NAVAL POSTGRADUATE SCHOOL
MONTEREY, CALIFORNIA

DISSERTATION

AN ANNULAR THERMOACOUSTIC PRIME MOVER

by

Lin, Hsiao-Tseng

September 1997

Thesis Advisor: Anthony A. Atchley

Approved for public release; distribution is unlimited.

REPORT DOCUMENTATION PAGE	Form approved OMB No. 0704-188

1. AGENCY USE ONLY (*Leave Blank*)	2. REPORT DATE	3. REPORT TYPE AND DATES COVERED
	September 1997	Ph.D. Dissertation

4. TITLE AND SUBTITLE
AN ANNULAR THERMOACOUSTIC PRIME MOVER

5. FUNDING NUMBERS

6. AUTHOR(S)
Lin, Hsiao-Tseng

7. PERFORMING ORGANIZATION NAME(S) AND ADDRESS(ES)
Naval Postgraduate School
Monterey, CA 93943-5000

8. PERFORMING ORGANIZATION REPORT NUMBER

9. SPONSORING/MONITORING AGENCY NAME(S) AND ADDRESS(ES)

10. SPONSORING/MONITORING AGENCY REPORT NUMBER

11. SUPPLEMENTARY NOTES
The views expressed in this thesis are those of the author and do not reflect the official policy or position of the Department of Defense or the U.S. Government.

12a. DISTRIBUTION/AVAILABILITY STATEMENT
Approved for public release; distribution is unlimited.

12b. DISTRIBUTION CODE

13. ABSTRACT (Maximum 200 words)

The dissertation constitutes the first detailed theoretical and experimental investigation of a thermoacoustic prime mover with periodic boundary conditions. There are five significant aspects to this research: (1) using DeltaE to analyze an annular prime mover, (2) developing an entirely new analysis program using MATLAB, (3) designing, building, and experimentally investigating a single stack, annular prime mover, (4) experimentally investigating a constricted, single stack annular prime mover, (5) predicting the performance of a two stack annular prime mover. The major conclusions are: (1) A single stack annular prime mover will not reach onset because the eigenmodes of the system do not support thermoacoustic growth. (2) A constricted annular prime mover will reach onset because the constriction forces dominating boundary conditions that alter the eigenmodes. (3) A two stack prime mover is predicted to reach onset because one of the eigenmodes of the symmetric system does support thermoacoustics.

14. SUBJECT TERMS
Acoustics, Thermoacoustics, Annular Resonator, Prime Mover

15. NUMBER OF PAGES
249

16. PRICE CODE

17. SECURITY CLASSIFICATION OF REPORT	18. SECURITY CLASSIFICATION OF THIS PAGE	19. SECURITY CLASSIFICATION OF THIS ABSTRACT	20. LIMITATION OF ABSTRACT
Unclassified	Unclassified	Unclassified	UL

NSN 7540-01-280-5500

Standard Form 298 (Rev. 2-89)
Prescribed by ANSI Std 239-18

Approved for public release; distribution is unlimited.

AN ANNULAR THERMOACOUSTIC PRIME MOVER

Lin, Hsiao-Tseng

Major, Republic of China Army

B.S., Chung Cheng Institute of Technology in Taiwan, 1984

M.S., Naval Postgraduate School, 1989

Submitted in partial fulfillment of

requirements for the degree of

DOCTOR OF PHILOSOPHY IN ENGINEERING ACOUSTICS

from the

NAVAL POSTGRADUATE SCHOOL

September 1997

Author: 林 發 增 Lin, Hsiao-Tseng

Lin, Hsiao-Tseng

Approved by:

Anthony A. Atchley
Professor of Physics
Dissertation Supervisor

Thomas J. Hofler
Professor of Physics

Andrés Larraza
Professor of Physics

Robert M. Keolian
Professor of Physics

Christopher Frenzen
Professor of Mathematics

James H. Miller
Professor of Ocean Engineering
University of Rhode Island

Approved by: _____
Anthony A. Atchley, Chair, Department of Physics

Approved by: _____
Herschel H. Loomis, Jr., Chair, Department of Electrical and Computer Engineering

Approved by: _____
Maurice D. Weir, Associate Provost for Instruction

ABSTRACT

The dissertation constitutes the first detailed theoretical and experimental investigation of a thermoacoustic prime mover with periodic boundary conditions. There are five significant aspects to this research: (1) using DeltaE to analyze an annular prime mover, (2) developing an entirely new analysis program using MATLAB, (3) designing, building, and experimentally investigating a single stack, annular prime mover, (4) experimentally investigating a constricted, single stack annular prime mover, (5) predicting the performance of a two stack annular prime mover. The major conclusions are: (1) A single stack annular prime mover will not reach onset because the eigenmodes of the system do not support thermoacoustic growth. (2) A constricted annular prime mover will reach onset because the constriction forces dominating boundary conditions that alter the eigenmodes. (3) A two stack prime mover is predicted to reach onset because one of the eigenmodes of the symmetric system does support thermoacoustics.

TABLE OF CONTENTS

LIST OF FIGURES

LIST OF TABLES

LIST OF SYMBOLS, SUBSCRIPTS AND SUPERSCRIPTS

A	area
amb	ambient duct
amb hx	ambient heat exchanger
c	sound speed
c_p	isobaric heat capacity per unit mass
E	energy
f	function in Eqs. (2.7) and (2.9), or frequency
f_0	real resonance frequency
h	function in Eqs. (2.6) and (2.8), or subscript for hot
hot	hot duct
hot hx	hot heat exchanger
$\dot{H}_2$	time averaged energy flux
Im	imaginary part of
$\boldsymbol{J}$	Jacobian matrix
L	resonator length
p	pressure
Q	quality factor
Re	real part of

Rs	area ratio of constriction
T	temperature
u	x component of velocity
$\overline{U}_1$	volume velocity
$\bar{v}$	velocity
$\dot{W}$	dissipated power
x	position along sound propagation
y	position perpendicular to sound propagation
y_0	plate half spacing
γ	ratio of isobaric to isochoric specific heats
δ	penetration depth
ω	complex angular frequency
κ	thermal conductivity, or the subscript for thermal
ρ	density
λ	wavelength
μ	dynamic viscosity
σ	Prandtl number
eff	effective
m	mean
pms	prime mover stack

st	stored
v	viscous
1	first order
2	second order
*	complex conjugate
\	LU factorization

ACKNOWLEDGMENTS

As we go through life, there are a few special people who share our trials and tribulations. It is for this reason, that I wish to express my sincere appreciation to all the individuals who assisted me in developing this research undertaken and preparing this dissertation.

I would like to first thanks my thesis advisor, Dr. Anthony Atchley who introduced me to the magnificent field of thermoacoustics. Through his busy schedule there was always time for me. His confidence, encouragement, and enthusiastic guidance made it all possible. The challenges of this research were always met and overcome through his dedication and perseverance. I would like to express my heartfelt thanks to Dr. Ralph Muehleisen, a never ending source of new ideas. His expertise provided me with solutions to many experimental and computer simulation problems.

I wish to thanks Dr. Thomas Hofler for his assistance in some inspired ideas in developing the simulation program. Special thanks are extended to the members of my doctoral committee: Dr. Robert Keolian, Dr. Andrés Larraza, Dr. Chris Frenzen, and Dr. James Miller for their guiding assistance and encouragement through the course of this research. My gratitude is also extended to Dr. Bill Ward of the Los Alamos National Laboratory for his guiding assistance in constructing the DeltaE program for this work.

Other individuals who made a significant contribution to this research are: Dr. Steven Baker, Dr. Wilson Oscar, Jr., Dr. Daphne Kapolka, Dr. James Sanders, Dr. Kevin Smith, Mr. Gary Beck, Mr. George Jaksa, Mr. Jay Adeff, Mr. Bill Gavlick, Mr. Robert Sanders, Miss Nancy Sharrock, and Prof. Tianmin Yu of Monterey Institute of International

Studies. I especially thank for all the prayer support from the members of Monterey Chinese Church.

I reserve special thanks to my parents who teach me the importance of education and support me throughout the entire course of research.

Finally, and most of all, to my wife, Szu-Mei, for her loving support, understanding, and encouragement to help me accomplish this dissertation. **You** are always the wind beneath **my** wings. As to my lovely children Chia-Wei and Chia-Yu, daddy is going back home.

DEDICATION

To my loving wife, Szu-Mei, and wonderful children, Chia-Wei and Chia-Yu.

I. INTRODUCTION

The subject of this dissertation is the investigation of thermoacoustic prime movers in an annular geometry. What sets this research apart from previous work in prime movers is the nature of the boundary conditions. To our knowledge this work is the first thorough investigation of thermoacoustic prime movers with periodic boundary conditions. The primary conclusion drawn from this work is that a full understanding of the eigenmodes of the system are required to design a functioning annular prime mover.

Thermoacoustic heat transport is a process through which an acoustic field generates, or is generated from, a flow of heat. Thermoacoustic engines are of two types: heat pumps and prime movers. A thermoacoustic heat pump utilizes a standing wave to transport heat along the boundary of a plate situated in the standing wave. The acoustically generated heat flow produces a temperature gradient across the stack. In other words, acoustic energy is converted into stored thermal energy. In contrast, a thermoacoustic prime mover produces acoustic work, by accepting heat from a high-temperature source and transferring it to a low-temperature sink. In this dissertation a prime mover in an annular resonator is investigated both theoretically and experimentally.

To illustrate how a prime mover operates, two conventional prime mover configurations are described. One type (as is shown in Fig. 1.1) is a rigid-rigid standing wave tube which contains a stack of plates called the prime mover stack (or, simply, the stack), which is in thermal contact with two heat exchangers. In operation, a temperature difference is imposed between the two heat exchangers, resulting in a temperature gradient along the stack. When the temperature gradient in the stack is sufficiently large, the gas in the resonator oscillates spontaneously at a certain frequency, with pressure antinodes at the

closed ends. The inception of spontaneous oscillation is known as *onset*. Once onset is reached, the acoustic amplitude in the resonator grows rapidly, typically reaching several percent of the mean gas pressure.

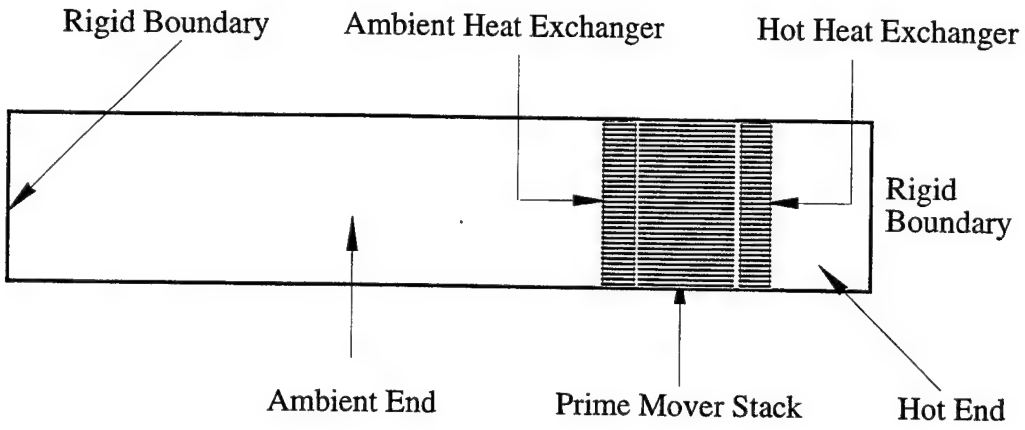

Figure 1.1 A typical rigid-rigid prime mover configuration.

The second prime mover configuration, called the Hofler tube, is a rigid-open resonator (as is shown in Fig. 1.2). In 1983, Hofler designed and built this simple thermoacoustic oscillator to demonstrate some thermoacoustic phenomena to his doctoral committee at the University of California, San Diego. The sound radiated from the open end of the pipe is impressively loud, about 100 dB re 20 μPa a meter away (Wheatley et al., 1985; Swift, 1988).

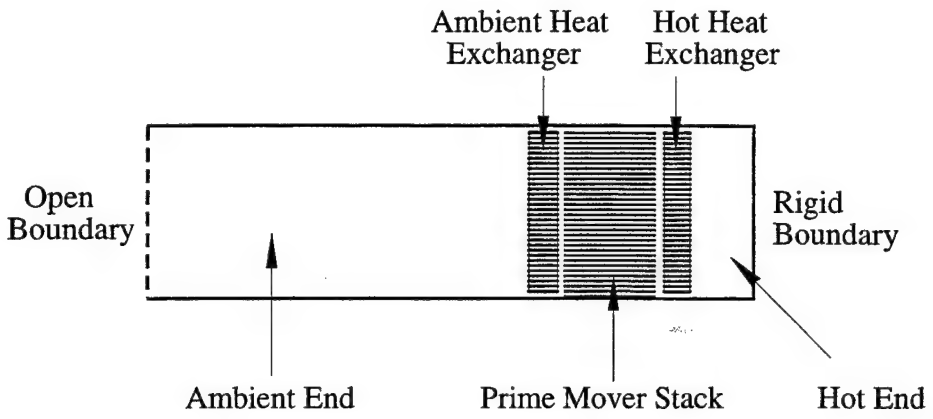

Figure 1.2 The Hofler tube, an example of a rigid-open prime mover.

The condition necessary for a prime mover to reach onset is that the amount of stored thermal energy converted to acoustic energy must exceed the total amount of acoustic energy dissipated by thermal-viscous losses in the prime mover. This ability to reach onset is determined by the geometry of the prime mover, in particular, the position of the stack relative to the nearest pressure antinode. The hot end of the stack is closer to a pressure antinode than is the ambient end. In the two examples of conventional prime movers described above, the node and antinode positions are fixed by incorporating well-defined acoustic boundary conditions into the system. This is an important common feature for all conventional prime movers. The "built-in" boundary conditions also serve as convenient starting points for computational analysis of the performance of a prime mover. Because the relative positions of the dominating boundaries and the stack are fixed, the stack position is optimized for only one acoustic mode. Also, the optimal stack position for onset is not necessarily the optimal position for high amplitude performance. One of the initial motivations for studying annular prime movers was to see if it would self-optimize the stack location relative to the acoustic field.

Unlike a conventional prime mover, an annular prime mover (as is shown in Fig. 1.3) does not have the typical dominating boundary condition to force a pressure or velocity node at any particular position. Design and analysis of a functional annular prime mover are thus made more difficult.

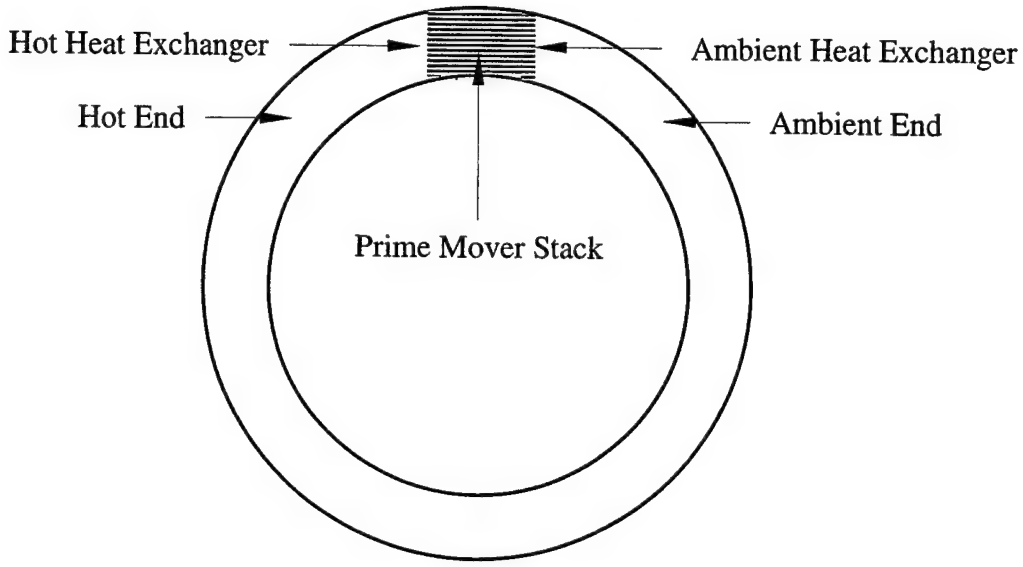

Figure 1.3 An annular prime mover configuration.

In a uniform cross-section annular resonator, the fundamental longitudinal mode corresponds to the circumference being approximately equal to one acoustic wavelength. There are two degenerate orthogonal modes that satisfy this condition. However, these modes have no preferred orientation. The presence of a nonuniformity (for example, the stack) breaks the degeneracy resulting in a frequency-splitting. The low frequency mode will have a pressure node at the stack, and the higher frequency mode will have a velocity node at the stack. (In what follows, the word "frequency" will be dropped and the modes

referred to, simply as "high" and "low".) Neither of these modes supports thermoacoustics.

Although in retrospect the answer now seems obvious, prior to a thorough study of the problem one might have argued that, once it becomes very strong, the thermoacoustic effect may dominate the situation and shift the orientation of the acoustic field to some preferable position. This suggests the possibility of the annular prime mover achieving onset. Even if the uniform cross section, single stack prime mover does not reach onset, other nonuniformities in cross section will have some effect on the spatial distribution of the acoustic field. Hence, by placing another constriction in the annulus, the previously mentioned pressure and velocity nodes may be displaced from the stack, providing the possibility of the annular prime mover reaching onset. These are some of the concepts that initiated this work.

It should be noted that a rigid-rigid prime mover can be considered a limiting case of a constricted, annular prime mover. All the previous work on thermoacoustic prime movers have dealt with engines that have some sort of well-defined boundary conditions imposed upon them. There has been no detailed analysis of prime movers with periodic boundary conditions.

A. BACKGROUND

Although thermoacoustic phenomena have been observed for a long time, significant advances in practical thermoacoustics are relatively recent. The earliest example of a thermoacoustic prime mover is the Sondhauss tube (Sondhauss, 1850). Over 100 years

ago, it was observed by glassblowers that a hot glass bulb attached to a cool glass tube sometimes emitted sound at the tip of the tube. Sondhauss quantitatively investigated the relationship between the pitch of the sound emitted and the dimensions of the tube. Lord Rayleigh explained the Sondhauss tube quantitatively in 1896, but no complete theoretical analysis of these phenomena was made before publication of the series of papers by Nikolaus Rott (Rott, 1969, 1980, 1983). Later, Wheatley (1985) and others at Los Alamos began the development of practical thermoacoustics devices.

B. PAST RELEVANT WORKS

Past works relevant to this research fall under three headings: (1) the thermoacoustic prime mover, (2) the acoustic Stirling Engine, and (3) the annular resonator.

1. The Thermoacoustic Prime Mover

The potential application of thermoacoustics as a heat-driven sound source has motivated theoretical developments (Rott, 1969; Wheatley and Cox, 1988; Swift, 1988). Work on prime movers has been focused on either rigid-rigid or rigid-open prime movers. Some examples are outlined below. Miglori and Swift (1988) constructed a thermoacoustic prime mover that used liquid sodium as its working fluid. A prime mover has also been used as a heat-driven sonar projector (Gabrielson, 1991). Swift (1992) built and analyzed a 5-inch thermoacoustic prime mover which, at its most powerful operating point, using 13.8-bar helium, delivered 630 W to an external acoustic load. With minor modifications, this device was used by Swift (1994) to research the application of similitude to nonlinear thermoacoustics.

The Naval Postgraduate School has been in the forefront of much thermoacoustic research. Atchley and the author first built and tested a heat driven prime mover (Lin and Atchley 1989), which generated a sound, at a temperature difference of 453 °C, with a peak acoustic amplitude of 7.9% of atmospheric pressure. Subsequently, other work was done on this device (Atchley 1992, 1993; Atchley and Kuo, 1994). In 1993, a thermoacoustic prime mover was constructed by Castro and Hofler to investigate the performance of heat exchangers and produced peak pressures of up to 20% of the mean pressure (Castro and Hofler, 1993).

DeltaE, a program developed at Los Alamos National Laboratory by Ward and Swift (1994, 1996) has been applied to several cases in the design and analysis of thermoacoustic prime movers. DeltaE stands for Design Environment for Low Amplitude Thermoacoustic Engines. It solves Rott's wave equation for a geometry defined by the user. For example, Swift (1992, 1996) used DeltaE to analyze the performance of a 5-inch thermoacoustic engine. Nessler (1994) used DeltaE to compare the performance of the pin stack with a conventional stack in a thermoacoustic prime mover (Swift and Keolian 1993). Yang (1995) and Meng (1996) also used DeltaE to predict onset of their thermoacoustic prime movers. More recently, DeltaE was applied to analyze the efficiency of a thermoacoustic prime mover with a pin stack (Gibson, Nessler, and Keolian, 1997).

2. The Acoustic Stirling Engine

Ceperley (1979, 1982 and 1985) has discussed acoustic engines using traveling waves. As recognized by Ceperley and several other authors (Swift, 1988, 1995; Hofler 1988; Organ 1992), the phasing between pressure oscillations and velocity within a Stirling engine regenerator is the same as those of an acoustic traveling wave. Ceperley proposed the replacement of the function of the pistons in a Stirling engine by acoustic processes, to

form what he called a *traveling-wave heat engine*. One of his concepts, a traveling-wave heat-driven refrigerator, is shown in Fig. 1.4. In this device, one regenerator and heat exchanger set functions as the prime mover, adding acoustic power onto the traveling wave as heat flows from a high-temperature heat source to a room temperature heat sink. The other set functions as a heat pump, using acoustic power from the traveling wave to transport heat from a low temperature to room temperature. His work was partly responsible for motivating the author to embark on this project. However, his analysis was overly simplistic and he never built a working device.

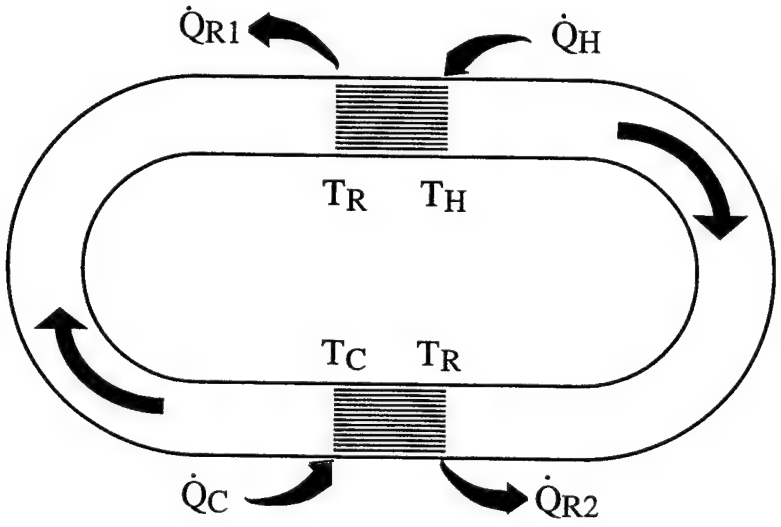

Figure 1.4 Ceperley's design for a traveling-wave heat-driven refrigerator. The arrows show the direction of wave propagation.

3. The Annular Resonator

Previous work on annular resonators is also relevant to the study of the annular prime mover. The eigenmodes for electromagnetic wave propagation in an annular cavity are of

fundamental interest in the radio-frequency (RF) heating of tokamak plasmas, besides having other applications in the microwave circuit theory (Cap and Deutsch 1978, 1980; Janaki and Dasgupta, 1990; Wu, 1992).

Another category of relevant work is the frequency splitting phenomenon found in different fields. As early as 1969, Rudnick *et al.* made observations of a superfluid helium persistent current using the Doppler-shifted splitting of an azimuthal resonant fourth-sound mode of the cylindrical resonator containing liquid helium (Rudnick et al. 1969). Heiserman investigated the persistent currents in superleaks in contact with bulk superfluid helium using the Doppler shifts of the acoustic modes of an annular resonator partially packed with a superleak, and with a simple gyroscopic technique (Heiserman, 1975). In plasma physics, in the presence of a finite plasma current, the axisymmetric magnetoacoustic wave resonance exhibits a frequency splitting for a finite annular mode number between oppositely directed traveling waves (Borg and Wit, 1991). A deformation of the cross section of a pinch of the plasma cross section also induces frequency shift and splitting of circular modes (Ring, 1988). In the microwave and RF field, frequency splitting can also be found in a nonuniform microstrip ring resonator (Wested and Andersen, 1972), in an asymmetrically coupled microstrip ring resonators (Al-Charchafchi and Dawson, 1990) and in a microstrip rhombic resonator with a step discontinuity in one of the arms (Al-Charchafchi and Boulkos, 1990; Al-Charchafchi and Schreck, 1994).

C. OUTLINE OF THIS WORK

This work constitutes the first detailed theoretical and experimental investigation of a thermoacoustic prime mover with periodic boundary conditions. There are five significant aspects to this research: (1) using DeltaE to analyze an annular prime mover, (2)

developing an entirely new analysis program using MATLAB, (3) designing, building, and experimentally investigating a single stack, annular prime mover, (4) experimentally investigating a constricted, single stack annular prime mover, (5) predicting the performance of a two stack annular prime mover.

The major conclusions are: (1) A single stack annular prime mover will not reach onset because the eigenmodes of the system do not support thermoacoustic growth. (2) A constricted annular prime mover will reach onset because the constriction forces dominating boundary conditions that alter the eigenmodes. (3) A two stack prime mover is predicted to reach onset because one of the eigenmodes of the symmetric system does support thermoacoustic growth.

II. THEORY

This chapter is divided into four parts. The first part is a brief review of the aspects of thermoacoustics pertinent to the annular prime mover problem. The review draws heavily from Swift's work (Swift, 1988 and 1997), and is intended to introduce the concepts required to understand the techniques used to analyze the annular prime mover. One of the central questions to be addressed in this dissertation is the ability of an annular prime mover to reach onset. The dependence of quality factor Q of the prime mover on the temperature difference ΔT applied to the stack is a key measure of this ability. In this research, the predicted Q will be determined from the complex eigenfrequency of the prime mover. Therefore, following the review of thermoacoustics, the complex eigenfrequency will be introduced.

Another important aspect of this dissertation is the numerical analysis of the annular prime mover. The techniques used will be discussed in the last part of this chapter. Some basic properties of the two-point boundary-value problem are discussed, followed by a discussion of the advantages and disadvantages of using DeltaE with the annular prime mover geometry. A MATLAB numerical analysis program is then described that is more tailored to the annular prime mover than is DeltaE. The validation of this program is discussed and the application of the MATLAB program to our annular prime mover is presented.

This chapter concludes with a discussion of the end corrections for constrictions in the cross section of annular resonators.

A. REVIEW OF THERMOACOUSTICS

Thermoacoustics is essentially the study of the acoustics of a fluid in which there exists a temperature gradient. The acoustics of such a fluid is contained in three differential equations which relate the complex acoustic pressure and volume velocity, and the temperature and enthalpy of the fluid. This method was first described by Wheatley et al. (Wheatley et al., 1983). The derivations of these relationships are summarized in this section. Once these concepts have been introduced, a description of the basic scheme used to analyze the performance of an annular prime mover is given.

This section is essentially a summary of pertinent aspects of thermoacoustics given in the articles by G. W. Swift (Swift, 1988 and 1997). Swift's quantitative thermoacoustic analysis is based on Rott's wave equation and energy-flux equation, which result from the momentum, mass continuity, and energy equations in the acoustic approximation. The results are valid for arbitrary phasing between the acoustic pressure and velocity; in other words, for both standing-wave and traveling-wave systems. The results presented in this section serve as the basis for the numerical analysis used in this dissertation.

First, the notation that will be used throughout this discussion is established. The acoustic wave is considered to propagate in the x direction within a duct of constant cross section. The usual complex notation is adopted for time-oscillatory acoustic quantities. Also, expansions to first order in the acoustic variables is assumed to suffice. Thus, the pressure, velocity and temperature can be written

$$p(x) = p_{\,\mathrm{m}} + p_1\,(x)\,\mathrm{e}^{i\omega t}, \tag{2.1}$$

$$u(x,\,y,\,z) = u_1\,(x,\,y,\,z)\,\mathrm{e}^{i\omega t}, \tag{2.2}$$

and

$$T(x, ,y, z) = T_m(x) + T_1(x, y, z)\, e^{i\omega t}, \qquad (2.3)$$

where $i = \sqrt{-1}$ and u_1 is the x-component of $\vec{v}$. The mean values (subscript m) are real, but the acoustic variables (subscript 1) are, in general complex, to account for the relative phasing of those oscillating quantities. It is assumed that the mean fluid velocity $u_m = 0$. All the time dependence appears in the $e^{i\omega t}$ term, with $\omega = 2\,\pi\, f$ being the angular frequency. For clarity, we consider here only the case of large solid heat capacity, so that the temperature of the solid material in the stack is simply $T_m(x)$, independent of t, y, and z.

The conservation of momentum of an incompressible viscous fluid is (Landau, 1975)

$$\frac{\partial \vec{v}}{\partial t} + (\vec{v} \bullet \text{grad})\, \vec{v} = -\frac{1}{\rho}\, \text{grad}\, p + \frac{\mu}{\rho}\, \nabla^2 \vec{v}, \qquad (2.4)$$

where $\vec{v}$ is the velocity, ρ is the density, p is the pressure and μ is the dynamic viscosity of the fluid in the resonator. This is called the *Navier-Stokes equation.* To develop a quantitative understanding including viscous effects, we begin by finding the y and z dependence of the velocity. Because of the viscous boundary layer in the y and z direction all other viscous derivatives can be neglected compared to $\mu\partial^2 u_1/\partial y^2$ and $\mu\partial^2 u_1/\partial z^2$. Equation (2.4) then reduces to

$$i\omega \rho_m u_1 = -\frac{dp_1}{dx} + \mu \left(\frac{\partial^2 u_1}{\partial y^2} + \frac{\partial^2 u_1}{\partial z^2} \right). \qquad (2.5)$$

Equation (2.5) is an ordinary differential equation for $u_1(y, z)$. The boundary condition at the solid surface is $u_1 = 0$. With this boundary condition Eq. (2.5) can be solved to yield

$$u_1(x,\ y,\ z) = \frac{i}{\omega\rho_m}\,[\,1 - h_v(y,\ z)]\frac{dp_1}{dx}\,, \tag{2.6}$$

where $h_v(y, z)$ depends on the specific geometry under consideration. The volume velocity is the spatial average over y and z of Eq. (2.6) and is thus

$$\overline{U}_1(x) = i\frac{A_{gas}}{\omega\rho_m}\,(1 - f_v)\,\frac{dp_1}{dx}\,, \tag{2.7}$$

where f_v is the spatial average of $h_v(y, z)$. For the case of parallel-plate geometry of the stack used in this work, it can be shown that (Swift 1988; Arnott et al. 1991)

$$h_v(y) = \frac{\cosh[(1+i)y/\delta_v]}{\cosh[(1+i)y_0/\delta_v]}, \tag{2.8}$$

and

$$f_v = \frac{\tanh[(1+i)y_0/\delta_v]}{[(1+i)y_0/\delta_v]}\,, \tag{2.9}$$

where $\delta_v = \sqrt{2\mu/\rho_m\omega}$ is the fluid's viscous penetration depth and y_0 is plate half-gap.

Calculation of the oscillating fluid temperature is accomplished using only the first order terms in the general equation of heat transfer (Landau, 1975). The entropy is expressed in terms of the acoustic pressure and temperature of the fluid and the resulting ordinary differential equation is solved subject to the appropriate boundary conditions. In the presence of a temperature gradient along the duct, the solution is (Swift 1988 and 1997)

$$T_1(x,\ y) = \frac{1}{\rho_m c_p}\,[\,1 - h_\kappa]\,p_1 + \frac{i}{\omega\,(1 - f_v)\,A_{gas}}\frac{dT_m}{dx}\,\left(1 - \frac{h_\kappa - \sigma h_v}{1 - \sigma}\right)\overline{U}_1\,, \tag{2.10}$$

where $\sigma = c_p\,\mu/\kappa$ is the Prandtl number, and c_p is the isobaric heat capacity per unit mass. The spatial average in (y, z)-direction of Eq. (2.10) can be written

$$\overline{T}_1(x) = \frac{1}{\rho_m c_p}\,[\,1 - f_\kappa\,]\,p_1 + \frac{i}{\omega\,(1-f_\nu)\,A_{gas}}\frac{dT_m}{dx}\,(\,1 - \frac{f_\kappa - \sigma f_\nu}{1-\sigma}\,)\,\overline{U}_1\,, \qquad (2.11)$$

where f_κ is the spatial average of h_κ. The functions h_κ and f_κ are the same as h_ν and f_ν, only with δ_ν replaced by $\delta_\kappa = \sqrt{2\kappa/\rho_m c_p \omega}$, the thermal penetration depth, where κ is the thermal conductivity of the fluid. The function f_κ and f_ν are very important in thermoacoustics and describe how viscous and thermal processes affect the oscillatory velocity and temperature in the acoustic field. A graph of f_ν as a function of y/δ_ν is shown in Fig. 2.1.

The equation of continuity is (Landau, 1975)

$$\frac{\partial \rho}{\partial t} + \nabla \bullet (\rho \vec{v}) = 0\,. \qquad (2.12)$$

To first order, the x-component of Eq. (2.12) can be reduced to the form

$$i\,\omega\,\rho_1 + \frac{\mathrm{d}(\rho_m\,u_1)}{\mathrm{d}x} = 0\,. \qquad (2.13)$$

Equation (2.13) can be rewritten in terms of volume velocity

$$i\,\omega\,\rho_1 + \frac{1}{A_{gas}}\frac{\mathrm{d}(\rho_m\,\overline{U}_1)}{\mathrm{d}x} = 0\,. \qquad (2.14)$$

Combining Eqs. (2.10) and (2.13) yields

$$\frac{d\overline{U}_1}{dx} = -\frac{i\omega A_{gas}}{\rho_m c^2}\left[1+(\gamma-1)f_\kappa\right]p_1 + \frac{(f_\kappa - f_\nu)}{(1-f_\nu)(1-\sigma)}\frac{1}{T_m}\frac{dT_m}{dx}\overline{U}_1\,, \qquad (2.15)$$

where c is the speed of sound in the gas, and γ is the ratio of isobaric to isochoric specific heats.

We pause to discuss the results derived in the last several paragraphs. Equation (2.7) shows that the gas which is much farther than δ_v from the nearest solid surface experiences essentially no viscous shear and moves with a velocity that depends only on x. The gas that is much closer than δ_v is nearly at rest. Gas that is between these extremes moves with a reduced velocity amplitude and significant phase change. The terms in Eq. (2.11) indicate that there are two contributions to the oscillatory temperature. The first term is simply due to the adiabatic compressions and expansions of the fluid. The second term comes from the convection of gas parcels along a temperature gradient. The net temperature oscillation is just a linear combination of these two effects. It should be pointed out that f_κ has the same functional dependence as y/δ_κ as is portrayed in Fig. 2.1 for f_v.

Equation (2.15) has an easy physical interpretation. It indicates that $d\overline{U}_1/dx$ comes from a density oscillation in the fluid. This density change can be caused by a pressure change or by convection of gas along the temperature gradient.

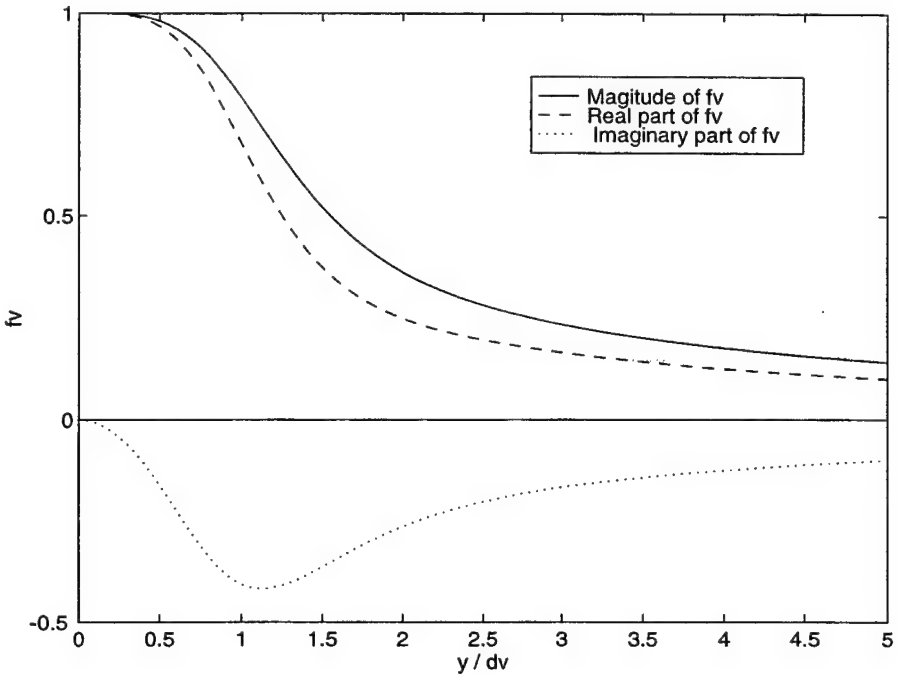

Figure 2.1 The real and imaginary parts and magnitude of f_v as functions of the ratio y/δ_v for the case of parallel plate geometry.

Next, following the derivation by Swift (1988 and 1997), the time averaged energy flux along the stack can be found as

$$\dot{H}_2 = \frac{1}{2}\,\mathrm{Re}\left[p_1\,\overline{U}_1^*\left(1-\frac{(f_\kappa - f_v^*)}{(1+\sigma)(1-f_v^*)}\right)\right] + \frac{\rho_m\,c_p\,\overline{U}_1^{\,2}}{2\omega\,A_{gas}(1-\sigma^2)\,|1-f_v|^2}\,\mathrm{Im}\left(f_\kappa + \sigma f_v^*\right)\frac{dT_m}{dx} - \left(A_{gas}\,\kappa + A_{soild}\,\kappa_{solid}\right)\frac{dT_m}{dx}, \tag{2.16}$$

where the superscripts * represent the complex conjugate of a complex quantity, and κ_{solid} is the thermal conductivity of the solid. On the basis of Swift's assumptions, in steady state for an engine without lateral heat flows to the surroundings, $\dot{H}_2$ along x must be a constant throughout the stack.

To numerically analyze the performance of thermoacoustic engines, it is recognized that Eqs. (2.7), (2.15) and (2.16) comprise a set of three second-order coupled complex differential equations in the five variables Re(p_1), Im(p_1), Re($\overline{U}_1$), Im($\overline{U}_1$) and T_m. These equations are the basis of both DeltaE and the MATLAB program presented later in this chapter.

In order to obtain a more useful form of the differential equation for $p_1(x)$, Eq. (2.7) can be written as

$$\frac{dp_1}{dx} = \frac{i\,\omega\rho_m}{A_{gas}(1-f_v)}\,\overline{U}_1(x)\,. \tag{2.17}$$

In a duct region, the integration is governed by Eqs. (2.15) and (2.17) and the temperature gradient dT_m/dx is determined by the measured temperature profile. It is assumed that there is no temperature gradient across the heat exchanger. As a result, in a heat exchanger, integration is carried out by Eq. (2.17) and a simplification of Eq. (2.15)

$$\frac{d\overline{U}_1}{dx} = -\frac{i\omega A_{gas}}{\rho_m c^2}\left[1+(\gamma-1)f_\kappa\right]p_1\,. \tag{2.18}$$

As for the stack region, integration is based on Eqs. (2.15), (2.17), and (2.19). In other words, the time averaged energy flux $\dot{H}_2$ is only used in the stack region and is a constant throughout the stack region.

The MATLAB numerical analysis method used in this work starts with specifying Re(p_1), Im(p_1), Re($\overline{U}_1$), Im($\overline{U}_1$), T_m, Re(f), and Im(f) at a point in the duct. The complex pressure and volume velocity just outside the starting end of the ambient heat exchanger can be determined by integrating Eqs. (2.15) and (2.17) in the boundary layer approximation limit. Next, the complex pressure and volume velocity can be determined just inside the

starting end of the ambient heat exchanger by invoking continuity of pressure and volume velocity at the end of the ambient heat exchanger. Then, Eqs. (2.17) and (2.18) are used to integrate over the ambient heat exchanger. Continuity of pressure and volume velocity is used to enter the stack. A value of $\dot{H}_2$ is specified to get dT_m/dx at the beginning of the stack. The solution in integrated to the heat exchanger. Again Eqs. (2.17) and (2.18) are integrated over the hot heat exchanger. Finally, the pressure, volume velocity, and the temperature at the exit of the hot heat exchanger are matched to those at the starting point.

B. COMPLEX EIGENFREQUENCY

The transition to onset in a prime mover is conveniently discussed in terms of the quality factor Q which can be defined as the ratio of 2π times the energy stored in the resonator to the energy dissipated per acoustic cycle. Letting $\dot{W}$ denote the dissipated power,

$$Q = \frac{\omega E_{st}}{\dot{W}}. \tag{2.19}$$

Both $\dot{W}$ and E_{st} are second order in the acoustic amplitude. A typical prime mover is comprised of five sections: the ambient duct, the ambient heat exchanger, the prime mover stack, the hot heat exchanger, and the hot duct. $\dot{W}$ is then the sum of the power dissipated in the five individual sections (Lin, 1989; Atchley, 1992 and 1994)

$$\dot{W} = \dot{W}_{amb} + \dot{W}_{amb\,hx} + \dot{W}_{pms} + \dot{W}_{hot\,hx} + \dot{W}_{hot}. \tag{2.20}$$

The subscripts *amb*, *amb hx*, *pms*, *hot hx*, and *hot* refer to the ambient duct, the ambient heat exchanger, the prime mover stack, the hot heat exchanger, and the hot duct,

respectively. The reader should refer to Atchley (Atchley et al., 1992) and Lin (Lin, 1989) for a full explanation.

Instead of Q, we prefer to use the reciprocal of Q, because $1/Q$ converges to zero at onset rather than diverging to infinity. Also, it is this quantity that is proportional to the acoustic power output of the prime mover. It is worth mentioning that $1/Q$ is a function of the prime mover geometry, the thermophysical properties of the gas, p_m, and the temperature difference. As the temperature difference along the stack increases from zero, the thermal losses in the stack decrease and eventually become negative, representing gain. In other words, below onset $1/Q$ is positive, at onset $1/Q$ is zero and above onset $1/Q$ is negative. A complete evolution of Q through onset for a prime mover is discussed by Atchley (Atchley, 1994).

In this work, the Q is determined by the complex eigenfrequency. Complex eigenvalues occur when a system has underdamped modes. The excitation of a resonator evolves in time as $\exp(i\omega_0 t)$ where the eigenfrequency is (Swift, 1988; Gamaletsos 1993; Arnott et al., 1994)

$$\omega_0 = 2\pi f_0 + i\frac{\pi f_0}{Q}, \tag{2.21}$$

where f_0 is the real resonance frequency. The quality factor Q thus can be found by

$$Q = \frac{\mathrm{Re}(\omega_0)}{2\,\mathrm{Im}(\omega_0)}. \tag{2.22}$$

It should be noted that the complex eigenfrequency approach accounts for power generation in the stack and dissipation everywhere in the resonator. If this approach were

not used, an artificial acoustic source would have to be introduced into the system to deliver power to match boundary conditions (Choe, 1997).

C. THE ANNULAR GEOMETRY FOR A PRIME MOVER

As discussed in the previous chapter, the major difference between conventional prime mover geometry and that of an annular prime mover is that there are no typical dominating boundary conditions in the latter. Instead, an annular prime mover satisfies the periodic conditions

$$p_1(r, \theta) = p_1(r, \theta + 2\pi), \tag{2.23}$$

and

$$\overline{U}_1(r, \theta) = \overline{U}_1(r, \theta + 2\pi). \tag{2.24}$$

At first glance, this difference does not seem to cause much difficulty in the design and analysis of an annular prime mover, until one realizes the fact that almost all the previous work on conventional prime movers employ some dominating boundary condition as a convenient starting point of their analysis. Elimination of these boundary condition makes research on an annular prime mover considerably different from that of a conventional prime mover.

It can be shown that an annular resonator can be modeled as a straight duct having an effect length L_{eff} that is related to the inner and outer radii of the annulus and the particular mode under consideration (Choe, 1997). Therefore, we will treat the annular prime mover as a straight duct having periodic boundary conditions. L_{eff} can be obtained by first writing the general solution of the wave equation in cylindrical coordinates which includes a linear

combination of the cylindrical Bessel and Neumann functions. Note that the Neumann function must be retained because the origin is excluded in the annular resonator. The effective circumference of the resonator can be then obtained by applying rigid boundary conditions at the inner and outer walls of the annulus. The annulus used in the experiments presented later has inner and outer radii of 10.0 and 15.3 cm, respectively. The height of the duct is 5.0 cm. The cutoff frequency for cross modes is approximately 6.6 kHz. We are interested in the fundamental longitudinal mode ($\lambda = L_{eff}$) corresponding to frequencies in the 400 ~ 450 Hz range, well below cutoff.

D. COMPUTER SIMULATION OF THE ANNULAR PRIME MOVER

This subsection discusses the numerical analysis techniques for the annular prime mover. For the purpose of numerical integration in a thermoacoustic engine, Eqs. (2.7), (2.15), and (2.16) can be rewritten as a set of five, first order, ordinary differential equations in terms of five independent acoustic variables: Re(p_1), Im(p_1), Re($\overline{U}_1$), Im($\overline{U}_1$) and T_m.

$$\frac{d\,\mathrm{Re}(p_1)}{dx} = \mathrm{Re}\left[-\frac{i\omega\rho_m A_{gas}}{(1-f_v)}\,\overline{U}_1(x)\right], \tag{2.25}$$

$$\frac{d\,\mathrm{Im}(p_1)}{dx} = \mathrm{Im}\left[-\frac{i\omega\rho_m A_{gas}}{(1-f_v)}\,\overline{U}_1(x)\right], \tag{2.26}$$

$$\frac{d\,\mathrm{Re}(\overline{U}_1)}{dx} = \mathrm{Re}\left\{-\frac{i\omega A_{gas}}{\rho_m c^2}\left[1+(\gamma-1)f_\kappa\right]p_1 + \frac{(f_\kappa - f_v)}{(1-f_v)(1-\sigma)}\frac{1}{T_m}\frac{dT_m}{dx}\overline{U}_1\right\}, \tag{2.27}$$

$$\frac{d\,\mathrm{Im}(\overline{U}_1)}{dx} = \mathrm{Im}\left\{ -\frac{i\omega A_{gas}}{\rho_m c^2}\left[1+(\gamma-1)f_\kappa\right]p_1 + \frac{(f_\kappa - f_v)}{(1-f_v)(1-\sigma)}\frac{1}{T_m}\frac{dT_m}{dx}\overline{U}_1 \right\}, \qquad (2.28)$$

and

$$\frac{dT_m}{dx} = \left\{ \frac{\dot{H}_2}{A_{gas}} - \frac{1}{2A_{gas}}\,\mathrm{Re}\left[p_1\,\overline{U}_1^*\left(1 - \frac{(f_\kappa - f_v^*)}{(1+\sigma)(1-f_v^*)}\right)\right]\right\} \div$$
$$\left\{ \frac{\rho_m\, c_p\, |\overline{U}_1|^2}{2A_{gas}^2(1-\sigma^2)\,|1-f_v|^2}\,\frac{\mathrm{Im}(f_\kappa + \sigma f_v^*)}{\mathrm{Re}(\omega)} - \kappa - \frac{A_{soild}}{A_{gas}}\kappa_{solid} \right\}. \qquad (2.29)$$

Our intention is to solve this set of coupled ordinary differential equations for $\mathrm{Re}(p_1)$, $\mathrm{Im}(p_1)$, $\mathrm{Re}(\overline{U}_1)$, $\mathrm{Im}(\overline{U}_1)$ and T_m, subject to the periodic boundary conditions at the ends of the prime mover. This is the same basic method employed by DeltaE.

1. Problem Statement

When ordinary differential equations are required to satisfy boundary conditions at more than one value of the independent variable, the resulting problem is called a *two point boundary value problem.* Determining the deflection of a bar rigidly fixed at both ends is a typical example where the conditions specified are the deflections of the elastic curve at the supports. Heat-flow problems often fall into this class when temperature or temperature gradients are given at two points. The problem encountered here is of this kind, too.

A major distinction between initial value problems and two point boundary value problems, as is pointed out by Press (Press et al., 1992), is that in the former case one is able to start an acceptable solution at its beginning (initial values) and just march it along by numerical integration to the end (final values). However in the latter case, the boundary conditions at the beginning point do not determine an unique solution to start with. For this

reason, two point boundary value problems require considerably more effort to solve than do initial value problems. Keller (Keller, 1992) has discussed the existence and uniqueness theory for two point boundary value problems.

Two different numerical approaches to the annular prime mover are applied in this dissertation: DeltaE and a MATLAB program.

2. DeltaE

DeltaE is a computer program, developed by Bill Ward and Greg Swift at Los Almos National Laboratory, for modeling and designing thermoacoustic and other one-dimensional acoustic apparatus. Basically, DeltaE solves the one-dimensional wave equation based on the usual low-amplitude acoustic approximation. It numerically integrates the wave equation in a gas or fluid, in a geometry provided by the user as a sequence of segments, such as ducts, transducers, compliances, heat exchangers and stacks. It uses continuity of oscillating pressure, oscillating volume velocity, and mean temperature to pass from the end of one segment to the beginning of the next. It uses the appropriate wave equation and temperature equation for each segment. The iteration is controlled by global parameters such as frequency and mean pressure, and by local parameters such as the geometry of a segment and enthalpy flow. By defining a series of inputs, global parameters (the guess vector), the desired outputs, and boundary conditions (the target vector), the problem is solved iteratively. Guesses are updated until targets are achieved. The number of elements in the target vector must equal the number of elements in the guess vector, otherwise the system is over- or under-determined. When the computed and specified targets agree to within a specific tolerance, the solution is said to

converge. All calculations in DeltaE are performed in double precision and the user may set the error tolerance for matching targets.

In general, because a pass of DeltaE's integration does not reach the end with targeted values of all variables, a shooting method is used to adjust chosen initial variables in order to hit the target values. The user provides guesses for chosen initial variables. A successful convergence of DeltaE depends heavily upon a good choice of guess and target members. A good guide to the choice of guess and target variables is discussed by Ward and Swift (Ward and Swift, 1996).

DeltaE is very versatile due to the fact that the elements of the guess vector are not limited to the conventional choices consisting of real and imaginary parts of p_1 and $\overline{U}_1$. Any variables that have an effect on the target vector variables can be used as a guess. This feature enables DeltaE to compute resonance frequency, temperature, and geometrical dimensions in order to satisfy specified boundary conditions. DeltaE is very efficient at converging to solutions for some complicated acoustic systems, however, it knows nothing about acoustics or physics. For example, it does not recognize that negative frequencies, negative pressures or negative lengths are physically meaningless. It simply does the integration. Therefore, the reasonableness of the solutions produced will almost always depend on the quality of the initial guess vector and choices of the guess-target vector.

To apply DeltaE to the annular prime mover the boundary conditions are incorporated into DeltaE's target vector. The unknown conditions at the *BEGIN* segment, which DeltaE is supposed to find, are in DeltaE's guess vector. To implement the periodic boundary conditions into DeltaE, a *SOFTEND* segment is inserted right after the initial *BEGIN* segment in the input file of the DeltaE program. Another *SOFTEND* segment (or they can both be *HARDEND* segments) is used at the end of the model. Four *DIFFTARGET*s are specified which match the amplitude and phase of p_1 and $\overline{U}_1$ at these two *SOFTEND*

segments (Ward, 1997). The *SOFTEND* segments serve only as a tool to calculate the outputs and will be ignored in the target vector. *SOFTEND*s do not force the impedance to be zero. A given temperature across the prime mover stack is achieved by selecting the temperature at the hot heat exchanger as a target and the amount of heat input to the ambient heat exchanger as a guess vector. We now have five targets and only one guess; four more guesses are still required. The other four guesses have been selected to be the amplitude and phase of p_1 and $\overline{U}_1$ at the beginning segment. These guesses and targets (as are shown in Appendix B) are summarized in Table 2.1.

Guess vector	Target vector
1. $\lvert p_1 \text{ (begin)} \rvert$	1. $\lvert p_1(\text{begin}) \rvert - \lvert p_1(\text{end}) \rvert < \varepsilon$
2. Phase[p_1 (begin)]	2. Phase[p_1(begin)] - phase[p_1(end)] $< \varepsilon$
3. $\lvert \overline{U}_1 \text{ (begin)} \rvert$	3. $\lvert \overline{U}_1 \text{ (begin)} \rvert - \lvert \overline{U}_1 \text{ (end)} \rvert < \varepsilon$
4. Phase[$\overline{U}_1$ (begin)]	4. Phase[$\overline{U}_1$ (begin)] - phase[$\overline{U}_1$ (end)] $< \varepsilon$
5. Heat input at ambient heat exchanger	5. Hot heat exchanger temperature

Table 2.1 Summary of the guess and target vectors in the DeltaE input file for the annular prime mover. ε represents the tolerance for convergence.

The important parameters for this work are the Q, the resonance frequency and the mode shape of the prime mover. To attain these desired quantities, more deliberation has to be made in determining the input file. Two methods can be utilized to find the Q with DeltaE (Ward, 1997). In the first method, the Q can be obtained indirectly by adding an artificial driver into the system, sweeping its frequency, and computing the frequency response of the system. The resonance frequency and half power points can be extracted

from this analysis. An alternate method is to compute the ratio of the stored energy to the dissipated energy. The stored energy is computed by adding an artificial driver, determining the pressure and velocity throughout the system and integrating the energy density. The dissipated energy is computed from the work done by the driver to excite the system. Since DeltaE only computes the pressure and velocity at the exit of a segment, the system must be broken into many segments to get a reasonable approximation to the stored energy. Thus the frequency response method was chosen to find the Q and resonance frequency. A side branch electroacoustic transducer was used as a driver, which has frequency independent parameters. A MATHEMATICA program (refer to Appendix A) was also developed to compute a least squares fit to the frequency response to find Q and resonance frequency. After finding resonance frequency, the system is then driven at resonance. To attain a detailed modal shape, the prime mover has to be divided into many small segments. The modal shape is a plot of the pressure at the end of each segments of the converged solution as a function of segment location.

DeltaE is a very useful tool to predict how a given thermoacoustic apparatus will perform, or for helping the user design an apparatus to achieve a desired performance. However, it does have several disadvantages when applied to the annular problem. As was mentioned in Chapter I, in the presence of a stack, an annular prime mover exhibits frequency splitting. The degree to which a particular mode is excited depends on the location of the driver relative to the stack. Because of dissipation, Q for each mode is finite, which means that the two modes may overlap in the frequency domain. In terms of a driven acoustic system, this manifests itself as a multimode excitation. When only one mode is excited, it is straightforward to find Q and resonance frequency by a least squares fit to the frequency response curve. However, in the case when the driver excites two

mode simultaneously, some other technique, for example pole-zero analysis, must be used to determine Q and resonance frequency for each individual mode.

Another disadvantage comes from trying to map out the mode shape with DeltaE. In DeltaE, values of acoustic pressure are only provided at the end of each segment. Therefore, to obtain a detailed mode shape, the prime mover must be divided into many small segments. This inherent property makes it is laborious and impractical to use DeltaE to find the mode shape.

The other disadvantage is that currently there is no straightforward way to apply an externally-imposed temperature gradient on a resonator duct (Ward, 1997). This limitation makes it very difficult to model an annular prime mover and incorporate measured temperatures along the duct into the numerical model.

Because of the disadvantages of applying the DeltaE program to our problem a decision was made to develop our own program. This program, written in MATLAB, was validated by comparing the results for a simplified annular prime mover with DeltaE results.

3. MATLAB Program

a. Approach

One important aspect of this dissertation is to develop a numerical analysis program that is more tailored to the annular resonator problem than DeltaE. The program implements the *shooting method* because it appears to be a straightforward way to solve boundary value problems. This method also provides a systematic approach to taking a set of ranging shots that allows us to improve our aim systematically (Keller, 1992; Press et al., 1992). The program uses functions that already exist in MATLAB where possible.

A complete explanation of the procedure of the shooting method can be found in Press (1992) and Gerald (1994). Only a summary is presented here. Most differential equations of order higher than first can be reduced to coupled sets of first-order differential equations. The two point boundary value problem is equivalent to obtaining the solution to a set of N coupled first-order differential equations, satisfying N periodic boundary conditions at the starting point x_a and at the end point x_b.

We start by writing Eqs. (2.25) through (2.29) in a general form

$$\frac{dy_i(x)}{dx} = f_i(x, y_1, y_2, ..., y_N), \quad i = 1, 2, ..., N, \tag{2.30}$$

with the periodic boundary conditions at the starting point x_a and final point x_b expressed as

$$y_i(x_a, y_1, y_2, ..., y_N) = y_i(x_b, y_1, y_2, ..., y_N), \quad i = 1, 2, ..., N, \tag{2.31}$$

where, in our problem, N equals five.

To solve this boundary value problem, an initial value problem is created by assuming five initial values. The MATLAB function *ode45*, which implements fourth and fifth order *Runge-Kutta formulas* is then used to integrate the differential equations from x_a to x_b. The local error term for the fourth-order Runge-Kutta method is $O(h^5)$ and the global error would be $O(h^4)$, where h is the step size of the integration (Celia and Gary, 1992; Gerald and Wheatley 1994). Now, at the final point x_b, a discrepancy vector $\boldsymbol{F}$ is defined with the dimension of N, whose components measure how far the first solution attempt is from satisfying the boundary conditions at x_b. The problem now becomes one of finding the vector $\boldsymbol{F}$ such that

$$F_i(y_1, y_2, ..., y_N) = 0, \quad i = 1, 2, ..., N. \tag{2.32}$$

To find the roots of this equation the *Newton-Raphson method* is employed. This method provides a very efficient means of converging to a solution, if a sufficiently good initial guess is given (Press, 1992).

Let $\boldsymbol{y}$ denote the entire vector of values y_i. In the neighborhood of $\boldsymbol{y}$, each of the functions F_i can be expanded in a Taylor series about $\boldsymbol{y}_0$ as (Press, 1992)

$$F_i(\boldsymbol{y}) = F_i(\boldsymbol{y}_0 + \delta\boldsymbol{y}) = F_i(\boldsymbol{y}_0) + \sum_{j=1}^{N} \frac{\partial F_i}{\partial y_i} \delta x_j + O(\delta y^2). \tag{2.33}$$

The matrix of partial derivatives, known as the *Jacobian* matrix, $\boldsymbol{J}$ is defined as

$$J_{ij} = \frac{\partial F_i}{\partial y_j}. \tag{2.34}$$

Since it is difficult to compute the matrix $\boldsymbol{J}$ analytically in this problem, finite differences are used to compute this matrix. In the MATLAB program, this is accomplished by perturbing each y_i individually and finding the value of the vector of $\Delta F_i/\Delta y_i(x_b)$.
Equation (2.34) can be expressed in the matrix form

$$\boldsymbol{F}(\boldsymbol{y} + \delta\boldsymbol{y}) = \boldsymbol{F}(\boldsymbol{y}) + \boldsymbol{J} \bullet \delta\boldsymbol{y} + O(\delta y^2). \tag{2.35}$$

To obtain a set of linear equations for the correction vector $\delta\boldsymbol{y}$, terms of order δy^2 and higher are neglected. Setting $\boldsymbol{F}(\boldsymbol{y}+\delta\boldsymbol{y}) = 0$, gives

$$\boldsymbol{J} \bullet \delta\boldsymbol{y} = - \boldsymbol{F}(\boldsymbol{y}). \tag{2.36}$$

Provided $\boldsymbol{J}$ is nonsingular, $\delta\boldsymbol{y}$ is given by

$$\delta\boldsymbol{y} = - \boldsymbol{J}^{-1} \boldsymbol{F}(\boldsymbol{y}). \tag{2.37}$$

In practice, $\boldsymbol{J}^{-1}$ is obtained by *LU* factorization. In MATLAB notation, $\delta\boldsymbol{y}$ is given by

$$\delta \boldsymbol{y} = -\boldsymbol{J} \backslash \boldsymbol{F}(\boldsymbol{y}), \tag{2.38}$$

where \ is used to denote left division.

The *LU* factorization implements *Gaussian elimination*. Because it involves the least amount of arithmetic operations, Gaussian elimination is generally considered to be one of the most efficient computation methods in the problem of solving a system of linear equations (Leon, 1994; Lindfield and Penny, 1995). It is worth pointing out that using $\boldsymbol{J} \backslash \boldsymbol{F}(\boldsymbol{y})$ instead of $inv(\boldsymbol{J})*\boldsymbol{F}(\boldsymbol{y})$ in MATLAB is two or three times faster and produces residuals on the order of machine accuracy relative to the magnitude of the data (The Math Works, 1994). Once $\delta \boldsymbol{y}$ is found, the solution vector is then updated as

$$\boldsymbol{y}_{new} = \boldsymbol{y}_{old} + \delta \boldsymbol{y}. \tag{2.39}$$

The process is iterated until the solution converges, i.e. when the value of the normalized norm of the discrepancy vector $\boldsymbol{F}$ is smaller than a desired threshold.

In order to formulate a program to model the annular prime mover, the parameters to be updated at each pass of the integrations must be identified. These parameters are selected to be: the real and imaginary parts of the volume velocity $\overline{U}_1$ and the complex frequency ω, and the time-averaged energy flux along the stack $\dot{H}_2$. $\mathrm{Re}(p_1)$ and $\mathrm{Im}(p_1)$ are kept constant at $x = 0$, which simply normalizes the amplitude of the pressure variation. In fact, for given values of $\mathrm{Re}(p_1)$ and $\mathrm{Im}(p_1)$, a unique solution can be obtained for a certain value of $\dot{H}_2$. The periodic boundary conditions are satisfied by matching the acoustic pressure p_1 and the acoustic volume velocity $\overline{U}_1$ between the starting and final points. Also the temperature at the hot heat exchanger is matched to a certain value while keeping the temperature of the ambient heat exchanger a constant.

b. Description

The complete MATLAB program is described in Appendix C. This section provides a brief explanation of how the program works. First, the coordinate system for the prime mover (as is shown in Fig. 2.2) is defined. The hot heat exchanger is at one end of the system. The end of the hot heat exchanger is at $x = L_{eff}$. The choice of the position of x = 0 is arbitrary, however by putting the stack and heat exchangers at the end, only four distinct regions are required. Had the stack been placed in the middle, there would have been five.

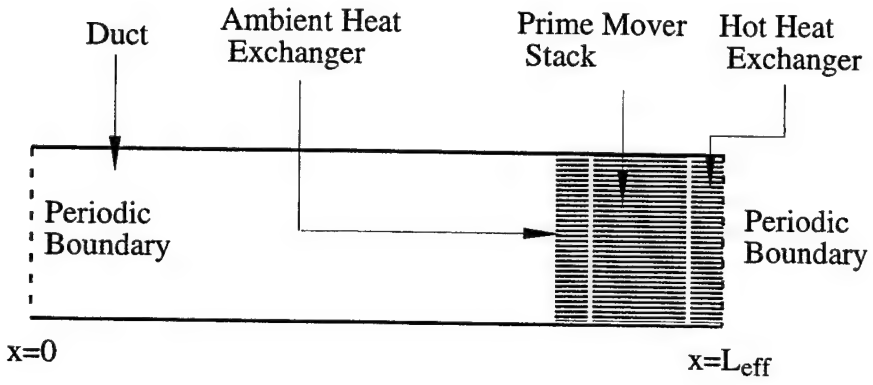

Figure 2.2 Coordinate system used in the numerical analysis of the annular prime mover.

Initial values of the real and imaginary parts of p_1, a measured temperature profile $T_m(x)$ along the duct and ambient heat exchanger, and a temperature for the hot heat exchanger, T_h are given. The real and imaginary parts of $\overline{U}_1$, the real and imaginary parts of the resonance frequency ω and the time-averaged energy flux along the stack $\dot{H}_2$ are guessed. It is assumed that the temperature of the duct and the ambient heat exchanger are

held at certain values by external means. A set of reasonable initial guesses, which can be estimated from the output of DeltaE, is the key to successful convergence of the program. The desired temperature of the hot heat exchanger (T_h in the program) is accomplished by adjusting the time-averaged energy flux along the stack $\dot{H}_2$. The targets to be matched are the real and imaginary parts of p_1 and $\overline{U}_1$ at $x = 0$ and $x = L_{\text{eff}}$, and the temperature of the hot heat exchanger. This matching is accomplished by adjusting the real and imaginary parts of $\overline{U}_1$, the real and imaginary parts the complex angular frequency ω, and the time-averaged energy flux along the stack. It is also assumed that there are no temperature gradients in the ambient and hot heat exchanger.

Once the required input parameters are determined. The program solves the system of equations for the five unknown variables. If the resulting new p_1, $\overline{U}_1$, and T_h differ significantly from the initial guesses it is necessary to update the guesses and do the integration again. During the integration, all the temperature dependent parameters and gas parameters are calculated according to the temperature distribution. This whole process is repeated to convergence.

c. Validation

This program was validated by comparing its solution to that using DeltaE for a simple case, in which it is assumed that the temperatures of the entire duct and the ambient heat exchanger are held at 293 K by some external means. The desired temperature of the hot heat exchanger is achieved by adjusting the quantity $\dot{H}_2$.

The comparisons of the results from the two programs are shown in Figs. 2.3 through 2.8. Figure 2.3 shows resonance frequency vs. ΔT, with ΔT increasing from 0 K to 240 K. Figure 2.4 shows $1/Q$ vs. ΔT over the same temperature difference span

as in Fig. 2.3. The overall agreement of resonance frequencies and $1/Q$ from the two methods is good. In fact, the normalized mean square errors of the resonance frequency between two methods are $1.48\times10^{-2}\%$ and $6.10\times10^{-3}\%$ for the low and high frequency mode, respectively. The normalized mean square error of $1/Q$ between two methods are 0.684% (low frequency mode) and 0.854%(high frequency mode). The value of $1/Q$ calculated from DeltaE is determined from a pole-zero analysis of the frequency response. The value of Q so determined is sensitive to the bandwidth and weighting used in the fit. The error bar attached to the $\Delta T = 200$ K data point indicates the uncertainty and accounts for most of the disagreement at higher values of ΔT. One reason for the dependence of Q on bandwidth is the multimode excitation. A driver was incorporated in the DeltaE program to find the frequency response, from which we obtain the required modal information. The driver locations are selected such that at $\Delta T = 0$ K there is only one mode being excited. However, as ΔT is increased, the mode shapes can be altered and the previous driver position may excite both modes simultaneously. This can be seen in Figs. 2.5 and 2.6 which show the frequency response of the low mode and high mode of the prime mover from DeltaE for three values of ΔT. For higher the ΔT, the effect of high mode excitation is clearly visible as a small bump in the frequency response of the low mode. However, no such bump is observed in the frequency response of the high mode.

Figures 2.7 and 2.8 show the mode shapes for the low frequency mode with $\Delta T = 0$ K and $\Delta T = 100$ K. Figures 2.9 and 2.10 show the mode shapes for high frequency mode with $\Delta T = 0$ K and $\Delta T = 100$ K. In these figures, the solid lines represent the results of the MATLAB program and the open circles represent the results of the DeltaE program. The mode shapes from DeltaE have been normalized to the highest value of the pressure amplitude. The amplitude of the mode shape from the MATLAB program is determined from a least squares fit to the DeltaE results.

It is seen that one of the advantages of the MATLAB program is the smooth mode shape curve. The agreement of the mode shapes are good in general. However the agreement of the low frequency mode is not as good as for the high frequency mode, particularly at high temperature difference. The reasons for this discrepancy at higher values of ΔT are not fully understood. It should be pointed out that the two programs treat the heat exchangers differently. The MATLAB program assumes that the mean gas temperature at the heat exchanger equals the temperature of the heat exchanger. However, DeltaE imposes a thermal impedance so that the gas and heat exchanger temperatures differ.

Figure 2.8 displays one interesting feature. Both program predict a low standing wave ratio. This feature is not present in the high mode.

Although there remain small disagreements between DeltaE and the MATLAB program, the major features are in good agreement. In the chapters to follow, the MATLAB program will be used to analyze the annular prime mover under more realistic conditions. The major difference is that the measured temperature profiles are incorporated in the program.

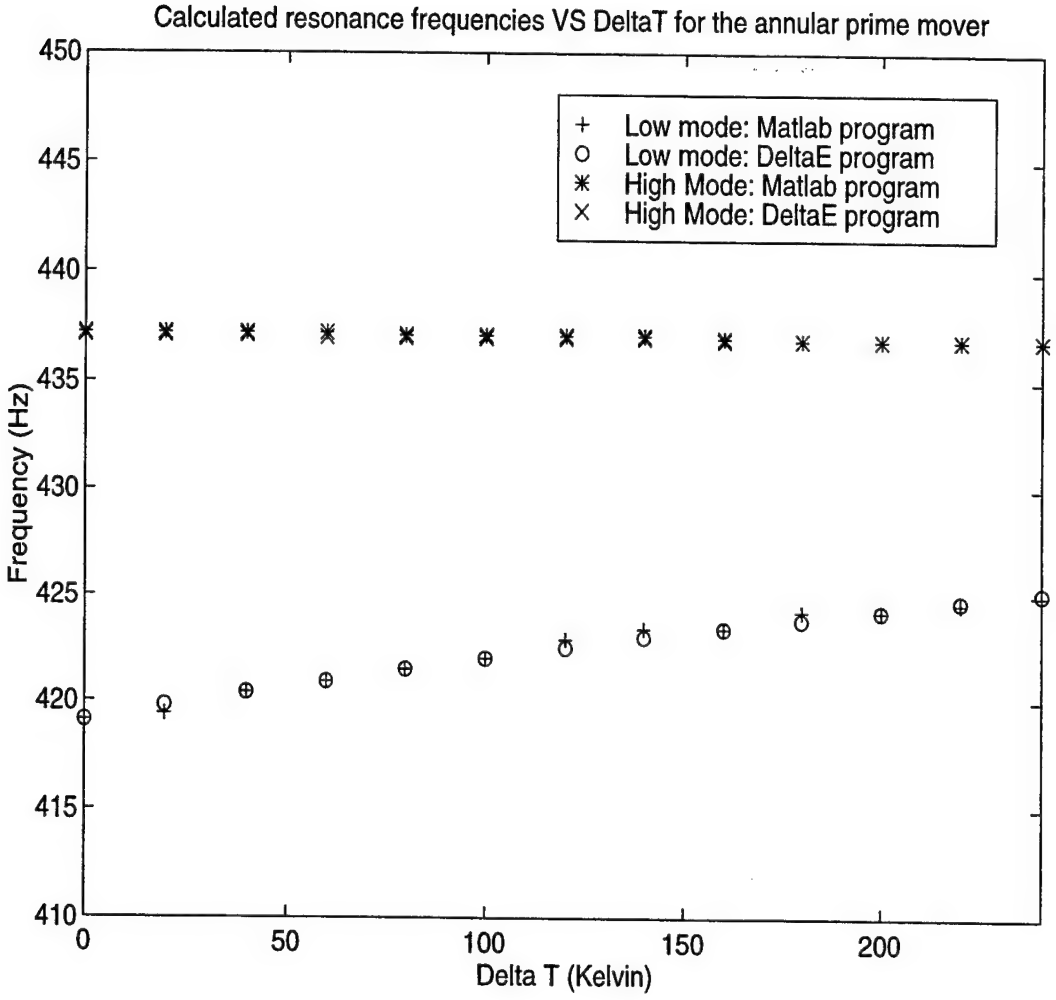

Figure 2.3 Comparison of the calculated resonance frequencies of the annular prime mover as determined from the MATLAB program and DeltaE. Symbols are explained in the legend. Agreement is excellent at all values of ΔT. The normalized mean square error is $1.48\times10^{-2}\%$ for the low mode and $6.10\times10^{-3}\%$ for the high mode.

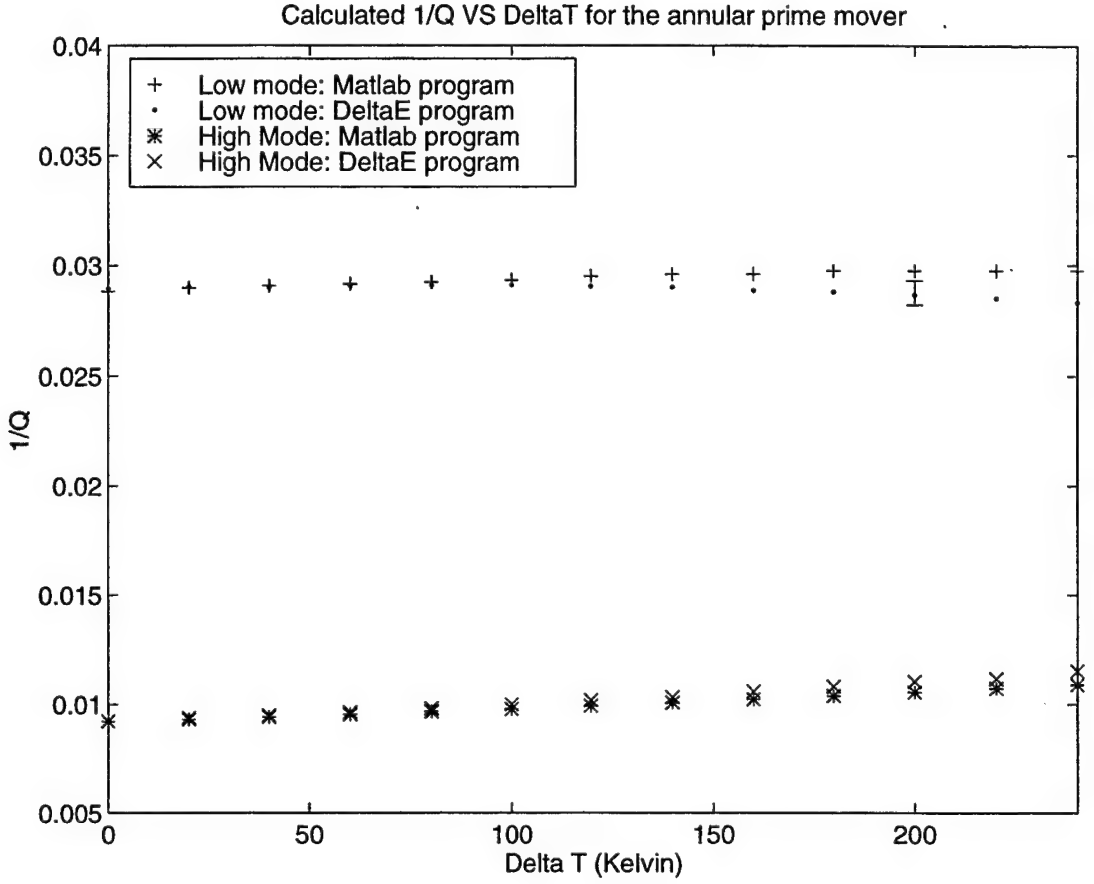

Figure 2.4 Comparison of $1/Q$ of the prime mover vs. ΔT as determined from the MATLAB and DeltaE. An error bar is indicated for the low mode at $\Delta T = 200$ K. Because of modal overlap, determination of $1/Q$ in DeltaE is not without uncertainty. Agreement is better at low ΔT. The normalized mean square error is 0.684% for the low mode and 0.854% for the high mode.

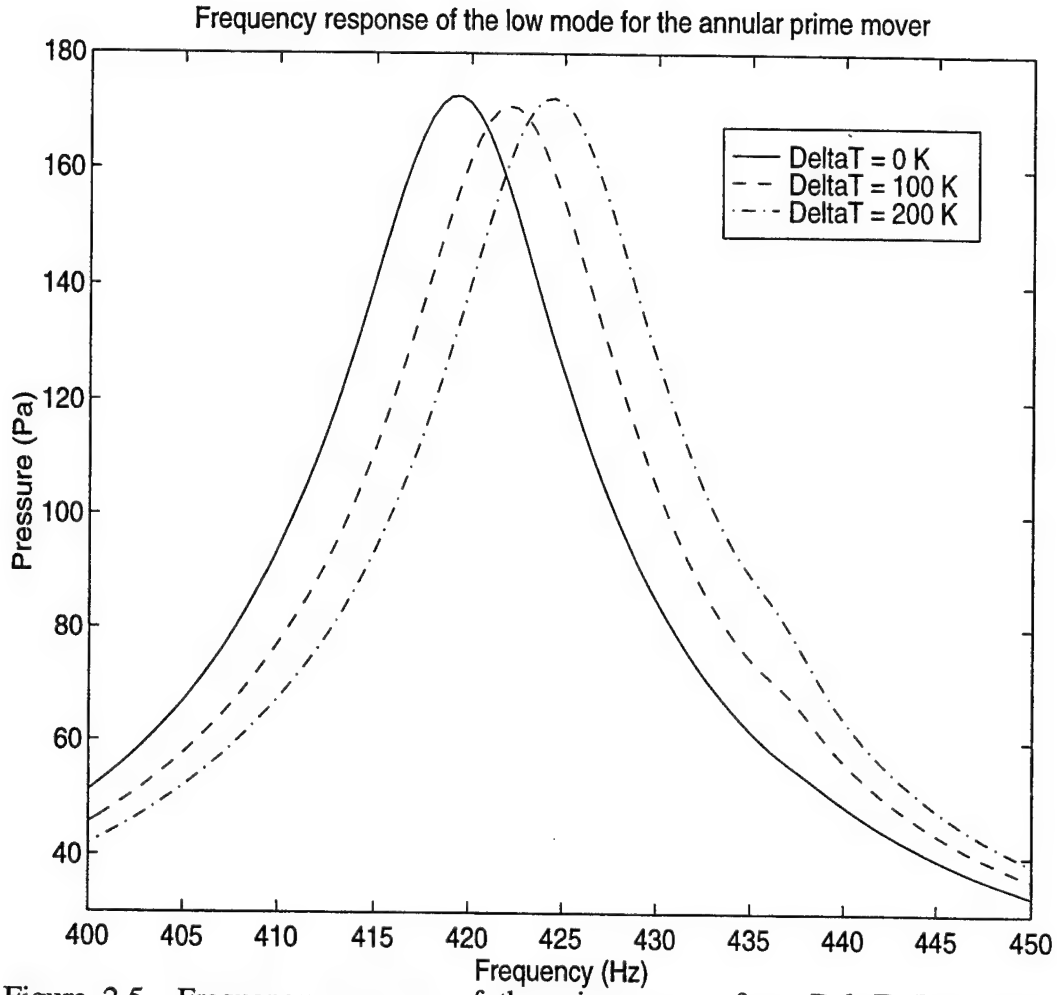

Figure 2.5 Frequency response of the prime mover from DeltaE (low mode) at $\Delta T = 0$ K, 100 K and 200 K. Note the small bump at about 436 Hz on $\Delta T = 100$ K and 200K curves which is a result of mode overlap.

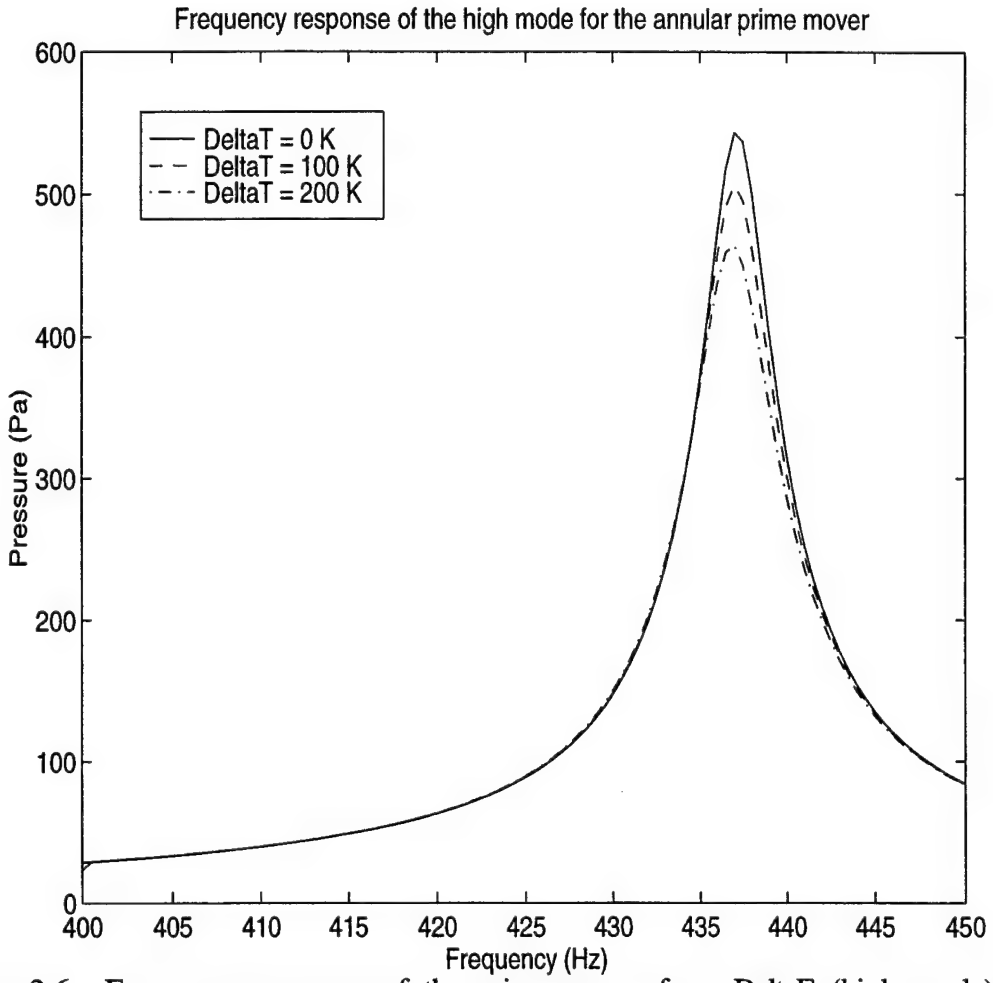

Figure 2.6 Frequency response of the prime mover from DeltaE (high mode) at $\Delta T = 0$ K, 100 K and 200 K. Notice that there is no visible bump from overlap.

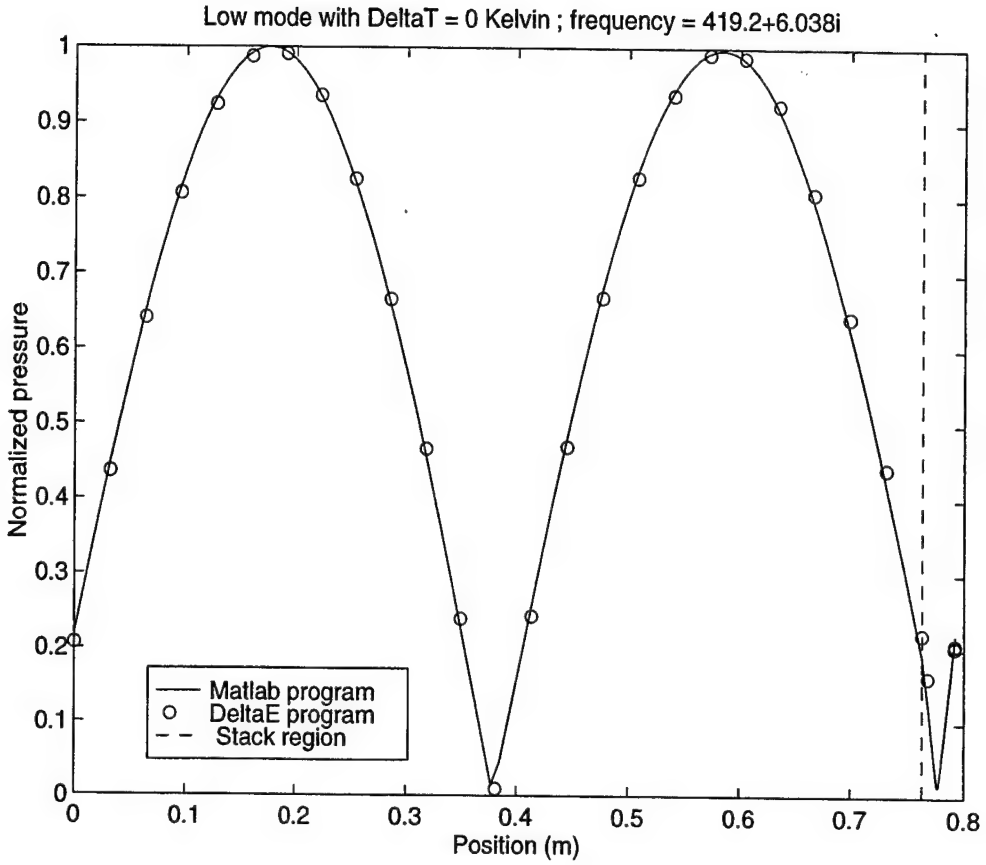

Figure 2.7 Comparison of mode shapes of the prime mover at $\Delta T = 0$ K for the low frequency mode as calculated with the MATLAB program and DeltaE. The beginning of the stack region is indicated by the dashed vertical line.

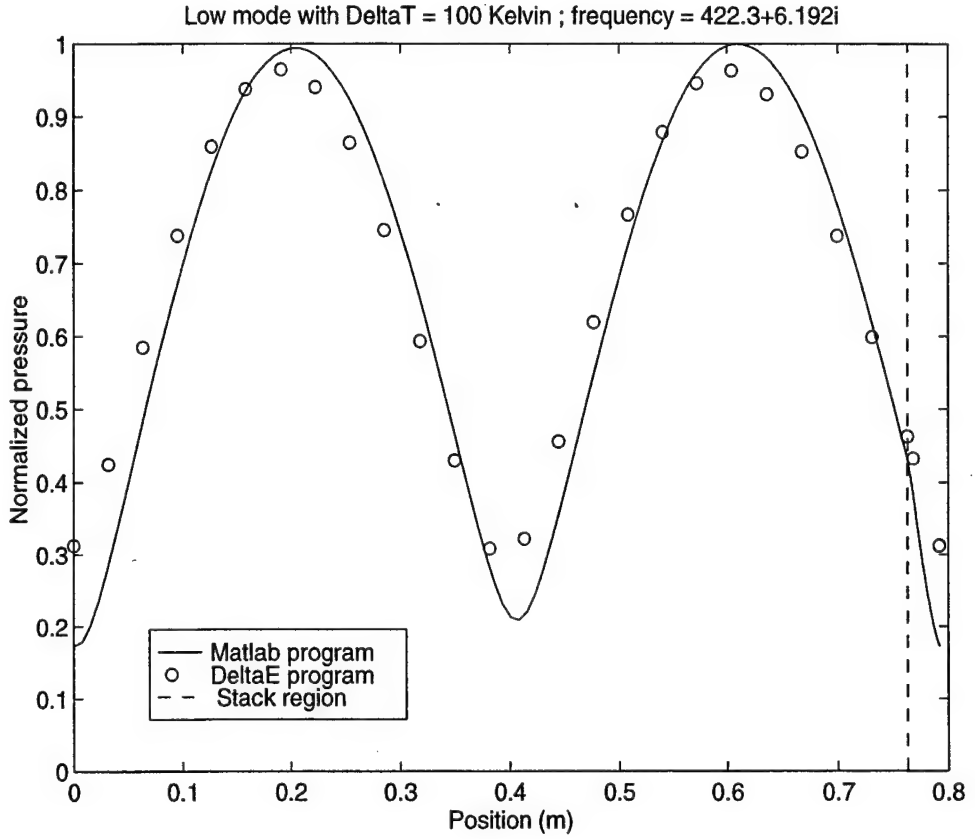

Figure 2.8 Comparison of mode shapes of the prime mover at $\Delta T = 100$ K for the low frequency mode as calculated with the MATLAB program and DeltaE. Although both programs predict the same general mode shape, the agreement is not as good at $\Delta T = 0$ K.

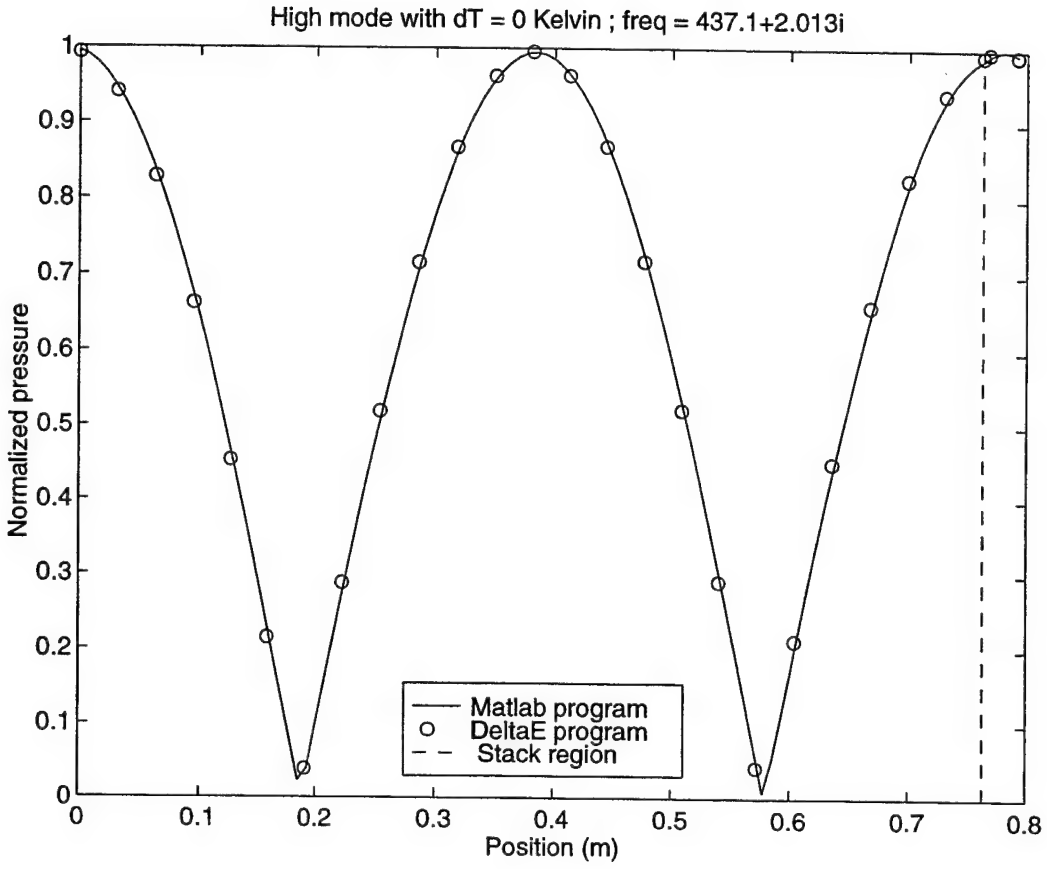

Figure 2.9 Comparison of mode shapes of the prime mover at $\Delta T = 0$ K for the high frequency mode as calculated with the MATLAB program and DeltaE.

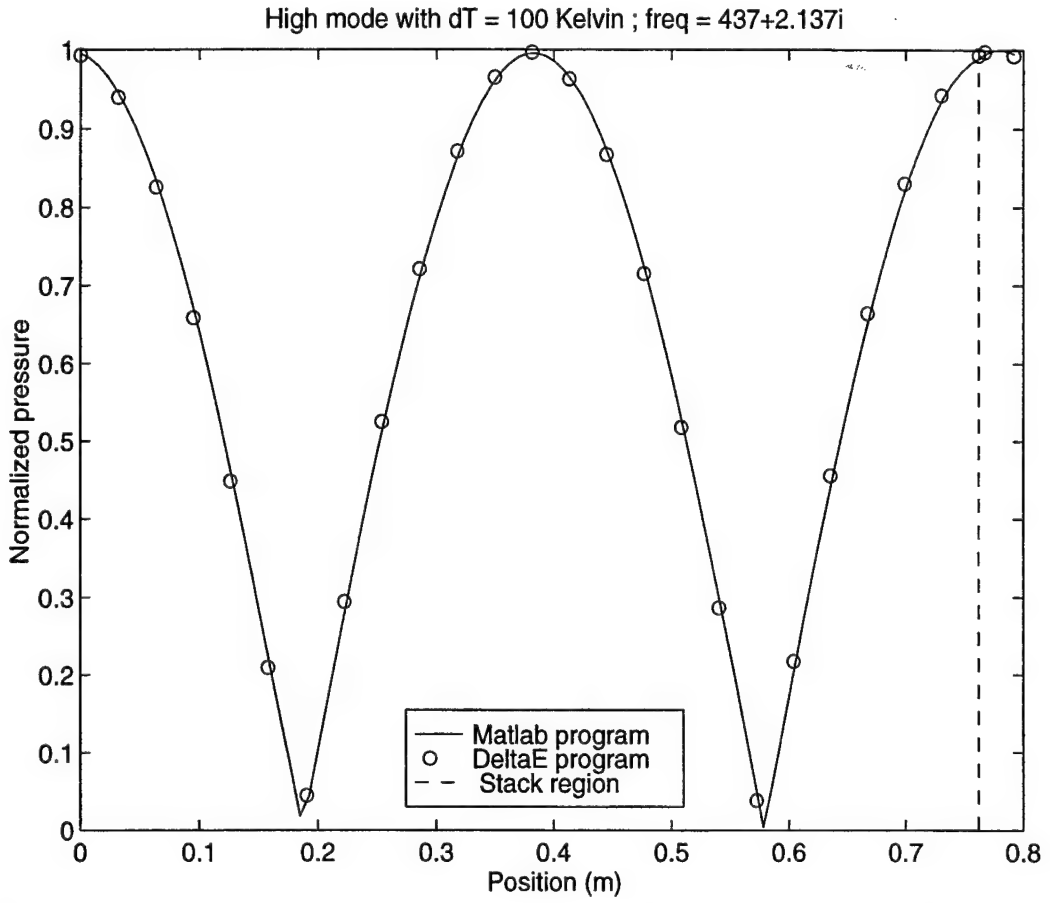

Figure 2.10 Comparison of mode shapes of the prime mover at $\Delta T = 100$ K for the high frequency mode as calculated with the MATLAB program and DeltaE. The agreement is much better than for the low mode at $\Delta T = 100$ K.

E. END EFFECTS

The usual boundary conditions applied to a change in cross section are continuity of pressure and volume velocity. However, at the discontinuity an additional acoustic impedance is introduced owing to the abrupt change of cross sectional area (Miles, 1946 and 1947; Karal, 1953; Pierce, 1991). As a matter of fact, we have shown (Choe, 1997) that it is critical to take into account end corrections at the constriction to get good agreement between the measured and predicted resonance frequency and mode shapes for a constricted annular resonator.

Sudden changes in duct cross section produce sudden changes in acoustic pressure amplitude. Below cutoff, the effect is equivalent to a lumped-parameter impedance. For example, a constriction in a duct gives rise to a concentration of flow through the constriction that consequently increases the kinetic energy density. As is discussed by Morse and Ingard (1968), if the net increase is concentrated in a region small compared to a wavelength, the total increase can be characterized by a lumped acoustic inductance. If the constriction also produces an increase in viscous energy loss, this addition can be modeled as a lumped acoustic resistance.

This equivalent lumped impedance can be obtained from various methods. Only two methods, the conformal transformation method and the higher order mode method, are discussed here.

After computing the analogous acoustical impedance Z, the boundary condition for the pressure becomes.

$$p_2(l) = p_1(l) - Z * U_1(l), \tag{2.40}$$

where p_1 is the pressure in the unconstricted region and p_2 is the pressure in the constriction. U_1 is the volume velocity in the unconstricted region and the constriction junction is at $x = l$. The volume velocity boundary condition is unchanged.

1. Conformal Transformation Method

The first method used to compute the lumped impedance introduced by a constriction is discussed by Morse and Ingard (1968). To obtain the analogous impedance of a constriction, they compute the extra kinetic energy and viscous-energy loss produced by steady flow through the constriction. To find the steady-state flow, the interior of the half-duct is first transformed to the upper half of a complex w plane by the Schwartz-Christoffel transformation. Next, depending on the geometry of a specific problem, a further transformation is required to go from the w plane to the velocity-potential plane in which the lumped impedance can be readily obtained.

Morse and Ingard applied this technique to the case of a rectangular duct of depth d and width b for $x < 0$ and a for $x > 0$ (as shown in Fig. 2.11). The lumped-circuit inductance and resistance corresponding to the sudden increase in the cross section of a rectangular duct are

$$L_a = \frac{\rho}{\pi d}\left[\frac{(a-b)^2}{2ab}\ln\frac{a+b}{a-b} + \ln\frac{(a+b)^2}{4ab}\right], \tag{2.41}$$

and

$$R_a = \frac{\rho\omega\delta_v}{2ad}\frac{a-b}{b}\left(1 + \frac{a^2-b^2}{\pi ab}\ln\frac{a+b}{a-b}\right). \tag{2.42}$$

Notice that both L_a and R_a vanish when $a = b$ (i.e., when there is no change in width).

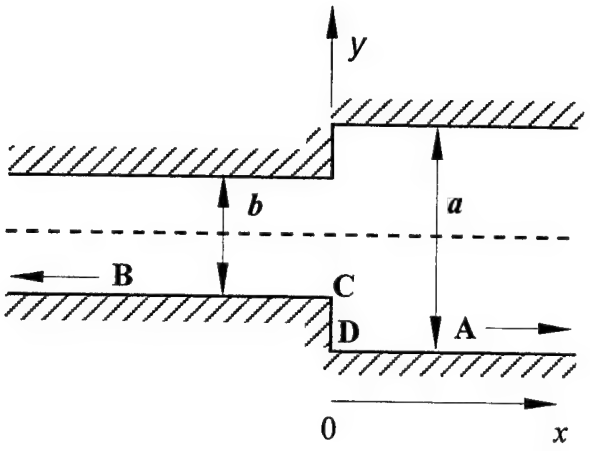

Figure 2.11 Section of a rectangular duct with sudden change of width in the y direction.

2. Higher Order Mode Method

This method involves including higher order modes near the constriction ends (Muehleisen, 1996). In this work, Muehleisen examines the reflection, transmission, radiation, and coupling of higher order modes at a discontinuity in finite length rigid wall rectangular ducts. Using a method of generalized scattering coefficients, an analytic expression for the reflection and transmission of higher modes at size discontinuities is developed.

From the scattering matrix formulation an expression for the lumped acoustic impedance can be found (Muehleisen, 1997). This method does not include losses, however, and so the resistance obtained by conformal mapping is added to the impedance.

III. EXPERIMENTAL APPARATUS AND PROCEDURE

A. INTRODUCTION

Descriptions of the experimental apparatus and data acquisition procedure are presented in this chapter. The chapter begins with a discussion of the annular resonator. This resonator was used in preliminary work to measure the modal properties of a constricted annular resonator in the absence of a stack (Choe, 1997). This discussion is followed by a detailed description of the annular prime mover. Next, the constricted annular prime mover is discussed, followed by a description of how the prime mover is instrumented with microphones and thermocouples. The calibration of the microphones is discussed in this subsection as well. The chapter concludes with a description of the procedure followed during data acquisition.

B. EXPERIMENTAL APPARATUS

1. Annular Resonator System

The annular resonator, shown in Fig. 3.1 (without the top) and Fig. 3.2 (with the top) has been used in a preliminary work to investigate the modal properties of a constricted annular resonator (Choe, 1997). The inner and outer radius of the resonator is 10.00 ± 0.01 cm and 15.30 ± 0.01 cm, respectively. The outer side wall is a 1 cm thick aluminum ring with 15.30 ± 0.01 cm inner radius. A solid aluminum 10 cm radius cylinder that is concentric with the outer ring forms the inner side wall. The height of the resonator is 5.00 ± 0.01 cm. The dimensions of the resonator were chosen to give a

longitudinal resonance frequency in the 300 to 500 Hz range, which is well below the cutoff frequency for the first cross mode, as discussed in Chapter II.

Since the prime mover will be operated at temperatures over 200 °C, the plexi-glass top described in Choe has been replaced by a 0.64 ± 0.01 cm thick aluminum top with a radius of 16.01 ± 0.01 cm. The top is bolted with a 10.7 cm long threaded rod at the center and three equally-spaced 7.1 cm long clamp bars on the edges. Ten microphones are installed in the top to measure the spatial pressure distribution inside the driven resonator below onset and observe the behavior of the sound generated above onset. To monitor the temperatures in the resonator, 5 type-E thermocouples are installed through the top and another 5 type-E thermocouples are installed in the stack/heat exchanger assembly. A detailed description of the microphone and thermocouple installation will be presented later in this chapter.

It is very difficult to move the stack and heat exchanger assembly after it has been put into the resonator because of the complex wiring and the fragility of the glass components. Therefore, three holes (3.50 mm diameter) were drilled in the bottom of the resonator to allow the driver location to be moved relative to the stack. Depending on which mode is to be excited, the driver was then connected to the desired hole via a 0.4 cm O.D., 3.5 cm long plastic tube. The two unused holes were plugged with thumbtacks that had some Dow Corning high vacuum grease applied to the tips.

To ensure tight sealing for a high Q, a thin layer of Dow Corning high vacuum grease was applied to the surface of the aluminum ring and the center piece before the top was put on and bolted down. In addition to the bolt in the center and the three clamps mentioned earlier, 6 extra equally spaced clamp bars are applied around the edge of the top to ensure a tight seal.

The instrumentation is shown in Fig. 3.3. The acoustic signal is generated by a 40W, 16 Ω external compression driver. The output of a Hewlett Packard 3562A dynamic signal analyzer was sent through a Techron 5507 power amplifier to the driver. The signal analyzer was used to determine the frequency response of the resonator. Typically, the resonator was driven with a random noise source of 1 Vrms source level. The pole-zero analysis function built into the signal analyzer was then used to determine the Q and the resonance frequency. To measure the mode shape, the source of the analyzer was changed to a 1Vrms fixed sinusoidal signal at the resonance frequency found in the previous measurement.

2. Stack Assembly

The prime mover stack assembly consists of the stack plates and the stack holder. The first challenge was to select a suitable material for stack. The stack needed to withstand high temperatures and the differential expansion imposed upon it from the high gradients. Glass has a low thermal conductivity in comparison to most metals (Johanson Companies, 1996) and is able to withstand higher temperatures than most plastics and other polymers. An AF-45 thin borosilicate glass slide (made by Precision Glass & Optics) was chosen to be the material for stack. Some properties of this AF-45 glass are provided in Appendix D. AF-45 is a modified borosilicate glass with a high content of BaO and Al_2O_3 and features a low thermal conductivity and a low coefficient of thermal expansion of $45.0 \times 10^{-7} K^{-1}$ (20~300° C). The glass was accurately cut to a size of: 43.65+/-0.05 mm wide and 23.90+/-0.10 mm long and is 0.145+/-0.02 mm thick.

The stack holder (detailed dimensions of which are given in Appendix E) consists of two horizontal bars (5.28 cm long) connected to two vertical bars (4.85 cm long) as shown

in Fig. 3.4. Tongue-and-groove joints are machined in the ends of the bars to ensure that they form a sturdy frame. Sixty-one 0.508 mm deep, 0.203 mm wide, equally-spaced slits were cut in the inside of each of the two horizontal bars. The center-to-center spacing between the slits is 0.762 mm. The gaps between the cover glass plates are 0.610 mm. After the stack holder was assembled, 61 glass slides were then carefully inserted into the slits. The overall porosity for the prime mover stack assembly, including the frame, is approximately 0.61.

3. Ambient Heat Exchanger Assembly

The ambient heat exchanger is used to remove heat from the stack and to maintain one end of the stack close to ambient temperature. The ambient heat exchanger assembly is constructed as shown in Fig. 3.5 and the detailed dimensions are given in Appendix E. The heat exchanger is designed to ensure that the temperature difference between the center and the edge of the heat exchanger is less than one degree C for a 35 W load. The ambient heat exchanger holder was made in the same way as the stack holder, except that it uses copper instead of aluminum and has only 10 slits. Also, a central bar was incorporated to supplement the heat transfer between the heat exchanger and the resonator body. The slits are 0.635 mm deep, 0.711 mm wide, and equally spaced at 4.064 mm (center to center). After the holder was made, twenty Alloy-100, 2.30 mm long, 5.10 mm wide, and 0.68 mm thick copper fins were cut and soft-soldered into the slits (10 on either side of the central bar). The overall porosity for the ambient heat exchanger is 0.62 (including the frame). The next step was to soft-solder a 5.256 cm $\times$ 4.977 cm rectangular copper woven wire cloth (20 $\times$ 20 mesh) on one side of the heat exchanger assembly. The function of

this wire cloth is to increase the thermal contact between the prime mover stack and the ambient heat exchanger.

The fin spacing is much larger than would be used in a practical prime mover. The acoustical properties of an constricted annular resonator are very sensitive to both the porosity and flow impedance of the constriction. It was decided to make the flow impedance of the heat exchangers small compared to that of the stack. This choice necessitated using large fin spacing, which reduced the effectiveness of the heat exchanger.

4. Hot Heat Exchanger Assembly

The function of the hot heat exchanger is to supply heat to the stack. It consists of nickel-chromium wire woven on a non-conducting frame. Since nickel-chromium wire is used to provide heat to the system, the hot heat exchanger has to provide electrical insulation to the aluminum resonator. Because of the need for electrical insulation and high temperature operation, virgin electrical grade PTFE (Teflon) is chosen for the hot heat exchanger frame. The hot heat exchanger assembly is shown in Fig. 3.6. Drawings of fabricated parts are provided in Appendix E. The Teflon frame has outer dimensions of 4.978 cm wide, 5.283 cm high, and 0.813 cm thick. The inside of this frame was milled out to a size of 4.470 cm wide and 4.663 cm high. Seventeen holes are drilled onto the two vertical sides with an equal spacing of 0.521 cm (8 on one side and 9 on the other side). Into each of the holes is inserted a 0-80 stainless steel screw. A 92.1 cm, # 28 gage nickel-chromium wire with a total resistance of 12 Ω was wound around the 17, 0-80 screws. To avoid direct contact between the nickel-chromium wire and the stack, stainless steel flat washers are used on the screws for spacers. The ends of the nickel-chromium wire are wrapped with heat shrinkable flexible PVC tubing to insulate the wire from the

resonator. The wire is then fed through Teflon tubing which is placed and epoxied in the bottom wall of the resonator.

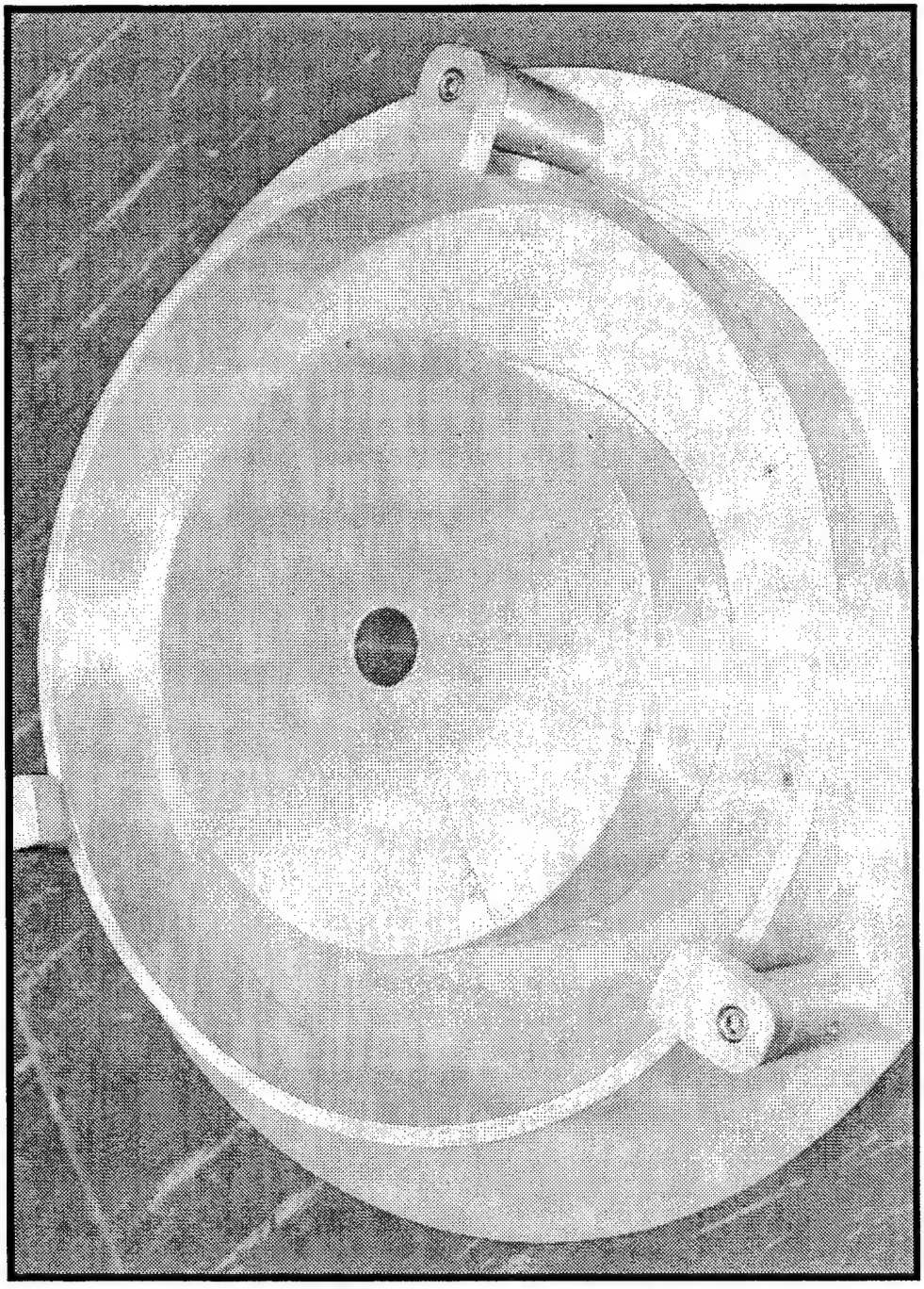

Figure 3.1 The annular resonator (without the top).

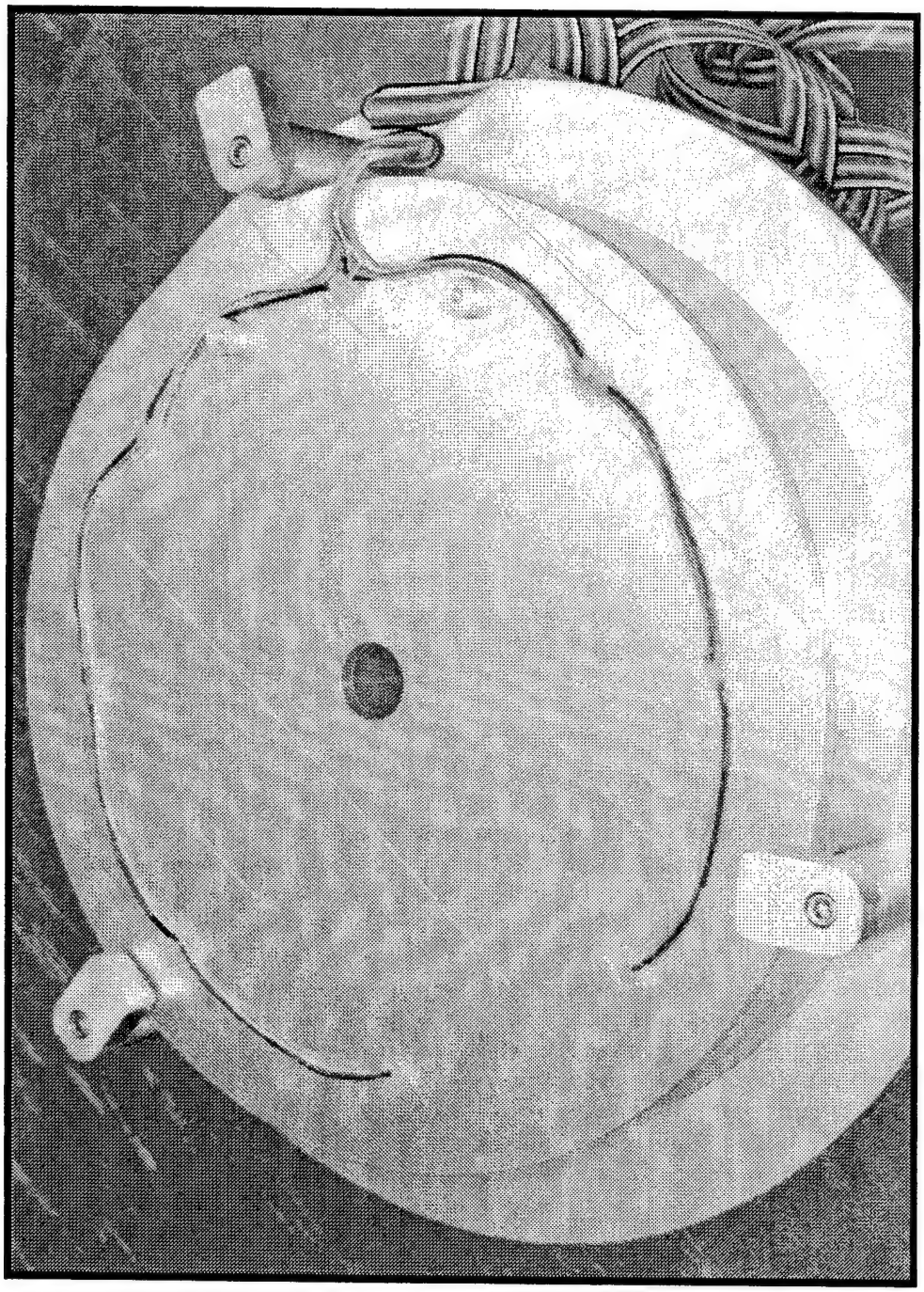

Figure 3.2 The annular resonator (with the top).

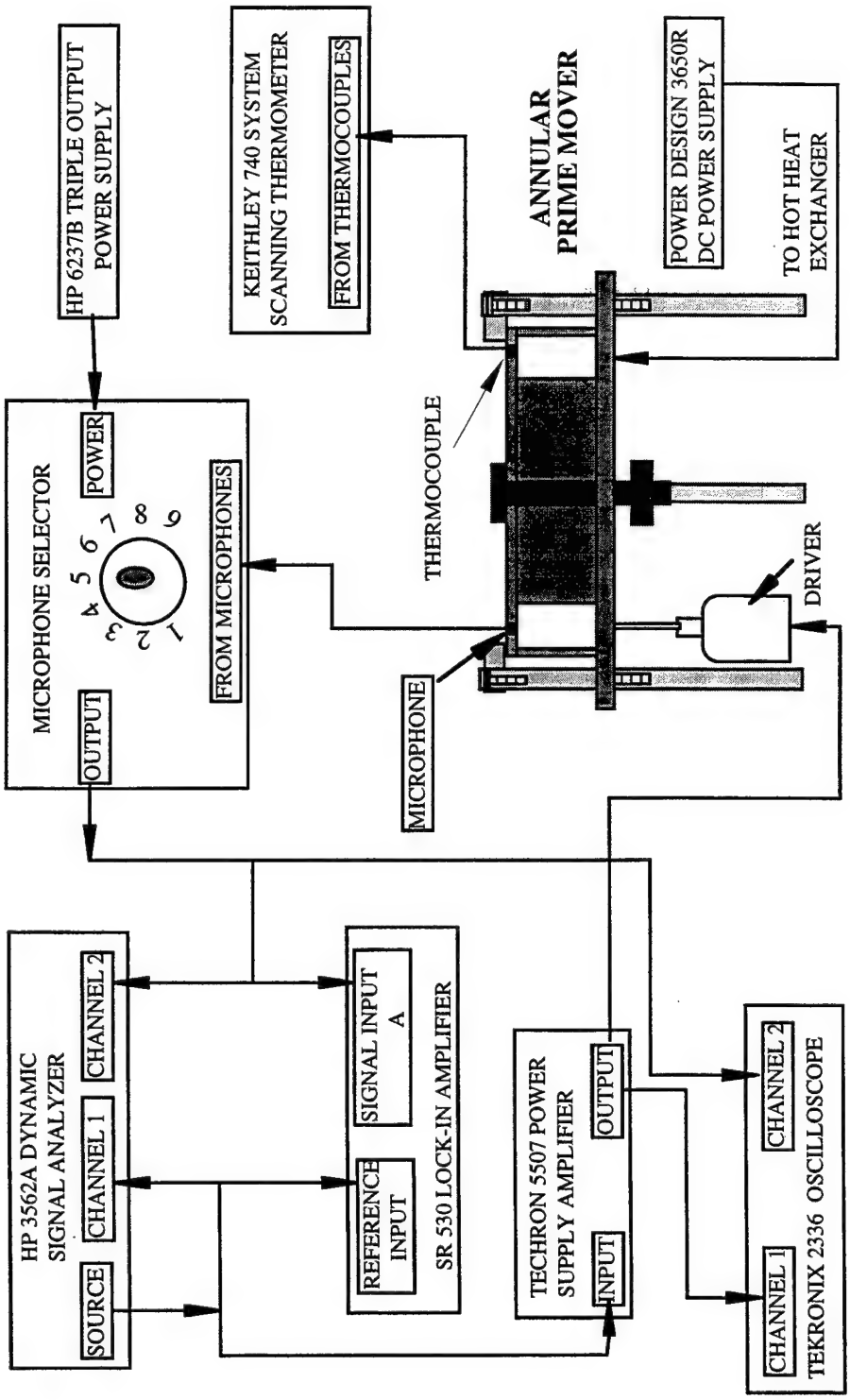

Figure 3.3 Block Diagram of Instrumentation Setup.

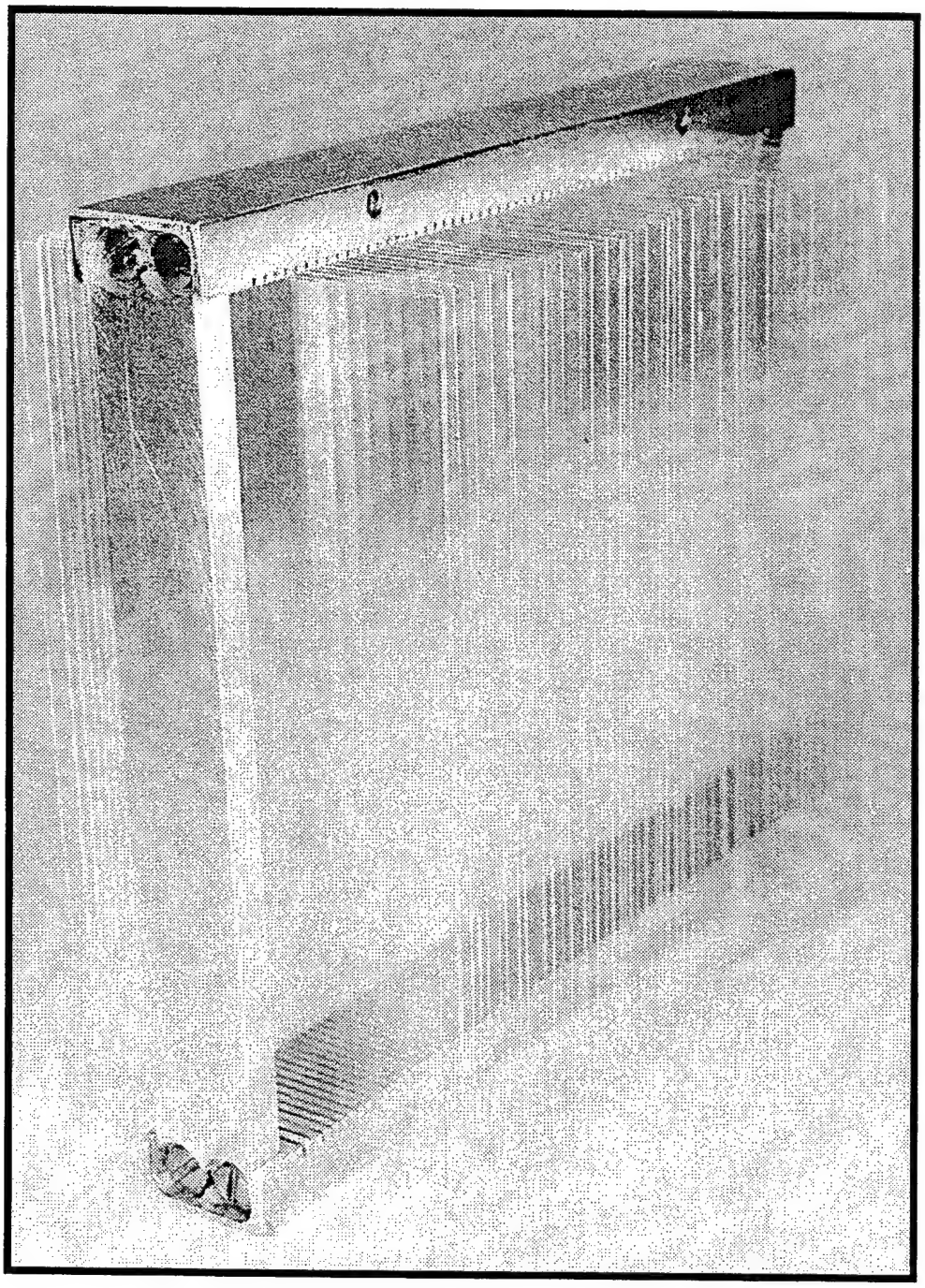

Figure 3.4 The prime mover stack assembly.

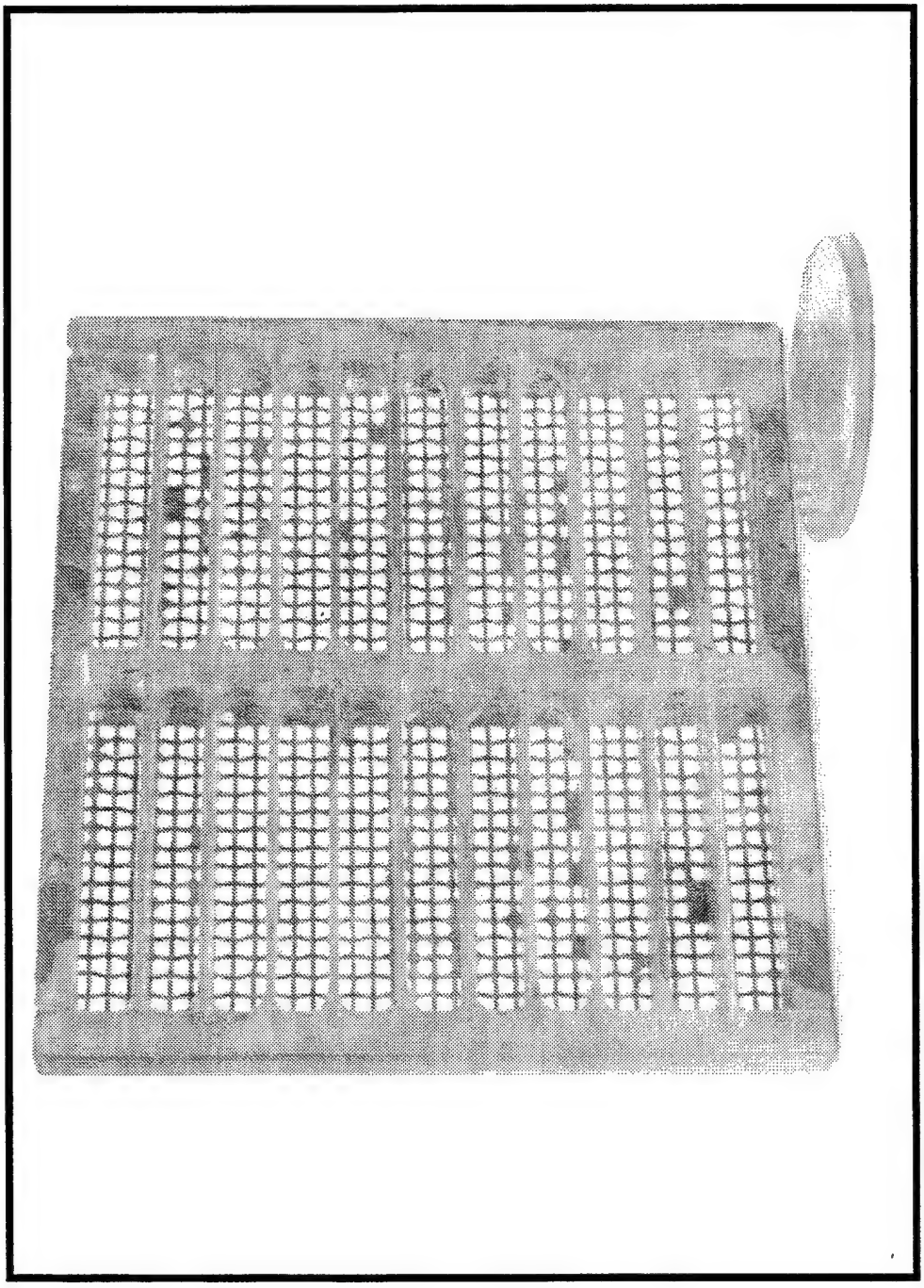

Figure 3.5 The ambient heat exchanger assembly.

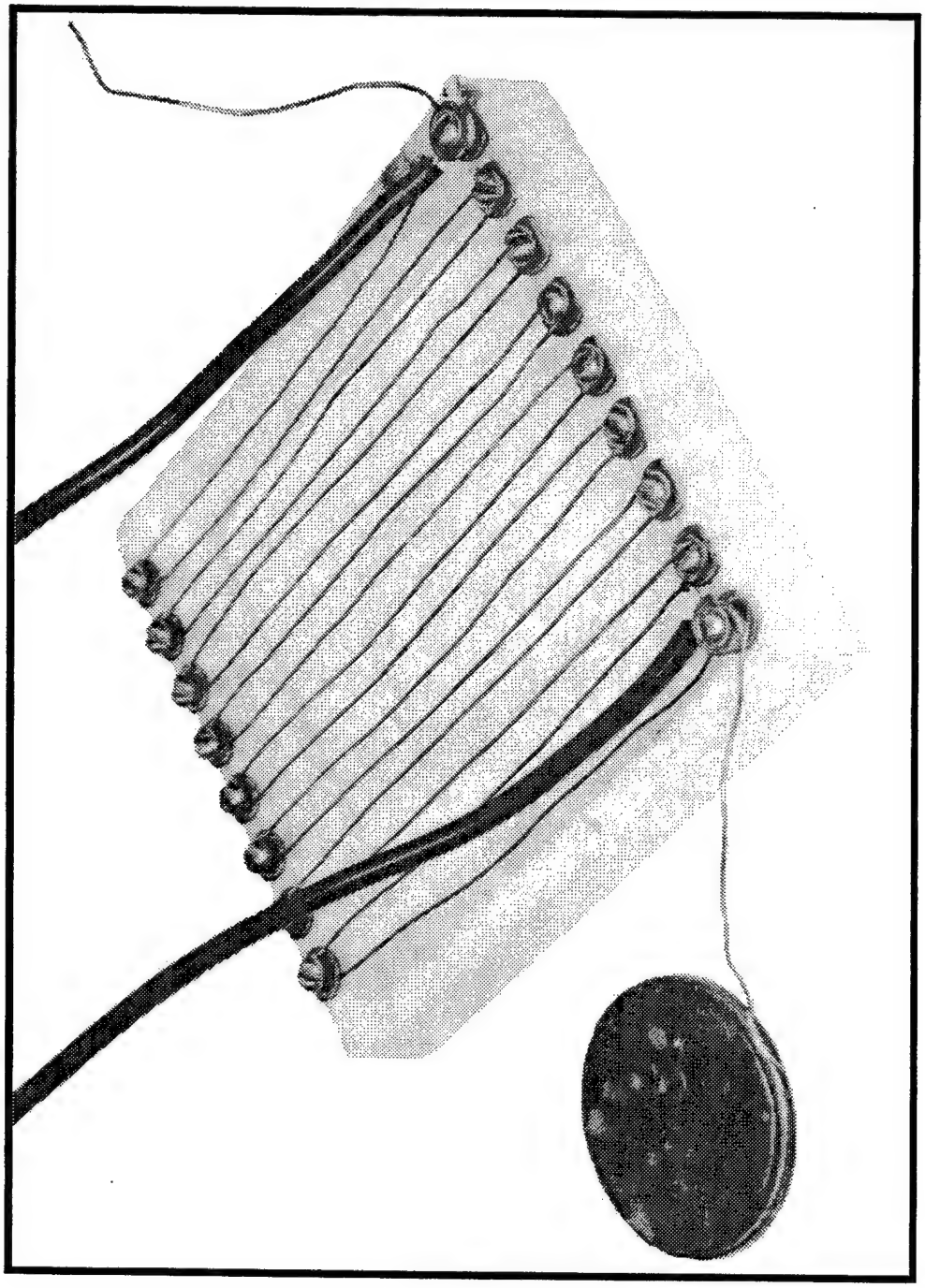

Figure 3.6 The hot heat exchanger assembly.

5. Stack/Heat Exchanger Assembly

The stack assembly, the ambient heat exchanger assembly, and the hot heat exchanger assembly were connected with four 5.08 cm long, 00-90 stainless steel threaded rods on the two horizontal sides (as shown in Fig. 3.7). Teflon spacers were used to ensure proper spacing between the stack and the heat exchangers. The spacing between the glass plate and the nickel-chromium wire is approximate 1 mm. Before the stack/heat exchanger assembly was placed into the resonator, a piece of thin Teflon tape was wrapped on the side of the hot heat exchanger to avoid electrical short circuit. A thin layer of silicone heat sink compound was applied to the side of the ambient heat exchanger frame to supplement the heat transfer between the ambient heat exchanger and the resonator wall and to seal any gaps between the frame and the resonator.

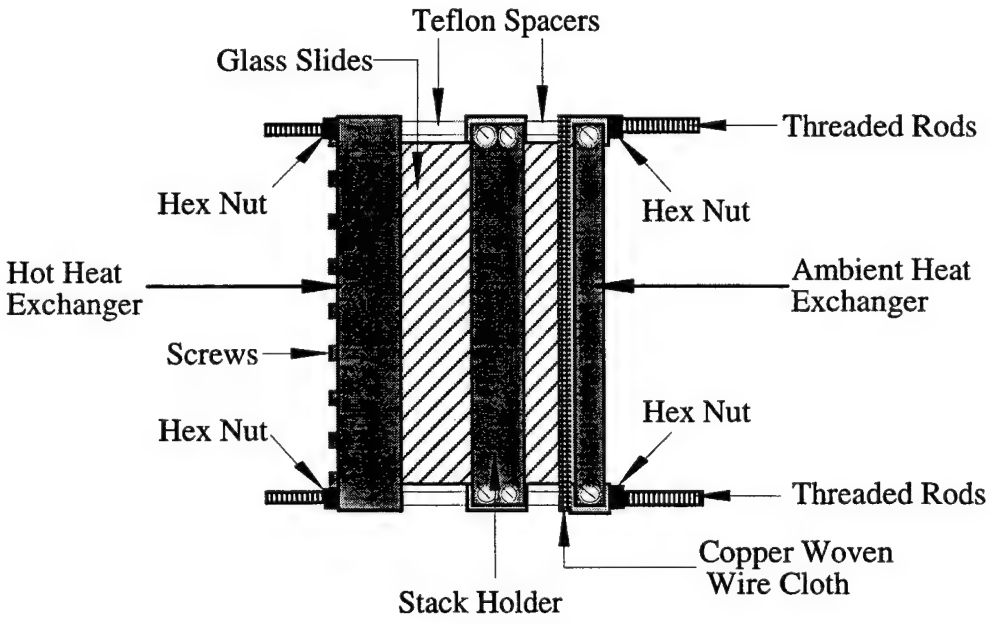

Figure 3.7 The stack/heat exchanger assembly.

6. Constriction

Placing another constriction in the resonator provides the possibility for an annular prime mover to reach onset. Such constrictions were previously used in related work by Choe (Choe, 1997). The constrictions are made of PVC (Ployvinylchloride) because of its rigidity and ease of fabrication. The area ratio is defined by the ratio of open area in the constriction (which is the shaded block in Fig. 3.8) to the cross-sectional area of the resonator. In Fig. 3.8, S_1 stands for the open area and S_2 stands for the open cross-sectional area of the constriction. The table in Figure 3.8 gives the geometrical parameters of the constrictions. Constrictions were used having area ratios of 0.7, 0.3 and 0.1 with a total length of 45°. The 45° length was achieved by stacking two 11.25° constrictions and one 22.5° constriction together. Vacuum grease was applied to the joining sides of the individual constrictions to ensure a tight fit.

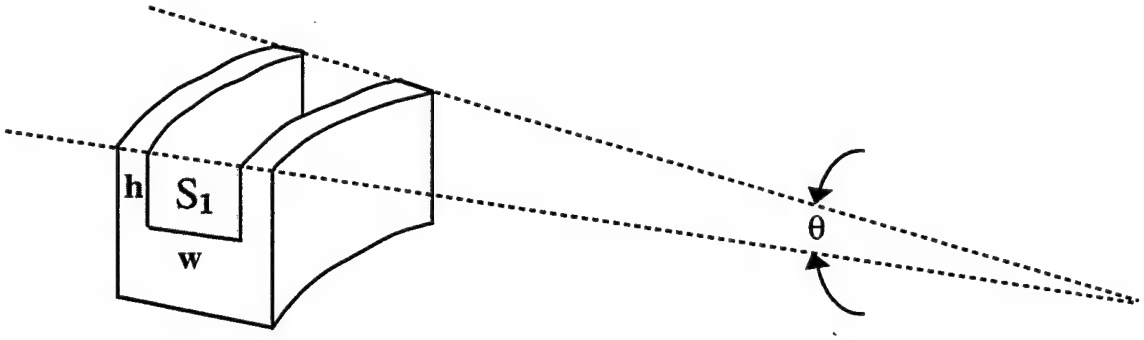

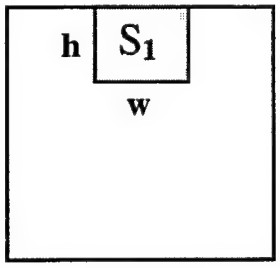

side view

Area ratio = S_1/S_2

$= S_1 / S_2$

unit : inch

θ	area ratio	w	h
22.5°	0.7	1.694	1.694
	0.3	1.109	1.109
	0.1	0.640	0.640
11.25°	0.7	1.694	1.694
	0.3	1.109	1.109
	0.1	0.640	0.640

Figure 3.8(a) Nominal geometry of the constrictions.

θ	S_1 (cm^2)	S_2 (cm^2)	area ratio (S_1/S_2)
22.53° ± 0.06	18.017 ± 0.005	26.447 ± 0.005	0.681 ± 0.005
	7.840 ± 0.005		0.296 ± 0.005
	2.591 ± 0.005		0.098 ± 0.005
11.25° ± 0.05	18.017 ± 0.005	26.447 ± 0.005	0.681 ± 0.005
	7.840 ± 0.005		0.296 ± 0.005
	2.591 ± 0.005		0.098 ± 0.005

Figure 3.8(b) Measured geometry of the constrictions.

7. Microphones

In this experiment, 8 Panasonic electret WM-60AT microphones and two ENDEVCO piezoresistive pressure transducers (Model #8510B-5, Serial # G63T, sensitivity 53.85 mV/psi, and Model #8530C-15, Serial # AGLC2, sensitivity 10.89 mV/psi) are used to measure the pressure distribution inside the resonator. The two ENDEVCO piezoresistive pressure transducers are intended to be used to observe the behavior of the sound generated above onset, in case the Pansonic microphones saturate. The Panasonic microphones are 6 mm in height and 5 mm in diameter, with a sensitivity of -44 dB ± 3 dB re 1 V/Pa. A Hewlett Packard 6237 Triple Output Power Supply provided 9V DC to each Panasonic microphone via a custom made microphone selector.

As shown in Fig. 3.9, the 8 Panasonic microphones were spaced by 45 degrees in pre-drilled holes (0.605 cm in diameter, 0.50 cm deep). They are glued into the holes with

silicone adhesive. At the bottoms of these holes, 0.82 mm diameter holes were drilled to expose the microphones to the resonator cavity. The two ENDEVCO piezoresistive pressure transducers were flush mounted in the cap through spacers with 0.404 cm in diameter threaded holes in the center.

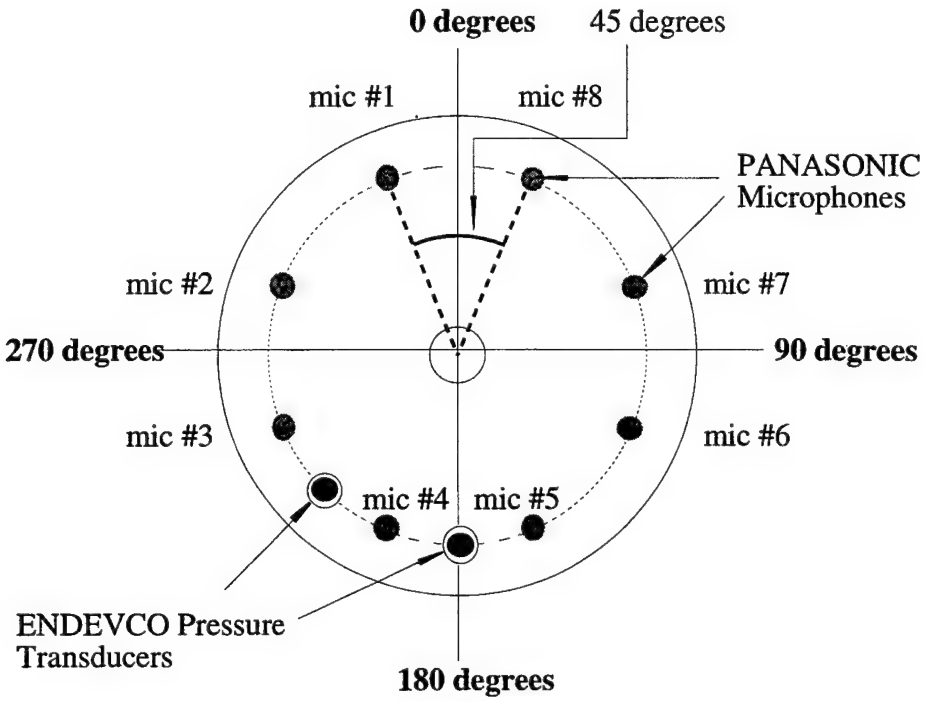

Figure 3.9 Installation of 10 microphones on the resonator top.

Prior to the experiment, the 8 Panasonic microphones were calibrated relative to Microphone # 1. The calibration apparatus is shown in Fig. 3.10. A calibrating chamber was made from a 19.6 mm long, 21.55 mm ID, and 27.22 mm OD circular PVC pipe. A Panasonic micro-speaker (Model #EAS-2P106C) was epoxied into one end of the pipe.

The resonator top was removed and the calibration chamber was positioned over each microphone. A thin layer of Dow Corning high vacuum grease is applied on the edge of the chamber to ensure a tight sealing. The frequency responses were then measured for each microphone over a 300 ~ 500 Hz frequency range using a Hewlett Packard 35665A Dynamic Signal Analyzer. For the calibration, the signal analyzer was set to swept sine mode with a integration time of 20 cycles, a settling time of 20 cycles, and a resolution of 200 pts/sweep.

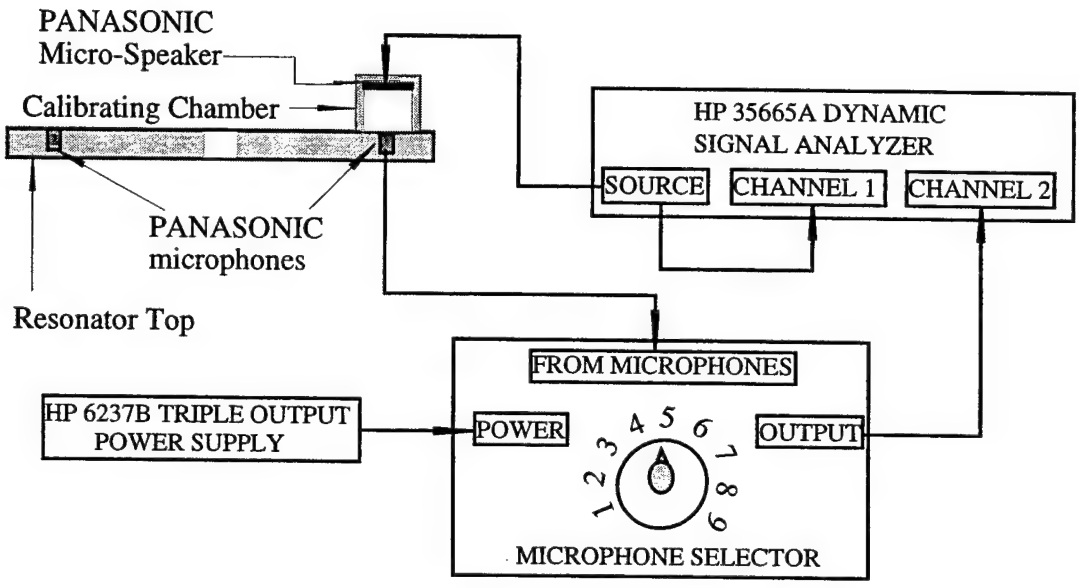

Figure 3.10 Calibration of the Panasonic microphones using a small chamber.

Microphone #1 was selected as the reference for the comparison calibration. The frequency response of microphone #1 when covered by the calibration chamber is shown in Fig. 3.11. Each microphone's frequency response was divided by that of microphone #1 to create a correction factor. A typical curve for the correction factor is shown in Fig.

3.12. After finishing the calibrations, one more measurement was made on Microphone #1 to ensure the reproducibility of the data. With this particular calibration chamber, a difference of less than 1% was achieved. The correction factor for the 8 microphones is usually in the range of 0.75 to 1.75.

When measuring the mode shape, the output from each microphone was divided by the appropriate correction factor to obtain the corrected amplitude at a particular location and driving frequency. A custom made microphone switch board selects each microphone to measure the pressure amplitude at different locations. The microphone output amplitude is measured using a Standford Research 530 Lock-in amplifier.

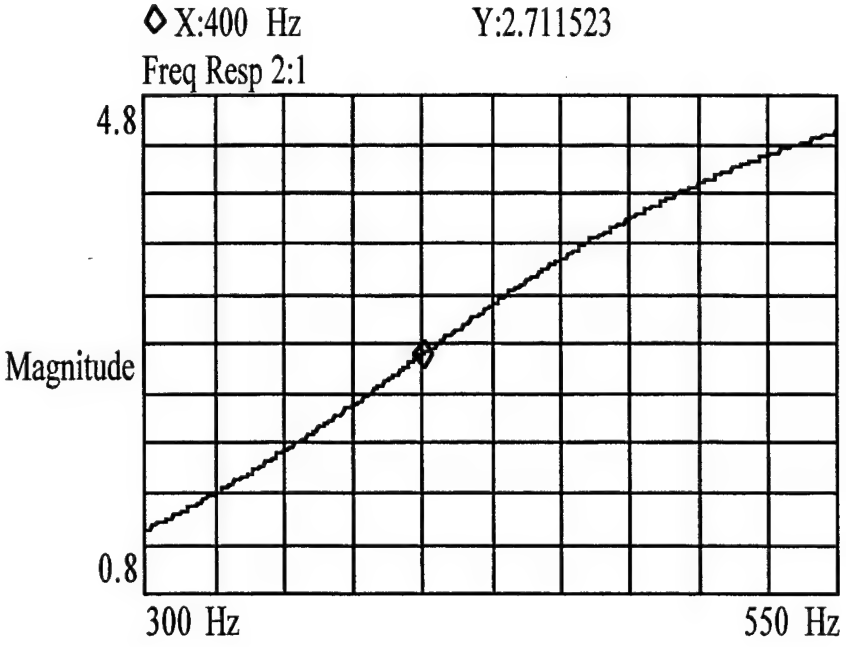

Figure 3.11 Frequency response of microphone #1 when covered by the small calibration chamber.

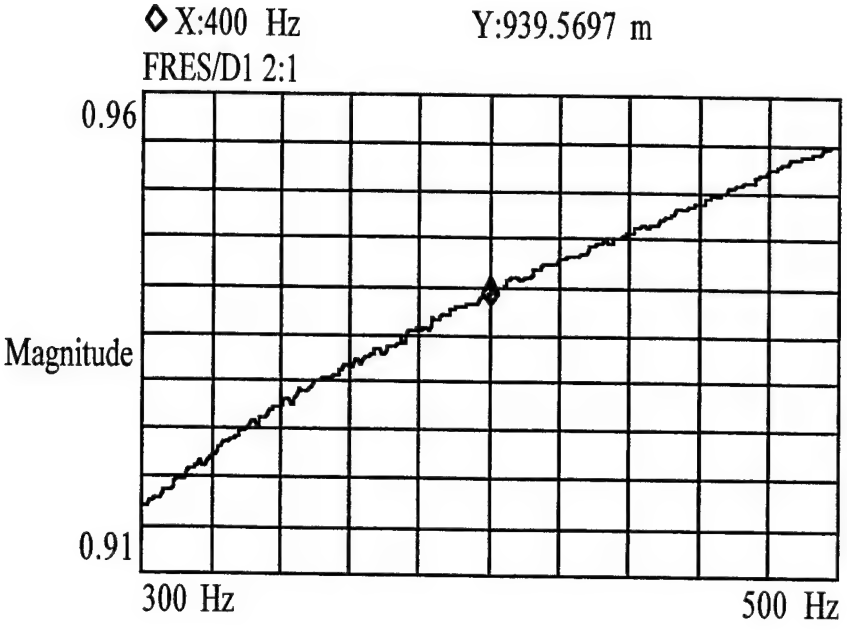

Figure 3.12 Plot of correction factor of microphone #2 referenced to microphone #1. The correction factor at 400 Hz is 0.940.

8. Thermocouple Instrumentation

Ten Omega type E (Model # 5TC-GC-E-30-72) chromel-constantan 0.254 mm diameter glass braid insulated thermocouples are used to monitor the temperatures of the stack, the heat exchanger, and inside the resonator. Type E thermocouples were selected over other types because they provide the greatest sensitivity (in V/°C) and because of their useful temperature range.

As shown in Fig. 3.13, five thermocouples are used to monitor the temperature of the stack and the ambient heat exchanger. Two thermocouples each are placed on the hot and ambient sides of the center glass slide, one in the center and the other at the edge. These thermocouples are fed through 1.4 mm diameter holes on the copper woven wire cloth of

the ambient heat exchanger. Another thermocouple (thermocouple # 6 in Fig. 3.13) was placed on one of the fins of the ambient heat exchanger. The thermocouples were attached to the glass plate using JB weld adhesive because its high temperature capability. The size of the glue spots is approximate 0.01 mm^2. These glue spots are approximate 0.5 mm from the edge the glass plate. The wires of the five thermocouples were individually threaded through 1.4 mm diameter holes in the resonator bottom adjacent to the ambient heat exchanger. The other five thermocouples were used to sense temperature inside the resonator, as is shown in Fig. 3.14. They were fed through 1.4 mm diameter holes in the top and positioned approximately 3 cm inside the resonator. All the holes in the resonator were then filled with BIPAX TRA-BOND epoxy to ensure a tight seal.

The temperature difference across the stack is adjusted by the voltage supplied to the hot heat exchanger which is controlled by a Power Design 3650R DC power supply. The temperatures inside the resonator and in the stack are measured by a Keithley 740 system scanning thermometer.

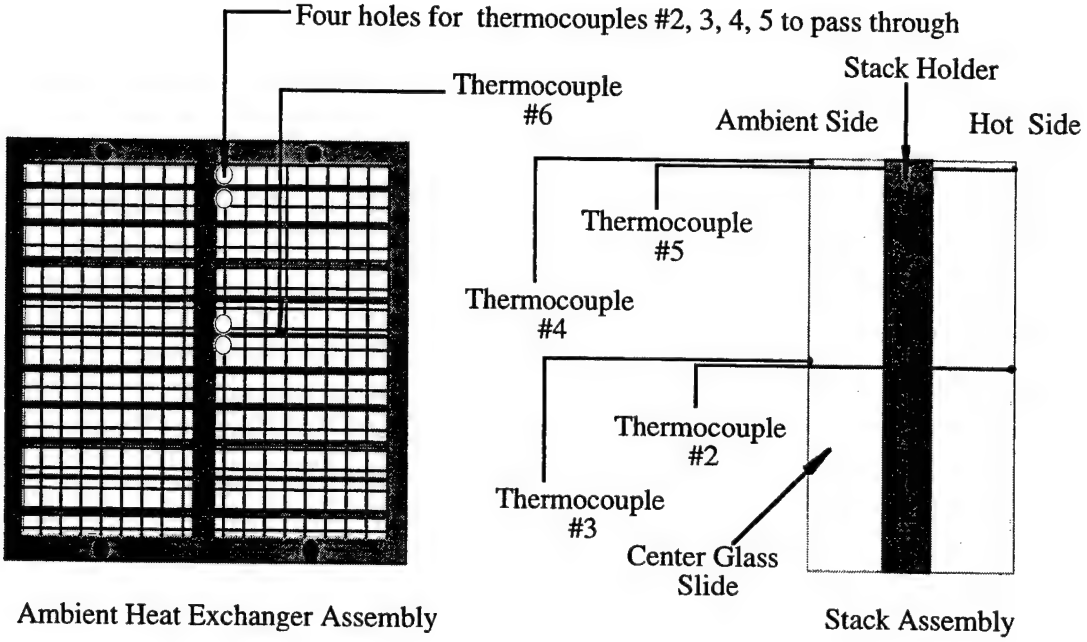

Figure 3.13 Thermocouple placement on the stack and the ambient heat exchanger.

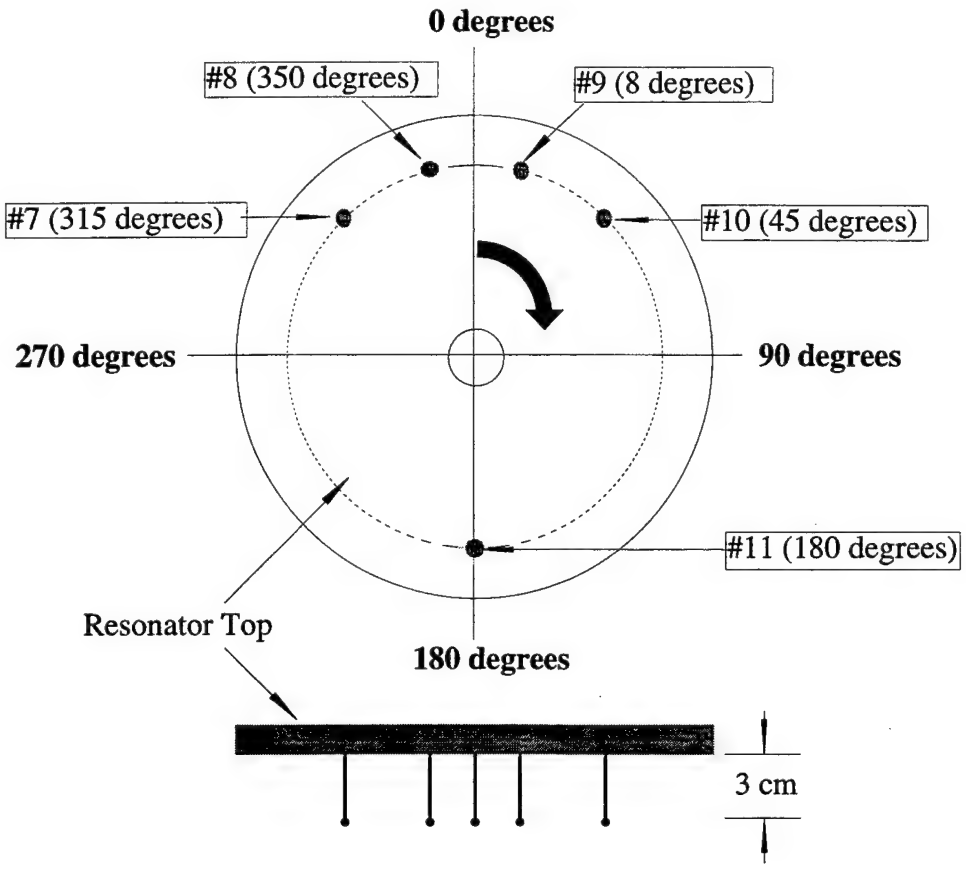

Figure 3.14 Thermocouple placement in the resonator top.

C. EXPERIMENTAL PROCEDURE

1. Resonator Setup

The stack/heat exchanger assembly is placed at a fixed location relative to the microphones and thermocouples. For the experiment, three driver positions are used: 45°, 90°, and 180° from the center line of the stack/heat exchanger assembly. Unused driver holes are plugged with thumbtacks with some vacuum grease applied to the tips. The resonator top is oriented so that 0° is set at the stack assembly center line. The 0° setting is

performed by rotation of the top by hand. To determine the error in positioning the top, the top was positioned five times. It was found that the error by rotation was less than ± 1.0°. So, with the mechanical error ± 0.25° in drilling the microphone holes, the total error of microphone positioning is less than ± 1.25°. With the stack/heat exchanger assembly positioned, the proper amount of vacuum grease is applied on the open surface of the resonator and the top is secured with the clamp bars.

For the measurements with a constriction in the prime mover, a 45° long constriction is inserted at a location that is 90° from the center line of the stack/heat exchanger assembly to the center of constriction.

2. Determining Resonator Characteristics

After the resonator was set, the Hewlett Packard 3562A Dynamic Signal Analyzer is used to characterize the resonator. The swept sine mode of the analyzer provides a sine wave signal to the system at a given range of frequencies. The frequency response of the system is used to determine the resonance frequency and Q of several modes of the resonator. When only one mode is excited, the peak pressure amplitude, frequency, and quality factor are same as the those given by pole-zero analysis. When two modes are excited simultaneously, pole-zero analysis is used to extract the resonance frequency and quality factor. The signal analyzer gives poles in the form $a + j\,b$. The resonance is simply the value of b and the quality factor can be obtained by b/2a. This method has been explained by Choe (1997). These measurements are performed for (1) annular prime mover without a constriction, and (2) annular prime mover with three different constrictions (45° long, porosities of 0.7, 0.3 and 0.1) placed at 90° relative to the center of the stack/heat exchanger assembly. The driver in the first experiment was located at 90°

(to excite the low frequency mode) or 180° (to excite the high frequency mode) from the center of the stack assembly. In experiment (2), the driver was placed at 45° from the center of the stack assembly, between the stack and constriction.

3. Data Collection

Data collection is performed in sets of annular prime mover without and with a constriction. Before data collection, the output of the Hewlett Packard 6237B Triple output power supply is set to DC 9V. The output voltage of the Power Design 3650R power supply is also adjusted to a certain value and the temperature at the hot end of the stack is allowed to reach steady state (temperature variation $\leq 0.1°C/10$ sec). The measurement is commenced by recording the temperatures measured by the Keithley 740 System Scanning thermometer. The resonance frequency and quality factor is measured by the Hewlett Packward 3562A Dynamic Signal Analyzer and the microphone switch board is set to the microphone that provides the maximum output. The procedure used to acquire the resonance frequency and quality factor was described in subsection 1. After finding the resonance frequency, a data run is commenced by changing the source of the Hewlett Packward 3562A Dynamic Signal Analyzer to a 1 V_{pp} fixed sine with a driving frequency equal to the resonance frequency obtained by previous procedure. The acoustic amplitude is measured with each microphone. With the driver running, the switch board selects a particular microphone and the value of amplitude at each position is measured with the Stanford SR530 Lock-In amplifier. The Lock-In amplifier is set to magnitude-phase display mode with a time constant of 1 second. At this time, the temperatures are recorded again and same measurement are repeated again. Before the entire set of experiments is finished, the final temperatures are recorded. Then, the output voltage of the Power Design

3650R power supply is changed to adjust the hot end temperature and the same procedure is followed. All data recorded from the 8 microphones are scaled by the correction factor obtained from the microphone calibration. The corrected data are then entered in a computer program to plot the mode shape. This concludes data acquisition of one mode.

IV. RESULTS AND DISCUSSION

This chapter shows the comparison between theoretical and measured results for two series of experiments on the annular prime mover. First, measured temperatures in the prime mover are presented. Next, results are presented for resonance frequency, $1/Q$ vs. ΔT, and mode shape for the unconstricted annular prime mover. Results for the annular prime mover with a constriction located 90° from the center of the stack/heat exchanger assembly are then discussed. Finally, an analysis of the potential for onset in a two-stack annular prime mover is presented.

A. ANNULAR PRIME MOVER

The measured resonance frequencies and Q's are determined as functions of ΔT from pole-zero analysis of the frequency response. The theoretical resonance frequencies and quality factors are determined from the complex frequency calculated using the measured temperature distribution in the prime mover as an input. Figures 4.1 and 4.2 show the measured temperatures as functions of the heater voltage at four locations on the center plate of the stack for the low mode and high mode of the prime mover.

Figure 4.1 shows that the transverse (center-to-edge) temperature difference on the ambient side of the stack is at most 5.4 K. However, there is a larger transverse temperature profile on the hot side. At the highest heater voltage the hot-side, center-to-edge, temperature difference is 14.8 K. The transverse temperature profile leads to some uncertainty in the value used for ΔT. The effects of a transverse ΔT profile on the performance of a stack is difficult to access. Therefore, the transverse profiles will be used

to place error bars on the ΔT values. Figure 4.2 shows the center-to-edge temperature difference for the high mode. It is seen that the ambient-side temperatures are essentially the same as in Fig. 4.1. However the hot side temperatures show a larger center-to-edge difference than in Fig. 4.1. The difference is attributed to the fact that the resonator top had to be removed to reposition the driver to switch from exciting the low mode to the high mode. It is entirely possible, and observed, that while removing and replacing the top the stack/heat exchanger assembly was disturbed. This could have slightly altered the hot heat exchanger/stack spacing, resulting in the observed differences.

In the results to follow, all the low mode data were taken, then the driver was repositioned and all the high mode data taken. Therefore, the temperatures displayed in Figs. 4.1 and 4.2 should be representative. Typical measured temperature distributions in the prime mover are shown in Figs. 4.3 (the low mode) and 4.4 (the high mode). The measured temperature profile in the duct (0 to 0.792 m) and the ambient heat exchanger temperature are used as inputs into the MATLAB program. The measured hot end stack temperature is a target.

Figure 4.5 shows the comparison of the measured and computed resonance frequency for the low mode and high mode. The driver location is 90° from the center of the stack/heat exchanger assembly for the low frequency mode and 180° for the high frequency mode. It is seen that there is good agreement between the measured and predicted resonance frequencies. The biggest differences between the measured and predicted resonance frequencies are approximately 0.86 % and 1.77 % for the low mode and high mode, respectively.

Figure 4.6 shows $1/Q$ of the low and high mode for the annular prime mover verses the temperature differences across the stack. In general the agreement is good, although there is a tendency to under predict the $1/Q$ (or over predict Q), indicating the presence of

unaccounted losses. For the low mode, $1/Q$ decreases as the temperature difference is increased while for the high mode $1/Q$ increases as the temperature increases. It is evident from these results that the annular prime mover will not reach onset under readily attainable conditions. As a matter of fact, an extrapolation of the $1/Q$ curve for the low mode gives an onset temperature difference of approximately 1400 K.

The larger discrepancies of the resonance frequency and $1/Q$ for the high mode at high temperature gradient can be caused by a misjudging of the stack temperature. In the original calculations, the temperatures of the hot (T_h) and ambient (T_a) sides of the prime mover stack are calculated by a weighted average of the temperatures at the edge and center of either side of the stack

$$T_h = \frac{2T_{hc} + T_{he}}{3} \tag{4.1}$$

and

$$T_a = \frac{2T_{ac} + T_{ae}}{3}, \tag{4.2}$$

where T_{hc} and T_{he} are the center and edge temperature of the hot side of the stack, respectively. T_{ac} and T_{ae} are the center and edge temperature of the ambient side of the stack, respectively. If the simple average of T_h and T_a are used in the computations as opposed to the weighted average, the resonance frequencies are almost unchanged (difference $\leq$ 0.03%). This negligible change is to be expected since the stack/heat exchanger assembly is very short compared to the effective length of the prime mover ($L_{stack\ assembly} / L_{eff} = 0.038$). As a results, the vertical error bars in Fig 4.5 are smaller than the symbols used to plot the data. However, $1/Q$ is more sensitive to uncertainties in T_h and T_a than is the resonance frequency since all thermoviscous effects are most important in the stack region. The sensitivity to uncertainties in ΔT is represented by the

vertical error bars shown in Fig. 4.6. There is also an uncertainty in the calculation of temperature difference across the stack. As shown in Fig. 4.1 and 4.2, the temperatures at the center of the hot end and ambient end differ from those at the edge. The largest differences at the hot end are 14.8 K and 33.3 K for the low and high mode, respectively (heater at 23 V in both cases). The differences of the center and edge temperatures in the ambient side are approximately 6 K for both cases. This spread is represented by horizontal error bars shown in Figs. 4.5 and 4.6. The other possible source of the discrepancies in resonance frequency and $1/Q$ at high ΔT for the high mode is the entire temperature distribution of the prime mover. As shown in Figs. 4.3 and 4.4, the major change in temperature profile is concentrated at the region adjacent to the hot heat exchanger and stack. It is difficult to accurately characterize the entire temperature distribution of the prime mover using only 10 thermocouples. This is an important difference between the conventional and annular prime movers. In a conventional prime mover, there is typically a hot temperature duct and an ambient temperature duct. In an annular prime mover the two temperatures must merge along the duct.

Figures 4.7(a), (b), and (c) show the mode shapes for the low mode at different temperature differences. The stack/heat exchanger assembly is located between $x = 0.768$ m and $x = 0.792$ m, indicated by the dashed line. In this experiment, the driver is located 90° from the center of the stack which corresponds to a position of 0.183 m. The driving frequencies are the resonance frequencies as computed by the MATLAB program and the ΔT's are calculated using Eqs. 4.1 and 4.2.

Figure 4.7(a) shows the mode shape for the low mode for $\Delta T = 0$ K. In this case, the stack/heat exchanger assembly acts simply like a constriction and there is a velocity antinode near the center of the stack/heat exchanger assembly. The agreement between the measured and calculated mode shape is good.

Figures 4.7(b) and (c) show the mode shapes for the low mode at temperature differences of 80 K and 200 K, respectively. The discrepancy between the measured and computed mode shape increases as the temperature difference increases. The discrepancy appears as a shift in mode shape. However, in both cases, the measured and predicted mode shapes show the same general features. In particular, the standing wave ratio decreases with increasing ΔT. Even with this obvious diminishing in the standing wave ratio, $1/Q$ only changes by 15% from $\Delta T = 0$ K to $\Delta T = 220$ K.

Figure 4.8(a) show the mode shape for the high mode with $\Delta T = 0$ K. The agreement between the measured and calculated mode shape is excellent. As one might expect, there is a pressure antinode near the center of the stack/heat exchanger assembly. Figures 4.8(b) and (c) show the mode shapes for high mode at temperature difference of 76 K and 192 K, respectively. The agreement between measured and calculated mode shapes are better than those of the low mode. In contrast to the low mode shapes, the high mode shapes do not change appreciably as ΔT increases. In particular, the standing wave ratio remains high. This difference between the two modes may be caused by the discontinuity in the acoustic impedance near the end of the stack. For the low mode, there is a velocity antinode near the center of the stack which results in a low acoustic impedance. However, the acoustic impedance of the stack is much larger for the high mode. As a result, as ΔT increases, the impedance discontinuity should have more effect on the low mode than the high mode.

The most important result of this section is that the annular prime mover will not reach onset under easily attainable conditions The reason is that neither mode shape supports thermoacoustic growth. In other words, the low mode has a velocity antinode centered on the stack/heat exchanger assembly whereas the high mode has a pressure antinode centered on the stack/heat exchanger assembly. It was also found that the standing wave ratio of the

low mode diminishes as ΔT increases. However, this alteration in mode shape does not correlate with increased attenuation in the prime mover.

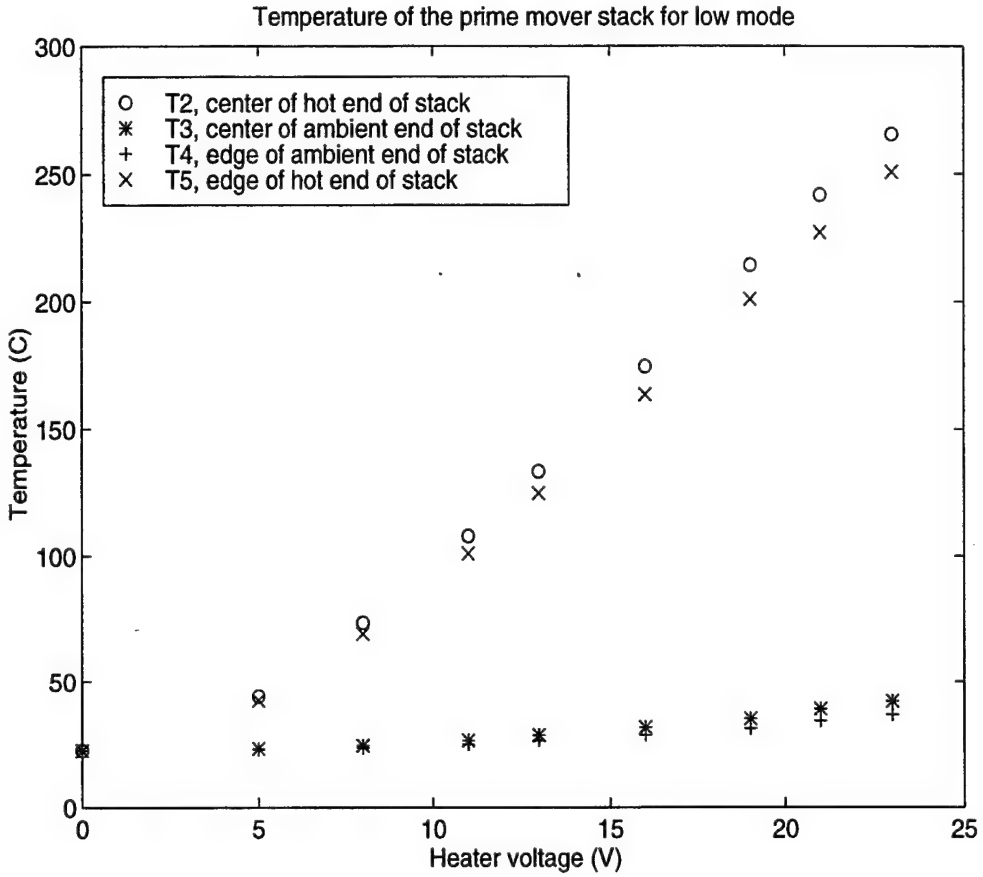

Figure 4.1 Temperature of the prime mover stack vs. the heater voltage (low mode).

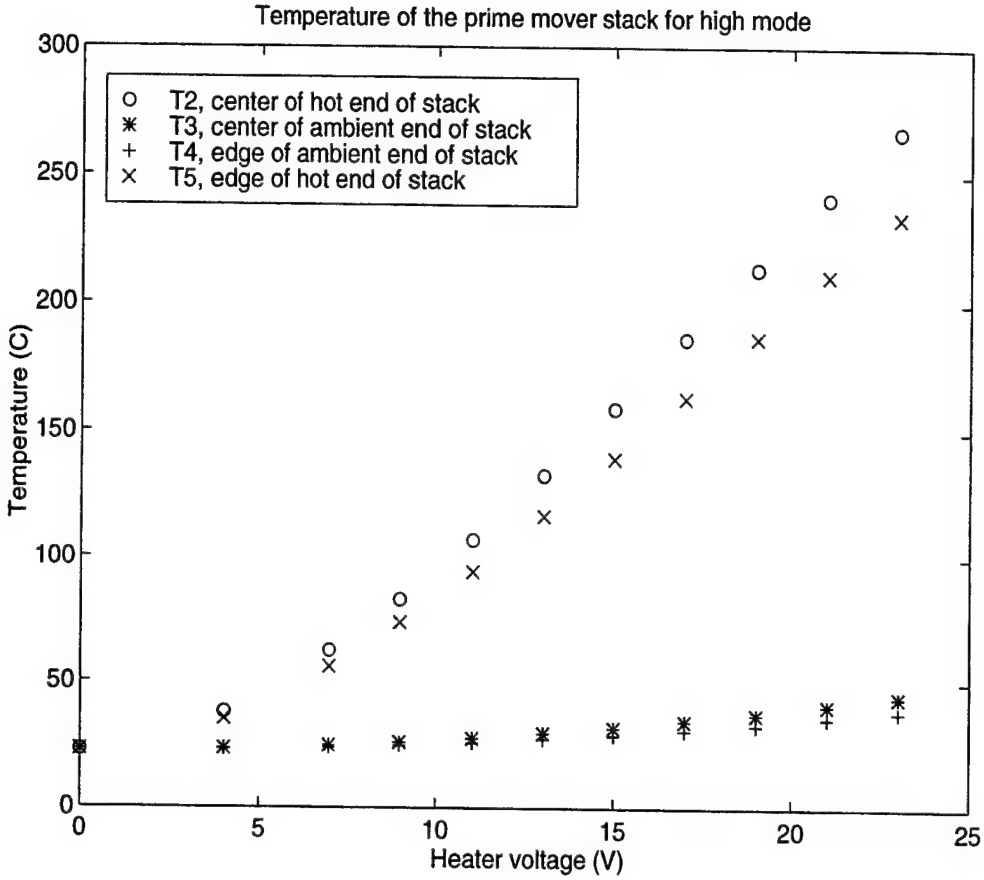

Figure 4.2 Temperature of the prime mover stack vs. the heater voltage (high mode).

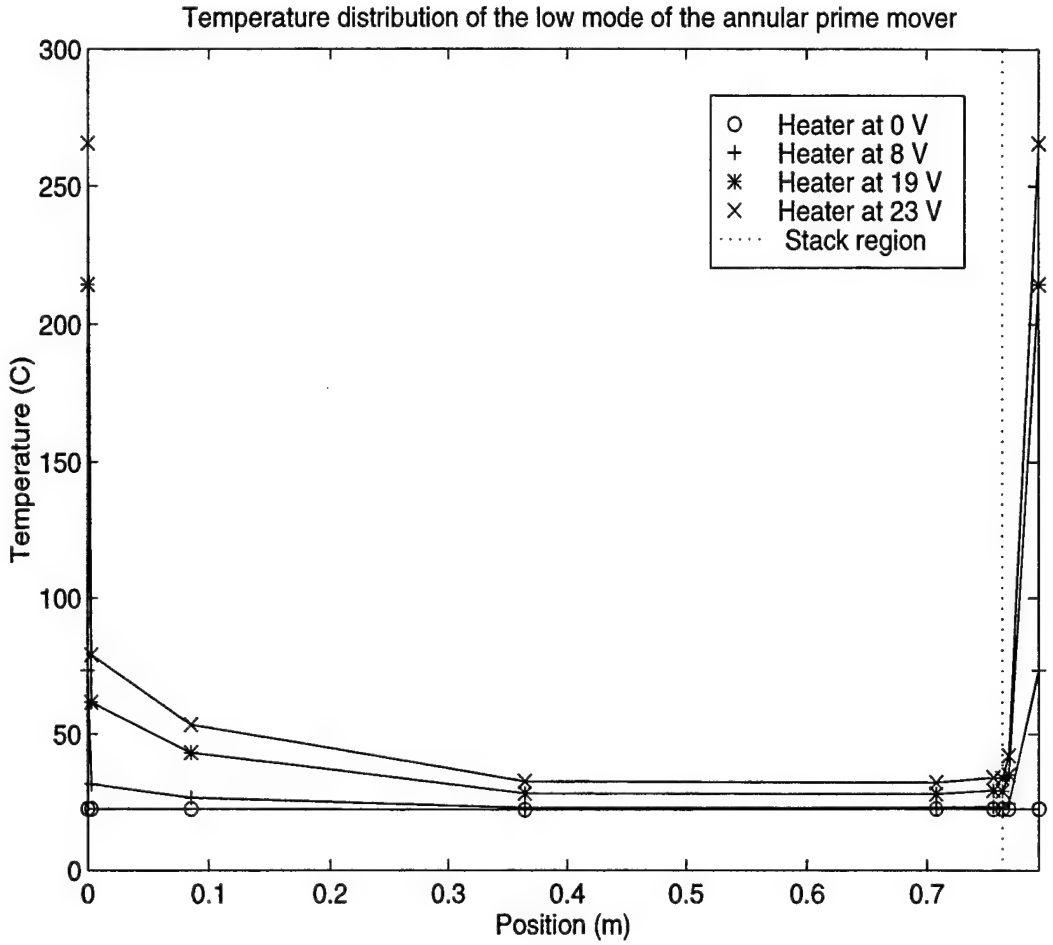

Figure 4.3 The measured temperature distribution of the prime mover (low mode, heater at 23 V). The stack is located to the right of the dotted line.

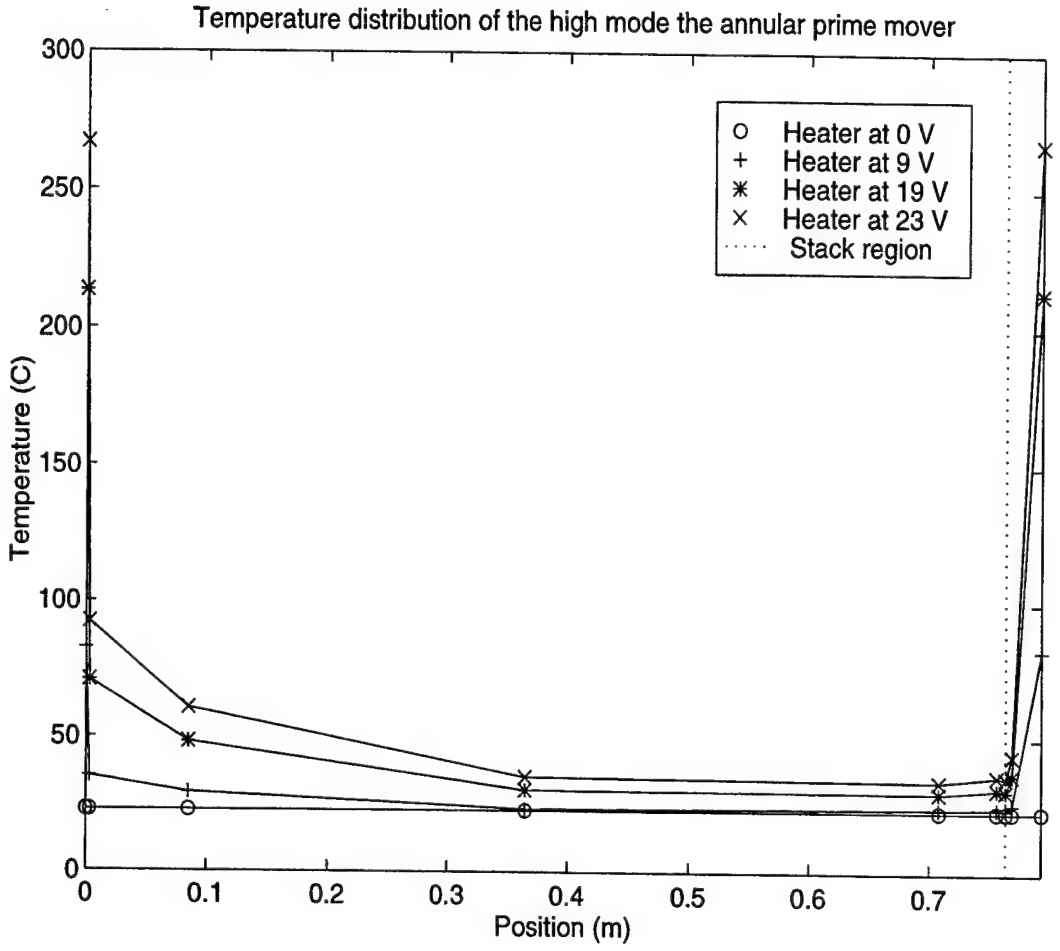

Figure 4.4 The measured temperature distribution of the prime mover (high mode, heater at 23 V). The stack is located to the right of the dotted line.

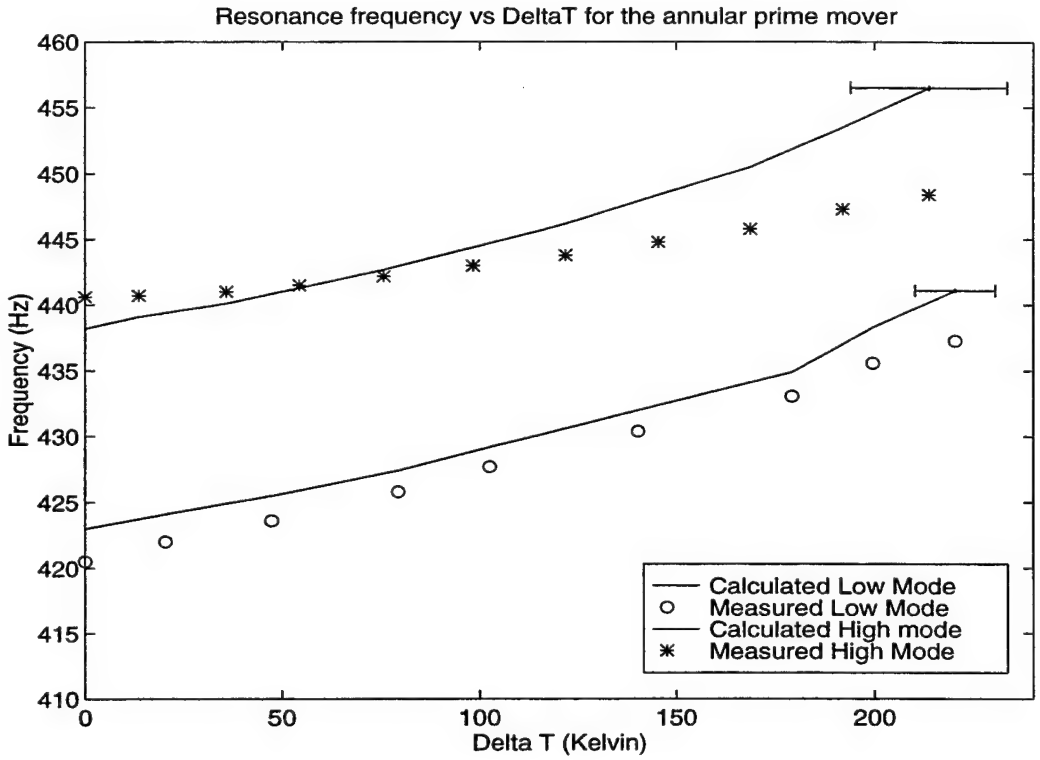

Figure 4.5 Comparison of calculated and measured resonance frequencies vs. ΔT for the annular prime mover.

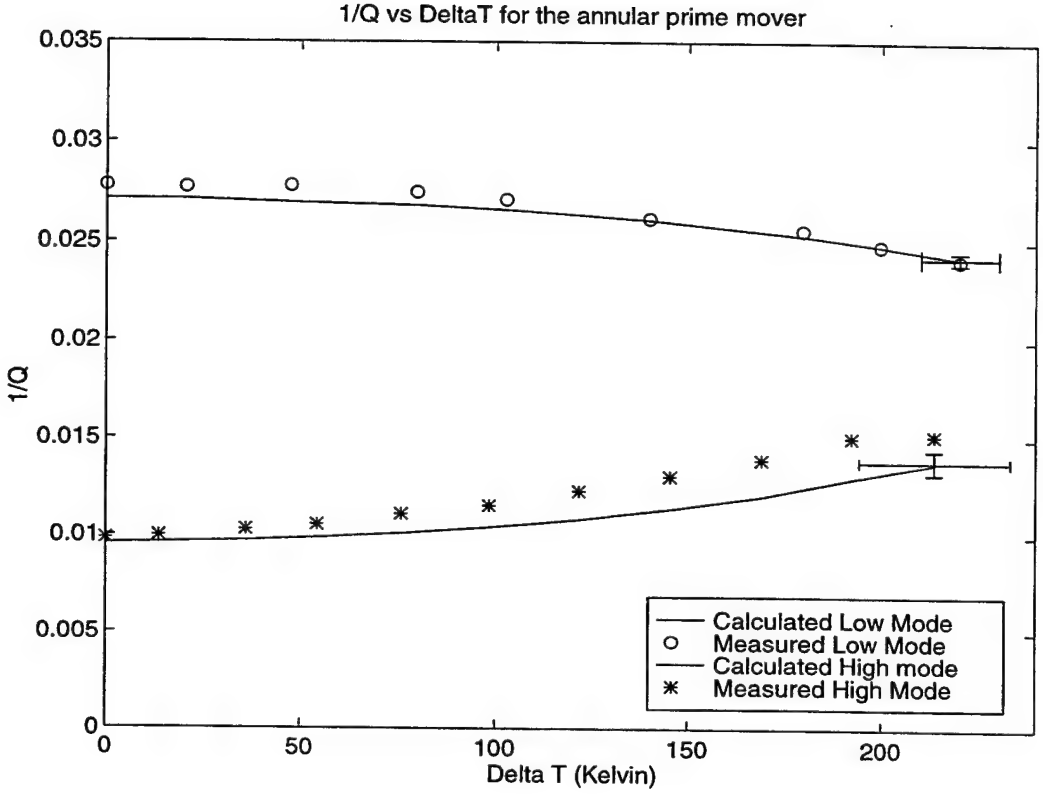

Figure 4.6 Comparison of calculated and measured $1/Q$ vs. ΔT for the annular prime mover.

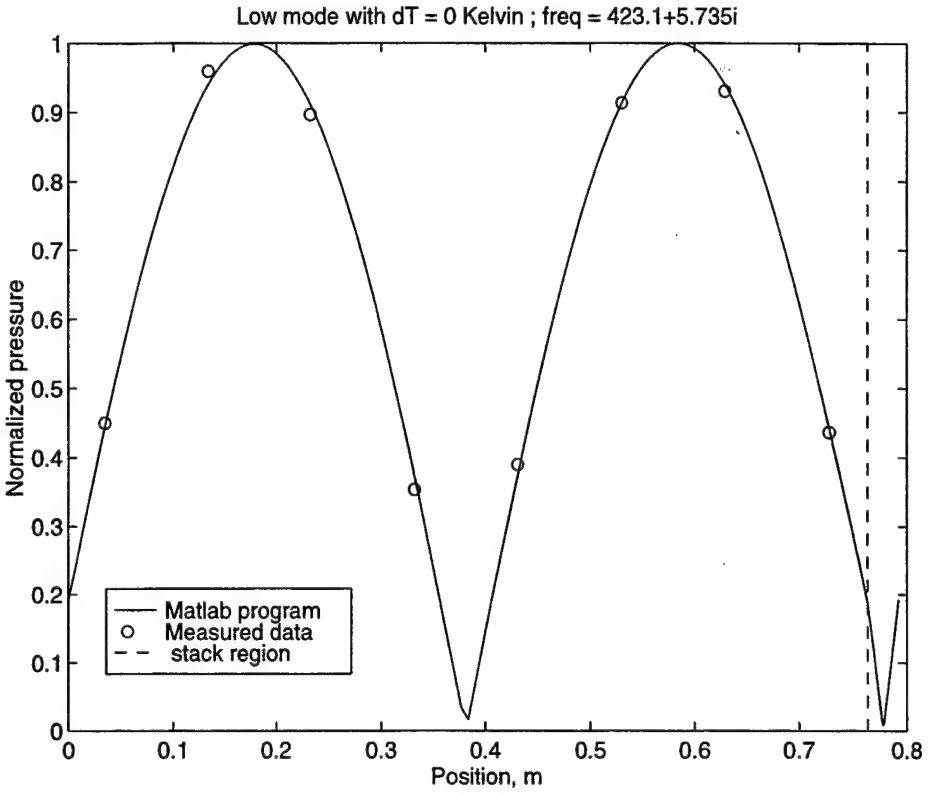

Figure 4.7(a) Mode shape for the low mode of the annular prime mover when the driver is located 90° from the stack and $\Delta T = 0$ K.

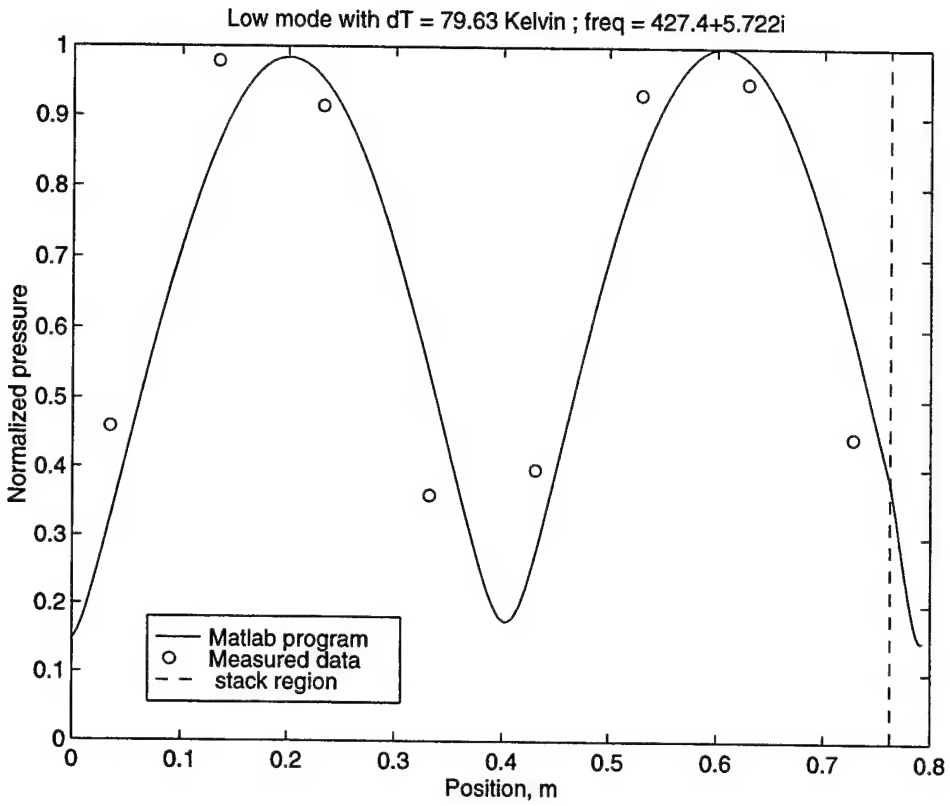

Figure 4.7(b) Mode shape for the low mode of the annular prime mover when the driver is located 90° from the stack and $\Delta T = 80$ K.

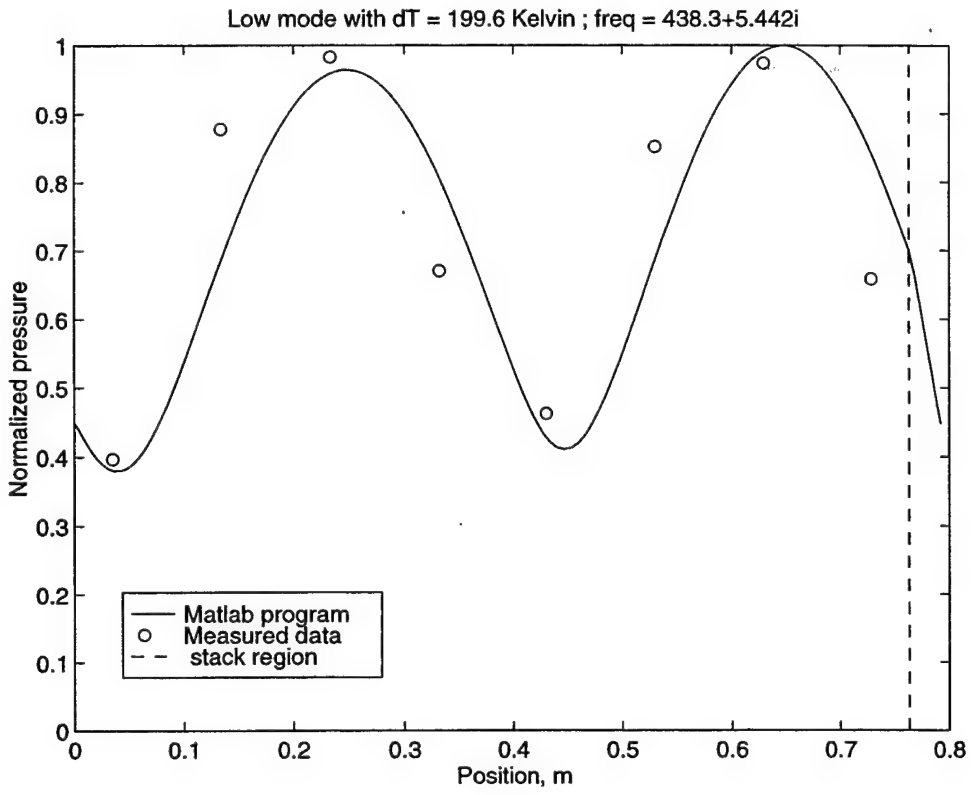

Figure 4.7(c) Mode shape for the low mode of the annular prime mover when the driver is located 90° from the stack and $\Delta T = 200$ K.

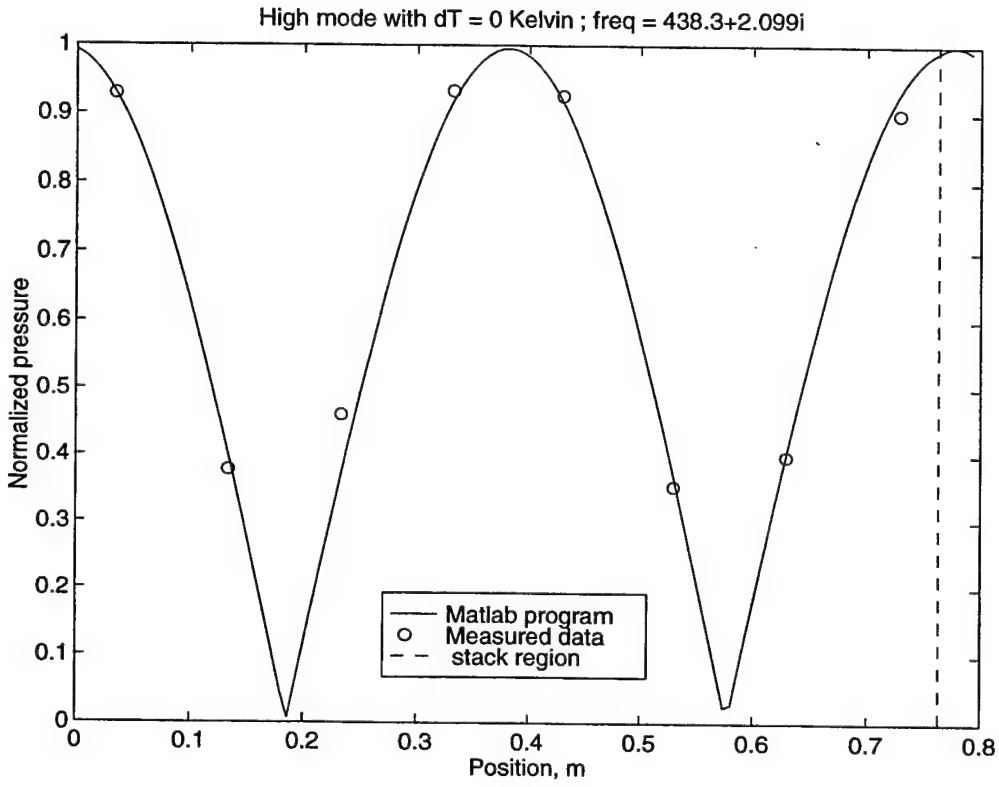

Figure 4.8(a) Mode shape for the high mode of the annular prime mover when the driver is located 180° from the stack and $\Delta T = 0$ K.

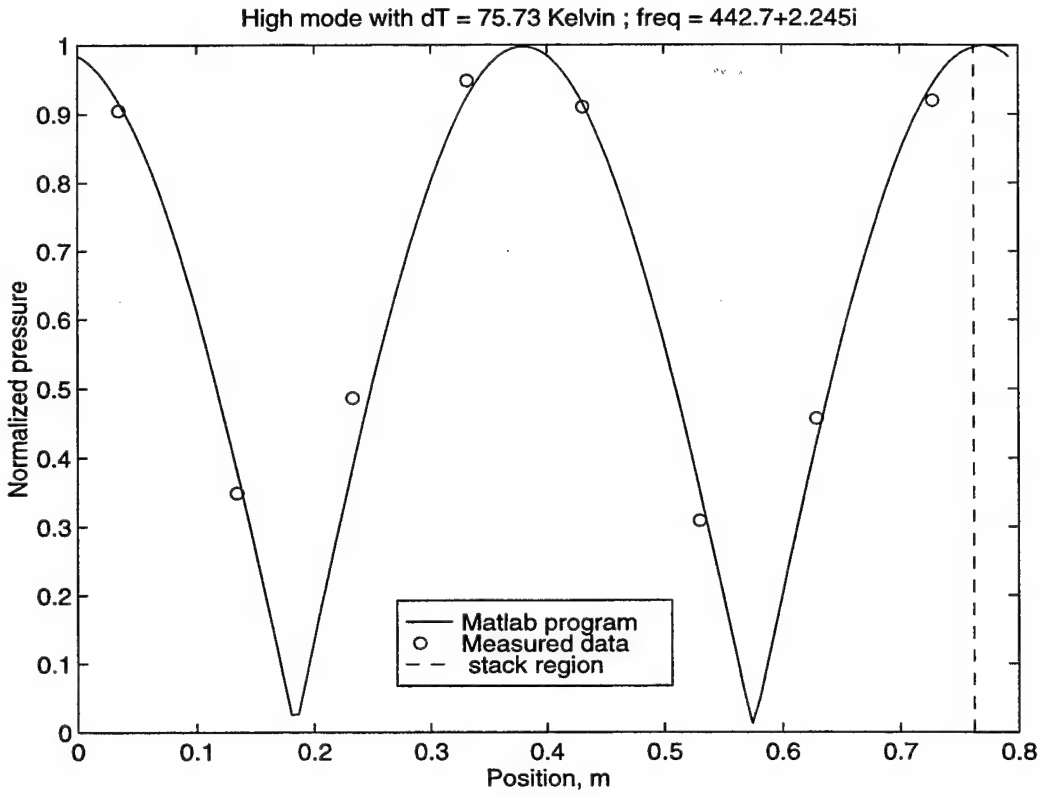

Figure 4.8(b) Mode shape for the high mode of the annular prime mover when the driver is located 180° from the stack and $\Delta T = 76$ K.

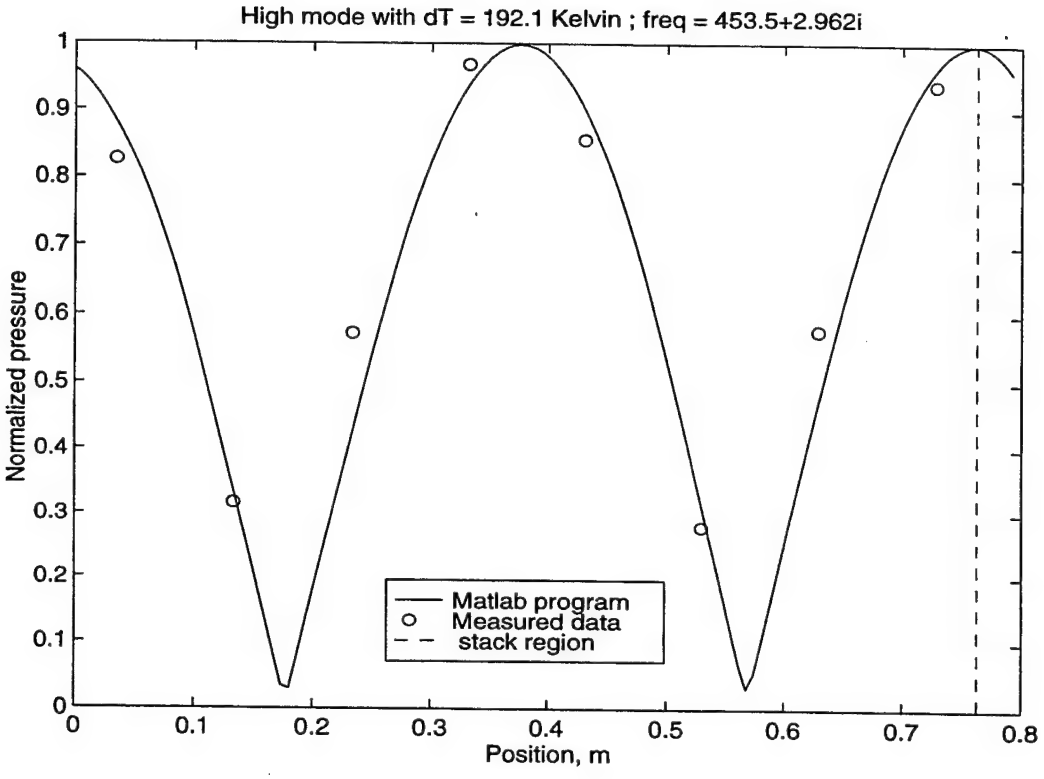

Figure 4.8(c) Mode shape for the high mode of the annular prime mover when the driver is located 180° from the stack and $\Delta T = 192$ K.

B. CONSTRICTED ANNULAR PRIME MOVER

In this section, results for the annular prime mover with a constriction located 90° from the center of the stack/heat exchanger assembly are presented. The constriction is 45° long and three different porosities 0.7, 0.3, and 0.1 are used. First, the comparisons of the measured and calculated resonance frequencies of the constricted prime mover are presented. Next, the comparisons of the measured and calculated Q of the constricted prime mover are discussed. The end corrections are included in the calculations using the two methods discussed in Chapter II. This section concludes with the comparisons of the measured and computed mode shapes for the constricted prime mover.

As mentioned earlier, the measured resonance frequencies and Q's are determined from pole-zero analysis of the frequency response. In the measurement, the driver is located 45° from the center of the stack assembly and the constriction. The theoretical resonance frequencies and Q's were calculated for four different cases, represented by A, B, C, and D. All the results are listed in Tables 4.1 and 4.2. In these tables, Column A represents the calculated results without any end corrections. Columns B and C represent the results with end corrections for the constriction using the conformal transformation method and higher order mode method, respectively. It is worth pointing out that there are no appreciable differences between of the results for $1/Q$ calculated from the conformal mapping transformation and the higher order mode method when the end corrections in the constriction are included. Column D gives the results for the case of applying end corrections to both the constriction and the stack using the higher order mode method. The end corrections in the prime mover stack are approximated by applying the end corrections to one slit and summing the impedance of the slits in parallel. The temperature differences were determined by Eqs. (4.1) and (4.2). Table 4.1 lists the calculated and measured

resonance frequencies for the low and high modes for the various constrictions. Table 4.2 lists the calculated and measured Q for the low and high modes for the various constrictions. In these tables, Rs represents the area ratio of the constriction, i.e., the porosity.

It is seen that the inclusion of end corrections has significant effects on the predictions for the low mode. For example, in the case of $Rs = 0.1$, the averaged differences between the calculated and measured resonance frequencies are 1.94 % (no end corrections), 0.67% (end corrections using conformal transformation method), and 0.39% (end corrections using higher order mode method). On the contrary, including end corrections for the constriction has little effect on the predictions for the high mode. This point is evident from Figs. 4.9 and 4.10, where it is seen that inclusion of end corrections in the constriction is important for the low mode only. However, inclusions of the end corrections in both the constriction and stack has more effect on the high mode than on the low mode.

The point to be taken from these figures is that the program does a good job of predicting the resonance frequencies, even in the absence of including end corrections. We have confidence in the end corrections applied to the constriction. This confidence is the result of preliminary work by Choe (Choe, 1997). Application of end corrections to the stack is only intended to be approximate, to indicate that they should have an effect. The contribution of this work is to point out the necessity of including end corrections. A detailed analysis of stack end corrections is an area for future work.

Figure 4.11 shows the comparisons of the calculated and measured $1/Q$ of the low mode for the unconstricted and constricted prime mover with various porosities. In this set of experiments, when the constriction porosity is 0.1, the prime mover reaches onset at a temperature difference of 260 K. The horizontal error bar in Fig. 4.11 indicates the

uncertainty in determining the onset temperature from the measure temperature distribution as discussed previously. In all cases, the calculated results under estimate $1/Q$. Therefore, the calculated results show a significantly lower onset value of ΔT in the case of $Rs = 0.1$. The reason for this discrepancy is not fully understood. Nonetheless, both the measured and calculated $1/Q$ indicate the same trends. First, the relative values for $1/Q$ are consistent. Also, both the predicted and measured results for the constricted prime mover intersect within a narrow range of ΔT. The predicted values intersect at $\Delta T \cong 100K$ and the measured data intersect at $\Delta T \cong 175$ K. The $1/Q$ curve for $Rs = 0.1$ begins with the highest value of the three constricted cases and ends with the lowest value after the intersection at $\Delta T \cong 100$ K. In contrast, $1/Q$ for $Rs = 0.7$ begins with the lowest value and ends with the largest value at higher ΔT. $1/Q$ for $Rs = 0.3$ remains in between $1/Q$ for the other two porosities.

The conclusion to be drawn from Fig. 4.11 is that it is predicted that a constricted annular prime mover will reach onset, and it does. Although, the agreement between the measured and calculated results are only fair, there is very good qualitative agreement. This indicates that although there are still some details to be investigated, the general behavior is understood.

Figure 4.12 shows the comparisons between the calculated and measured $1/Q$ for the high mode for the unconstricted and constricted prime mover. It is seen that the temperature difference has less effect on $1/Q$ for the high mode than for the low mode. Over the temperature span from $\Delta T = 0$ K to $\Delta T = 200$ K, the change in $1/Q$ is less than 30 % in all cases. The same comments about the general qualitative agreement apply to the high mode results as they do to the low mode results.

The question to be addressed now is why does a constricted annular prime mover reach onset. The answer lies in the effects that a constriction has on mode shapes.

Figures 4.13(a) and (b) show the comparison of the measured and computed mode shapes of the low mode for $Rs = 0.1$. In this case the constriction is much longer than the stack assembly ($L_{constriction}/L_{stack} \cong 3.33$) and the porosity of the constriction is much smaller than that of the stack assembly. As a result, the mode shape is dominated by the constriction. There is a pressure node near the center of the constriction and a pressure antinode between the constriction and the stack assembly nearest (but not at) the hot end of the stack. End corrections for the constriction are included using the higher order mode method. Figure 4.13(a) is for $\Delta T = 0$ K and Fig. 4.13(b) is for $\Delta T = 288$ K. The frequencies are the calculated values. It is observed that there is a good agreement between the measured and predicted mode shape at $\Delta T = 0$ K. This mode shape is favorable to thermoacoustic growth. The agreement in mode shape worsens at $\Delta T = 288$ K. It should be noticed that the imaginary part of the calculated resonance frequency is negative, which suggests the onset has been reached.

Figures 4.14(a) and (b) show the comparison of the measured and computed mode shapes of the high mode for $Rs = 0.1$. The agreement between the measured and calculated mode shape is good. As one would expect, there is a pressure antinode near the center of the constriction.

One important common feature of Figs. 4.13 and 4.14 is that the mode shapes are essentially determined by the constriction and are independent of the temperature difference. This is a key to making the annular prime mover reach onset.

The main conclusion from this section is that to build a functional annular prime mover, the relative locations of the constriction and the stack, and their relative porosities are the crucial factors. This is equivalent to incorporating some type of dominating boundary conditions into the prime mover to alter the mode shapes.

Rs=0.1 Low mode	**A**	**B**	**C**	**D**	
DeltaT (K)	f, cal (Hz)	f, cal (Hz)	f, cal (Hz)	f, cal (Hz)	f, mea (Hz)
0	300.9	297.1	296.2	295.6	295.6
41.1	302.3	298.6	297.6	296.9	296.9
70.8	303.6	299.9	298.9	298.3	298.1
103.9	305.1	301.2	300.3	299.7	299.2
175.4	309.0	304.9	304.2	303.6	302.6
228.2	312.3	308	307.4	306.8	305.1
Rs=0.1 High mode	**A**	**B**	**C**	**D**	
DeltaT (K)	f, cal (Hz)	f, cal (Hz)	f, cal (Hz)	f, cal (Hz)	f, mea (Hz)
0	474.2	474	474.0	468.8	470.5
41.1	476.6	476.5	476.4	471.6	474
70.8	478.8	478.7	478.6	473.9	476.9
103.9	481.1	481	481.0	476.4	479.6
175.4	487.7	487.6	487.6	483.2	486.7
228.2	493.3	493.1	493.1	488.9	491.8
Rs=0.3 Low mode	**A**	**B**	**C**	**D**	
DeltaT (K)	f, cal (Hz)	f, cal (Hz)	f, cal (Hz)	f, cal (Hz)	f, mea (Hz)
0	368.4	363	361.7	361.3	362
42.1	368.6	363.2	361.9	361.6	361.6
71.7	369.3	363.9	362.6	362.3	361.9
105.6	370.4	364.9	363.6	363.4	362.5
175.4	373.4	367.7	366.6	366.3	364.4
226.4	376.8	370.9	369.9	369.6	366.7
Rs=0.3 High mode	**A**	**B**	**C**	**D**	
DeltaT (K)	f, cal (Hz)	f, cal (Hz)	f, cal (Hz)	f, cal (Hz)	f, mea (Hz)
0	467.3	467	466.9	461.9	464.2
42.1	468.1	467.8	467.7	463.1	465.8
71.7	469.2	468.8	468.7	464.2	467.2
105.6	470.8	470.5	470.4	466	469.3
175.4	475.3	474.9	474.9	470.7	473.7
226.4	480.0	479.7	479.6	475.5	478
Rs=0.7 Low mode	**A**	**B**	**C**	**D**	
DeltaT (K)	f, cal (Hz)	f, cal (Hz)	f, cal (Hz)	f, cal (Hz)	f, mea (Hz)
0	419.3	418.4	417.9	417.8	417.8
46.8	419.9	419	418.5	418.4	418.2
77.1	421.9	421	420.5	420.4	418.8
112.2	423.5	422.5	422.1	421.9	419.9
179.2	426.9	425.9	425.4	425.2	422
231	433.9	429.6	429.2	428.8	424.5
Rs=0.7 High mode	**A**	**B**	**C**	**D**	
DeltaT (K)	f, cal (Hz)	f, cal (Hz)	f, cal (Hz)	f, cal (Hz)	f, mea (Hz)
0	438.9	438.8	438.7	434.2	436.2
46.8	442.5	442.4	442.3	438.1	440.2
77.1	445.2	445.1	445.0	440.9	442.2
112.2	448.2	448.1	448.0	444	444.4
179.2	454.2	454.1	454.0	450.2	448.5
231	460.2	460	460.0	456.3	452

Table 4.1 Comparisons of the calculated and measured resonance frequencies for the constricted annular prime mover. Case A: without end corrections; Cases B, C, D: End corrections with different methods.

Rs=0.1 Low mode	**A**	**B**	**C**	**D**	
DeltaT (K)	Qlow, cal	Qlow, cal	Qlow, cal	Qlow, cal	Qlow, mea
0	50.4	45.5	45.4	38.2	43.3
41.1	68.8	60.8	60.9	48.9	51.5
70.8	92.3	80.2	80.2	61.3	60.5
103.9	148.3	122.6	123.4	84.8	73.8
175.4	-519.6	-1089	-1029	421	127
228.2	-124.3	-123.3	-131.9	-225	239.5
Rs=0.1 High mode	**A**	**B**	**C**	**D**	
DeltaT (K)	Qlow, cal	Qlow, cal	Qlow, cal	Qlow, cal	Qhigh, mea
0	36.4	36.4	36.4	24.3	32.6
41.1	37.9	37.9	37.9	24.9	33.7
70.8	39.2	39.1	39.1	25.4	34.2
103.9	40.8	40.8	40.8	26	35.9
175.4	45.7	45.6	45.7	27.8	37.9
228.2	51.3	51.2	51.2	29.6	41.3
Rs=0.3 Low mode	**A**	**B**	**C**	**D**	
DeltaT (K)	Qlow, cal	Qlow, cal	Qlow, cal	Qlow, cal	Qlow, mea
0	74.9	69.6	69.1	62.7	65.1
42.1	90.2	84.8	83.7	75.6	73.8
71.7	105.5	98.6	98.1	87.7	81.1
105.6	129.2	122	123	107	90.9
175.4	235.2	234	248	196	121.7
226.4	514.4	590	690	435	157
Rs=0.3 High mode	**A**	**B**	**C**	**D**	
DeltaT (K)	Qhigh, cal	Qhigh, cal	Qhigh, cal	Qhigh, cal	Qhigh, mea
0	35.7	35.7	35.7	24	32.8
42.1	36.9	36.9	36.9	24.5	33.7
71.7	37.9	37.8	37.8	24.9	34.3
105.6	39.2	39.1	39.1	25.3	35.1
175.4	42.6	42.4	42.4	26.6	37.4
226.4	45.8	45.8	45.8	27.8	38.8
Rs=0.7 Low mode	**A**	**B**	**C**	**D**	
DeltaT (K)	Qlow, cal	Qlow, cal	Qlow, cal	Qlow, cal	Qlow, mea
0	98.8	97.3	97.2	94.2	85.4
46.8	108.2	106.8	106.6	103.4	95
77.1	118.4	116.8	116.7	114.4	98.2
112.2	136.7	134.5	134.5	133.6	103
179.2	216.3	207	205.8	210	114
231	312.5	407.1	398.2	444.3	119.1
Rs=0.7 High mode	**A**	**B**	**C**	**D**	
DeltaT (K)	Qhigh, cal	Qhigh, cal	Qhigh, cal	Qhigh, cal	Qhigh, mea
0	36.6	36.6	36.6	24.7	35.2
46.8	36.5	36.5	36.5	24.7	36.4
77.1	36.1	36.1	36.2	24.3	36.3
112.2	35.7	35.7	35.8	24	35.2
179.2	34.5	34.8	34.9	23.4	36.4
231	33.7	34	34.1	22.8	37.2

Table 4.2 Comparisons of the calculated and measured Q for the constricted annular prime mover. Case A: without end corrections; Cases B, C, D: End corrections with different methods.

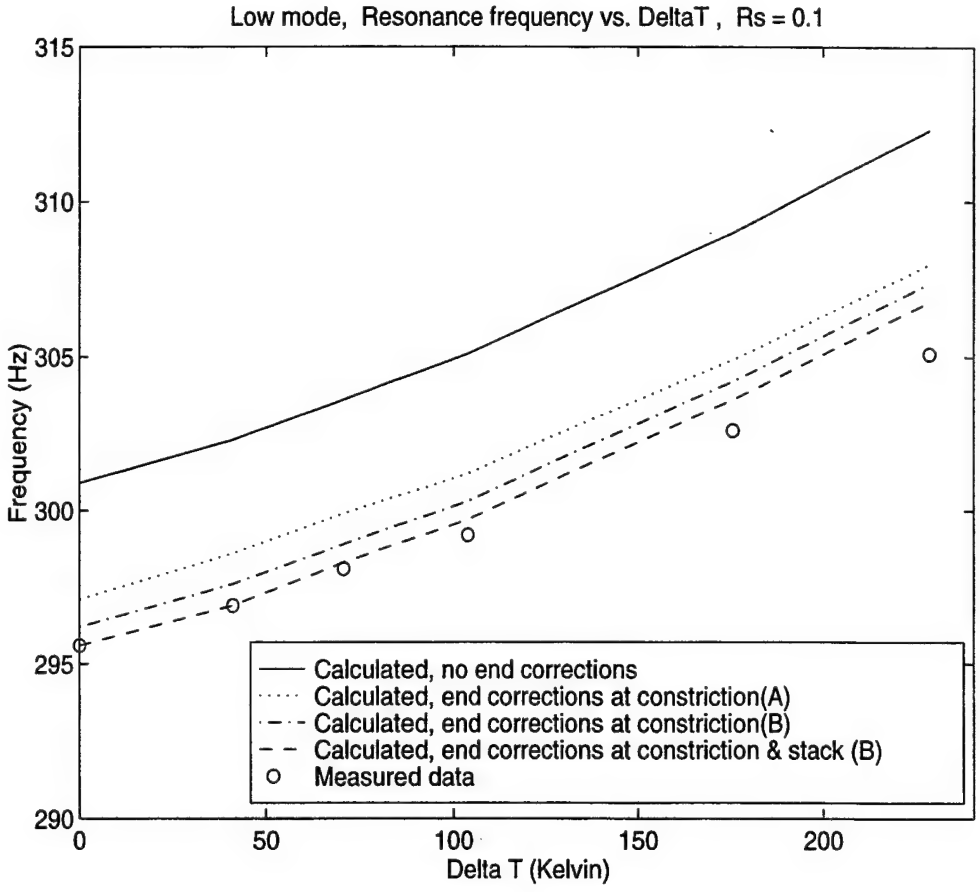

Figure 4.9 Comparisons of the measured and calculated resonance frequencies of the low mode for the constricted prime mover with a porosity of 0.1. Method A is the conformal mapping transformation and Method B is the higher order mode.

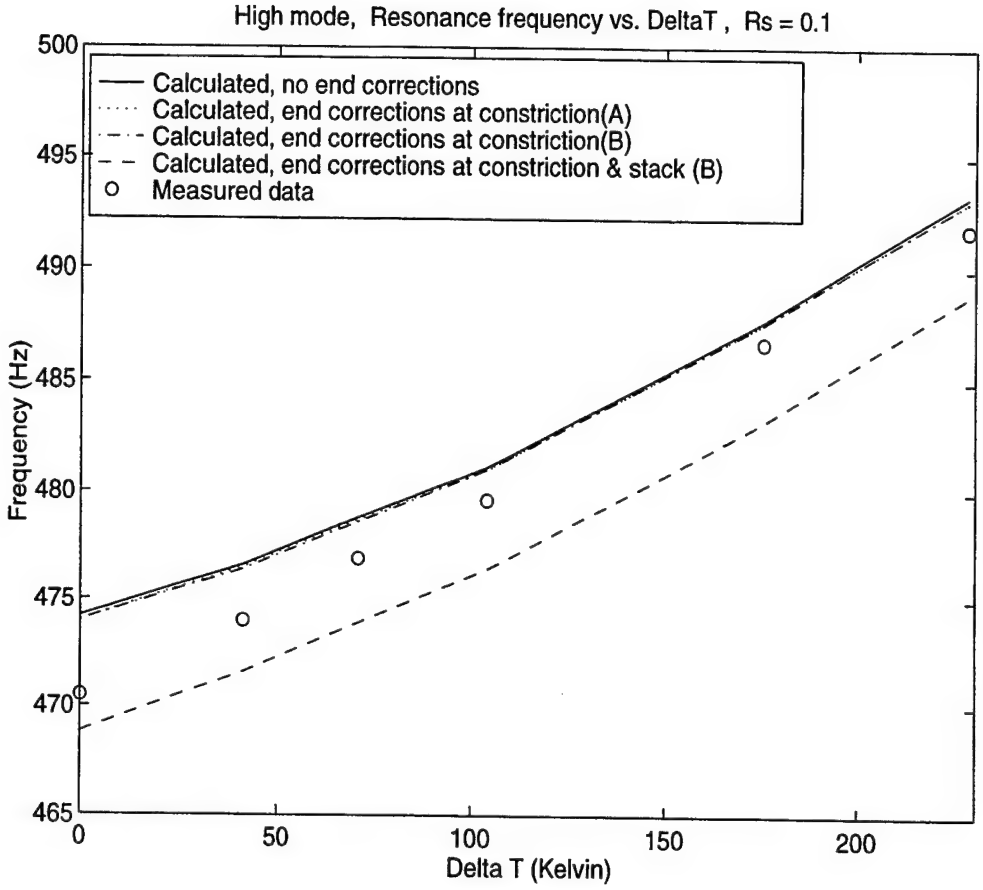

Figure 4.10 Comparisons of the measured and calculated resonance frequencies of the high mode for the constricted prime mover with a porosity of 0.1. Method A is the conformal mapping transformation and Method B is the higher order mode.

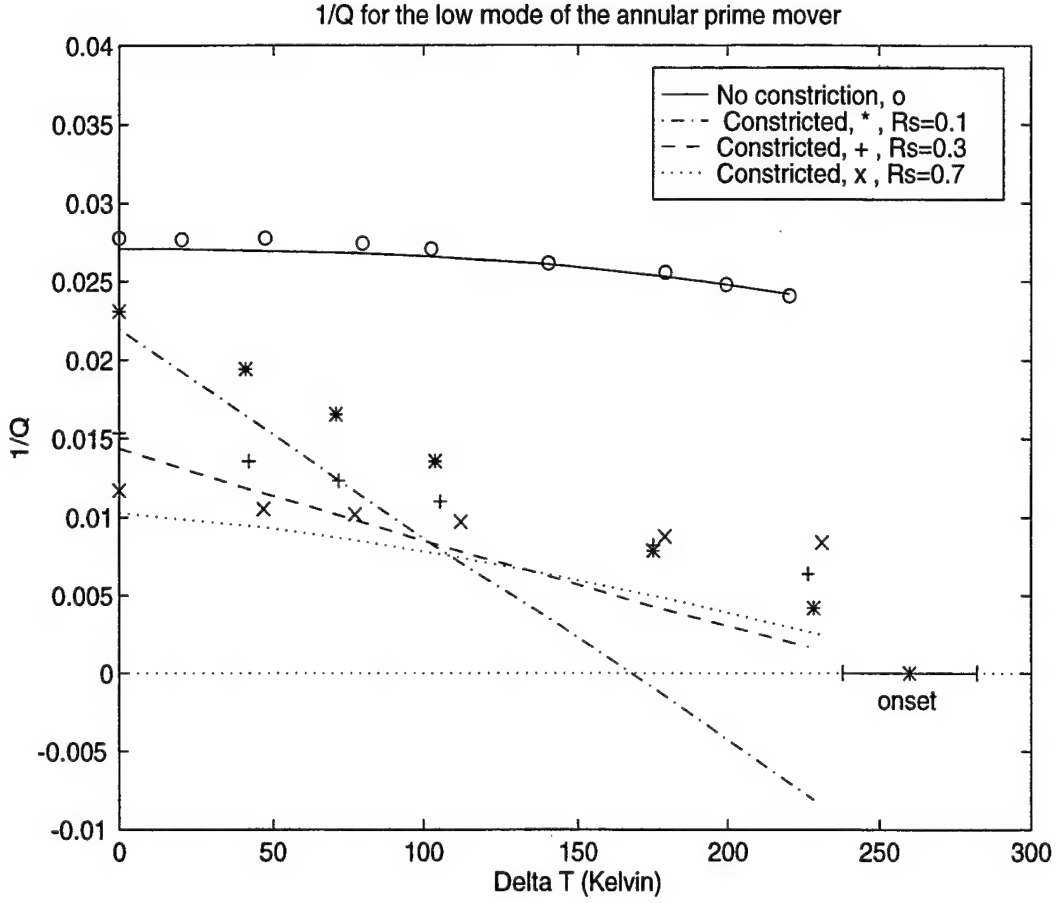

Figure 4.11 Comparisons of the measured and predicted $1/Q$ of the low mode for the unconstricted and constricted prime mover. Symbol **o** represents the measured $1/Q$ of unconstricted prime mover. Symbols *, +, and × represent the measured $1/Q$ for the constricted prime mover with porosities of 0.1, 0.3, and 0.7, respectively. The lines represent the predicted values. No end corrections are included in the predicted values for the unconstricted prime mover.

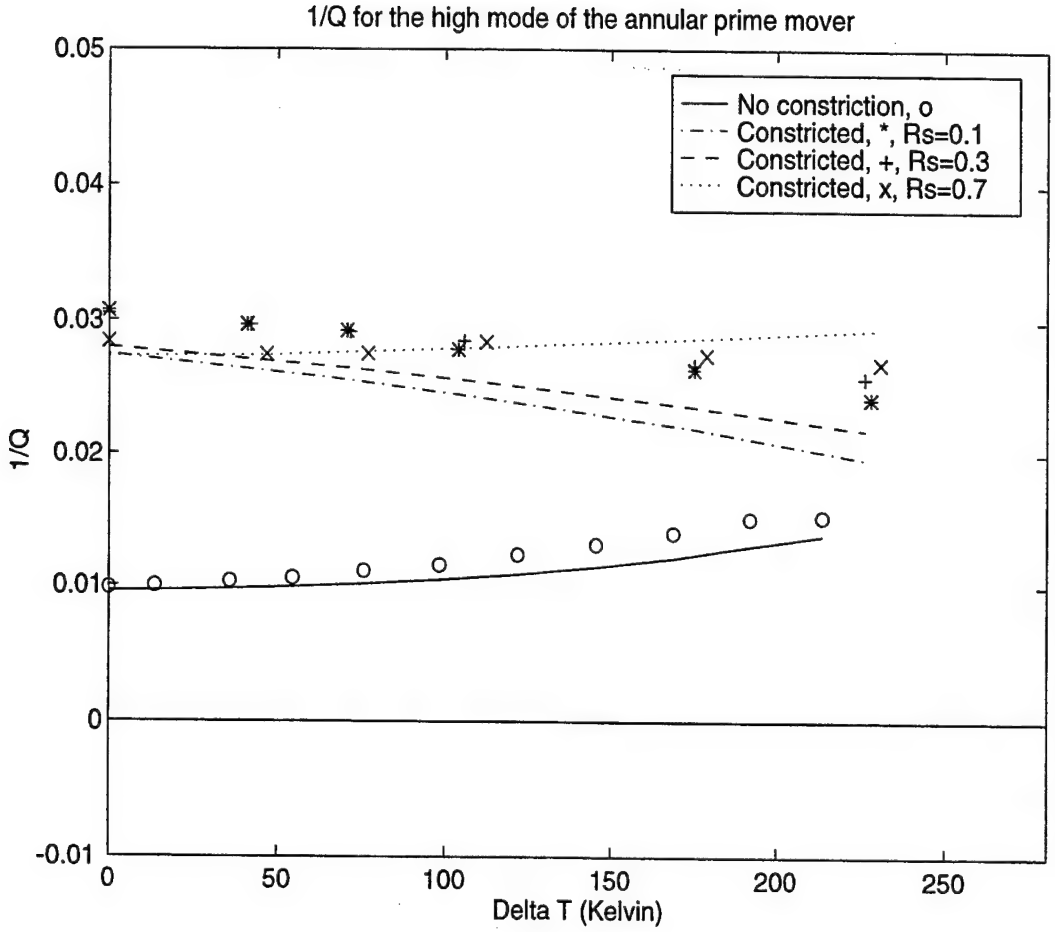

Figure 4.12 Comparisons of the measured and predicted $1/Q$ of the high mode for the unconstricted and constricted prime mover. Symbol **o** represents the measured $1/Q$ of unconstricted prime mover. Symbols *, +, and × represent the measured $1/Q$ for the constricted prime mover with porosities of 0.1, 0.3, and 0.7, respectively. The lines represent the predicted values. No end corrections are included in the predicted values for the unconstricted prime mover.

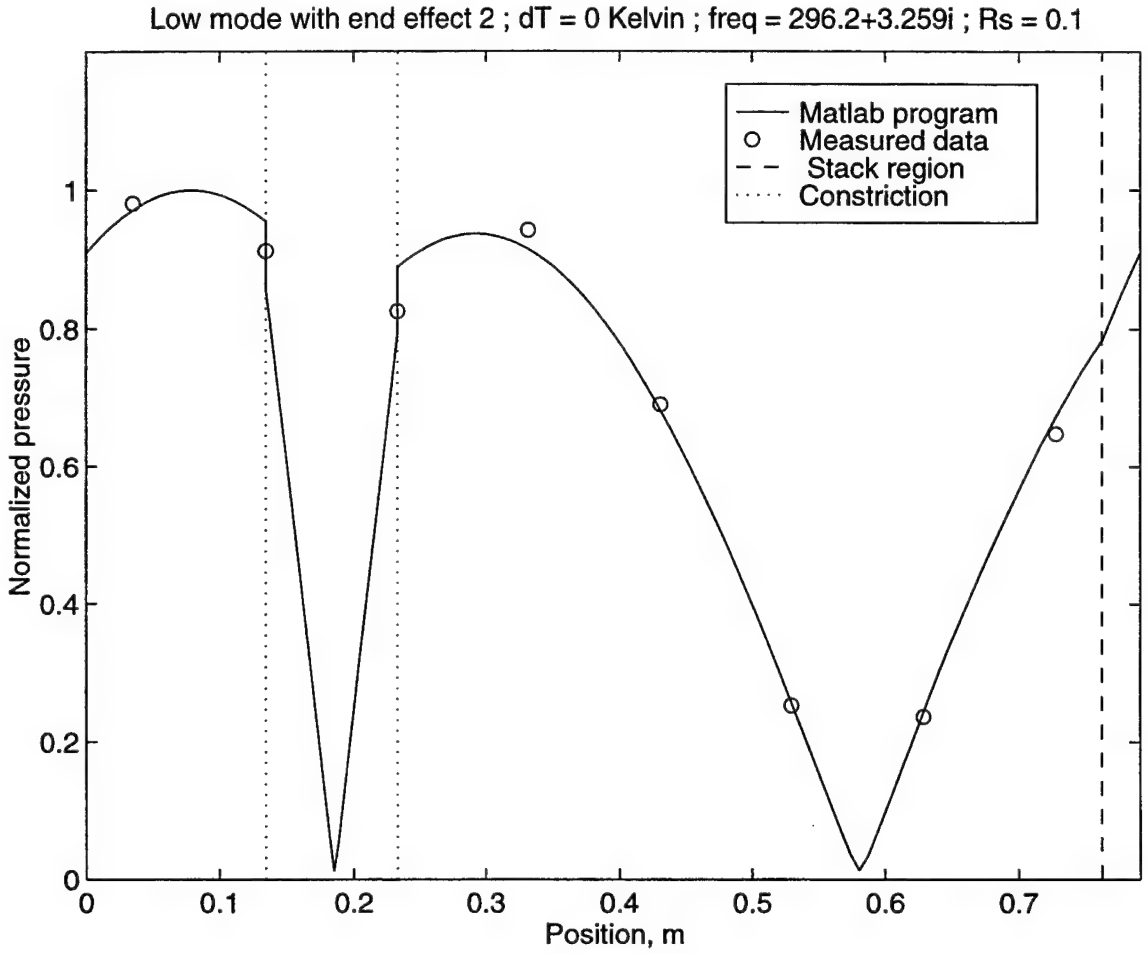

Figure 4.13(a) Mode shape of the low mode of the constricted prime mover (Rs = 0.1) when the driver is located 45° from the stack and $\Delta T = 0$ K. The calculated results are based on the higher order mode method. The frequency is the calculated value.

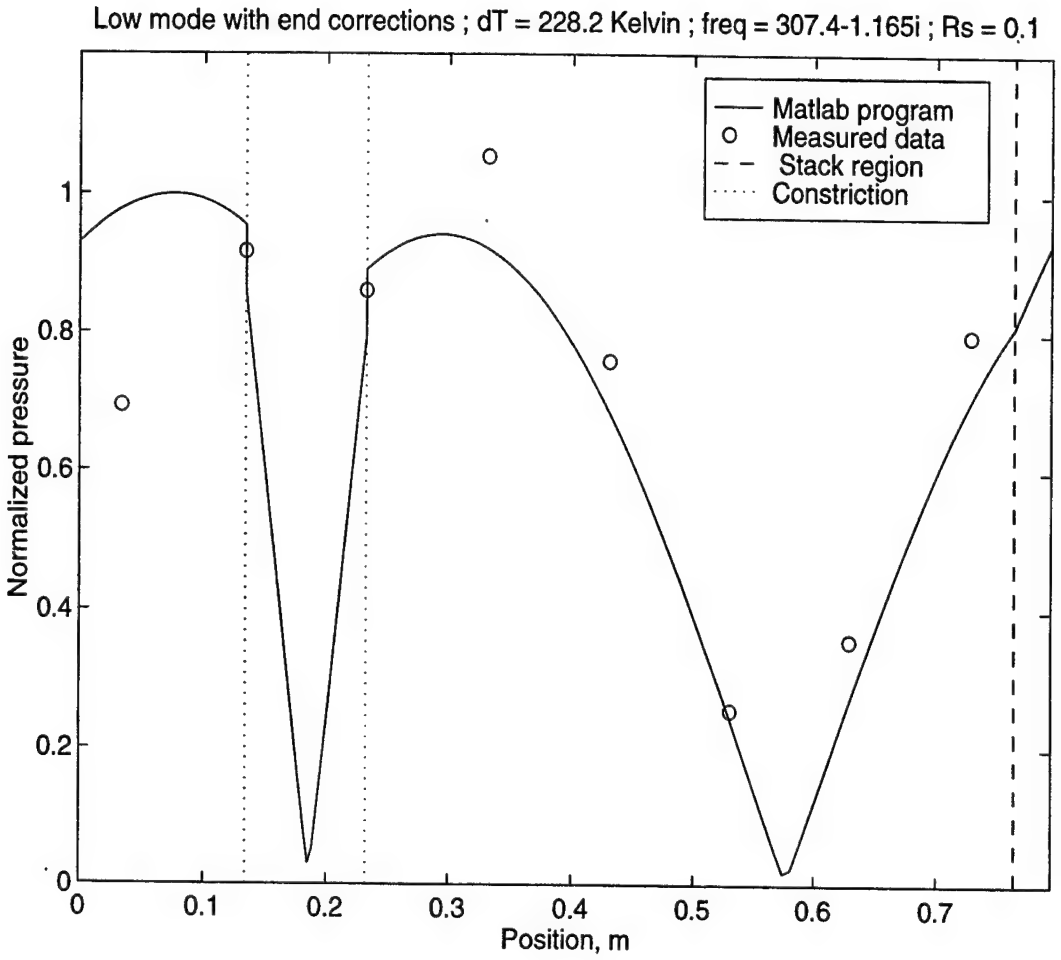

Figure 4.13(b) Mode shape of the low mode of the constricted prime mover (Rs = 0.1) when the driver is located 45° from the stack and ΔT = 228 K. The calculated results are based on the higher order mode method. The frequency is the calculated value.

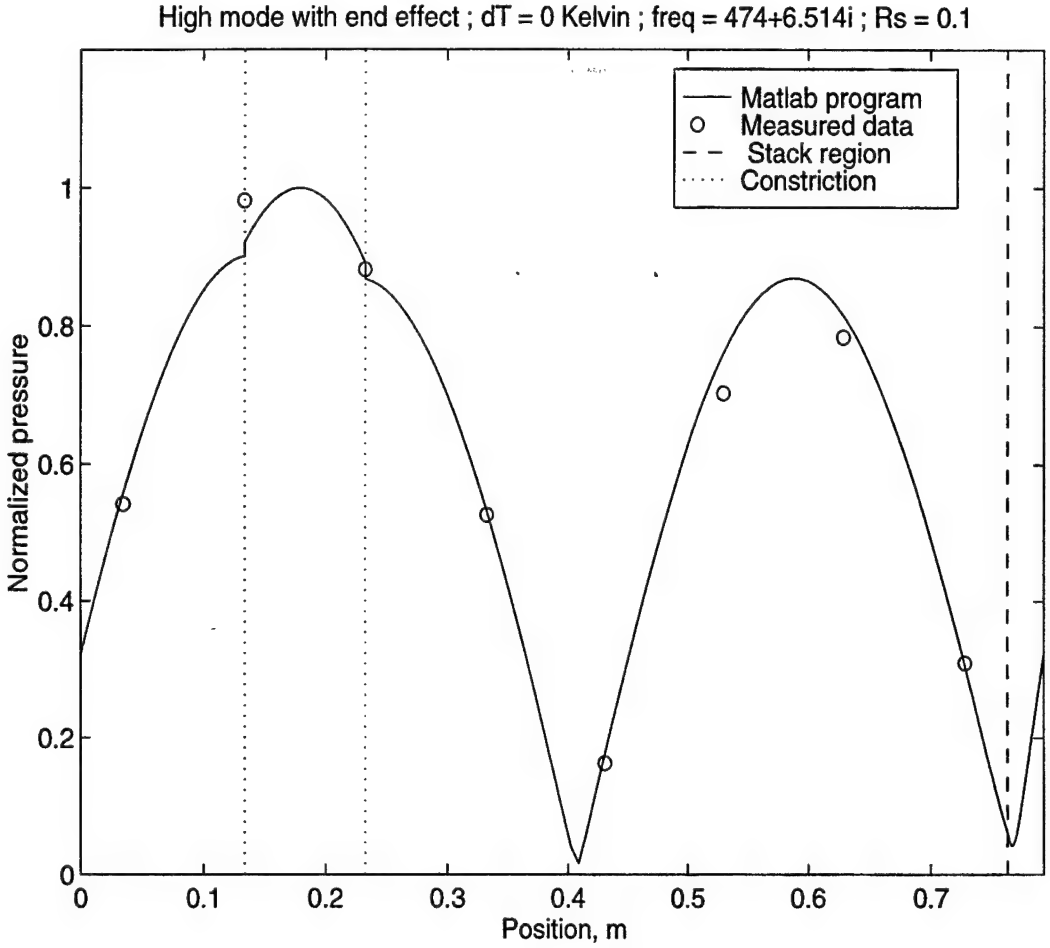

Figure 4.14(a) Mode shape of the high mode of the constricted prime mover (Rs = 0.1) when the driver is located 45° from the stack and $\Delta T = 0$ K. The calculated results are based on the higher order mode method. The frequency is the calculated value.

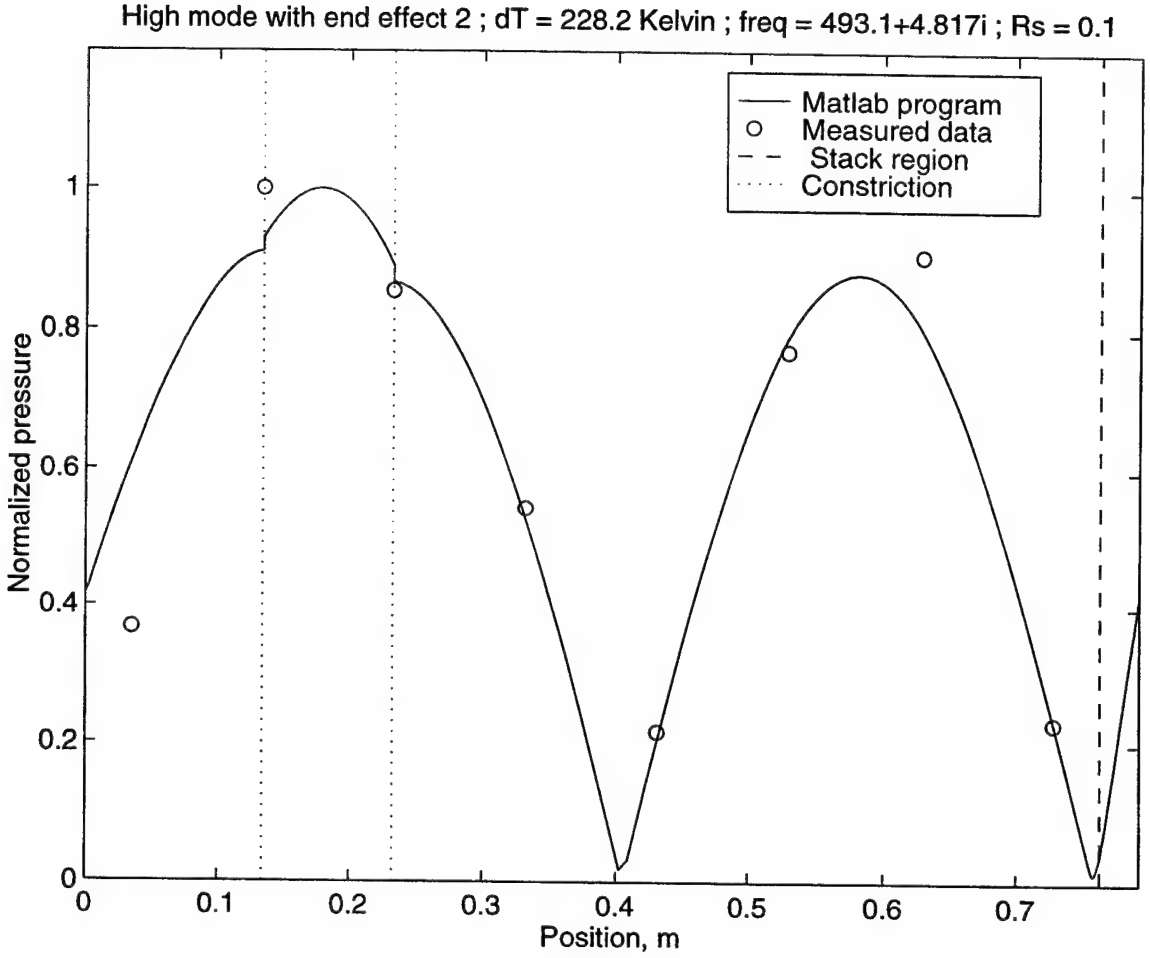

Figure 4.14(b) Mode shape of the high mode of the constricted prime mover (Rs = 0.1) when the driver is located 45° from the stack and ΔT = 228 K. The calculated results are based on the higher order mode method. The frequency is the calculated value.

C. TWO STACK ANNULAR PRIME MOVER

The knowledge gained from the last two sections leads to the design of a symmetric two stack annular prime mover in which the constriction in the last section is replaced by a stack assembly. This proposed design of the annular prime mover, as shown in Fig. 4.15, has two identical stack/heat exchanger assemblies. The two stack assemblies are placed such that the hot heat exchangers face each other.

The MATLAB program was modified to predict the performance of this two stack annular prime mover, by adding one more guess of the time-averaged energy flux $\dot{H}_2$ along the second stack to match the temperature of the hot heat exchanger. Two different cases are studied here. In case 1 the duct between the two heat exchangers is held at ambient temperature $T_a = 293$ K while in case 2 it is held at the desired temperature of the hot heat exchanger T_h. The reason for studying case 1 is that the current apparatus can be easily modified to conduct the experiment. However, because of the temperature discontinuity near the junction of the duct and hot heat exchanger, it is difficult to model this case theoretically and computationally. It is known that the temperature discontinuity in the duct will also create a small discontinuity in the work flow (Rott, 1969). On the contrary, although the theoretical analysis of case 2 is simpler than case 1, investigating it requires a new apparatus.

Figure 4.16 shows the calculated resonance frequencies of the two-stack prime mover for the two cases. In case 1, it is seen that the resonance frequencies for the high mode increase approximately linearly with temperature difference. However, ΔT has little effect on the resonance frequencies of the low mode in case 1. The resonance frequencies for both the low and high mode in case 2 increase approximately linearly with temperature difference. Because the duct between the two hot heat exchangers is held at T_h, the

increase in resonance frequency is bigger than that in case 1. It should be pointed out that in case 1 at very low temperature difference ($\Delta T \leq 50$ K), the resonance frequencies of the low mode and high mode are very nearly equal. The MATLAB program always converges to only one mode. For example, at $\Delta T = 0$ K, the program always converges to the high mode, while at $\Delta T = 25$ K it always converges to the low mode. As ΔT increases, the modes are well separated and no such condition was observed. This condition is not present in case 2. It was always possible to distinguish between the low mode and high mode. It should also be pointed out that for case 1 at $\Delta T = 0$ K, the resonance frequency for the high mode is 424.6 Hz and is 424.0 Hz for the low mode. The results indicate the possibility of mode level repulsion (Pippard, 1985 and 1989; Laraza and Denardo 1997).

Figure 4.17 shows the calculated $1/Q$ of the low mode and high mode for the two-stack prime mover for the two cases. It is evident that the high mode reaches onset at $\Delta T \cong 190$ K for case 1. The onset temperature difference for the high mode in case 2 is approximately 350 K. An interesting feature different from the $1/Q$ for the constricted prime mover is the linearly increase and decrease in $1/Q$ for the low mode and high mode, respectively. Similar dependence has been observed for a rigid-rigid prime mover (Lin, 1989; Atchley, et al., 1992).

Frequency splitting in the two-stack annular prime mover offers the possibility that the harmonics of the fundamental frequency and the overtones of the resonator will not coincide, thus detuning the system. This means that if high amplitudes are achieved above onset, waveform distortion and shocking should not be a problem (Coppens, 1971; Atchley and Hofler, 1990; Atchley *et. al.* 1993).

Figures 4.18 to 4.21 show the calculated mode shapes for the low mode and high mode for the two cases. As one would expect from symmetry, there is a pressure antinode

between the two stacks for the high mode and a pressure node between the two stack assembly for the low mode. It is evident that only the high modes in both cases support thermoacoustic growth, as is confirmed by Fig. 4.17.

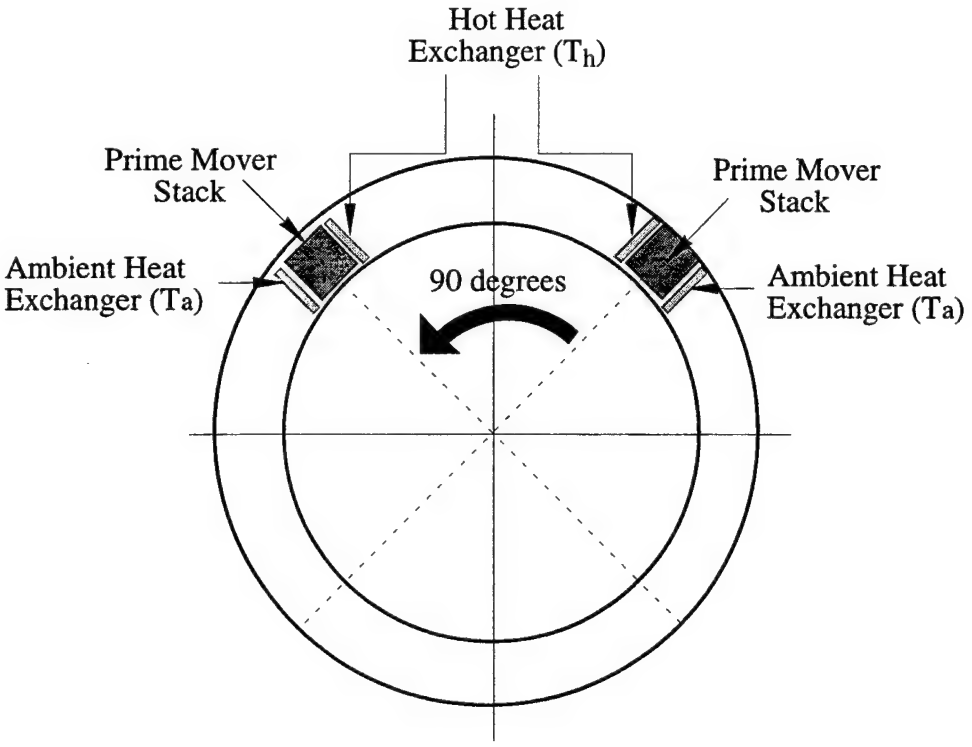

Figure 4.15 The two-stack annular thermoacoustic prime mover.

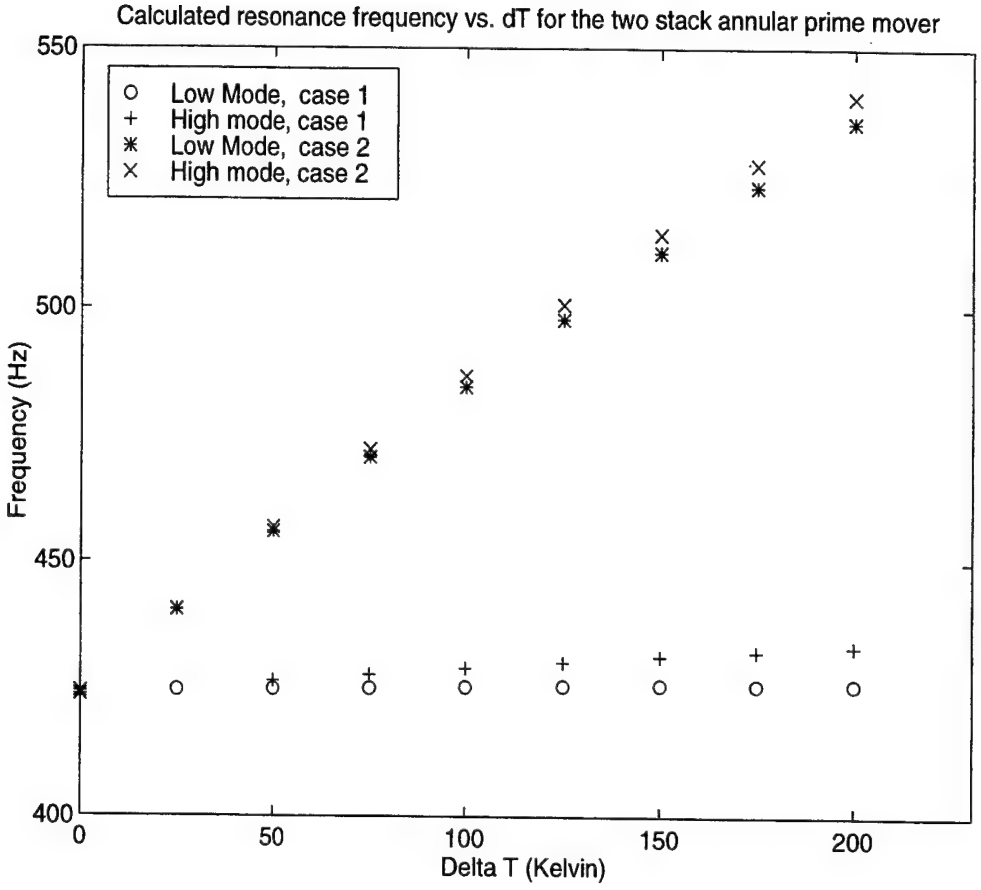

Figure 4.16 The calculated resonance frequencies for the two stack annular prime mover. Case 1: The duct between the two hot heat exchangers is held at T_a. Case 2: The duct between the two hot heat exchangers is held at T_h.

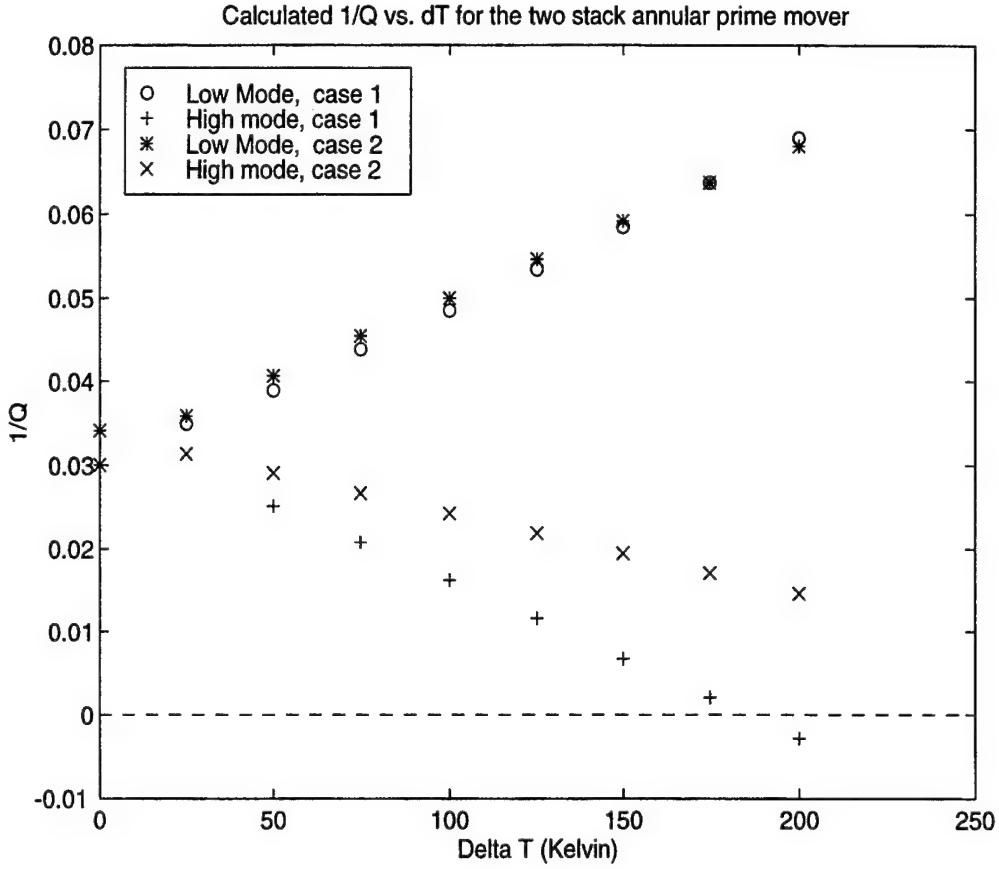

Figure 4.17 The calculated $1/Q$ for the low mode and high mode for the two stack annular prime mover. Case 1: The duct between the two hot heat exchangers is held at T_a. Case 2: The duct between the two hot heat exchangers is held at T_h.

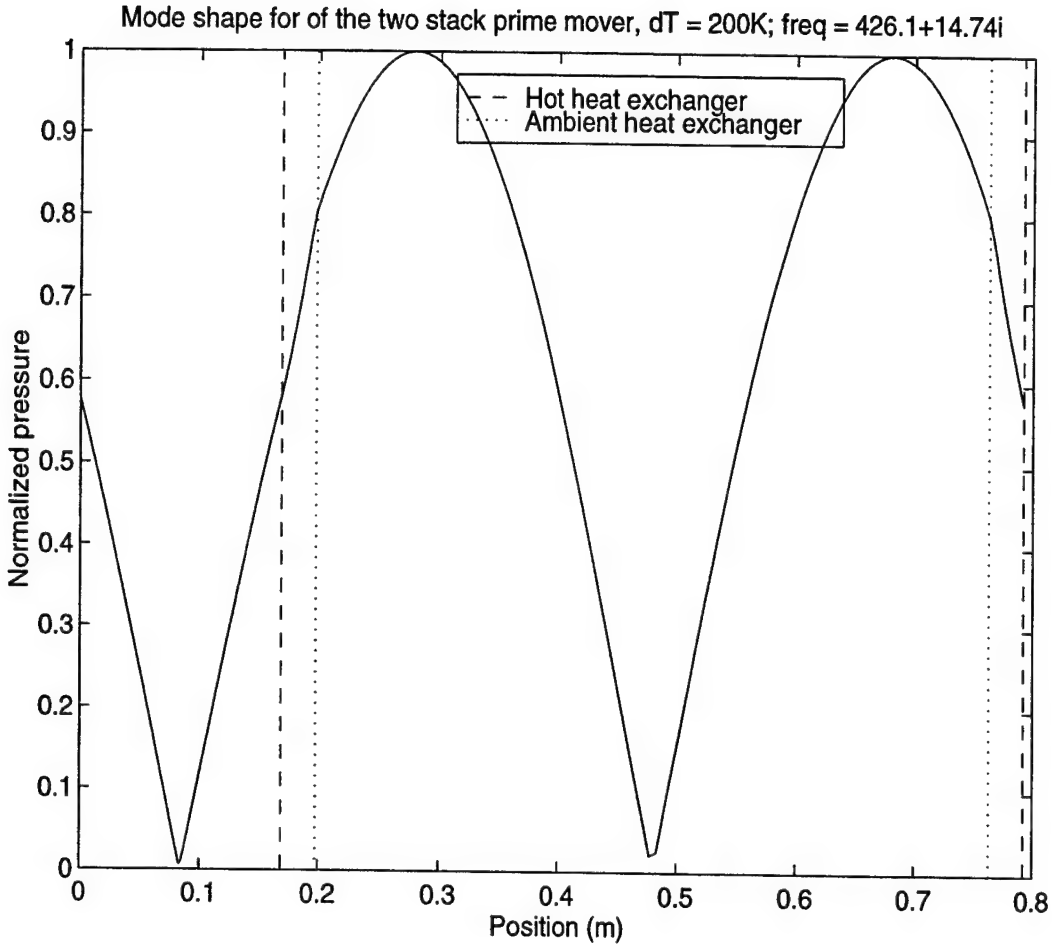

Figure 4.18 The calculated mode shape of the low mode of the two stack annular prime mover at $\Delta T = 200$ K. Case 1: The duct between the two hot heat exchangers is held at $T_a = 293$ K.

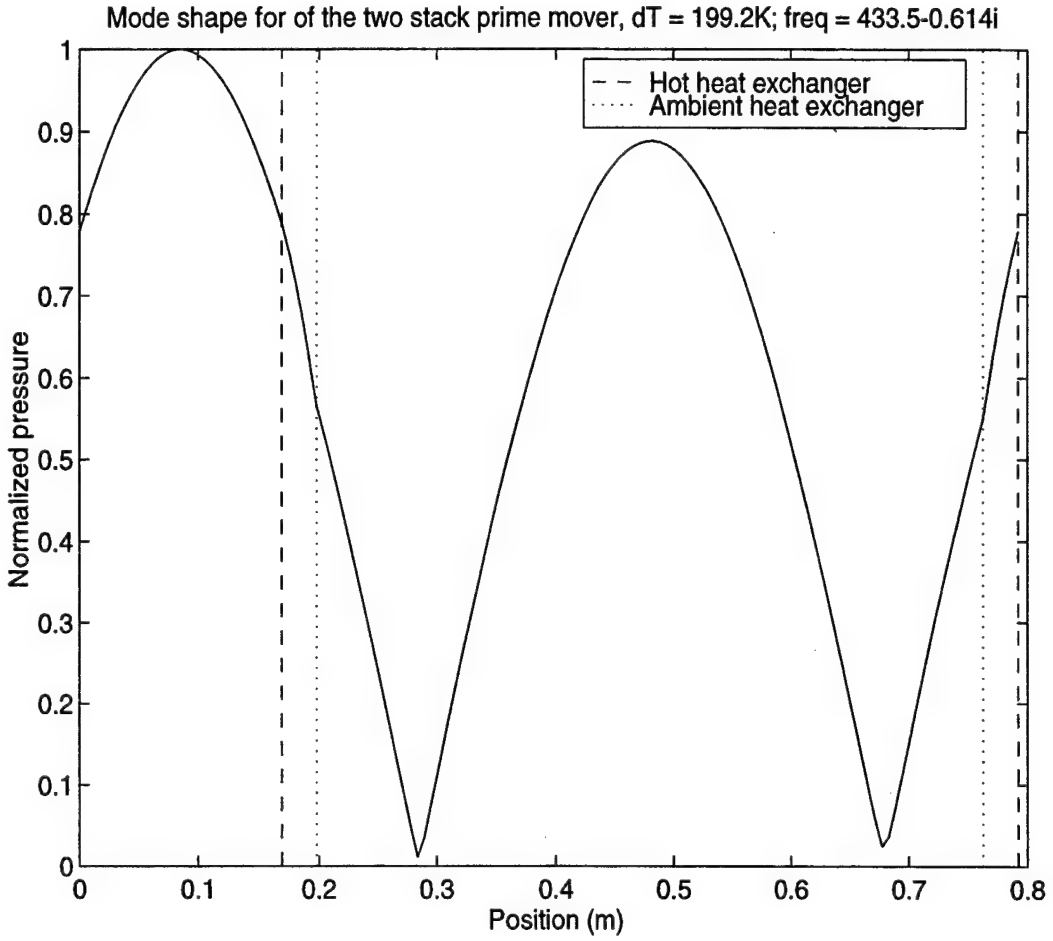

Figure 4.19 The calculated mode shape of the high mode of the two stack annular prime mover at ΔT = 200 K. Case 1: The duct between the two hot heat exchangers is held at T_a = 293 K.

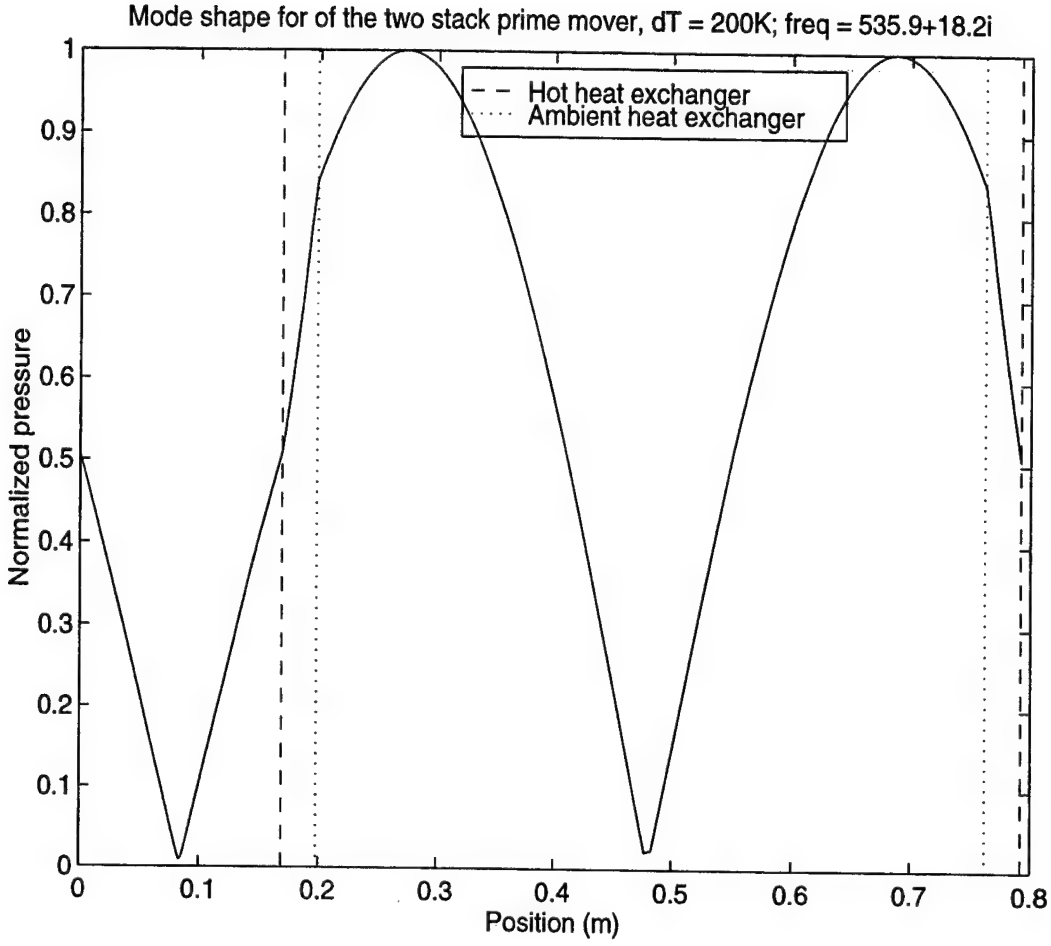

Figure 4.20 The calculated mode shape of the low mode of the two stack annular prime mover at $\Delta T = 200$ K. Case 2: The duct between the two hot heat exchangers is held at $T_h = 493$ K.

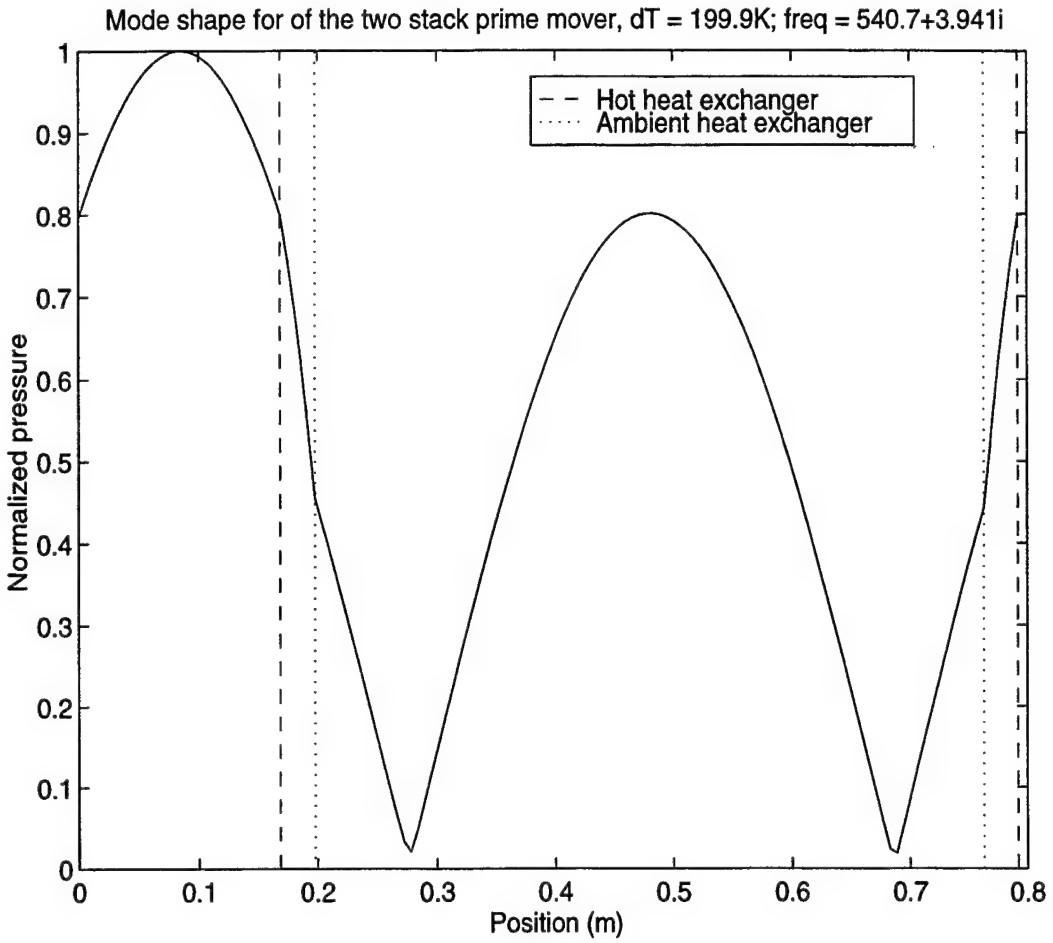

Figure 4.21 The calculated mode shape of the high mode of the two stack annular prime mover at $\Delta T = 200$ K. Case 2: The duct between the two hot heat exchangers is held at $T_h = 493$ K.

V. SUMMARY AND CONCLUSION

The objective of this dissertation is to investigate a thermoacoustic prime mover having periodic boundary conditions both experimentally and theoretically. The experimental approach has been to design, build, and test an annular thermoacoustic prime mover. The resonance frequencies, quality factors, and the mode shapes of the prime mover are measured as functions of the temperature difference across the prime mover stack. The experimental resonance frequencies and Q's are determined from pole-zero analysis of the measured frequency response.

An important aspect of this dissertation is the computational analysis of a thermoacoustic device with periodic boundary conditions. Two approaches were taken. First an existing program, DeltaE, was applied to this novel geometry. It was found that DeltaE can be applied to the problem, but has some disadvantages. It is difficult to extract Q's below onset and awkward to extract mode shapes. It is also difficult to include temperature gradients in ducts.

Because of these problems, a new program was developed. It uses the same basic approach as DeltaE, but overcomes the disadvantages. The complex eigenfrequency is used to extract resonance frequencies and Q's.

The results of this dissertation indicate that under all but perhaps extreme conditions an annular prime mover will not reach onset. The reason is well understood. The eigenmodes of a single-stack annular prime mover do not support thermoacoustic growth. This finding lead to the investigation of a constricted annular prime mover. The idea is that the constriction could impose dominating boundary conditions on the prime mover thus

altering the eigenmodes. It was shown that decreasing the porosity of the constriction forced the prime mover into onset. The porosity and location of the constriction is used to adjust the eigenmodes of the system so that thermoacoustic growth is supported.

Another way to produce eigenmodes that support thermoacoustic growth is to introduce a symmetry into the system which shifts the nodes and antinodes of the modes off the stacks, such that for one of the modes a pressure antinode is near the hot end of the stacks. It is predicted that a two-stack annular prime mover will reach onset. This design is an area for future research.

Another area for future study is end correction for stacks. It was shown in this dissertation that inclusion of end corrections does affect the predicted resonance frequencies and Q's. Determining the proper end corrections for realistic stack geometries is likely to be a nontrivial project.

APPENDIX A.1 THE DELTAE INPUT FILE FOR THE LOW FREQUENCY MODE OF THE ANNULAR THERMOACOUSTIC PRIME MOVER

```
TITLE Annular resonator  (file : to2dTflowC.in)
!Created@23:18:35 02-MAY-97 with DeltaE Vers. 3.0b1 for the Power Macintosh
!---------------------------------  0 ---------------------------------
BEGIN     Initial
1.0130E+05     a Mean P   Pa          16.63          A |p|@0  G( 0d)    P
427.0          b Freq.    Hz          -43.90         B Ph(p)0 G( 0e)    P
293.0          c T-beg    K           6.7062E-04     C |U|@0  G( 0f)    P
16.63          d |p|@0    Pa      G   38.50          D Ph(U)0 G( 0g)    P
-43.90         e Ph(p)0   deg     G   -1.8309E-03    E HeatIn G(27e)    P
6.7062E-04     f |U|@0    m^3/s   G
38.50          g Ph(U)0   deg     G
air       Gas type
ideal          Solid type
!---------------------------------  1 ---------------------------------
SOFTEND   1
0.0000         a Re(Z)        (t)     16.63          A |p|      Pa
0.0000         b Im(Z)        (t)     -43.90         B Ph(p)    deg
                                      6.7062E-04     C |U|      m^3/s
                                      38.50          D Ph(U)    deg
                                      7.3673E-04     E Hdot     W
                                      7.3673E-04     F Work     W
                                      2.0847E-02     G Re(Z)
sameas 0       Gas type               -0.1564        H Im(Z)
ideal          Solid type             293.0          I  T       K
!---------------------------------  2 ---------------------------------
ISODUCT   Duct
2.6300E-03     a Area     m^2         42.05          A |p|      Pa
0.2050         b Perim    m           -48.73         B Ph(p)    deg
3.1788E-02     c Length   m           6.2404E-04     C |U|      m^3/s
                                      38.20          D Ph(U)    deg
sameas 0       Gas type               7.0088E-04     E Hdot     W
```

ideal	Solid type		7.0088E-04	F Work	W
!---------- 3 ----------					
ISODUCT	Duct				
2.6300E-03	a Area	m^2	64.95	A |p|	Pa
0.2050	b Perim	m	-49.96	B Ph(p)	deg
3.1788E-02	c Length	m	5.3889E-04	C |U|	m^3/s
			37.86	D Ph(U)	deg
sameas 0	Gas type		6.6858E-04	E Hdot	W
ideal	Solid type		6.6858E-04	F Work	W
!---------- 4 ----------					
ISODUCT	Duct				
2.6300E-03	a Area	m^2	83.85	A |p|	Pa
0.2050	b Perim	m	-50.55	B Ph(p)	deg
3.1788E-02	c Length	m	4.2045E-04	C |U|	m^3/s
			37.36	D Ph(U)	deg
sameas 0	Gas type		6.4101E-04	E Hdot	W
ideal	Solid type		6.4101E-04	F Work	W
!---------- 5 ----------					
ISODUCT	Duct				
2.6300E-03	a Area	m^2	97.57	A |p|	Pa
0.2050	b Perim	m	-50.93	B Ph(p)	deg
3.1788E-02	c Length	m	2.7606E-04	C |U|	m^3/s
			36.44	D Ph(U)	deg
sameas 0	Gas type		6.1820E-04	E Hdot	W
ideal	Solid type		6.1820E-04	F Work	W
!---------- 6 ----------					
ISODUCT	Duct				
2.6300E-03	a Area	m^2	105.3	A |p|	Pa
0.2050	b Perim	m	-51.21	B Ph(p)	deg
3.1788E-02	c Length	m	1.1484E-04	C |U|	m^3/s
			33.10	D Ph(U)	deg
sameas 0	Gas type		5.9903E-04	E Hdot	W
ideal	Solid type		5.9903E-04	F Work	W
!---------- 7 ----------					
ISODUCT	Duct				
2.6300E-03	a Area	m^2	106.4	A |p|	Pa P

0.2050	b Perim	m	-51.45	B Ph(p)	deg
3.1788E-02	c Length	m	5.5371E-05	C |U|	m^3/s
			-130.1	D Ph(U)	deg
sameas 0	Gas type		5.8148E-04	E Hdot	W
ideal	Solid type		5.8148E-04	F Work	W

!---------- 8 ----------

ISODUCT	Duct				
2.6300E-03	a Area	m^2	101.0	A |p|	Pa
0.2050	b Perim	m	-51.67	B Ph(p)	deg
3.1788E-02	c Length	m	2.1977E-04	C |U|	m^3/s
			-138.8	D Ph(U)	deg
sameas 0	Gas type		5.6316E-04	E Hdot	W
ideal	Solid type		5.6316E-04	F Work	W

!---------- 9 ----------

ISODUCT	Duct	7			
2.6300E-03	a Area	m^2	89.39	A |p|	Pa
0.2050	b Perim	m	-51.92	B Ph(p)	deg
3.1788E-02	c Length	m	3.7131E-04	C |U|	m^3/s
			-140.0	D Ph(U)	deg
sameas 0	Gas type		5.4183E-04	E Hdot	W
ideal	Solid type		5.4183E-04	F Work	W

!---------- 10 ----------

ISODUCT	Duct	8			
2.6300E-03	a Area	m^2	72.22	A |p|	Pa
0.2050	b Perim	m	-52.23	B Ph(p)	deg
3.1788E-02	c Length	m	4.9997E-04	C |U|	m^3/s
			-140.6	D Ph(U)	deg
sameas 0	Gas type		5.1603E-04	E Hdot	W
ideal	Solid type		5.1603E-04	F Work	W

!---------- 11 ----------

ISODUCT	Duct				
2.6300E-03	a Area	m^2	50.59	A |p|	Pa
0.2050	b Perim	m	-52.75	B Ph(p)	deg
3.1788E-02	c Length	m	5.9773E-04	C |U|	m^3/s
			-140.9	D Ph(U)	deg
sameas 0	Gas type		4.8535E-04	E Hdot	W

ideal	Solid type		4.8535E-04	F Work W
!---------- 12 ----------				
ISODUCT	Duct			
2.6300E-03	a Area	m^2	25.84	A |p| Pa
0.2050	b Perim	m	-54.17	B Ph(p) deg
3.1788E-02	c Length	m	6.5855E-04	C |U| m^3/s
			-141.1	D Ph(U) deg
sameas 0	Gas type		4.5059E-04	E Hdot W
ideal	Solid type		4.5059E-04	F Work W
!---------- 13 ----------				
ISODUCT	Duct			
2.6300E-03	a Area	m^2	1.340	A |p| Pa
0.2050	b Perim	m	-165.9	B Ph(p) deg
3.1788E-02	c Length	m	6.7865E-04	C |U| m^3/s
			-141.3	D Ph(U) deg
sameas 0	Gas type		4.1353E-04	E Hdot W
ideal	Solid type		4.1353E-04	F Work W
!---------- 14 ----------				
ISODUCT	Duct			
2.6300E-03	a Area	m^2	26.91	A |p| Pa
0.2050	b Perim	m	131.0	B Ph(p) deg
3.1788E-02	c Length	m	6.5679E-04	C |U| m^3/s
			-141.5	D Ph(U) deg
sameas 0	Gas type		3.7652E-04	E Hdot W
ideal	Solid type		3.7652E-04	F Work W
!---------- 15 ----------				
ISODUCT	Duct			
2.6300E-03	a Area	m^2	51.56	A |p| Pa
0.2050	b Perim	m	129.7	B Ph(p) deg
3.1788E-02	c Length	m	5.9432E-04	C |U| m^3/s
			-141.6	D Ph(U) deg
sameas 0	Gas type		3.4190E-04	E Hdot W
ideal	Solid type		3.4190E-04	F Work W
!---------- 16 ----------				
ISODUCT	Duct			
2.6300E-03	a Area	m^2	73.03	A |p| Pa

0.2050	b Perim	m	129.2	B Ph(p) deg
3.1788E-02	c Length	m	4.9511E-04	C |U| m^3/s
			-141.8	D Ph(U) deg
sameas 0	Gas type		3.1142E-04	E Hdot W
ideal	Solid type		3.1142E-04	F Work W

!---------- 17 ----------

ISODUCT	Duct			
2.6300E-03	a Area	m^2	89.99	A |p| Pa
0.2050	b Perim	m	128.9	B Ph(p) deg
3.1788E-02	c Length	m	3.6528E-04	C |U| m^3/s
			-142.1	D Ph(U) deg
sameas 0	Gas type		2.8583E-04	E Hdot W
ideal	Solid type		2.8583E-04	F Work W

!---------- 18 ----------

ISODUCT	Duct			
2.6300E-03	a Area	m^2	101.4	A |p| Pa
0.2050	b Perim	m	128.8	B Ph(p) deg
3.1788E-02	c Length	m	2.1289E-04	C |U| m^3/s
			-142.6	D Ph(U) deg
sameas 0	Gas type		2.6468E-04	E Hdot W
ideal	Solid type		2.6468E-04	F Work W

!---------- 19 ----------

ISODUCT	Duct			
2.6300E-03	a Area	m^2	106.5	A |p| Pa
0.2050	b Perim	m	128.7	B Ph(p) deg
3.1788E-02	c Length	m	4.7479E-05	C |U| m^3/s
			-146.9	D Ph(U) deg
sameas 0	Gas type		2.4644E-04	E Hdot W
ideal	Solid type		2.4644E-04	F Work W

!---------- 20 ----------

VDUCER	Driver			
1.0000E-09	a Re(Ze)	ohms	106.5	A |p| Pa P
0.0000	b Im(Ze)		128.7	B Ph(p) deg
1.0000E+04	c Re(T1)	V-s/m^3	1.4217E-04	C |U| m^3/s
0.0000	d Im(T1)	V-s/m^3	-169.5	D Ph(U) deg
-1.0000E+04	e Re(T2)	Pa/A	3.5727E-03	E Hdot W

0.0000	f Im(T2) Pa/A	3.5727E-03	F Work W
1.0000E-09	g Re(Zm) Pa-s/m^3	3.3263E-03	G WorkIn W
1.0000E-09	h Im(Zm) Pa-s/m^3	1.000	H Volts V
1.000	i AplVol V	1.0651E-02	I Amps V
		-51.35	J Ph(Ze) deg
sameas 0	Gas type	1.0000E-04	K |Ux| m^3/s
ideal	Solid type	-180.0	L Ph(-Ux deg

!---------- 21 ----------

ISODUCT	Duct		
2.6300E-03	a Area m^2	108.1	A |p| Pa
0.2050	b Perim m	127.3	B Ph(p) deg
3.1788E-02	c Length m	7.9112E-05	C |U| m^3/s
		93.49	D Ph(U) deg
sameas 0	Gas type	3.5543E-03	E Hdot W
ideal	Solid type	3.5543E-03	F Work W

!---------- 22 ----------

SODUCT	Duct		
2.6300E-03	a Area m^2	103.1	A |p| Pa
0.2050	b Perim m	125.9	B Ph(p) deg
3.1788E-02	c Length m	2.2143E-04	C |U| m^3/s
		53.91	D Ph(U) deg
sameas 0	Gas type	3.5352E-03	E Hdot W
ideal	Solid type	3.5352E-03	F Work W

!---------- 23 ----------

ISODUCT	Duct		
2.6300E-03	a Area m^2	91.74	A |p| Pa
0.2050	b Perim m	124.2	B Ph(p) deg
3.1788E-02	c Length m	3.7161E-04	C |U| m^3/s
		46.13	D Ph(U) deg
sameas 0	Gas type	3.5132E-03	E Hdot W
ideal	Solid type	3.5132E-03	F Work W

!---------- 24 ----------

ISODUCT	Duct		
2.6300E-03	a Area m^2	74.83	A |p| Pa
0.2050	b Perim m	122.0	B Ph(p) deg
3.1788E-02	c Length m	5.0174E-04	C |U| m^3/s

			42.72	D Ph(U) deg
sameas 0	Gas type		3.4867E-03	E Hdot W
ideal	Solid type		3.4867E-03	F Work W
!---------- 25 ----------				
ISODUCT	Duct			
2.6300E-03	a Area	m^2	53.48	A |p| Pa
0.2050	b Perim	m	118.2	B Ph(p) deg
3.1788E-02	c Length	m	6.0191E-04	C |U| m^3/s
			40.63	D Ph(U) deg
sameas 0	Gas type		3.4553E-03	E Hdot W
ideal	Solid type		3.4553E-03	F Work W
!---------- 26 ----------				
ISODUCT	Duct			
2.6300E-03	a Area	m^2	29.40	A |p| Pa
0.2050	b Perim	m	108.6	B Ph(p) deg
3.1788E-02	c Length	m	6.6543E-04	C |U| m^3/s
			39.08	D Ph(U) deg
sameas 0	Gas type		3.4195E-03	E Hdot W
ideal	Solid type		3.4195E-03	F Work W
!---------- 27 ----------				
HXFRST	Ambient HX			
sameas 3a	a Area	m^2	23.02	A |p| Pa
0.6290	b GasA/A		103.2	B Ph(p) deg
5.0800E-03	c Length	m	6.6930E-04	C |U| m^3/s
1.7018E-03	d y0	m	38.94	D Ph(U) deg
-1.8309E-03	e HeatIn	W G	1.5886E-03	E Hdot W
293.0	f Est-T	K (t)	3.3455E-03	F Work W
sameas 0	Gas type		-1.8309E-03	G Heat W
copper	Solid type		293.0	H MetalT K
!---------- 28 ----------				
STKSLAB	Prime Mover Stack			
2.6300E-03	a Area	m^2	16.26	A |p| Pa
0.6220	b GasA/A		-43.67	B Ph(p) deg
2.4000E-02	c Length	m	6.7080E-04	C |U| m^3/s
3.0480E-04	d y0	m	38.51	D Ph(U) deg
7.5000E-05	e Lplate	m	1.5886E-03	E Hdot W

```
                                7.4220E-04      F Work     W
                                293.0           G T-beg    K
sameas  0       Gas type        293.0           H T-end    K
kapton          Solid type      -2.6033E-03     I StkWrk   W
!-------------------------------- 29 --------------------------------
HXLAST    Cold HX
sameas  3a      a Area     m^2   16.63           A |p|      Pa
 0.7050         b GasA/A         -43.90          B Ph(p)    deg
3.0480E-04      c Length   m     6.7062E-04      C |U|      m^3/s
1.2540E-03      d y0       m     38.51           D Ph(U)    deg
0.0000          e HeatIn   W (t) 7.3668E-04      E Hdot     W
293.0           f Est-T    K =29H? 7.3668E-04    F Work     W
sameas  0       Gas type        -8.5195E-04     G Heat     W
copper          Solid type      293.0           H MetalT   K
!-------------------------------- 30 --------------------------------
SOFTEND
0.0000          a Re(Z)       (t) 16.63         A |p|      Pa
0.0000          b Im(Z)       (t) -43.90        B Ph(p)    deg
                                6.7062E-04      C |U|      m^3/s
                                38.51           D Ph(U)    deg
                                7.3668E-04      E Hdot     W
                                7.3668E-04      F Work     W
                                2.0846E-02      G Re(Z)
sameas  0       Gas type        -0.1564         H Im(Z)
ideal           Solid type      293.0           I T        K
!-------------------------------- 31 --------------------------------
DIFFTAR         |p| mismatch
0.0000          a TargDi    =31A?   8.0065E-05  A D1-D2
1A b D1Addr
30A c D2Addr
!-------------------------------- 32 --------------------------------
DIFFTAR         Ph(p) mismatch
0.0000          a TargDi    =32A?   3.3780E-04  A D1-D2
1B b D1Addr
30B c D2Addr
!-------------------------------- 33 --------------------------------
```

```
DIFFTAR      |U|  mismatch
0.0000       a TargDi        =33A?   1.3884E-09   A D1-D2
1C b D1Addr
30C c D2Addr
!-------------------------------- 34 --------------------------------
DIFFTAR      Ph(U) mismatch
0.0000       a TargDi        =34A?   -1.0691E-04 A D1-D2
1D b D1Addr
30D c D2Addr

! The restart information below was generated by a previous run
! You may wish to delete this information before starting a run
! where you will (interactively) specify a different iteration
! mode.  Edit this table only if you really know your model!
INVARS     5  0  4  0  5  0  6  0  7 27  5
TARGS      5 29  6 31  1 32  1 33  1 34  1
SPECIALS   0
PLTVAR     7  0  2 -1  1  0  1  0  2  0  3  0  4  0  5  7  1 20  1
! Plot start, end, and step values.  May be edited if you wish.
! Outer Loop:                    | Inner Loop .
   410.0       427.0       0.2000       1.000        1.000        1.000
```

APPENDIX A.2 THE DELTAE INPUT FILE FOR THE HIGH FREQUENCY MODE OF THE ANNULAR THERMOACOUSTIC PRIME MOVER

```
TITLE     Annular resonator (file :: to2dTfhighC.in)
!Created@12:00:08 02-MAY-97 with DeltaE Vers. 3.0b1 for the Power Macintosh
!-------------------------------- 0 --------------------------------
BEGIN     Initial
1.0130E+05     a Mean P   Pa          0.0000    A |p|@0  G( 0d)    P
430.5          b Freq.    Hz          0.0000    B Ph(p)0 G( 0e)    P
293.0          c T-beg    K           0.0000    C |U|@0  G( 0f)    P
500.0          d |p|@0    Pa    G     0.0000    D Ph(U)0 G( 0g)    P
0.0000         e Ph(p)0   deg   G     0.0000    E HeatIn G(27e)    P
2.9000E-04     f |U|@0    m^3/s G
0.0000         g Ph(U)0   deg   G
air            Gas type
ideal          Solid type
!-------------------------------- 1 --------------------------------
SOFTEND   1
0.0000         a Re(Z)          (t)   0.0000    A |p|      Pa
0.0000         b Im(Z)          (t)   0.0000    B Ph(p)    deg
                                       0.0000    C |U|      m^3/s
                                       0.0000    D Ph(U)    deg
                                       0.0000    E Hdot     W
                                       0.0000    F Work     W
                                       0.0000    G Re(Z)
sameas  0  Gas type                    0.0000    H Im(Z)
ideal      Solid type                  0.0000    I  T       K
!-------------------------------- 2 --------------------------------
ISODUCT   Duct
2.6300E-03     a Area     m^2         0.0000    A |p|      Pa
0.2050         b Perim    m           0.0000    B Ph(p)    deg
3.1788E-02     c Length   m           0.0000    C |U|      m^3/s
                                       0.0000    D Ph(U)    deg
sameas  0      Gas type                0.0000    E Hdot     W
ideal          Solid type              0.0000    F Work     W
```

```
!-------------------------------- 3 --------------------------------
ISODUCT   Duct
2.6300E-03    a Area    m^2          0.0000    A |p|     Pa
0.2050        b Perim   m            0.0000    B Ph(p)   deg
3.1788E-02    c Length  m            0.0000    C |U|     m^3/s
                                     0.0000    D Ph(U)   deg
sameas 0      Gas type               0.0000    E Hdot    W
ideal         Solid type             0.0000    F Work    W
!-------------------------------- 4 --------------------------------
ISODUCT   Duct
2.6300E-03    a Area    m^2          0.0000    A |p|     Pa
0.2050        b Perim   m            0.0000    B Ph(p)   deg
3.1788E-02    c Length  m            0.0000    C |U|     m^3/s
                                     0.0000    D Ph(U)   deg
sameas 0      Gas type               0.0000    E Hdot    W
ideal         Solid type             0.0000    F Work    W
!-------------------------------- 5 --------------------------------
ISODUCT   Duct
2.6300E-03    a Area    m^2          0.0000    A |p|     Pa
0.2050        b Perim   m            0.0000    B Ph(p)   deg
3.1788E-02    c Length  m            0.0000    C |U|     m^3/s
                                     0.0000    D Ph(U)   deg
sameas 0      Gas type               0.0000    E Hdot    W
ideal         Solid type             0.0000    F Work    W
!-------------------------------- 6 --------------------------------
ISODUCT   Duct
2.6300E-03    a Area    m^2          0.0000    A |p|     Pa
0.2050        b Perim   m            0.0000    B Ph(p)   deg
3.1788E-02    c Length  m            0.0000    C |U|     m^3/s
                                     0.0000    D Ph(U)   deg
sameas 0      Gas type               0.0000    E Hdot    W
ideal         Solid type             0.0000    F Work    W
!-------------------------------- 7 --------------------------------
ISODUCT   Duct
2.6300E-03    a Area    m^2          0.0000    A |p|     Pa
0.2050        b Perim   m            0.0000    B Ph(p)   deg
```

3.1788E-02	c Length	m	0.0000	C |U|	m^3/s
			0.0000	D Ph(U)	deg
sameas 0	Gas type		0.0000	E Hdot	W
ideal	Solid type		0.0000	F Work	W

!---------- 8 ----------

ISODUCT	Duct				
2.6300E-03	a Area	m^2	0.0000	A |p|	Pa
0.2050	b Perim	m	0.0000	B Ph(p)	deg
3.1788E-02	c Length	m	0.0000	C |U|	m^3/s
			0.0000	D Ph(U)	deg
sameas 0	Gas type		0.0000	E Hdot	W
ideal	Solid type		0.0000	F Work	W

!---------- 9 ----------

ISODUCT	Duct				
2.6300E-03	a Area	m^2	0.0000	A |p|	Pa
0.2050	b Perim	m	0.0000	B Ph(p)	deg
3.1788E-02	c Length	m	0.0000	C |U|	m^3/s
			0.0000	D Ph(U)	deg
sameas 0	Gas type		0.0000	E Hdot	W
ideal	Solid type		0.0000	F Work	W

!---------- 10 ----------

ISODUCT	Duct				
2.6300E-03	a Area	m^2	0.0000	A |p|	Pa
0.2050	b Perim	m	0.0000	B Ph(p)	deg
3.1788E-02	c Length	m	0.0000	C |U|	m^3/s
			0.0000	D Ph(U)	deg
sameas 0	Gas type		0.0000	E Hdot	W
ideal	Solid type		0.0000	F Work	W

!---------- 11 ----------

ISODUCT	Duct				
2.6300E-03	a Area	m^2	0.0000	A |p|	Pa
0.2050	b Perim	m	0.0000	B Ph(p)	deg
3.1788E-02	c Length	m	0.0000	C |U|	m^3/s
			0.0000	D Ph(U)	deg
sameas 0	Gas type		0.0000	E Hdot	W
ideal	Solid type		0.0000	F Work	W

```
!-------------------------------- 12 --------------------------------
ISODUCT   Duct
2.6300E-03    a Area     m^2          0.0000    A |p|      Pa
0.2050        b Perim    m            0.0000    B Ph(p)    deg
3.1788E-02    c Length   m            0.0000    C |U|      m^3/s
                                      0.0000    D Ph(U)    deg
sameas  0     Gas type                0.0000    E Hdot     W
ideal         Solid type              0.0000    F Work     W
!-------------------------------- 13 --------------------------------
ISODUCT   Duct
2.6300E-03    a Area     m^2          0.0000    A |p|      Pa
0.2050        b Perim    m            0.0000    B Ph(p)    deg
3.1788E-02    c Length   m            0.0000    C |U|      m^3/s
                                      0.0000    D Ph(U)    deg
sameas  0     Gas type                0.0000    E Hdot     W
ideal         Solid type              0.0000    F Work     W
!-------------------------------- 14 --------------------------------
VDUCER    Driver
1.0000E-09    a Re(Ze)   ohms         0.0000    A |p|      Pa
0.0000        b Im(Ze)                0.0000    B Ph(p)    deg
1.0000E+04    c Re(T1)   V-s/m^3      0.0000    C |U|      m^3/s
0.0000        d Im(T1)   V-s/m^3      0.0000    D Ph(U)    deg
-1.0000E+04   e Re(T2)   Pa/A         0.0000    E Hdot     W
0.0000        f Im(T2)   Pa/A         0.0000    F Work     W
1.0000E-09    g Re(Zm)   Pa-s/m^3     0.0000    G WorkIn   W
1.0000E-09    h Im(Zm)   Pa-s/m^3     0.0000    H Volts    V
1.000         i AplVol   V            0.0000    I Amps     V
                                      0.0000    J Ph(Ze)   deg
sameas  0     Gas type                0.0000    K |Ux|     m^3/s
ideal         Solid type              0.0000    L Ph(-Ux   deg
!-------------------------------- 15 --------------------------------
ISODUCT   Constriction
2.6300E-03    a Area     m^2          0.0000    A |p|      Pa
0.2050        b Perim    m            0.0000    B Ph(p)    deg
3.1788E-02    c Length   m            0.0000    C |U|      m^3/s
                                      0.0000    D Ph(U)    deg
```

```
sameas  0       Gas type                0.0000   E Hdot     W
ideal           Solid type              0.0000   F Work     W
!-------------------------------- 16 --------------------------------
ISODUCT   Duct          7
2.6300E-03      a Area      m^2         0.0000   A |p|      Pa
0.2050          b Perim     m           0.0000   B Ph(p)    deg
3.1788E-02      c Length    m           0.0000   C |U|      m^3/s
                                        0.0000   D Ph(U)    deg
sameas  0       Gas type                0.0000   E Hdot     W
ideal           Solid type              0.0000   F Work     W
!-------------------------------- 17 --------------------------------
ISODUCT   Duct          8
2.6300E-03      a Area      m^2         0.0000   A |p|      Pa
0.2050          b Perim     m           0.0000   B Ph(p)    deg
3.1788E-02      c Length    m           0.0000   C |U|      m^3/s
                                        0.0000   D Ph(U)    deg
sameas  0       Gas type                0.0000   E Hdot     W
ideal           Solid type              0.0000   F Work     W
!-------------------------------- 18 --------------------------------
ISODUCT   Duct
2.6300E-03      a Area      m^2         0.0000   A |p|      Pa
0.2050          b Perim     m           0.0000   B Ph(p)    deg
3.1788E-02      c Length    m           0.0000   C |U|      m^3/s
                                        0.0000   D Ph(U)    deg
sameas  0       Gas type                0.0000   E Hdot     W
ideal           Solid type              0.0000   F Work     W
!-------------------------------- 19 --------------------------------
ISODUCT   Duct
2.6300E-03      a Area      m^2         0.0000   A |p|      Pa
0.2050          b Perim     m           0.0000   B Ph(p)    deg
3.1788E-02      c Length    m           0.0000   C |U|      m^3/s
                                        0.0000   D Ph(U)    deg
sameas  0       Gas type                0.0000   E Hdot     W
ideal           Solid type              0.0000   F Work     W
!-------------------------------- 20 --------------------------------
ISODUCT   Constriction
```

```
2.6300E-03    a Area     m^2          0.0000    A |p|      Pa
0.2050        b Perim    m            0.0000    B Ph(p)    deg
3.1788E-02    c Length   m            0.0000    C |U|      m^3/s
                                      0.0000    D Ph(U)    deg
sameas  0     Gas type                0.0000    E Hdot     W
ideal         Solid type              0.0000    F Work     W
!-------------------------------- 21 --------------------------------
ISODUCT   Duct
2.6300E-03    a Area     m^2          0.0000    A |p|      Pa
0.2050        b Perim    m            0.0000    B Ph(p)    deg
3.1788E-02    c Length   m            0.0000    C |U|      m^3/s
                                      0.0000    D Ph(U)    deg
sameas  0     Gas type                0.0000    E Hdot     W
ideal         Solid type              0.0000    F Work     W
!-------------------------------- 22 --------------------------------
ISODUCT   Duct
2.6300E-03    a Area     m^2          0.0000    A |p|      Pa
0.2050        b Perim    m            0.0000    B Ph(p)    deg
3.1788E-02    c Length   m            0.0000    C |U|      m^3/s
                                      0.0000    D Ph(U)    deg
sameas  0     Gas type                0.0000    E Hdot     W
ideal         Solid type              0.0000    F Work     W
!-------------------------------- 23 --------------------------------
ISODUCT   Duct
2.6300E-03    a Area     m^2          0.0000    A |p|      Pa
0.2050        b Perim    m            0.0000    B Ph(p)    deg
3.1788E-02    c Length   m            0.0000    C |U|      m^3/s
                                      0.0000    D Ph(U)    deg
sameas  0     Gas type                0.0000    E Hdot     W
ideal         Solid type              0.0000    F Work     W
!-------------------------------- 24 --------------------------------
ISODUCT   Duct
2.6300E-03    a Area     m^2          0.0000    A |p|      Pa
0.2050        b Perim    m            0.0000    B Ph(p)    deg
3.1788E-02    c Length   m            0.0000    C |U|      m^3/s
                                      0.0000    D Ph(U)    deg
```

sameas 0	Gas type	0.0000	E Hdot	W
ideal	Solid type	0.0000	F Work	W

!---------- 25 ----------

ISODUCT	Duct			
2.6300E-03	a Area m^2	0.0000	A |p|	Pa
0.2050	b Perim m	0.0000	B Ph(p)	deg
3.1788E-02	c Length m	0.0000	C |U|	m^3/s
		0.0000	D Ph(U)	deg
sameas 0	Gas type	0.0000	E Hdot	W
ideal	Solid type	0.0000	F Work	W

!---------- 26 ----------

ISODUCT	Duct			
2.6300E-03	a Area m^2	0.0000	A |p|	Pa
0.2050	b Perim m	0.0000	B Ph(p)	deg
3.1788E-02	c Length m	0.0000	C |U|	m^3/s
		0.0000	D Ph(U)	deg
sameas 0	Gas type	0.0000	E Hdot	W
ideal	Solid type	0.0000	F Work	W

!---------- 27 ----------

HXFRST	Ambient HX			
sameas 3a	a Area m^2	23.02	A |p|	Pa
0.6290	b GasA/A	103.2	B Ph(p)	deg
5.0800E-03	c Length m	6.6930E-04	C |U|	m^3/s
1.7018E-03	d y0 m	38.94	D Ph(U)	deg
-1.8309E-03	e HeatIn W G	1.5886E-03	E Hdot	W
293.0	f Est-T K (t)	3.3455E-03	F Work	W
sameas 0	Gas type	-1.8309E-03	G Heat	W
copper	Solid type	293.0	H MetalT	K

!---------- 28 ----------

STKSLAB	Prime Mover Stack			
2.6300E-03	a Area m^2	16.26	A |p|	Pa
0.6220	b GasA/A	-43.67	B Ph(p)	deg
2.4000E-02	c Length m	6.7080E-04	C |U|	m^3/s
3.0480E-04	d y0 m	38.51	D Ph(U)	deg
7.5000E-05	e Lplate m	1.5886E-03	E Hdot	W
		7.4220E-04	F Work	W

```
                                293.0          G T-beg     K
sameas  0       Gas type        293.0          H T-end     K
kapton          Solid type     -2.6033         E-03 I StkWrk    W
!-------------------------------- 29 --------------------------------
HXLAST    Cold HX
sameas  3a      a Area     m^2  16.63          A |p|       Pa
0.7050          b GasA/A        -43.90         B Ph(p)     deg
3.0480E-04      c Length   m    6.7062E-04     C |U|       m^3/s
1.2540E-03      d y0       m    38.51          D Ph(U)     deg
0.0000          e HeatIn   W (t) 7.3668E-04    E Hdot      W
293.0           f Est-T    K =29H? 7.3668E-04  F Work      W
sameas  0       Gas type        -8.5195E-04    G Heat      W
copper          Solid type      293.0          H MetalT    K
!-------------------------------- 30 --------------------------------
SOFTEND
0.0000          a Re(Z)       (t) 0.0000       A |p|       Pa
0.0000          b Im(Z)       (t) 0.0000       B Ph(p)     deg
                                  0.0000       C |U|       m^3/s
                                  0.0000       D Ph(U)     deg
                                  0.0000       E Hdot      W
                                  0.0000       F Work      W
                                  0.0000       G Re(Z)
sameas  0       Gas type          0.0000       H Im(Z)
ideal           Solid type        0.0000       I  T        K
!-------------------------------- 31 --------------------------------
DIFFTAR         |p|  mismatch
 0.0000         a TargDi     =31A?   8.0065E-05   A D1-D2
1A b D1Addr
30A c D2Addr
!-------------------------------- 32 --------------------------------
DIFFTAR         Ph(p) mismatch
0.0000          a TargDi      =32A? 3.3780E-04   A D1-D2
1B b D1Addr
30B c D2Addr
!-------------------------------- 33 --------------------------------
DIFFTAR         |U|  mismatch
```

```
0.0000          a TargDi        =33A?   1.3884E-09   A D1-D2
1C b D1Addr
30C c D2Addr
!-------------------------------- 34 --------------------------------
DIFFTAR         Ph(U) mismatch
0.0000          a TargDi        =34A?   -1.0691E-04 A D1-D2
1D b D1Addr
30D c D2Addr

! The restart information below was generated by a previous run
! You may wish to delete this information before starting a run
! where you will (interactively) specify a different iteration
! mode.  Edit this table only if you really know your model!
INVARS      5  0  4  0  5  0  6  0  7 27  5
TARGS       5 29  6 31  1 32  1 33  1 34  1
SPECIALS    0
```

APPENDIX B. THE MATHEMATICA PROGRAM FOR THE LEAST SQUARE FIT TO THE FREQUENCY RESPONSE

```
(* This mathematica program read the plotting data file generated by *)
(* DeltaE  and perform a least square fit to find the resonance frequency      *)
ClearAll["Global`*"]
(* Read the data file generated by the DeltaE program. *)
(* In this example, the data file is flowDT100.de        *)
datfile=ReadList["flowDT100.de",Table[Number,{8}]];(* There are eight columns in  *)
                                                    (* the data file               *)
(* Select the data range used in the least square fit, column 1 is the frequencies *)
(* and column 7 is the pressure amplitude                                          *)
data=datfile[[Range[2,19],{1,7}]] (* Determine the bandwidth of fitting      *)
(* Initial guesses of A, f0, and Q *)
soln = {A->150,f0->437,Q->100};

Attributes[y]={Listable};

y[f_,A_,f0_,Q_] := A (f/f0)^2 Abs[Cot[Pi (f/f0-I/(2 Q))]/(Pi (f/f0-I/(2 Q)))];
Attributes[yy] = {Listable};
yy[f_] = y[f,A,f0,Q] /.soln;
xlist = Transpose[data][[1]];
ylist = Transpose[data][[2]];
rmserror[A_,f0_,Q_] := Sqrt[ Apply[Plus,(ylist - y[xlist, A,f0,Q])^2]];
rmserror[A,f0,Q]/.soln;
FindMinimum[rmserror[A,f0,Q],{A,{100,200}},{f0,{435,439}},{Q,{90,110}}]
(* A is an arbitrary constant, f0 the resonance frequency, Q the quality factor  *)
(* End of program  *)
```

APPENDIX C. THE MATLAB PROGRAM FOR THE ANNULAR THERMOACOUSTIC PRIME MOVER

Function **updateF.m**: The function performs the actual iteration to find the solutions for the constricted annular prime mover.

```
% Begin of function %
function  [y,iterations]=updateF(y);
%
%       usage [newy,iterations] = updateF(y)
%       This function implements picards method for updating y
%       solving f(y,x)=0 for an annular resonator
%       The input y vector is a 8 by 1 vector: [Tm;pre;pim;Ure;Uim;fre;fim;H2dot]
%       only the last 5 elements (i.e. Ure, Uim, fre, fim and H2) are updated
%       newy = y - inv(J)*f(y,x);
%       where J is the Jacobian of f(y)
%       REQUIRES: fdjacF.m, funcvF.m, computeL.m,
%       Note: Before run this program, make sure to adjust the area ratio and select the
%             right temperature (Just active the line for the temperature profile)
% Declare the global variables
global T2 T3 T4 T5 T6 T7 T8 T9 T10 T11 Th Tc Tmatrix Rs La Las R Rst r
r = 2.565e-2;           % Equivalent radius of the annular resonator, m
Rs = 0.7;               % The area ratio for the constriction
% Compute the equivalent inductance of constriction
      d = 0.0529;                 % Width of annulus, m
      h = 0.0497;                 % Height of annulus, m
      dc = d*sqrt(Rs);            % Width of the constriction, m
      hc = h*sqrt(Rs);            % Height of annulus, m
      dst = 4.28e-2;              % Width of a slit in the stack m
      hst = 6.12e-4;              % Height of a slit in the stack m
      La = computeL(d,h,dc,hc);   % Compute the equivalent inductance of constriction
      Las = computeL(d,h,dst,hst); % Compute the equivalent inductance of a slit in the
                                  % stack
      R = sqrt((dc*hc)./(d.*h));
```

```
Rst = sqrt((dst*hst)./(d.*h));    % Compute the equivalent area ratio for one slit
% The measured temperature profiles for all the measurements
% When run this main program, select the profile based on the porosity
% The low mode and high mode share the same temperature profile
% These temperatures are in °C
% Low mode and high mode with constriction Rs=0.1                    % Heater voltage
% Tmatrix=[21.0 21 21 21 21 21 21 21 21 20.6];                       % heater = 0V
% Tmatrix=[66.9 23.4 22.5 58.8 22.2 21.9 22.2 32.5 25.7 21.4];       % heater = 8V
% Tmatrix=[100.7 25.8 24.3 86.8 23.8 23.2 23.7 41.2 30.4 22.6];      % heater = 11V
% Tmatrix=[137.8 28.5 26.2 119.2 25.4 24.4 25.2 51.7 36.2 23.6];     % heater = 14V
% Tmatrix=[218.6 36.6 32.4 194.5 30.6 28.7 30.2 82.1 51.8 27.3];     % heater = 20V
% Tmatrix=[278.6 43.9 38 253.1 35.2 32.3 34.5 113.1 66.2 30.2];      % heater = 25V
% Low Mode and high mode with constriction Rs=0.3
% Tmatrix=[29.7 29.5 29.4 29.6 29.5 29.4 29.4 29.3 29.5 29.5];       % heater = 0V
% Tmatrix=[74.3 30 29.1 66.8 28.9 28.5 28.8 37.8 32.2 28.4];        % heater = 8V
% Tmatrix=[106.6 31.1 29.6 93.8 29.1 28.4 29.0 44.5 35.1 28.2];     % heater = 11V,
% Tmatrix=[143.9 33.1 30.7 126 29.9 28.9 29.7 54.2 39.4 28.4];      % heater = 14V,
% Tmatrix=[220.7 38.5 34.4 196.2 32.6 30.6 32.1 81.4 50.8 29.5];    % heater = 20V
% Tmatrix=[278.4 44.9 39.1 251.5 36.3 33.2 35.5 110.3 63.1 31.5];   % heater = 25V
% Low and high Mode with constriction Rs=0.7
% Tmatrix=[23.5 23.5  23.5 23.5 23.5 23.5 23.5 23.5 23.4];          % heater = 0V
% Tmatrix=[74.9 25.3 24.3 65.7 24 23.6 23.9 55.1 23.7 23.4];        % heater = 8V
% Tmatrix=[108.5 27.2 25.5 94 24.9 24.2 24.8 74.5 30.4 23.9];       % heater = 11V
% Tmatrix=[147.7 29.8 27.3 128.2 26.3 25.1 26.0 100.1 34.5 24.6];   % heater = 14V
% Tmatrix=[221.9 35.6 31.2 196 29.4 27 28.8 157.1 43.6 26.2];       % heater = 20V
% Tmatrix=[280.7 42.5 36.2 252.9 33.3 29.7 32.4 219.2 53.5 29.5];   % heater = 25V
Tmatrix = Tmatrix+273;          % Change temperature to Kelvin
T2=Tmatrix(1);
T3=Tmatrix(2);
T4=Tmatrix(3);
T5=Tmatrix(4);
T6=Tmatrix(5);
T7=Tmatrix(6);
T8=Tmatrix(7);
T9=Tmatrix(8);
T10=Tmatrix(9);
```

```
T11=Tmatrix(10);
Th = (2*T2+T5)/3;     % Weighted hot end targeted temperature, K
Tc = (2*T3+T4)/3;     % Weighted cold end  temperature, K
Nmax = 100;           % Maximum number of integration
y=y(:);               % Make sure the input vector y is a column vector
y(1,1) = Th;          % Fixed the starting temperature at T_h
iterations=0;
% Main loop for iterations
while(1)
        iterations = iterations + 1;
        fvec=funcvF(y);              % Compute the difference between the targets and %
                                     % calculated results                              %
        checky = norm(fvec./y(1:5))  % Check the norm of the ratio of the difference %
        if checky<1.0E-3             % Set the converging threshold                    %
                fprintf(1,'Done\n');
                y = y'               % Print out the solution %
                [fvec,yend] = funcvF(y);
                yend = yend'  % print out the integration results at the ends %
                Q = yend(1,6)/(2*yend(1,7))  % Find the quality factor %
        elseif iterations == Nmax    % Terminate the iteration if iteration ≥ N_max %
                fprintf(1,'Exceed max # of iterations');
                return
        else
        J = fdjacF(y,fvec);      % calculate the Jacobian %
        diffy = -J\fvec;         % Use the LU factorization %
        if checky<1.0e-1
                diffy = diffy/2; % Close to converge, adjust the step size %
        elseif checky<5.0e-2
                diffy = diffy/4;
        elseif checky<1.0e-2
                diffy = diffy/6;
        end
        newy=y
        newy(4:8) = y(4:8)+diffy;    % Perform a Newton iteration to update y %
        y=newy;                      % only update Ure, Uim, fre, fim and H2 %
        fprintf(1,'Computing Update, iterations %4.0f \n',iterations)
```

```
        end
end
%
% End of updateF.m %
```

Function **funcvF.m**: The function integrate the coupled ordinary differential equations of the annular prime mover.

% Begin of function %

```
function [fvec,yend] = funcvF(yin)
%
% Includes the ends effect from high order mode method
% This function integrates the annular resonator with the stack/heat exchanger assembly
% at the end of the resonator (including ambient and hot heat exchanger)
% constriction locates between xcon1 to xcon2
% Requires: ductfunc2.m, ductfunc21.m, ductcon.m,
%       , stackfun.m, ode45.m, ambhxfunc.m, hothxfunc, zstuff.m
% Declare the global variables
global T2 T3 T4 T5 T6 T7 T8 T9 T10 T11 Th Tc Tmatrix Rs La Las R Rst
yin=yin(:);
d = 0.0529;     % Width of annulus m
h = 0.0497;     % Height of annulus m
dc = d*sqrt(Rs);        % Width of the constriction m
hc = h*sqrt(Rs);        % Height of constriction m
cp=1005;                % Isobaric heat capacity per unit mass
% These are the positions of the thermocouples, m
xp0= 0;
xp11=0.00293;           % Thermocouple # 9
xp12=0.084345;          % Thermocouple # 10
xp13=0.39615;           % Thermocouple # 11
xp14=0.707955;          % Thermocouple # 7
xp15=0.7556;            % Thermocouple # 8
xp1 =0.76292;           % Ambient heat exchanger
xp2 = 0.768;            % Prime mover stack
xp3 = 0.7920;           % Hot heat exchanger
xcon1=0.133863;         % 45° long constriction, 90° from the center of the stack assembly
xcon2= 0.23290;
xpL=0.7923;             % Effective length of the annular resonator, m %
% These are not the resolution of the integration
% These are the points in which the results are extracted
```

```
xn1 = 20;       xn2 = 30;
xn3 = 50;       xn4 = 10;
fvec = zeros(5,1);      % Set up the fvec vector
x11span = linspace(xp0,xp11,xn1);
x12span = linspace(xp11,xp12,xn2);
x13aspan = linspace(xp12,xcon1,xn2);
x13bspan = linspace(xcon1,xcon2,xn2);
x13cspan = linspace(xcon2,xp13,xn2);
x14span = linspace(xp13,xp14,xn3);
x15span = linspace(xp14,xp15,xn2);
x16span = linspace(xp15,xp1,xn1);
x2span = linspace(xp1,xp2,xn1);
x3span = linspace(xp2,xp3,xn2);
x4span = linspace(xp3,xpL,xn1);
y0 = yin(1:7); % make sure y0 is column vector and only the first 7 elements used in a duct
y0 = y0(:);     % Set up the starting boundary conditions
 [x11,y11] = ode45('ductfunc2',x11span,y0); % Use the MATLAB built in ODE45 function
y011 = y11(xn1,:);     % Set up the boundary condition for next integration
[x12,y12] = ode45('ductfunc21',x12span,y011);
y012 = y12(xn2,:);     % Set up the boundary condition for next integration
[x13a,y13a] = ode45('ductfunc22a1',x13aspan,y012);
% From duct to a constriction, U is continuous but p2=p1-U1Za
gamma = 1.4;            % Ratio, isobaric to isochoric specific heats
rh = 1.2825e-2;         % Hydraulic radius of the resonator, rh=r/2, m
rhc = rh*sqrt(Rs);      % Hydraulic radius in the constriction, m
omega = 2*pi*(y13a(xn2,6) + j.*y13a(xn2,7));% Extract the complex frequency
rho = 353.065./y13a(xn2,1);     % Density of air as a function of temperature (K)
c = 20.0447.*sqrt(y13a(xn2,1)); % Speed of sound in air as a function of temperature (K)
mue = 1.846e-5.*(y13a(xn2,1)/300).^1.5.*(410.4./(y13a(xn2,1)+110.4)); % Viscosity of air
K=2.624e2.*(y13a(xn2,1)./300).^1.5.*(523.831./(y13a(xn2,1)+...
        245.4.*exp(27.6./y13a(xn2,1))));      % Thermal conductivity, Air
Pr = 0.60928+0.23017.*exp(-0.0028565.*y13a(xn2,1)); % Prandtl number
dV = sqrt(2.*mue./(rho.*omega));    % Viscous penetration depth %
dK = sqrt(2.*K./(rho.*cp.*omega));  % Thermal penetration depth %
fv = (1-j)*dV/(2*rh);
fvc = (1-j)*dV/(2*rhc);
```

```
fk = fv/sqrt(Pr);
fkc = fvc/sqrt(Pr);
k = omega/c *sqrt((1+(gamma-1)*fk)/(1-fv));    % Wave number in a regular duct
kc = omega/c *sqrt((1+(gamma-1)*fkc)/(1-fvc)); % Wave number in the constriction
[H,Hm0,mymz2,nynz2]=zstuff(d,h,dc,hc);
Y1=diag(-j*sqrt(mymz2-k.^2)./(k.*rho*c));
Y2=diag(-j*sqrt(nynz2-kc.^2)./(kc.*rho*c));
Zimag=(Hm0.'*((H*Y2*H.'+Y1)\Hm0))/(Rs*4*r^2); % Compute the acoustic impedance
                                              % caused by the constriction, using
                                              % higher order mode method
Ra1 = rho.*omega.*dV.*(1-R)./R.*(1+(1-R.^2)./(pi*R).*log((1+R)./(1-R)))/(Rs*4*r^2);
Za1 = Ra1+ Zimag;
%Za1=0;        % If do not want to included end correction, just set the impedance to zero
               % by activating this line
U1 = y13a(xn2,4) + j.*y13a(xn2,5); % Volume velocity at entrance of the constriction
y013b = y13a(xn2,:);
y013b(1,2) = y013b(1,2) - real(Za1*U1);      % Correct real part of pressure
y013b(1,3) = y013b(1,3) - imag(Za1*U1);      % Correct imag part of pressure
[x13b,y13b] = ode45('ductcon',x13bspan,y013b); % Constriction region
% From a constriction to a duct , U is continuous but p3=p2-U2Za
rho = 353.065./y13b(xn2,1);
c = 20.0447.*sqrt(y13b(xn2,1));
mue = 1.846e-5.*(y13b(xn2,1)/300).^1.5.*(410.4./(y13b(xn2,1)+110.4));
K = 2.624e-2.*(y13b(xn2,1)./300).^1.5.*(523.8306./(y13b(xn2,1)+...
245.4.*exp(-.27.6./y13b(xn2,1))));% Thermal conductivity, Air
Pr = 0.60928+0.23017.*exp(-0.0028565.*y13b(xn2,1));%Prandtl number
dV = sqrt(2.*mue./(rho.*omega));              % Viscous penetration depth %
dK = sqrt(2.*K./(rho.*cp.*omega));            % Thermal penetration depth %
fv = (1-j)*dV/(2*rh);
fvc = (1-j)*dV/(2*rhc);
fk = fv/sqrt(Pr);
fkc = fvc/sqrt(Pr);
k = omega/c*sqrt((1+(gamma-1)*fk)/(1-fv)); % Wave number in regular duct
kc = omega/c*sqrt((1+(gamma-1)*fkc)/(1-fvc)); % Wave number in the constriction
Y1=diag(-j*sqrt(mymz2-k.^2)./(k.*rho*c));
Y2=diag(-j*sqrt(nynz2-kc.^2)./(kc.*rho*c));
```

```
Zimag=(Hm0.'*((H*Y2*H.'+Y1)\Hm0))/(Rs*4*r^2);
Ra2 = rho.*omega.*dV.*(1-R)./R.*(1+(1-R.^2)./(pi*R).*log((1+R)./(1-R)))/(Rs*4*r^2);
Za2 = Ra2 + Zimag;
%Za2 = 0;
U2 = y13b(xn2,4) + j*y13b(xn2,5);% Volume velocity at start of the constriction
y013c = y13b(xn2,:);
y013c(1,2) = y013c(1,2)-real(Za2*U2);      % Correct real part of pressure
y013c(1,3) = y013c(1,3)-imag(Za2*U2);      % Correct imag part of pressure
[x13c,y13c] = ode45('ductfunc22a2',x13cspan,y013c);
y013 = y13c(xn2,:);
[x14,y14] = ode45('ductfunc23',x14span,y013);
y014 = y14(xn3,:);
[x15,y15] = ode45('ductfunc24',x15span,y014);
y015 = y15(xn2,:);
[x16,y16] = ode45('ductfunc25',x16span,y015);
y016 = y16(xn1,:);
[x2,y2] = ode45('ambhxfunc',x2span,y016); % Integrate in the ambient heat exchanger
% Compute the end corrections for the stack
% Activate these command to include the end corrections in the stack region
        %nslit = 57;            % Number of the slit
        %Aslit = 2.61936e-5;    % Area for one slit, m^2
        %y0=3.06e-4;            % Half spacing of the stack, m
        %ds = 4.28e-2;          % Width of  one slit in the stack region, m
        %hs = 6.12e-4;          % Height of one slit in the stack region, m
        %omega = 2*pi*(y2(xn1,6) + j.*y2(xn1,7)); % Complex frequency
        %rho = 353.065./y2(xn1,1);
        %c = 20.0447.*sqrt(y2(xn1,1));
        %mue = 1.846e-5.*(y2(xn1,1)/300).^1.5.*(410.4./(y2(xn1,1)+110.4));
        %dV = sqrt(2.*mue./(rho.*omega));  % Viscous penetration depth in regular duct
        %dK = sqrt(2.*K./(rho.*cp.*omega));  % Thermal penetration depth in regular duct
        %fv = (1-j)*dV/(2*rh);
        %fk = fv/sqrt(Pr);
        %fvs = tanh((1+j)*y0/dV)/((1+j)*y0/dV);      % fv for Parallel plate
        %fks = fvs/sqrt(Pr);                         % fk for Parallel plate
        %k = omega/c *sqrt((1+(gamma-1)*fk)/(1-fv));  % Wave number in regular duct
        %ks = omega/c *sqrt((1+(gamma-1)*fks)/(1-fvs));% Wave number in the constriction
```

```
        %[H,Hm0,mymz2,nynz2]=zstuff(d,h,ds,hs);
        %Y1=diag(-j*sqrt(mymz2-k.^2)./(k.*rho*c));
        %Y2=diag(-j*sqrt(nynz2-ks.^2)./(ks.*rho*c));
        %Zimag=(Hm0.'*((H*Y2*H.'+Y1)\Hm0))/(Aslit);
        %Rast3 = rho.*omega.*dV.*(1-Rst)./Rst.*(1+(1-Rst.^2)./(pi*Rst).*log((1+Rst)./(1-...
                Rst)))/(Aslit);
        %Zast1 = (Rast3 + Zimag)/nslit;  % Effective impedance for end corrections of the
                                         % stack
        %Ust1 = y2(xn1,4) + j.*y2(xn1,5); % Volume velocity at entrance of the constriction
Zast1=0;                        % No end corrections for stack if this line is active
y02 = [y2(xn1,:) yin(8)];           % Add the 8th element (i.e. H2) in the stack region
        %y02(1,2) = y02(1,2) - real(Zast1*Ust1);      % Correct real part of pressure
        %y02(1,3) = y02(1,3) - imag(Zast1*Ust1);      % Correct imag part of pressure
[x3,y3] = ode45('stackfun',x3span,y02); % Integrate in the prime mover stack region
% Activate these commands to include the end corrections in the stack region
        %Aslit = 2.61936e-5;                  % Area for one slit
        %rho = 353.065./y3(xn2,1);
        %c = 20.0447.*sqrt(y3(xn2,1));
        %mue = 1.846e-5.*(y3(xn2,1)/300).^1.5.*(410.4./(y3(xn2,1)+110.4));
        %dV = sqrt(2.*mue./(rho.*omega));  % Viscous penetration depth in regular duct
        %dK = sqrt(2.*K./(rho.*cp.*omega));% Thermal penetration depth in regular duct
        %fv = (1-j)*dV/(2*rh);
        %fk = fv/sqrt(Pr);
        %fvs = tanh((1+j)*y0/dV)/((1+j)*y0/dV);      % fv for Parallel plate
        %fks = fvs/sqrt(Pr);                         % fk for Parallel plate
        %k = omega/c*sqrt((1+(gamma-1)*fk)/(1-fv));% Wave number in regular duct
        %ks = omega/c*sqrt((1+(gamma-1)*fks)/(1-fvs));% Wave number in the constriction
        %[H,Hm0,mymz2,nynz2]=zstuff(d,h,ds,hs);
        %Y1=diag( -j*sqrt(mymz2-k.^2)./(k.*rho*c));
        %Y2=diag( -j*sqrt(nynz2-ks.^2)./(ks.*rho*c));
        %Zimag=(Hm0.'*((H*Y2*H.'+Y1)\Hm0))/(Aslit);
        %Rast4 = rho.*omega.*dV.*(1-Rst)./Rst.*(1+(1-Rst.^2)./(pi*Rst).*log((1+Rst)./(1-...
                Rst)))/(Aslit);
        %Zast2 = (Rast4 + Zimag)/nslit;% Effective impedance for end corrections of stack
Zast2=0; % If this line ic active, no end corrections for the stack is included
        %Ust2 = y3(xn2,4) + j.*y3(xn2,5);     % Volume velocity at start of the constriction
```

```
y03 = y3(xn2,1:7);      % only the first 7 elements are used in the hot heat exchanger
        %y03(1,2) = y03(1,2) - real(Zast2*Ust2);      % Correct real part of pressure
        %y03(1,3) = y03(1,3) - imag(Zast2*Ust2);      % Correct imag part of pressure
[x4,y4] = ode45('hothxfunc',x4span,y03);
yend = [y4(xn1,:) yin(8)]';      % This is the result at the end of the hot heat exchanger
fvec(1,1) = yend(1,1)-Th;      % Find the difference of the targeted hot temperature
fvec(2:5,1)= yin(2:5,1)-yend(2:5,1);% Find the differences of the target pre, pim, Ure , Uim
yend = yend(:);                % Show results of the integration at the end
%
```

% End of funcvF.m

Function **fdjacF.m**: This function computes the Jacobian using finite difference.

```
% Begin of function %
function df=fdjacF(yin,fin)
% USAGE: df=fdjacF(yin,fin)
%
% Inputs:  y, funcvF input vector to compute Jacobian about
%              f evaluation of funcv at y
% Outputs: df = matrix with df(i,j) = dfuncv(i),dy(j)
% This function compute an numerical approximation to the Jacobian matrix
% for the function funcvF
%
% INPUTS: yin in the original guess vector
%          fin is the original differences of the target
% Requires: funcvF.m
%

yin=yin(:);
fin=fin(:);
h=1E-10.*abs(yin)+eps;  % make y perturbation be 1E-10 of y's current value
% Perturb with respect to U_r, U_i, f_r, f_i and H_2 . i.e.        y(4:8)
% DON'T perturb with respect to  Tm, pr or pi
df=zeros(5,5);  % Initialize the Jacobian matrix (5 by 5)
for i=4:8
% perturb the only ith element of y %
ypert=yin;
ypert(i)=h(i)+yin(i);
% find f with the perturbed y %
pert = funcvF(ypert);
% Forward difference formula %
df(:,i-3) = (fpert(:)-fin(:))./h(i); % Jacobian array
fprintf(1,'.');
end
%
% End of funcvF.m %
```

Function **ductfunc2.m**: This function contains the differential equations in a duct region.

% Begin of function %

```
function ydot = ductfunc2(x,y)
% This function contains the differential equation in a dust region
%       dp1/dx = -jw*rho*U1/((1-fv)*Area)
%       dU1/dx = -jw*Area*(1+(gamma-1)*fk)*p1/(rho*c^2), U1 is the volumetric velocity
% The input y is a column vector with the component of
%       y=[Tm;pre;pim;Ure;Uim;frc;fim;H2];
%        in a duct region, H2 is not used, only y(1:7) is used in duct region
%
%
global T2 T3 T4 T5 T6 T7 T8 T9 T10 T11 Th Tc r    % All input temperature in C
xp11 = 0.00293;         % Location of the thermocouple #9
y(1) = Th;
y=y(1:7);
r_h = r/2 ;             % Hydraulic radius of the resonator
Area = 4*r^2;           % Cross-section area of the duct, m^2
Tm = y(1);
prl = y(2);
pim = y(3);
Url = y(4);
Uim = y(5);
frl = y(6);
fim = y(7);
U = Url + j.*Uim;       % The volumetric velocity, s/m^3
p = prl + j.*pim;       % Acoustic pressure
f = frl + j*fim;        % Complex frequency
w = 2*pi*f;

% Gas constants for air , Tm in Kelvin, at 1 ATM %
% Thermal      conductivity     %
K = 2.624e-2*(Tm/300)^1.5*(523.8306/(Tm+245.4*exp(-27.6/Tm)));
% Viscosity of Air                %
mue = 1.846e-5.*(Tm/300).^1.5.*(410.4./(Tm+110.4));
```

```
gamma = 1.4;            % Ratio, isobaric to isochoric specific heats
cp=1005;                % Isobaric heat capacity per unit mass
% Compute gas properties and the f function
[fv,fk,c,rho,K,Ksolid,Prandtl]=airproperty(Tm,w,1);
Tmdot = (T9-Th)/xp11;       % Set the temperature gradient along the duct

% set up the ODE equation in a duct region
temp1 = -j.*w.*rho.*U./((1-fv)*Area);
temp2 = -j.*w.*Area.*(1+(gam-1).*fk).*p./(rho.*c.^2)+...
((fk-fv)*Tmdot*U)/((1-fv)*(1-Prandtl)*Tm);
% Set up the  ordinary differential equations
prdot =  real(temp1);
pidot =  imag(temp1);
Urdot =  real(temp2);
Uidot =  imag(temp2);
frldot = 0;
fimdot = 0;
ydot =[Tmdot;prdot;pidot;Urdot;Uidot;frldot;fimdot];
%
```

% End of ductfunc2.m %

Function **ambhxfunc.m**: This function contains the differential equations in the ambient heat exchanger.

% Begin of function %

```
function ydot = ambhxfunc(x,y)
% This function contains the differential equations in the ambient heat exchanger
%       dp1/dx = -jw*rho*U1/((1-fv)*Area)
%       dU1/dx = -jw*Area*(1+(gamma-1)*fk)*p1/(rho*c^2), U1 is the volumetric velocity
% The input y is a column vector with the component of
%       y=[Tm;pre;pim;Ure;Uim;fre;fim;H2];
% in the ambient heat exchanger region, H2 is not used
% Note that only y(1:7) is used here
%

global T2 T3 T4 T5 T6 T7 T8 T9 T10 T11 Th Tc     % All input temperature in C
y = y(1:7);
y=y(:);                         % Make sure y0 is a column vector
Aambgas = 1.6547e-03;           % Gas area. m^2
y0amb = 1.7018e-03;             % Half spacing of plates for ambient heat exchanger, m
y(1)=T6;                        % Ambient heat HX at T6 Kelvin
Tm = y(1);
prl = y(2);
pim = y(3);
Url = y(4);
Uim = y(5);
frl = y(6);
fim = y(7);
U = Url + j.*Uim;       % The volumetric velocity, s/m^3
p = prl + j.*pim;       % Acoustic pressure
f = frl + j*fim;        % Complex frequency
w = 2*pi*f;

% Gas properties for air , Tm in Kelvin, at 1 atm %
% Thermal conductivity
K = 2.624e-2*(Tm/300)^1.5*(523.8306/(Tm+245.4*exp(-27.6/Tm)));
```

```
c = 20.0447*sqrt(Tm);          % speed of sound in the air
mue = 1.846e-5.*(Tm/300).^1.5.*(410.4./(Tm+110.4)); % Viscosity of Air
rho = 353.065/Tm;      % Density of air
gam = 1.4;             % Ratio, isobaric to isochoric specific heats
cp=1005;               % Isobaric heat capacity per unit mass
deltaK = sqrt(2.*K./(rho.*cp.*w));  % Thermal penetration depth, m
deltaV = sqrt(2.*mue./(rho.*w));        % Viscous penetration depth, m
rootPrandtl=sqrt(mue.*cp./K);
fv = tanh((1+j)*y0amb/deltaV)/((1+j)*y0amb/deltaV);% fv for Parallel plate
fk = fv./rootPrandtl;                                   % fk for Parallel plate
% set up the ODE equations in the ambient heat exchanger region
temp1 = -j.*w.*rho.*U./((1-fv)*Aambgas);
temp2 = -j.*w.*Aambgas.*(1+(gam-1).*fk).*p./(rho.*c.^2);

Tmdot = 0;     % Note that it is assumed no temperature gradient across the ambient heat
               % exchanger
prdot =  real(temp1);
pidot =  imag(temp1);
Urdot =  real(temp2);
Uidot =  imag(temp2);
frldot = 0;
fimdot = 0;
ydot =[Tmdot;prdot;pidot;Urdot;Uidot;frldot;fimdot];
%
```

% End of ambhxfunc.m %

Function **ductcon.m**: This function contains the differential equations in the constricted duct.

% Begin of function %

```
function ydot = ductcon(x,y)
% This function contains the differential equations in the constriction
%       dp1/dx = -jw*rho*U1/((1-fv)*Area)
%       dU1/dx = -jw*Area*(1+(gamma-1)*fk)*p1/(rho*c^2), U1 is the volumetric velocity
% The input y is a column vector with the component of
%       y=[Tm;pre;pim;Ure;Uim;fre;fim;H2];
% in a duct region, H2 is not used, only y(1:7) is used in duct region
%

global T2 T3 T4 T5 T6 T7 T8 T9 T10 T11 Th Tc Rs r
% Define the locations of the constriction and thermoacoustics (in m)
xp12 = 0.084345;      % Thermocouple # 10
xp13 = 0.39615;       % Thermocouple # 11
xcon1=0.133863;       % Constriction locates at xcon1 to xcon2
xcon2= 0.23290;       % 45° long constriction, 90° from center of stack
y=y(1:7);
r_h = r/2*sqrt(Rs) ;  % Hydraulic radius of the constricted duct. m
Area = Rs*4*r^2;      % Cross-section area of the duct, m^2
Tm = y(1);
prl = y(2);
pim = y(3);
Url = y(4);
Uim = y(5);
frl = y(6);
fim = y(7);
U = Url + j.*Uim;     % Volumetric velocity, s/m^3
p = prl + j.*pim;     % Acoustic pressure
f = frl + j*fim;      % Complex frequency
w = 2*pi*f;

% Gas properties for air , Tm in Kelvin, at 1 atm %
```

```
cp=1005;                % Isobaric heat capacity per unit mass
c=20.0447.*sqrt(Tm); % Speed of sound in air
rho=353.065./Tm;        % Density of air
gam = 1.4;              % Ratio, isobaric to isochoric specific heats
% Thermal conductivity, Air, Tm in Kelvin
K = 2.624e-2.*(Tm./300).^1.5.*(523.8306./(Tm+245.4.*exp(-27.6./Tm)));
mue = 1.846e-5.*(Tm/300).^1.5.*(410.4./(Tm+110.4));      % Viscosity of Air
Prandtl = 0.60928+0.23017.*exp(-0.0028565.*Tm);          % Prandtl number

deltaK = sqrt(2.*K./(rho.*cp.*w));     % Thermal penetration depth in the constriction, m
deltaV = sqrt(2.*mue./(rho.*w));       % Viscous penetration depth in the constriction, m
fv = (1-j).*deltaV./(2*r_h);           % f_v of the constriction
fk = fv./sqrt(Prandtl);                % f_k of the constriction
Tmdot = (T11-T10)/(xp13-xp12);         % Temperature gradient across the constriction

% set up the ODE equation in a  constricted duct region
temp1 = -j.*w.*rho.*U./((1-fv)*Area);
temp2 = -j.*w.*Area.*(1+(gam-1).*fk).*p./(rho.*c.^2)+...
        ((fk-fv)*Tmdot*U)/((1-fv)*(1-Prandtl)*Tm);
prdot =  real(temp1);
pidot =  imag(temp1);
Urdot =  real(temp2);
Uidot =  imag(temp2);
frldot = 0;
fimdot = 0;

ydot =[Tmdot;prdot;pidot;Urdot;Uidot;frldot;fimdot];
```

% End of ductcon.m %

Function **stackfun.m**: This function contains the differential equations in the prime mover stack.

% Begin of function %

```
function ydot = stackfun(x,y)
% This function contains the differential equations in the prime mover stack
% to integrate in the stack region
% The input y is a column vector with the component of
%       y=[Tm;pre;pim;Urc;Uim;frc;fim;H2];
%
% Requires: airproperty.m
%

global T2 T3 T4 T5 T6 T7 T8 T9 T10 T11 Th Tc
y=y(:);
Agas = 1.7995e-3;       % Total gas cross section area, m^2, 56 cover glasses
AsAgas = 0.2237;        % Asolid/Agas in the stack region
y(1) = Tc;              % Ambient side's temperature of the prime mover stack
Tm = y(1);
prl = y(2);
pim = y(3);
Url = y(4);
Uim = y(5);
frl = y(6);
fim = y(7);
H2 =  y(8);             % Time-averaged energy flux, constant along the stack
U = Url + j.*Uim;       % Volumetric velocity, s/m^3
p = prl + j.*pim;       % Acoustic pressure
f = frl + j*fim;        % Complex frequency
w = 2*pi*f;
% Gas properties for air
[fv,fk,c,rho,K,Ksolid,Prandtl] = airproperty(Tm,w,2);   % index == 2 for parallel plates
                                                        % geometry
gam = 1.4;              % Ratio, isobaric to isochoric specific heats
cp=1005;                % Isobaric heat capacity per unit mass
```

```
% H2 is the time-averaged energy flux, constant along the stack %
dTmdx1 = H2/Agas-0.5/Agas*real(p*U'*(1-((fk-fv')/((1+Prandtl)*(1-fv')))));
dTmdx2 = 0.5*rho*cp*abs(U)^2*imag(fk+Prandtl*fv')/(real(w)*(1-Prandtl^2)*abs(1-...
         fv)^2*Agas^2) - K- AsAgas*Ksolid;
dTmdx = dTmdx1/dTmdx2;   % Temperature gradient in the stack region
temp1 = -j.*w.*rho.*U./((1-fv)*Agas);
temp2 = -j.*w.*Agas.*(1+(gam-1).*fk).*p./(rho.*c.^2)+((fk-fv)*dTmdx*U)/((1-fv)*(1-...
        Prandtl)*Tm);
Tmxdot = dTmdx;
prdot =  real(temp1);
pidot =  imag(temp1);
Urdot =  real(temp2);
Uidot =  imag(temp2);
frldot = 0;
fimdot = 0;
H2dot = 0;      % H2 is constant through the stack
ydot =[Tmxdot;prdot;pidot;Urdot;Uidot;frldot;fimdot;H2dot];
```

% End of stackfun.m %

Function **airproperty.m**: This function compute the properties for air.

% Begin of function %

```
function  [fv,fk,c,rho,K,Ksolid,Prandtl] = airproperty(T,w,index)
% This function compute the air properties at 1 atm and T Kelvin
% if    index == 1 >> BL approximation for  regular duct
%       index == 2 >> Parallel plate for stack region
%       index == 3 >> BL approximation for constricted duct
global Rs
r_h = 2.5654E-2/2;      % Hydraulic radius of the resonator is r/2
y0 = 3.06e-4;           % Half spacing of plates for stack, m
cp=1005;                % Isobaric heat capacity per unit mass
c=20.0447.*sqrt(T);     % Speed of sound in air
rho=353.065./T;
% Thermal conductivity, Air
K = 2.624e-2.*(T./300).^1.5.*(523.8306./(T+245.4.*exp(-27.6./T)));
Ksolid = 0.2*(1-exp(-T/100)); % Thermal conductivity, kapton
mue = 1.846e-5.*(T/300).^1.5.*(410.4./(T+110.4));  % Viscosity of Air
Prandtl = 0.60928+0.23017.*exp(-0.0028565.*T);   % Prandtl number
deltaK = sqrt(2.*K./(rho.*cp.*w));      % Thermal penetration depth, m
deltaV = sqrt(2.*mue./(rho.*w));        % Viscous penetration depth, m
if index == 1
        fv = (1-j).*deltaV./(2*r_h);    % fv for boundary layer approximation
        elseif index == 2
                fv = tanh((1+j)*y0/deltaV)/((1+j)*y0/deltaV); % fv for Parallel plate
        elseif index == 3
                fv = (1-j).*deltaV./(2*r_h*sqrt(Rs));% fv for boundary layer approximation
                                                %       in the constricted duct
        else
                fprintf(1,' Wrong index number !!')
                return
end
fk = fv./sqrt(Prandtl);
```

% End of airproperty.m %

Function **plotpUF.m**: This function plot the acoustic pressure distribution in the annular prime mover prime mover stack

```
% Begin of function %
function [x,y,pnorm]= plotpUF(yin)
% This function plot the acoustic pressure amplitude of the auunlar prime mover
% It uses the solution from "updataF.m" and integrates "yin" from x=0 to x=xL
%
%       Note:   The first section of this function which is not included here,
%               contains the function "funcvF.m".  It uses funcvF.m to integrate
%               the solution from "updateF.m" from x0 to xL

%
% Put :funcvF.m here
%

dT = Th-Tc;                     % Temperature difference across the prime mover stack, K
freq = y0(6,1) +j*y0(7,1);      % Complex frequency
% Combine the solution vector
% x is the position vector, y is the solution matrix
x=[x11;x12;x13a;x13b;x13c;x14;x15;x16;x2;x3;x4];
y=[y11(:,1:7);y12(:,1:7);y13a(:,1:7);y13b(:,1:7);y13c(:,1:7);y14(:,1:7);y15(:,1:7);...
    y16(:,1:7);y2(:,1:7);y3(:,1:7);y4(:,1:7)];
T = y(:,1);
p =y(:,2)+j*y(:,3);      % Complex acoustic pressure
U =y(:,4)+j*y(:,5);      % Complex volume velocity
pm=zeros(8,1);
% Find the theoretical pressure amplitude at the locations of each microphones
% There are 8 microphones used in the measurement
for i=1:8
        xm(i) = 0.03483+(i-1)*9.90375e-2;  % Microphone location, m
        [Y,index] = min(abs(x-xm(i)));     % Compute the corresponding index
        pc(i)=pnorm(index);                % Compute the theoretical values at
                                           % each microphones' locations
end
```

```
pc=pc(:);
% These are the calibrated measured pressure amplitude at each microphones
% For the constricted annular prime mover
% Note that all these measurements are subjected to the measured temperature profile listed
% in the function "updateF.m"
%
% Low mode, With constriction
% Rs = 0.7, low mode
%pm=[34.64;20.63;14.82;31.92;31.18;13.42;12.07;28.41]';  % Heater = 0V
%pm=[35.44;21.3;15;32.63;31.94;13.78;12.16;29.07]';      % Heater = 8V
%pm=[35.72;21.77;14.95;33.05;32.53;14.09;12.17;29.39]'; % Heater = 11V
%pm=[36.26;22.37;15.14;33.77;33.16;14.5;12.3;30.03]';    % Heater =14V
%pm=[37.38;23.76;15.3;35.39;35.24;15.57;12.62;31.45]';   % Heater = 20V
%pm=[37.98;24.63;15.46;36.71;36.71;16.29;13.1;32.65]';   % Heater = 25

% Rs=0.3, low mode
%pm=[34.89;26.09;12.32;34.67;28.18;10.54;11.6;26.91]';   % Heater = 0V
%pm=[39.74;29.49;14.06;38.56;31.29;11.57;13.08;29.95]'; % Heater =V8
%pm=[43.11;32.27;15.82;42.16;34.18;12.56;14.41;32.77]'; % Heater = 11V
%pm=[47.39;35.68;18.16;46.65;37.88;13.71;16.1;36.31]';   % Heater = 14V
%pm=[58.26;45.57;24.5;60.3;48.71;17.44;21.35;47.11]';    % Heater = 20V
%pm=[55.92;55.06;30.23;74.79;60.53;21.48;27.1;58.8]';    % Heater = 25V

% Rs=0.1, low mode
%pm=[40.57;37.74;34.13;38.99;28.57;10.43;9.76;26.8]';    % Heater = 0V
%pm=[47.45;44.12;39.87;45.48;33.24;11.91;11.76;31.61]'; % Heater = 8V
%pm=[53.45;50.17;45.87;52.2;38;13.43;13.95;36.4]';       % Heater = 11V
%pm=[62.9;59.89;54.71;62.74;45.34;15.77;17.47;43.7]';    % Heater = 14V
%pm=[91.08;97.23;89.03;104.3;75.09;25.35;32.76;73.7]';   % Heater = 20V
%pm=[117.4;155.5;145.9;178.6;128.7;43.3;60.38;135.1]';   % Heater = 25V

% High mode, With constriction
% Rs=0.7, high mode
%pm=[7.29;12.45;11.79;6.47;4.78;9.75;12.213;6.14]';      % Heater = 0V
pm=[8.03;13.09;11.48;5.6;5.44;10.19;11.67;5.17]';       % Heater = 8V
%pm=[8.14;12.99;11.19;5.43;5.66;10.14;11.3;4.92]';       % Heater = 11V
```

```
%pm=[8.41;13.22;11.19;5.39;5.97;10.3;11.23;4.84]';        % Heater = 14V
%pm=[8.7;13.29;10.96;5.38;6.43;10.35;10.94;4.75]';        % Heater = 20V
%pm=[8.59;13.07;10.67;5.5;6.65;10.26;10.7;4.79]';         % Heater = 25V
% Rs=0.3, high mode
%pm=[6.86;12.83;6.18;6.49;2.87;9.72;11.99;4.47]';         % Heater = 0V
%pm=[7.24;13.41;6.43;6.56;3.05;10;12.12;4.32]';           % Heater = 8V
%pm=[7.38;13.64;6.69;6.62;3.19;10.18;12.21;4.22]';        % Heater = 11V
%pm=[7.45;13.83;6.95;6.63;3.32;10.34;12.27;4.06]';        % Heater = 14V
%pm=[7.41;14.4;7.48;6.81;3.67;10.87;12.71;3.87]';         % Heater = 20V
%pm=[5.56;14.5;7.61;6.89;3.89;11.16;12.93;3.67]';         % Heater = 25V
% Rs=0.1, high mode
%pm=[8.75;15.87;14.26;8.5;2.63;11.37;12.68;4.99]';        % Heater = 0V
%pm=[9;16.27;14.48;8.59;2.83;11.67;12.85;4.76]';          % Heater = 8V
%pm=[8.98;16.33;14.65;8.6;2.94;11.79;13;4.56]';           % Heater = 11V
%pm=[8.98;16.8;15.07;8.84;3.13;12.21;13.66;4.48]';        % Heater = 14V
%pm=[7.69;17.31;15.12;8.99;3.5;12.87;15.10;4.17]';        % Heater = 20V
%pm=[6.39;17.4;14.87;9.46;3.77;13.43;15.79;4.01]';        % Heater = 25V

% A least fit is applied to the predicted values and the measured data
A=pm*pc/(pc'*pc);     % Find the least square fit constant
pmscal=pm./A;         % Normalized microphone voltage by the constant A
% These are the actual positions of the microphones, m
xpm=[0.03483;0.13387;0.23291;0.33195;0.43099;0.53003;0.62907;0.72811];
clg
lx =[0.7629  0.7629];          % Mark the starting location for stack assembly
ly = [0 1.2];
lx1=[0.133863  0.133863 ];     % Mark the location of the constriction
ly1=[0  1.2];
lx2=[0.2329  0.2329 ];         % Mark the location of the constriction
ly2=[0  1.2];
% Plot the predicted pressure amplitude vs. the least square of the measured data
plot(x,abs(p)./max(abs(p)),'b-',xpm,pmscal,'ro',lx,ly,'g--',lx1,ly1,'g:',lx2,ly2,'g:')
legend('Matlab program ','Measured data',' Stack region', 'Constriction');
%title(['Low mode with end effect 3 ; dT = ',num2str(dT),' Kelvin ;...   % Title for low mode
%       freq = ',num2str(freq),' ; Rs = ',num2str(Rs)])
title(['High mode with end effect 3 ; dT = ',num2str(dT),' Kelvin ;...    % Title for high mode
```

```
    freq = ',num2str(freq),' ; Rs = ',num2str(Rs)])
xlabel('Position, m')
ylabel('Normalized pressure')
axis([0 0.7923 0 1.2])
```

% End of plotpUF.m %

Function **computeL.m**: This function computes the equivalent inductance for the series acoustic impedance Za(w) of a size discontinuity between a duct dxh and dcxhc using higher order mode theory.
This function is contributed by Ralph T. Muehleisen

% Begin of function %

```
function La=computeL(d,h,dc,hc);
%
% Inputs
%       d = depth of main channel
%       h = height of main channel
%       dc = depth of constriction
%       hc = height of constriction
% Outputs
%       La = equivalent inductance of constriction
%
% This function computes the equivalent inductance for the
% series acoustic impedance Za(w) of a size discontinuity between a
% duct dxh and dcxhc using higher order mode theory.
% The discontinuity is assumed to be symmetric
% in the y direction and asymmetric in the z direction
% (i.e. going from a1xb1 to a2xb2 the open area in duct 2 is
%  (d-dc)/2<y<(d+dc)/2 and (h-hc)<z<h
%
% To use this add the following lines to your code
%
% In the beginning:
%       La = computeL(d,h,dc,hc)
%       R=sqrt((dc*hc)./(d.*h));
%       Ra = rho.*w.*dV.*(1-R)./R.*( 1+ (1-R.^2)./(pi*R).*log((1+R)./(1-R)) );
%       Za = Ra + j*w*La;

R=sqrt((dc*hc)./(d.*h));

% compute the coupling matrix H, using n2=3 modes in small constriction
```

```
% and select n1 based on relative sizes
n2=3;
n1=round(n2/sqrt(R));

% call h2d to get the full coupling matrix
[Hfull,my,mz,ny,nz] = h2d(R,n1,n2);
[MH,NH] = size(Hfull);

H00= Hfull (1,1);

% extract out the higher order mode terms
H = Hfull(2:MH,2:NH);

% Extract out the plane wave terms
Hm0 = Hfull(2:MH,1);
my = my(2:MH);
mz = mz(2:MH);
ny = ny(2:NH);
nz = nz(2:NH);

mymz2 = (my.*pi./d).^2 + (mz.*pi./h).^2;
nynz2 = (ny.*pi./dc).^2 + (nz.*pi./hc).^2;
% The inductance approximation, it assumes k2 << my2mz2 or ny2nz2 and k~kc

Y1n = diag(sqrt(mymz2));
Y2n = diag(sqrt(nynz2));
La = rho* (Hm0.' *inv(H*Y2n*H.' + Y1n)*Hm0)/(hc*dc);
return
```

% End of computeL.m %

Function **zstuff.m**: This function computes the scattering matrices used in computation of series acoustic impedance Za(w) of a size discontinuity between a duct dxh and dcxhc using higher order mode theory.
This function is contributed by Ralph T. Muehleisen

% Begin of function %

```
function [H,Hm0,mymz2,nynz2]=zstuff(d,h,dc,hc);
% usage  [H,Hm0,mymz2,nynz2]=zstuff(d,h,dc,hc);
%
% Inputs
%       d = depth of regular duct
%       h = height of regular duct
%       dc = depth of constriction
%       hc = height of constriction
%
% Outputs
%       H = higher order mode scattering matrix
%       Hm0 = scattering vector back to plane wave modes
%       mymz2, nynz2 = indices of higher order modes
%
% This function computes the scattering matrices used in computation
% of series acoustic impedance Za(w) of a size discontinuity between a
% duct dxh and dcxhc using higher order mode theory.
% The discontinuity is assumed to be symmetric
% in the y direction and asymmetric in the z direction
%       . (i.e. going from a1xb1 to a2xb2 the open area in duct 2 is
%       d-dc)/2<y<(d+dc)/2 and (h-hc)<z<h
%
% Add the following lines to your program
% somewhere in the beginning add
% [H,Hm0,mymz2,nynz2]=zstuff(d,h,dc,hc);
%
% In the frequency dependent part add following. If the constriction is on the right
%       Y1=diag( -j*sqrt( mymz2-k.^2)./(k*rho*c));
%       Y2=diag( -j*sqrt(nynz2-kc.^2)./(kc.*rho*c));
```

```
%       Zimag=(Hm0.'*((H*Y2*H.'+Y1)\Hm0))/Sc;
%       R=sqrt((dc*hc)./(d.*h))
%       Ra = rho.*w.*dV.*(1-R)./R.*(1+(1-R.^2)./(pi*R).*log((1+R)./(1-R)));
%       Za = Ra+ Zimag;
%

R=sqrt((dc*hc)./(d.*h));
% Compute the coupling matrix H, using n2=3 modes in small constriction
% and select n1 based on relative sizes
n2=3;
n1=round(n2/R);
if n1> 10
        n1=10;
end
% Call h2d.m to get the full coupling matrix
[Hfull,my,mz,ny,nz]=h2d(R,n1,n2);
[MH,NH]=size(Hfull);

H00=Hfull(1,1);

% Extract out the higher order mode terms
H=Hfull(2:MH,2:NH);

% extract out the plane wave terms
Hm0 =Hfull(2:MH,1);
my=my(2:MH);
mz=mz(2:MH);
ny=ny(2:NH);
nz=nz(2:NH);

mymz2 = (my.*pi./d).^2 + (mz.*pi./h).^2;
nynz2= (ny.*pi./dc).^2 + (nz.*pi./hc).^2;
return
```

% End of zstuff.m %

Function **h2d.m**: This function is used to calculate the coupling matrix H for a change of size of a square duct (axa)->(bxb) with R=b/a.
This function is contributed by Ralph T. Muehleisen

% Begin of function %

```
function [H,my,mz,ny,nz]=h2d(R,N1,N2)
%
% Inputs:
%       Ry = a2/a1 = width ratio of duct,
%       Rz = b2/b1 = height ratio of duct
%       N1= # of modes in large duct region and
%       N2 = # of modes in small duct in one direction.
%
% Outputs:
%       H = coupling matrix
%       Mx = large duct y mode matrix
%       Mz= large duct z mode matrix
%       Ny = small duct y mode matrix
%       Ny = small duct z mode matrix
%
% The routine uses the N1 and N2 lowest frequency modes in each section.
% It assumes that the y direction constriction is symmetric (i.e b is
% centered on a) and the z constriction is asymmetric (b is at one
% edge of a
%

Nt2=N2.^2;
Nt1=N1.^2;
% Generate ny, nz
temp=(0:N2-1)';
ny=zeros(Nt2,1);
nz=ny;
for i=0:N2-1
        ny(i*N2 + (temp+1),1)=[i.*ones(size(temp))];
        nz(i*N2 + (temp+1),1)=temp;
```

```
end

% now sort the modes by frequency
f2=sqrt(ny.^2 + nz.^2);          % Compute relative freq of each mode
[y,I]=sort(f2);                  % Sort the freq.
ny=ny(I);                        % Pull out ny and nz
nz=nz(I);
% Generate my,mz
temp=(0:N1-1)';
my=zeros(Nt1,1);
mz=my;
for i=0:N1-1
        my(i*N1 + (temp+1),1)=[i.*ones(size(temp))];
        mz(i*N1 + (temp+1),1)=temp;
end
f1=sqrt(my.^2 + mz.^2);          % Compute relative freq of each mode
[y,I]=sort(f1);                  % Sort the freq.
my=my(I);                        % Pull out ny and nz
mz=mz(I);
% convert my,mz,ny,nz into the matrices used to compute H=Hy*Hy;
[Ny,My]=meshgrid(ny,my);
[Nz,Mz]=meshgrid(nz,mz);
Mypio2=My.*pi/2;
Hy=zeros(size(My));
Hz=Hy;
% first compute H for the symmetric y direction
e=(1-R)/2;
sme=sin(My*pi*e);
cme=cos(My*pi*e);
smepr=sin(My*pi*(e+R));
smep2r=sin(My*pi*(e+2*R));
% first fill in the general terms
Hy=-2*R.^(3/2).*My.*(sme-(-1).^Ny.*smepr)./(pi*((My.*R).^2-Ny.^2+eps));
% find the n=m*R terms (including m=n=0) and set them to (-1)^(m+n)*Sqrt(R)
I=find(abs(Ny-R*My)<10*eps);
temp=(2*My.*pi.*R.*cme-sme+smep2r)./(4*My*pi*sqrt(R)+eps);
```

```
Hy(I)=temp(I);
% find the m=0 terms and set them to zero
I=find(My==0);
Hy(I)=0*I;
% Find the n=0 terms.  they were computed above by the general expression
% but are sqrt(2) too big
I=find(Ny==0);
Hy(I)=Hy(I)/sqrt(2);
% find the m=n=0 terms and set them equal to sqrt(R)
I=find(My==0 & Ny==0);
Hy(I)=sqrt(R)*ones(size(I));
% second compute H for the asymmetric z direction
e=(1-R);
sme=sin(Mz*pi*e);
cme=cos(Mz*pi*e);
smepr=sin(Mz*pi*(e+R));
smep2r=sin(Mz*pi*(e+2*R));
% first fill in the general terms
Hz=-2*R.^(3/2).*Mz.*(sme-(-1).^Nz.*smepr)./(pi*((Mz.*R).^2-Nz.^2+eps));
% find the n=m*R terms (including m=n=0) and set them to (-1)^(m+n)*Sqrt(R)
I=find(abs(Nz-R*Mz)<10*eps);
temp=(2*Mz.*pi.*R.*cme-sme+smep2r)./(4*Mz*pi*sqrt(R)+eps);
Hz(I)=temp(I);
% Find the m=0 terms and set them to zero
I=find(Mz==0);
Hz(I)=0*I;
% find the n=0 terms.  they were computed above by the general expression
% but are sqrt(2) too big
I=find(Nz==0);
Hz(I)=Hz(I)/sqrt(2);
% find the m=n=0 terms and set them equal to sqrt(R)
I=find(Mz==0 & Nz==0);
Hz(I) = sqrt(R)*ones(size(I));
H = Hy.*Hz;
```

% End of h2d.m %

Function **update2st.m**: This function iterates the ordinary differential equation for a two-stack annular prime mover.

% Begin of function %

```
function  [y,iterations]=update2st(y);
%
%
%       usage [newy,iterations] = update2st(y)
%
%
%       This function implements picards method for updating y
%       solving f(y,x)=0 for a resonator
%  The input y vector is a 8 by 1 vector: [T_m;p_re;p_im;U_re;U_im;f_re;f_im;H_2a;H_2b]
%  only the last 6 elements (i.e. U_re, U_im, f_re, f_im, H_2a, and H_2b) are updated
%
%       newy = y - inv(J)*f(y,x);
%       where J is the Jacobian of f(y)
%       REQUIRES: fdjac2st.m, func2st.m

Nmax = 50;
y = y(:);
iterations = 0;
while(1)
        iterations = iterations + 1;
        fvec=func2st(y);
        checky = norm(fvec./y(1:6))   % check the norm of the ratio of the diffenence %
        if checky < 1.0E-2            % to the solution, be sure to use "./" not "/"  %
                fprintf(1,'Done\n');
                y = y'                % Print out the solution %
                [fvec,yend] = func2st(y);
                yend = yend'          % print the integration results at the ends %
                Q = yend(1,6)/(2*yend(1,7))   % Find the quality factor %
                return
        elseif iterations == Nmax
                fprintf(1,'Exceed max # of iterations');
```

```
            return
        else
        J = fdjac2st(y,fvec);     % calculate the Jacobian %
        diffy = -J\fvec;          % Use LU factorization to find the correction to the guess %
        if checky<1.0e-1          % Reduce the step size when close to solution %
                        diffy = diffy/2;
                elseif checky < 5.0e-2
                        diffy = diffy/4;
                elseif checky < 5.0e-3
                        diffy = diffy/6;
        end
        newy = y;
        newy(4:9) = y(4:9) + diffy;     % Do a Newton iteration to update y %
        y = newy                  % only update Ure, Uim, fre, fim, H2a, and H2b %
        fprintf(1,'Computing Update, iterations %4.0f \n',iterations)
        end
end
```

% End of update2st.m %

Function **fdjac2st.m**: This function computes the Jacobian for the two-stack annular prime mover using finite difference.

% Begin of function %

```
function df=fdjac2st(yin,fin)
% USAGE: df=fdjac2st(yin,fin)
%
% INPUTS:  y funcv input vector to compute Jacobian about
%       f evaluation of funcv at y
% OUTPUTS: df = matrix with df(i,j) = dfuncv(i),dy(j)
% This function compute an numerical approximation to the Jacobian matrix
% for the function funcv
% INPUTS:
%       yin in the original guess vector
%       fin is the original differences of the target
%
% Requires: func2st.m

yin = yin(:);
fin = fin(:);
h = 1E-10.*abs(yin)+eps;  % make y perturbation be 1E-10 of y's current value
% Perturb with respect to Ur, Ui, fr, fi and H2a H2b . i.e. y(4:9)
% DON'T perturb with respect to  Tm, pr or pi
df = zeros(6,6);          % Initialize the Jacobian matrix (6 by 6)
for I = 4:9
% perturb the only ith element of y
        ypert=yin;
        ypert(i) = h(i)+yin(i);
% find f with the perturbed y
        fpert = func2st(ypert);
% Forward difference formula %
        df(:,i-3) = (fpert(:)-fin(:))./h(i); % Jacobian matrix %
        fprintf(1,'.');
end
```

% End of fdjac2st.m %

Function **funcv2st.m**: The function integrate the coupled ordinary differential equations of the two-stack annular prime mover.

% Begin of function %

```
function [fvec,yend] = func2st(yin)
% This function integrates coupled ODE for the two stack annular prime move
% Requires:
%       duct2st1.m, hothx2st1.m, stack1.m, stack2.m, ambhx2st1.m, ambhx2st2.m,
%       hothx2st1.m, hothx2st2.m, ode45.m
%       Note: Most of these functions are similar to the functions for the constricted
%       annular prime mover. Therefore, only the main functions are included here.

global  Th Tc           % All input temperature in K
% Before to execute the program, be sure to adjust                    %
% the target hot heat exchanger temperature to the desired value      %
Th = 393;
Tc = 293;
yin = yin(:);
xp0 = 0;
xp1 = 0.16869;          % Starting location for the first satck assembly
xp2 = 0.1689948;
xp3 = 0.1929948;        % End of the first stack assembly
xp4 = 0.198075;
xp5 = 0.76292;          % Starting location for the second satck assembly
xp6 = 0.768;
xp7 = 0.792;            % End of the second stack assembly
xpL = 0.7923;           % Effective length of the resonator, m
xn1 = 50;
xn2 = 10;
xn3 = 20;
fvec = zeros(6,1);
x1span = linspace(xp0,xp1,xn1);
x2span = linspace(xp1,xp2,xn2);
x3span = linspace(xp2,xp3,xn3);
x4span = linspace(xp3,xp4,xn2);
```

```
x5span = linspace(xp4,xp5,xn1);
x6span = linspace(xp5,xp6,xn2);
x7span = linspace(xp6,xp7,xn3);
x8span = linspace(xp7,xpL,xn2);
%
% Make sure that y0 is column vector, only the first 7 elements are used in the duct%
y0 = yin(1:7);
y0 = y0(:);
[x1,y1] = ode45('duct2st1',x1span,y0);
y01 = y1(xn1,:);
y01(1,1) = Th;
[x2,y2] = ode45('hothx2st1',x2span,y01);% Temperature at Th
y02 = [y2(xn2,:) yin(8)]';      % Add the 8th element (i.e. H2a) for the ist stack
[x3,y3] = ode45('stack1',x3span,y02);
y03 = y3(xn3,1:7);              % only the first 7 elements are used in the hot heat exchanger
[x4,y4] = ode45('ambhx2st1',x4span,y03);% Target Tc at the 1st ambient heat exchanger
y04 = y4(xn2,:);
[x5,y5] = ode45('duct2st1',x5span,y04);
y05 = y5(xn1,:);
y05(1,1) = Tc;
[x6,y6] = ode45('ambhx2st2',x6span,y05);% Temperature at Tc
y06 = [y6(xn2,:) yin(8) yin(9)]';      % Add the 8th element (i.e. H2) for the 2nd stack
[x7,y7] = ode45('stack2',x7span,y06);
y07 = y7(xn3,1:7);     % only the first 7 elements are used in the hot heat exchanger
[x8,y8] = ode45('hothx2st2',x8span,y07);      % Target Th at 2nd hot heat exchanger
% Combine results of the integration
% This is the result at the end of the 2nd hot heat exchanger
yend = [y8(xn2,:) yin(8) yin(9)]';
% Compute the target values %
fvec(1,1) = y03(1,1)-Tc; % Find the difference of the targeted cold temperature at ambhx2st1
fvec(6,1) = yend(1,1)-Th;% Find the difference of the targeted hot temperature at hothx2st2
% Find the differences of the target pre, pim, Ure and Uim %
fvec(2:5,1)= yin(2:5,1)-yend(2:5,1);
yend = yend(:);         % Show results of the integration at the end
```

% End of funcv2st.m %

APPENDIX D. PROPERTIES OF AF 45 GLASS

Mechanical properties:

Density at 20 °C (68 °F): $\rho = 2.72$ g/cm^3

Young's modulus: c = 66.0 kN/mm^2

Torsional modulus: E = 26.7 kN/mm^2

Poisson's ratio: $\gamma = 0.235$

Electrical properties:

Dielectric constant (1 MHz): $\varepsilon_r = 6.2$

Dielectric loss factor (1 MHz): $\tan \delta = 9 \times 10^{-4}$

Temperature for a specific electrical resistivity of 10^8 Ω cm: $T_{\kappa 100} = 610$ °C (1130 °F)

Thermal properties:

Viscosity and corresponding temperatures

Viscosity log η (d Pas)	Temperature in °C	(°F)	Designation
14.5	627	(1161)	Strain point
13.0	663	(1225)	Annealing point
7.60	883	(1621)	Softening point

Transformation temperature: $T_g = 662$ °C (1224 °F)

Coefficient of mean linear thermal expansion: $\alpha_{20\text{-}300} = 4.5 \times 10^{-6}$ K^{-1}

Optical properties:

Refractive indices at 20°C (68°F): $n_e(\lambda = 546$ nm) = 1.5275, n_d ($\lambda = 546$ nm) = 1.5255

Abbe value: $\nu_o = 62.2\%$

Luminous transmittance (glass thickness 1.1 mm): $\tau_{VD65} = 91.2\%$

APPENDIX E.1 CONSTRUCTION DRAWINGS FOR THE PRIME MOVER STACK HOLDER

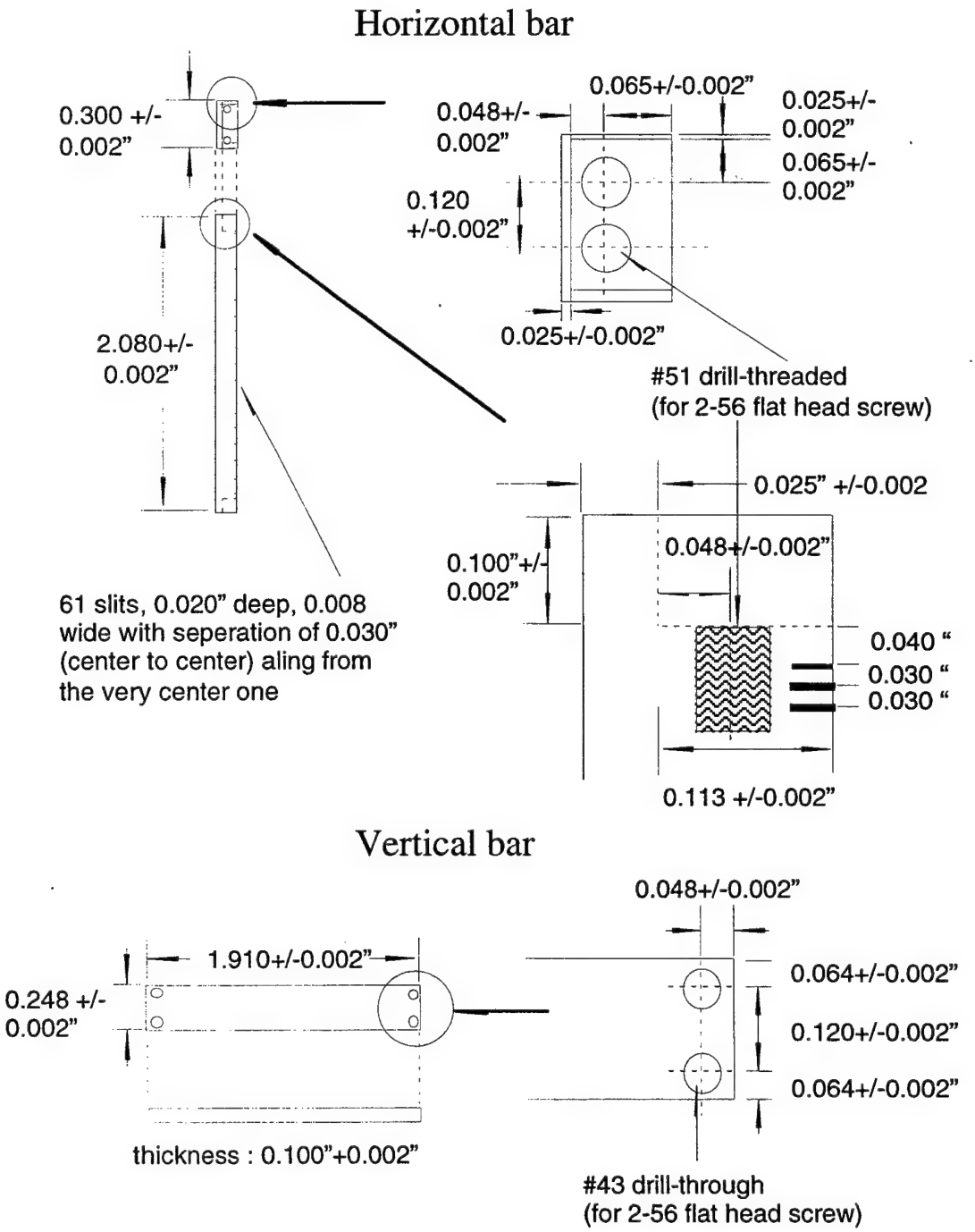

APPENDIX E.2 CONSTRUCTION DRAWINGS FOR THE AMBIENT HEAT EXCHANGER

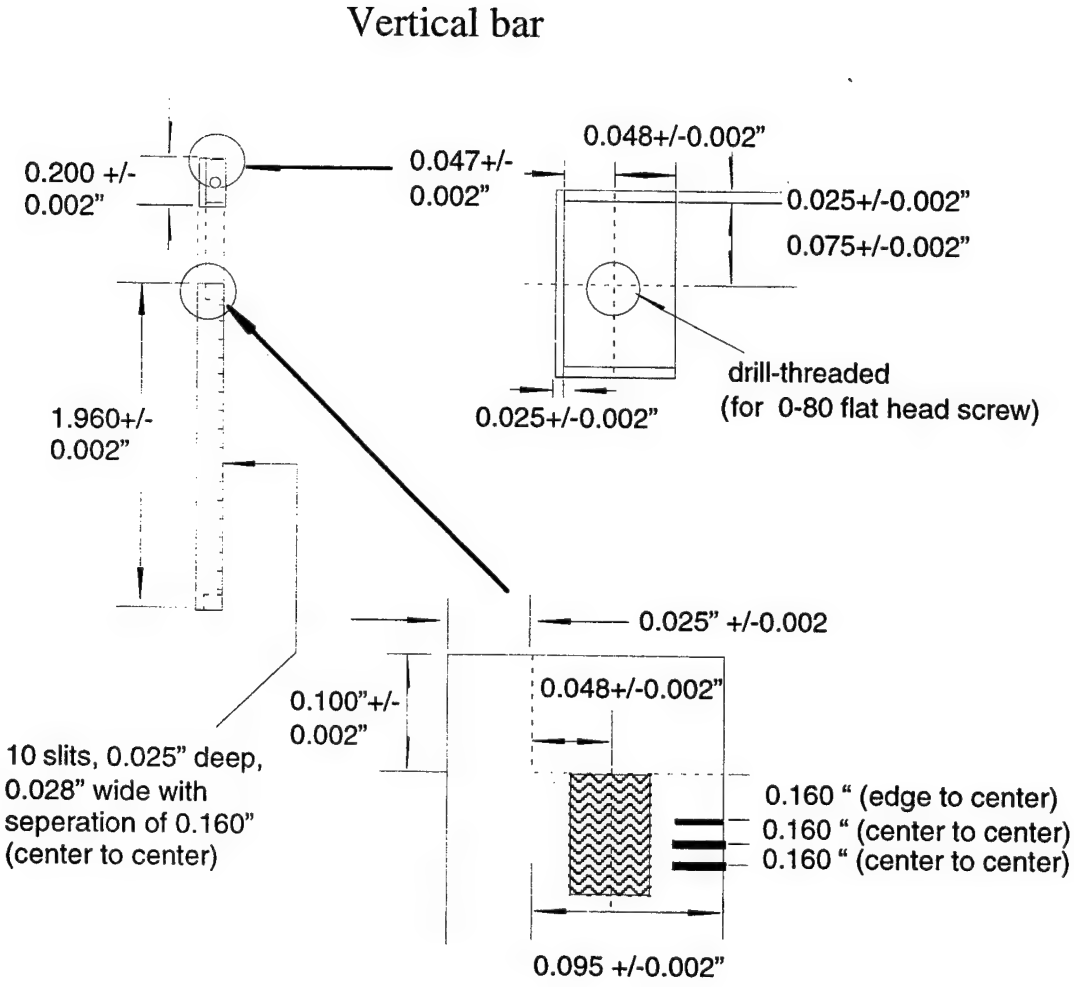

APPENDIX E.2(CONTINUED) CONSTRUCTION DRAWINGS FOR THE AMBIENT HEAT EXCHANGER

Horizontal bar

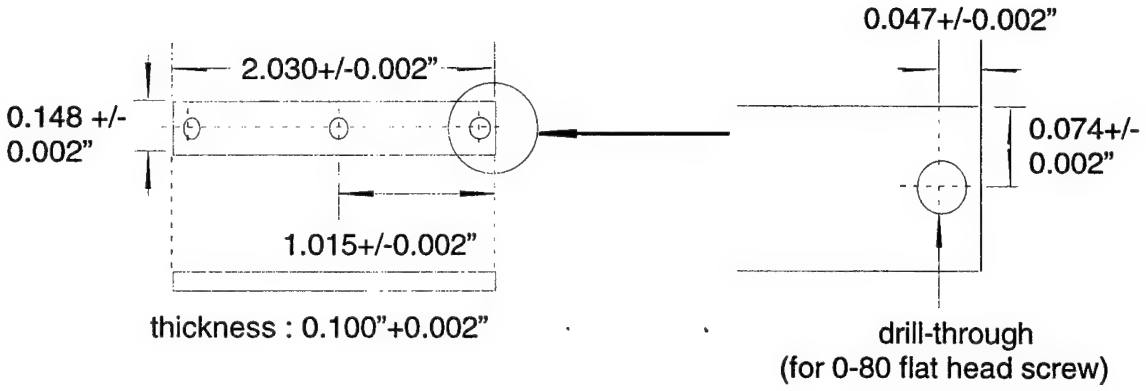

Central bar

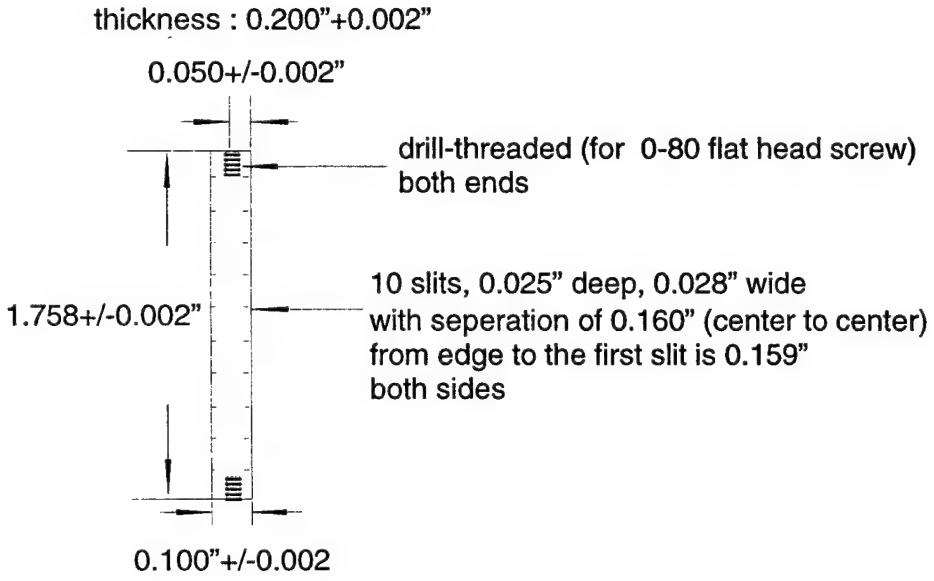

APPENDIX E.3 CONSTRUCTION DRAWINGS FOR THE HOT HEAT EXCHANGER

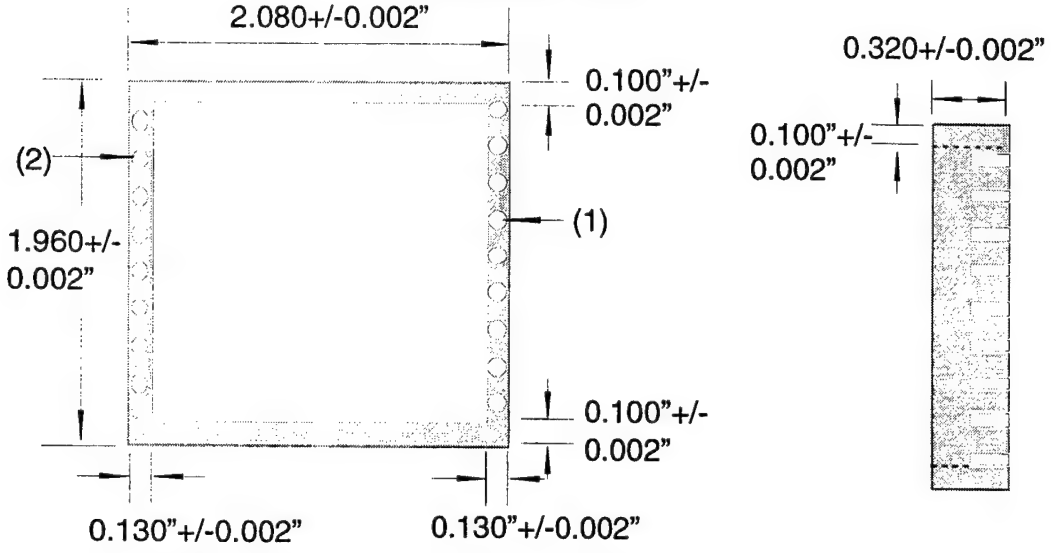

(1). 9 threaded holes of spacing 0.205"(center to center) for 0-80 3/16" fine screw
(2). 8 threaded holes of spacing 0.205" (center to center) for 0-80 3/16" fine screw

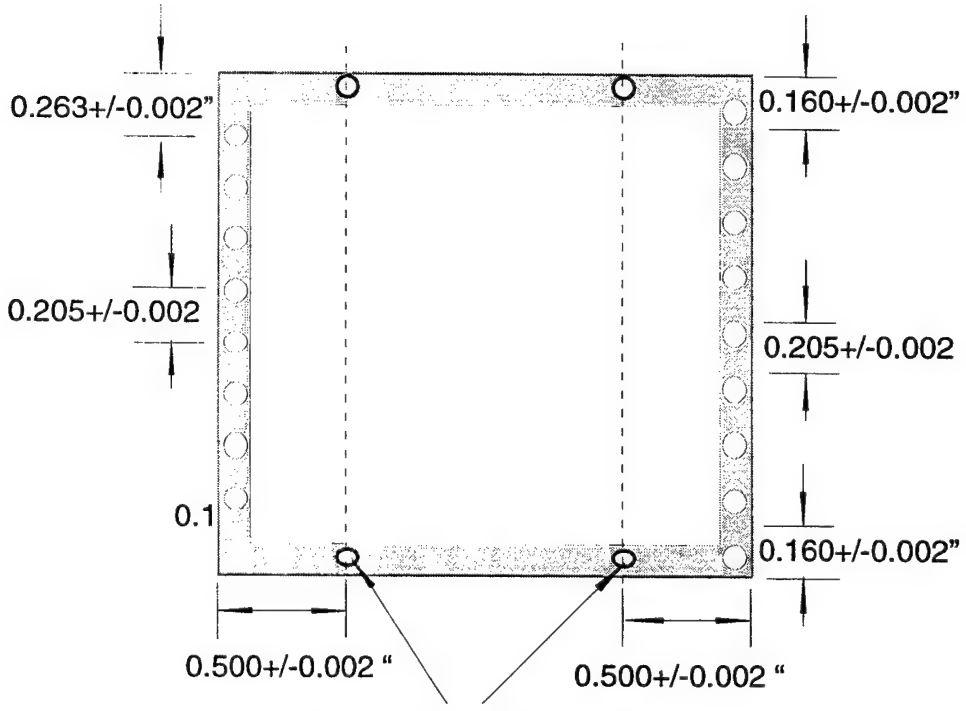

drill holes for 00-90 threaded rod

APPENDIX F. GRAPHS OF MATLAB AND MEASURED RESULTS

This section which is divided into two subsections contains graphs of the results of the MATLAB program and measurements. First, results of the constricted annular prime mover are presented. Next, some predictied results for the two stack annular prime mover are provided.

APPENDIX F.1 RESULTS OF THE CONSTRICTED ANNULAR PRIME MOVER

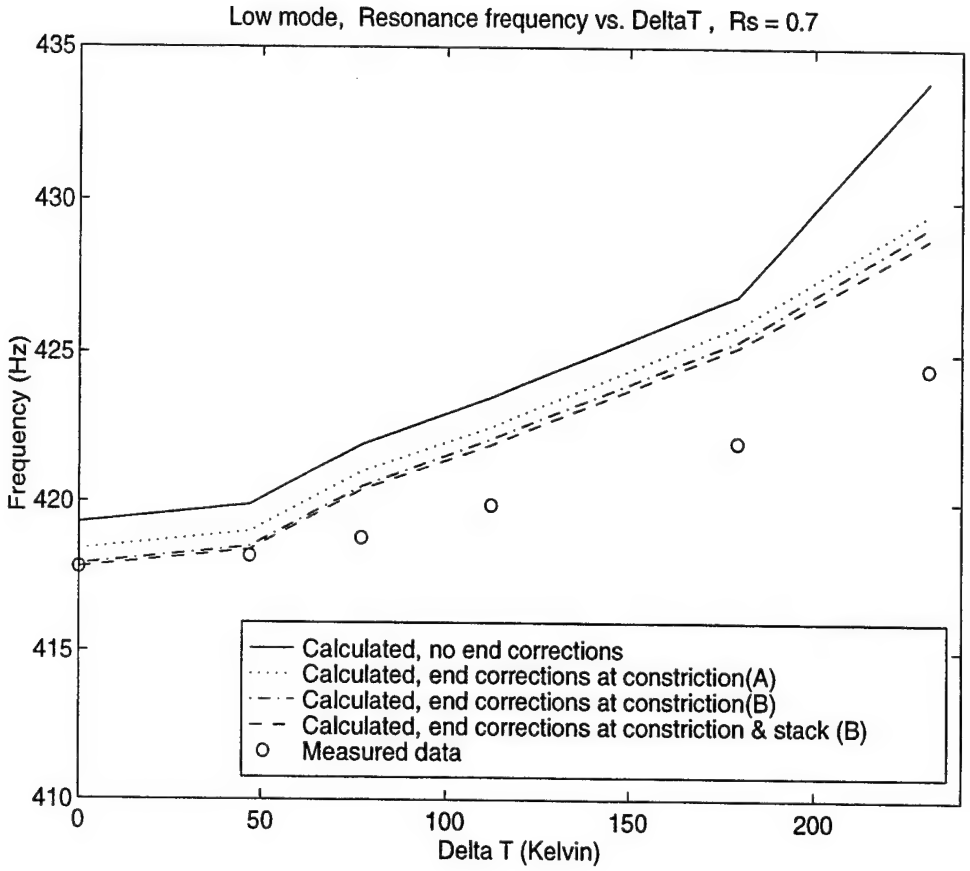

Figure F.1-1 Comparisons of the measured and calculated resonance frequencies of the low mode for the constricted prime mover with the porosity of 0.7. Method A is the conformation transformation and Method B is the higher order mode.

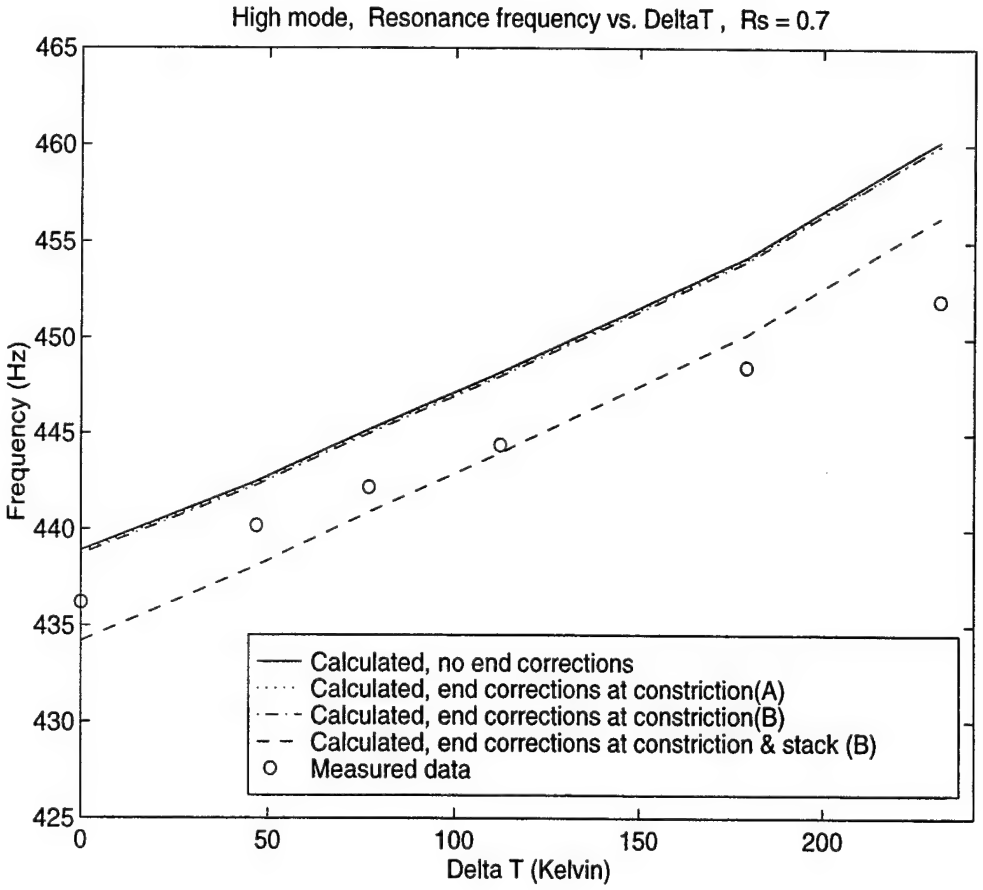

Figure F.1-2 Comparisons of the measured and calculated resonance frequencies of the high mode for the constricted prime mover with the porosity of 0.7. Method A is the conformation transformation and Method B is the higher order mode.

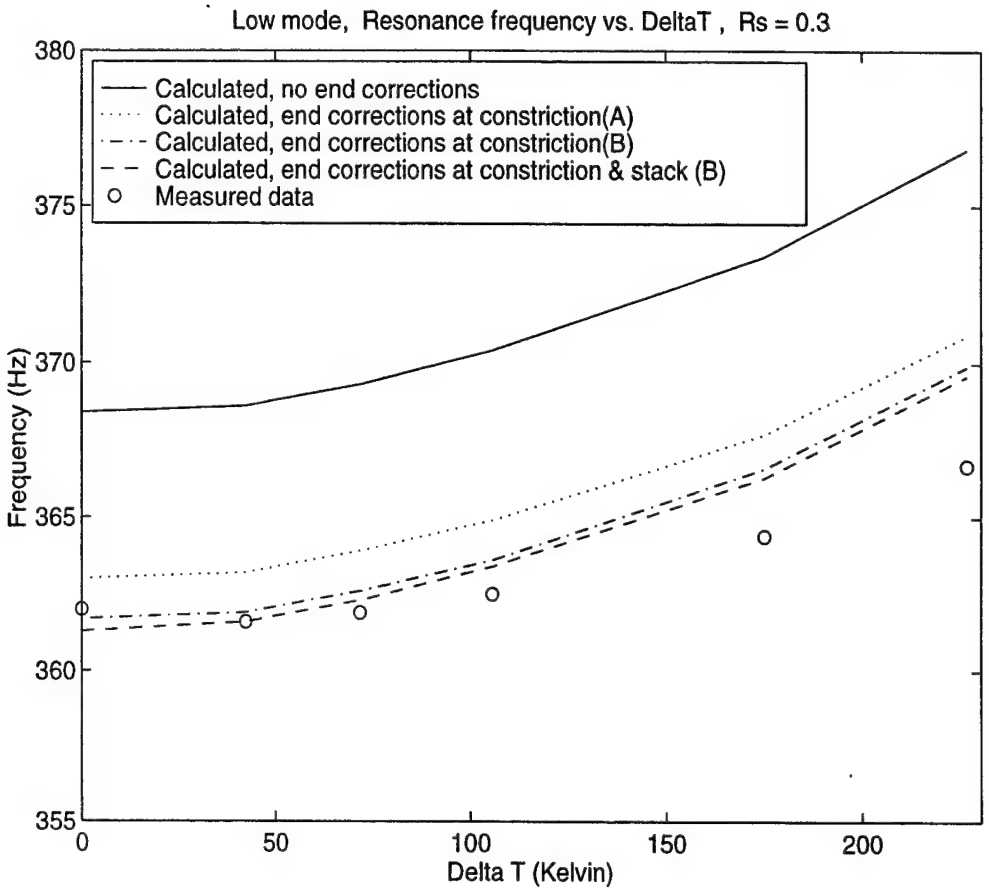

Figure F.1-3 Comparisons of the measured and calculated resonance frequencies of the low mode for the constricted prime mover with the porosity of 0.3. Method A is the conformation transformation and Method B is the higher order mode.

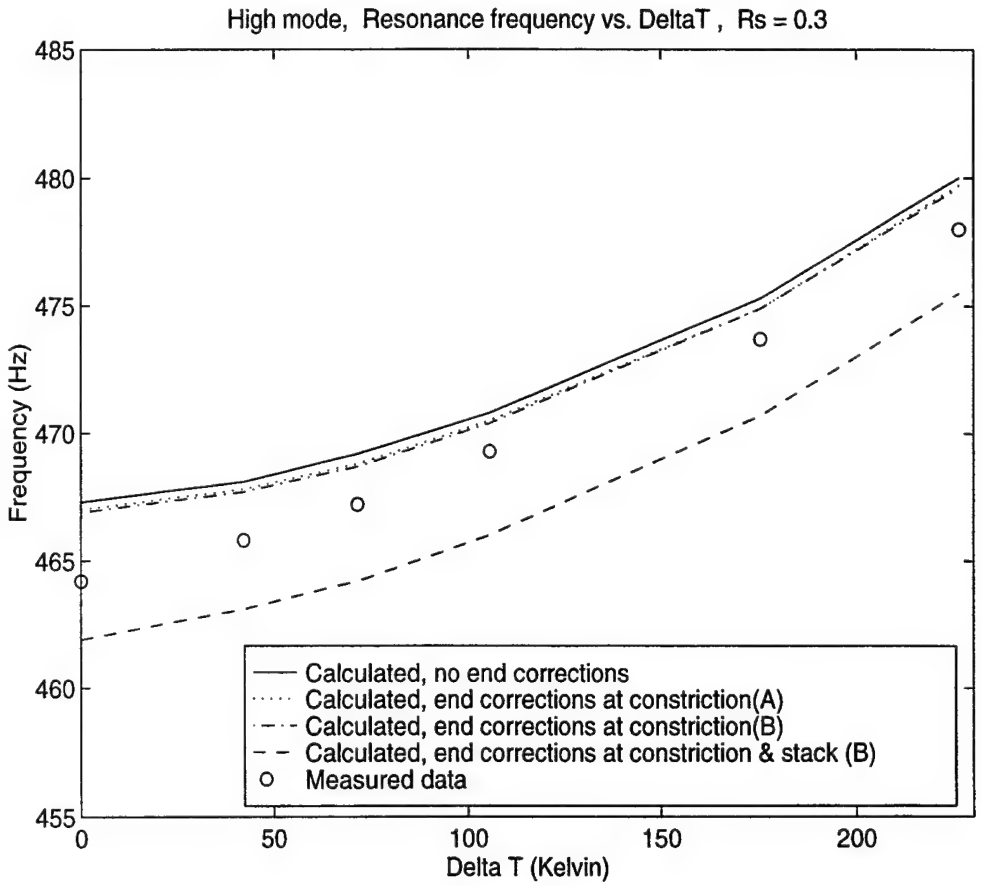

Figure F.1-4 Comparisons of the measured and calculated resonance frequencies of the high mode for the constricted prime mover with the porosity of 0.3. Method A is the conformation transformation and Method B is the higher order mode.

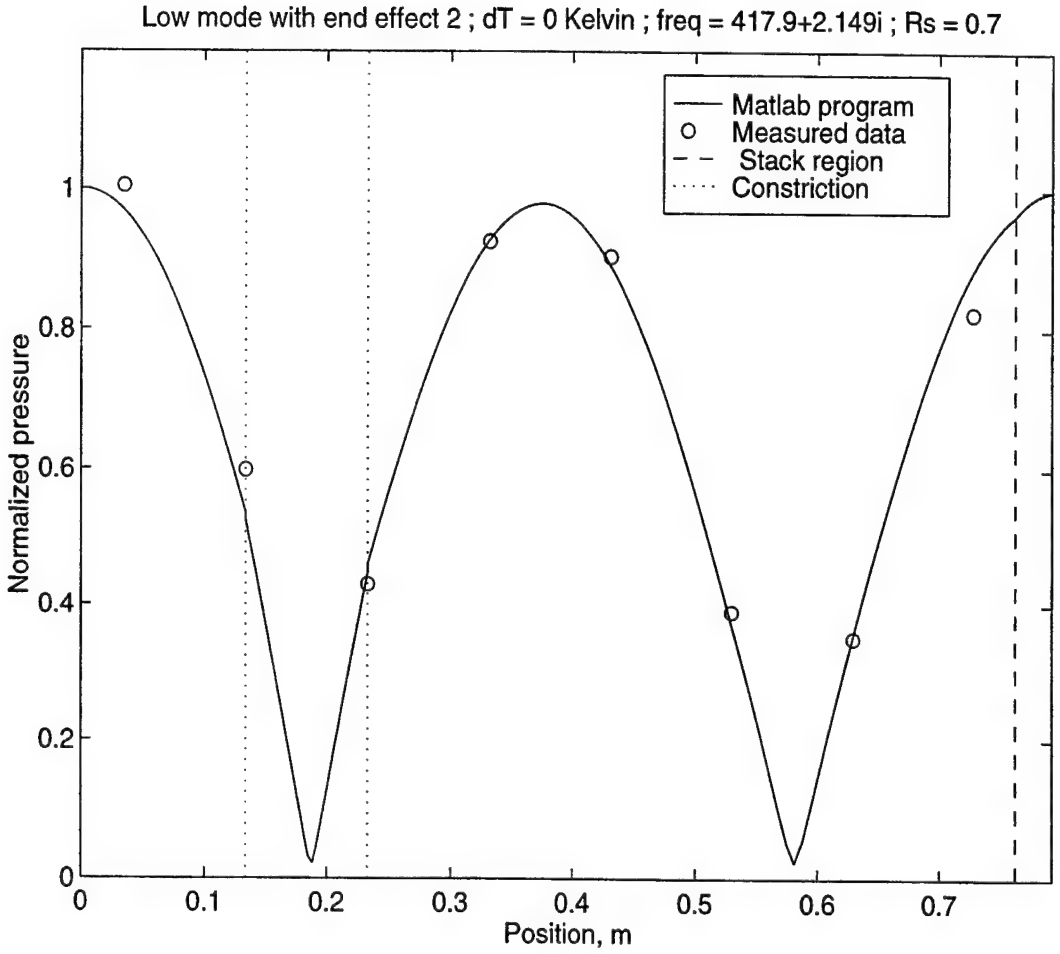

Figure F.1-5 Mode shape of the low mode of the constricted prime mover (Rs=0.7) when the driver is located 45° from the stack and ΔT=0 K. The calculated results are based on the higher order mode method. The frequency is the calculated value.

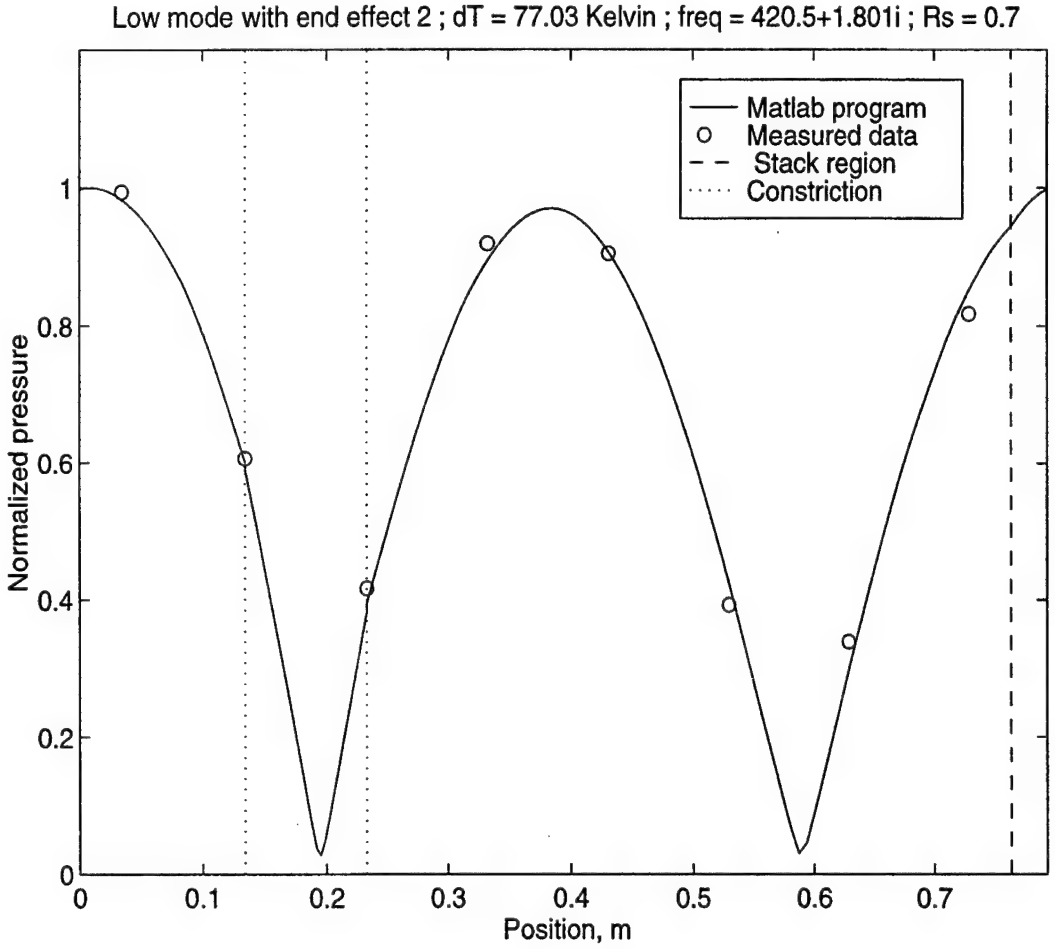

Figure F.1-6 Mode shape of the low mode of the constricted prime mover (Rs=0.7) when the driver is located 45° from the stack and ΔT=77 K. The calculated results are based on the higher order mode method. The frequency is the calculated value.

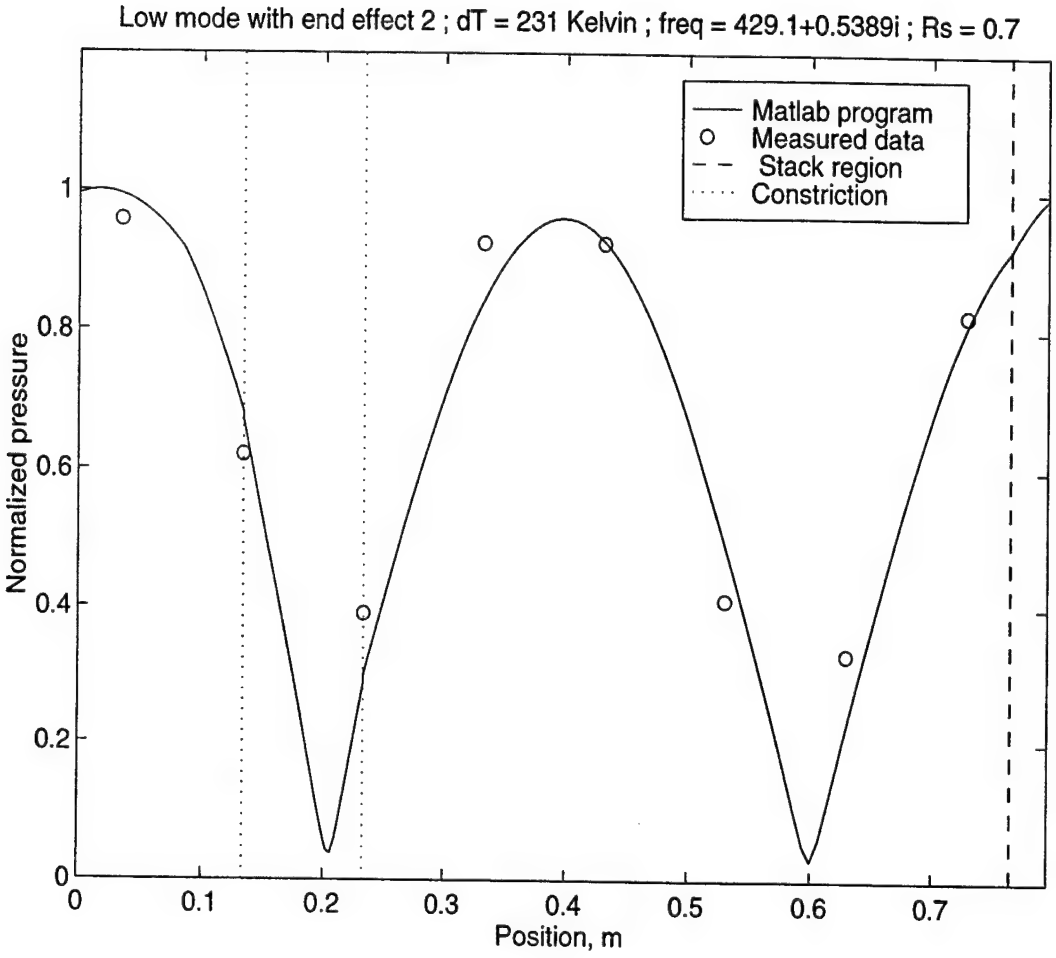

Figure F.1-7 Mode shape of the low mode of the constricted prime mover (Rs=0.7) when the driver is located 45° from the stack and ΔT=231 K. The calculated results are based on the higher order mode method. The frequency is the calculated value.

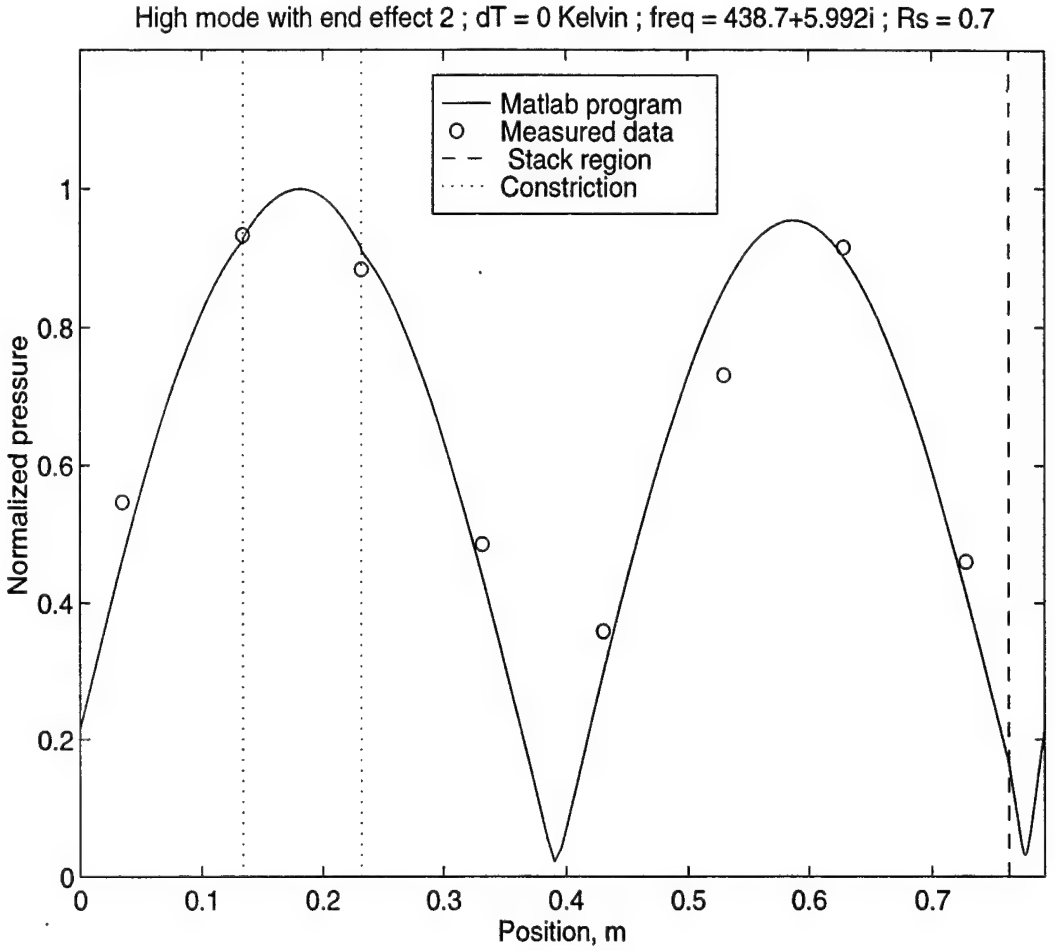

Figure F.1-8 Mode shape of the high mode of the constricted prime mover (Rs=0.7) when the driver is located 45° from the stack and ΔT=0 K. The calculated results are based on the higher order mode method. The frequency is the calculated value.

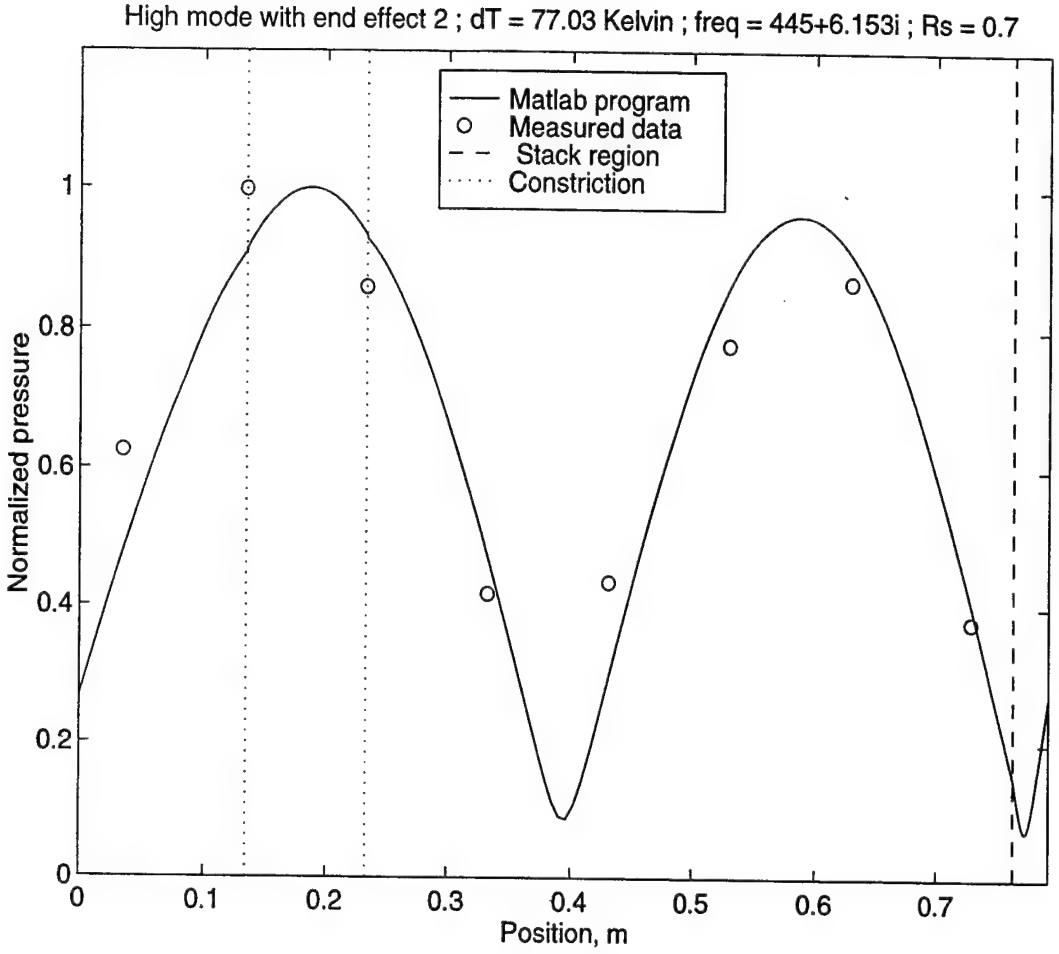

Figure F.1-9 Mode shape of the high mode of the constricted prime mover (Rs=0.7) when the driver is located 45° from the stack and ΔT=77 K. The calculated results are based on the higher order mode method. The frequency is the calculated value.

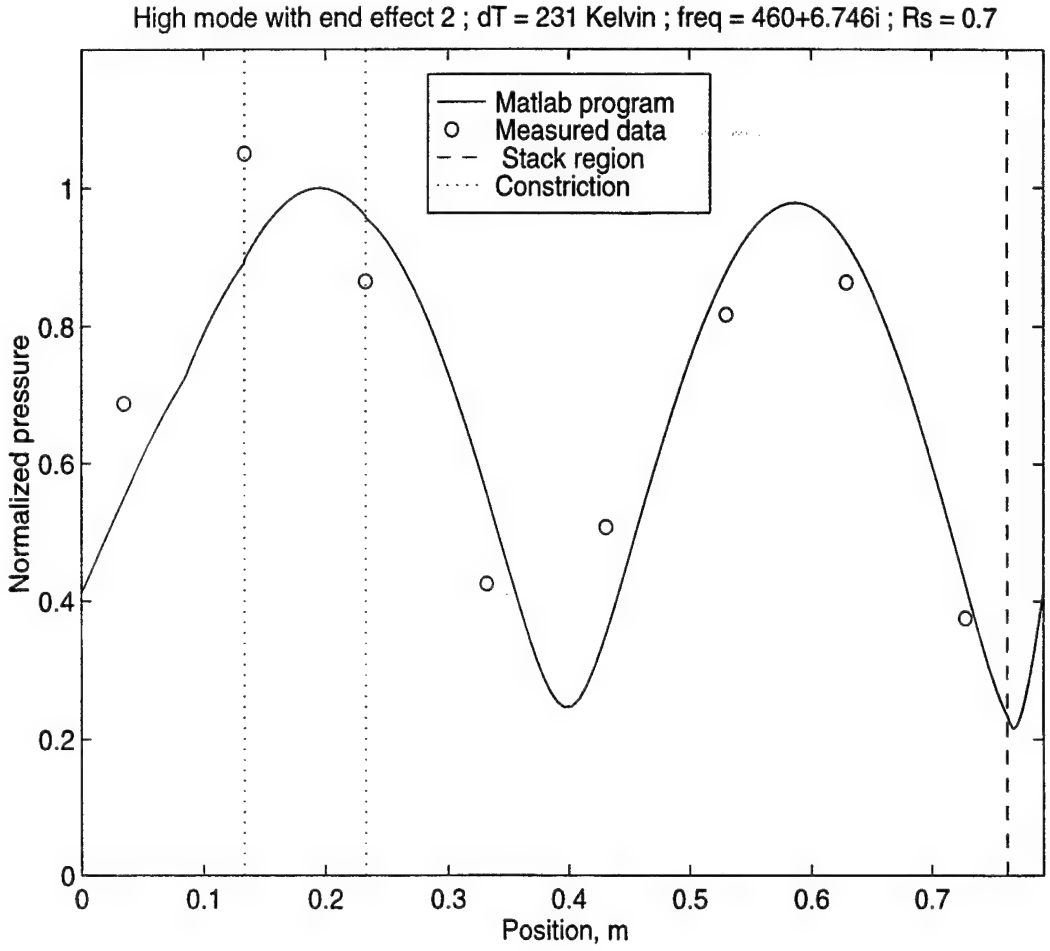

Figure F.1-10 Mode shape of the high mode of the constricted prime mover (Rs=0.7) when the driver is located 45° from the stack and ΔT=231 K. The calculated results are based on the higher order mode method. The frequency is the calculated value.

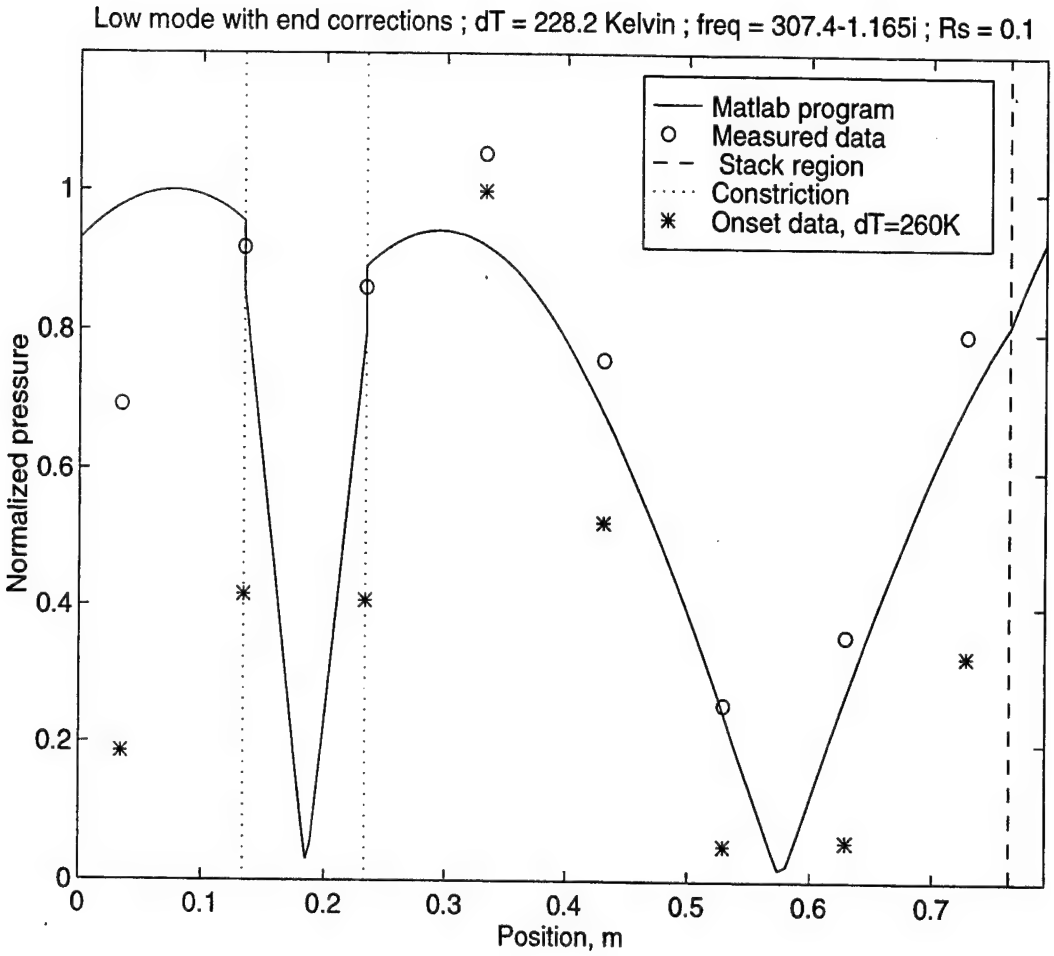

Figure F.1-11 Mode shape of the low mode of the constricted prime mover (Rs=0.1) when the driver is located 45° from the stack and ΔT=228 K. The calculated results are based on the higher order mode method. The frequency is the calculated value. Symbol * represents the mode shape above onset, the measured frequency is 312 Hz.

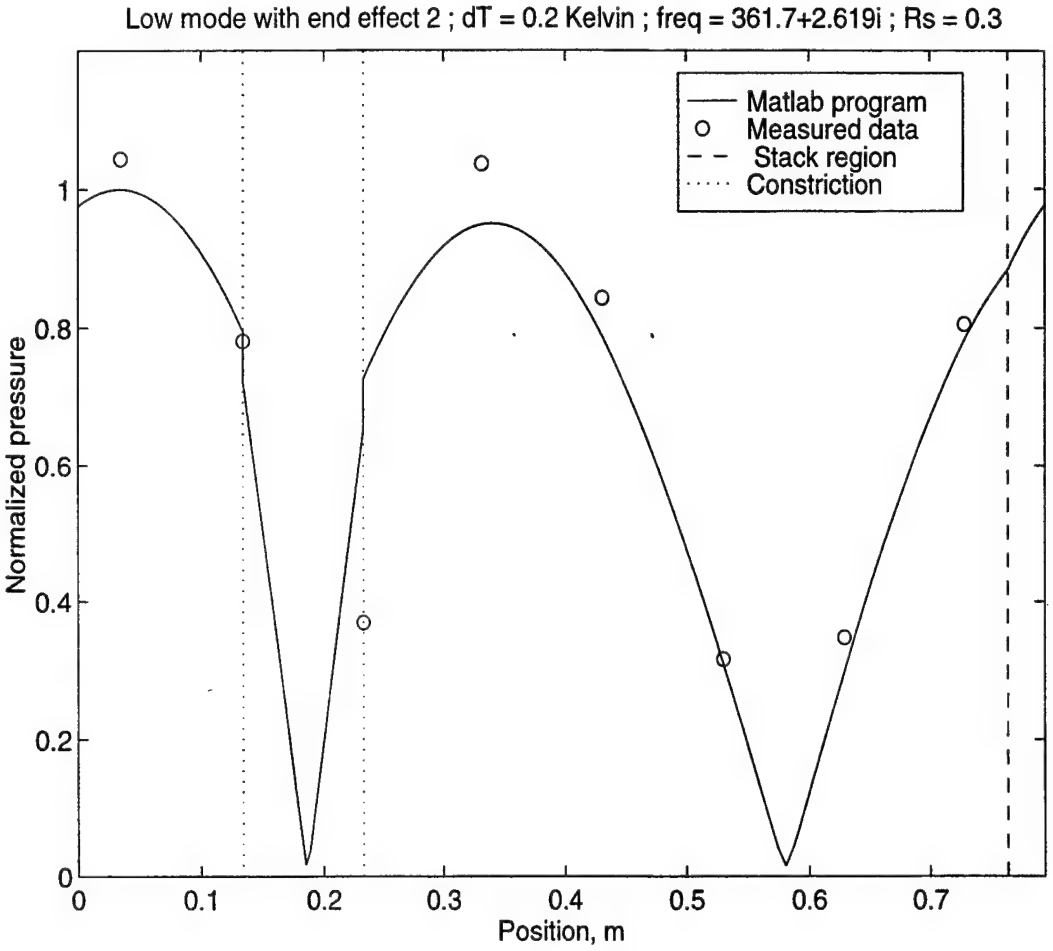

Figure F.1-12 Mode shape of the low mode of the constricted prime mover (Rs=0.3) when the driver is located 45° from the stack and ΔT=0 K. The calculated results are based on the higher order mode method. The frequency is the calculated value.

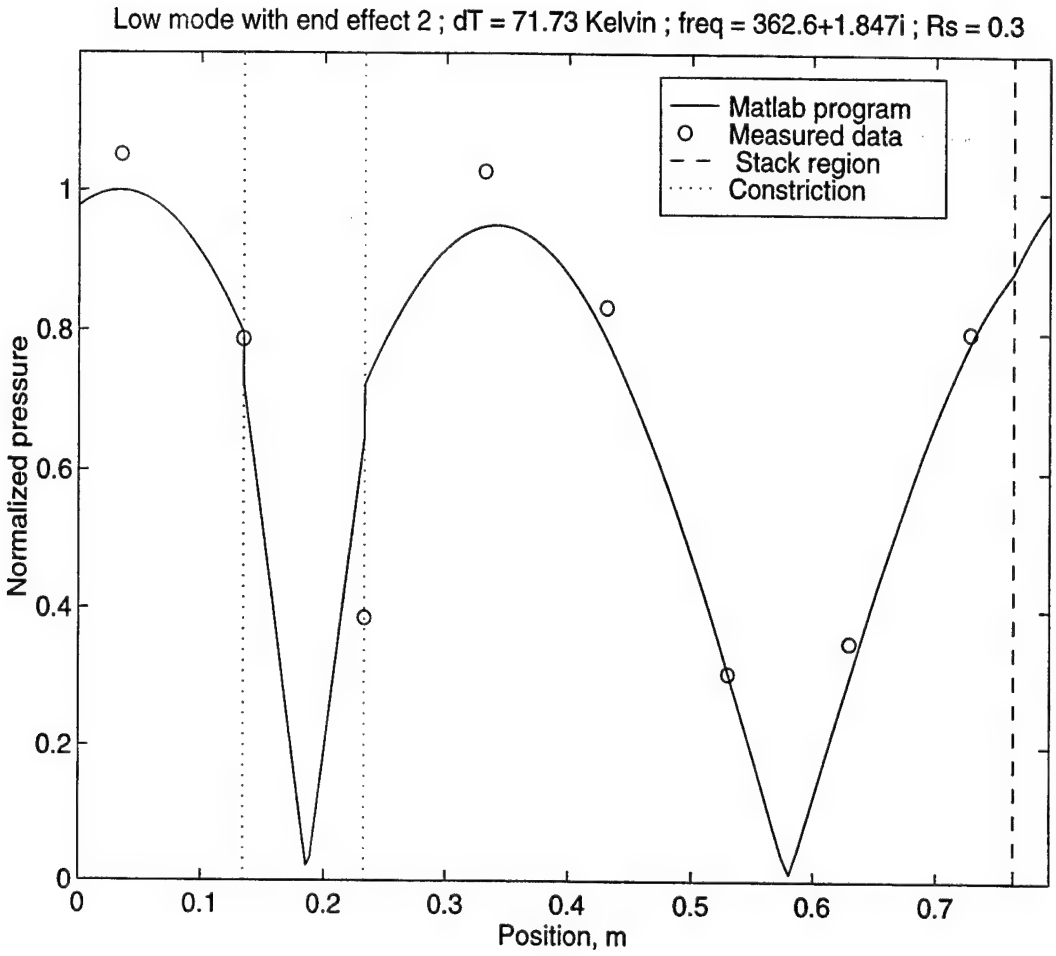

Figure F.1-13 Mode shape of the low mode of the constricted prime mover (Rs=0.3) when the driver is located 45° from the stack and ΔT=72 K. The calculated results are based on the higher order mode method. The frequency is the calculated value.

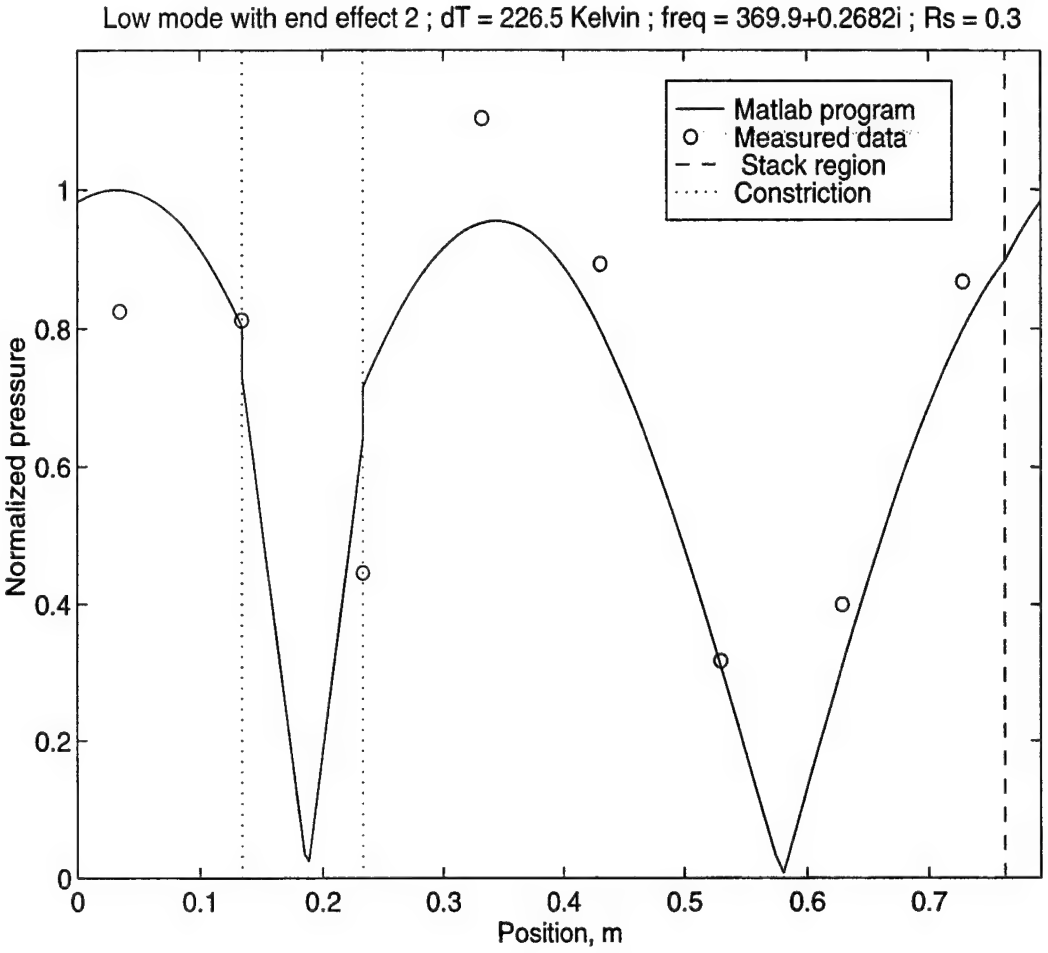

Figure F.1-14 Mode shape of the low mode of the constricted prime mover (Rs=0.3) when the driver is located 45° from the stack and ΔT=227 K. The calculated results are based on the higher order mode method. The frequency is the calculated value.

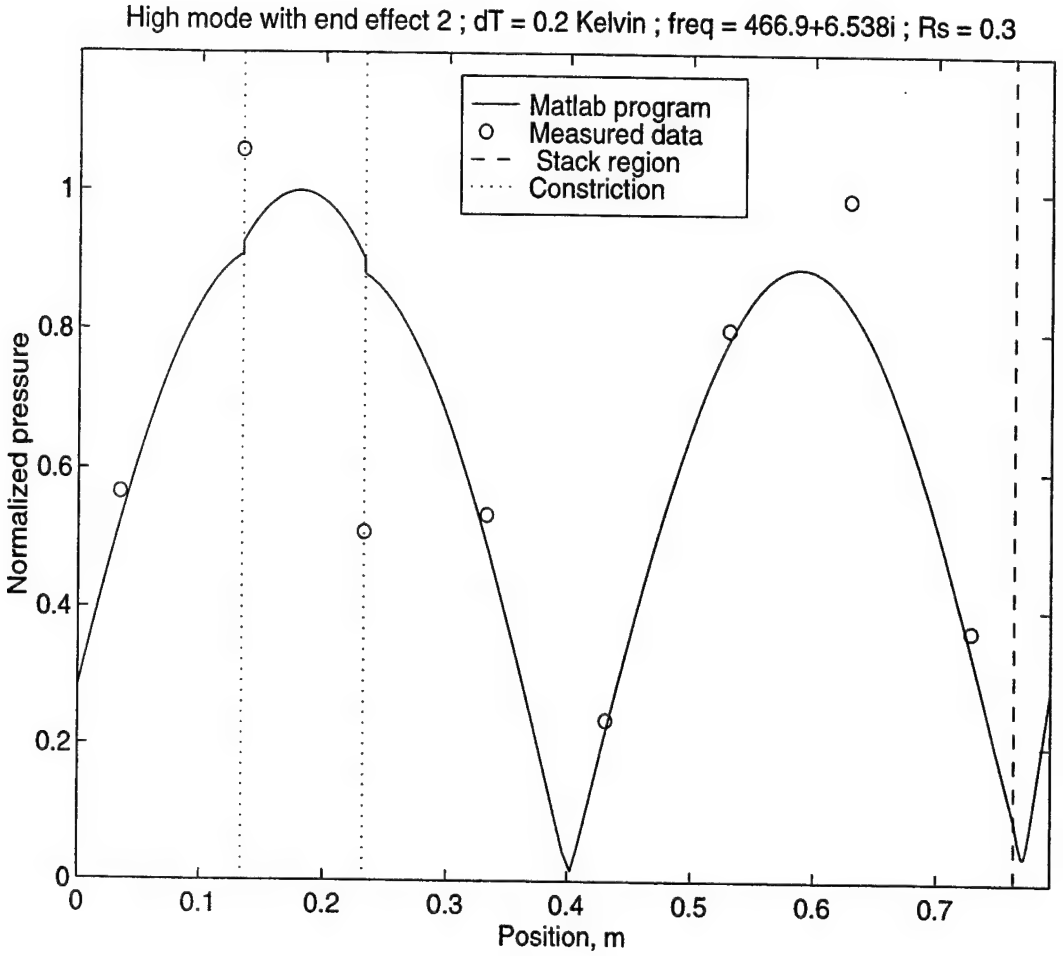

Figure F.1-15 Mode shape of the high mode of the constricted prime mover (Rs=0.3) when the driver is located 45° from the stack and ΔT=0 K. The calculated results are based on the higher order mode method. The frequency is the calculated value.

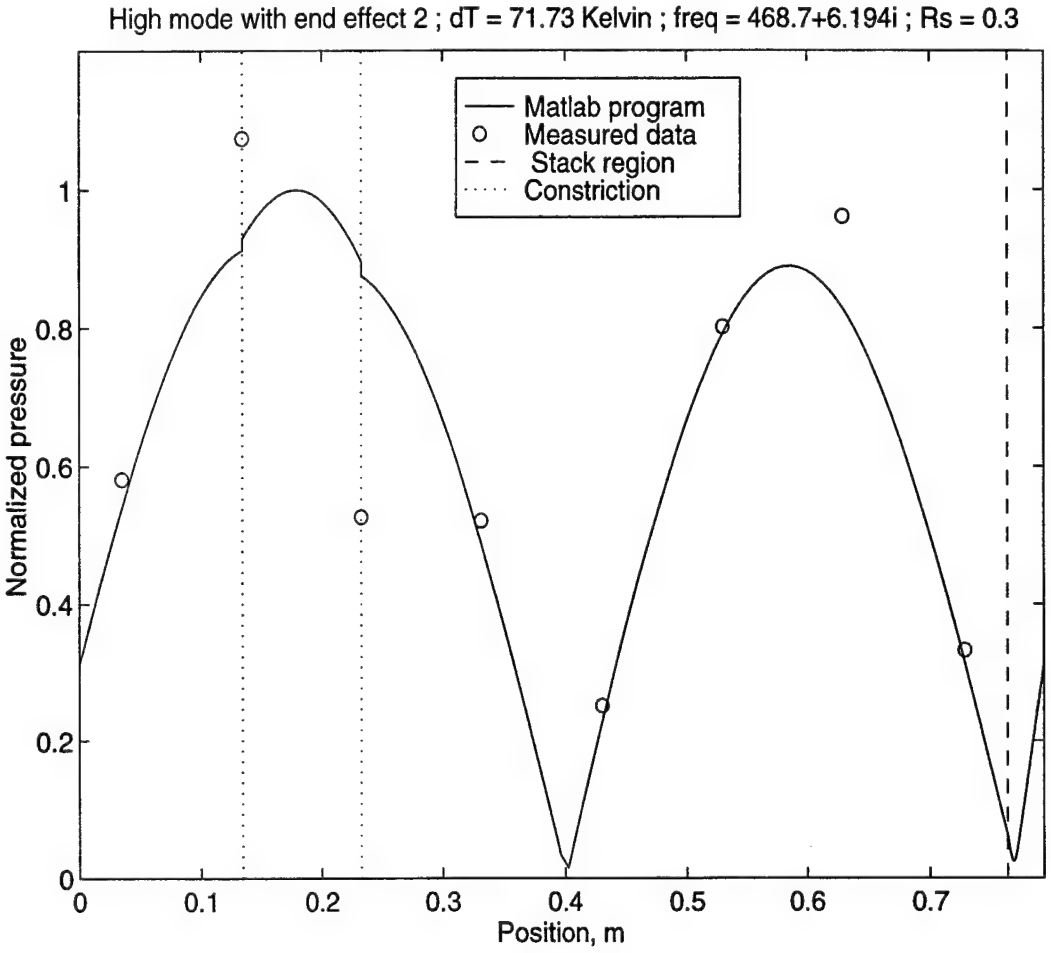

Figure F.1-16 Mode shape of the high mode of the constricted prime mover (Rs=0.3) when the driver is located 45° from the stack and ΔT=72 K. The calculated results are based on the higher order mode method. The frequency is the calculated value.

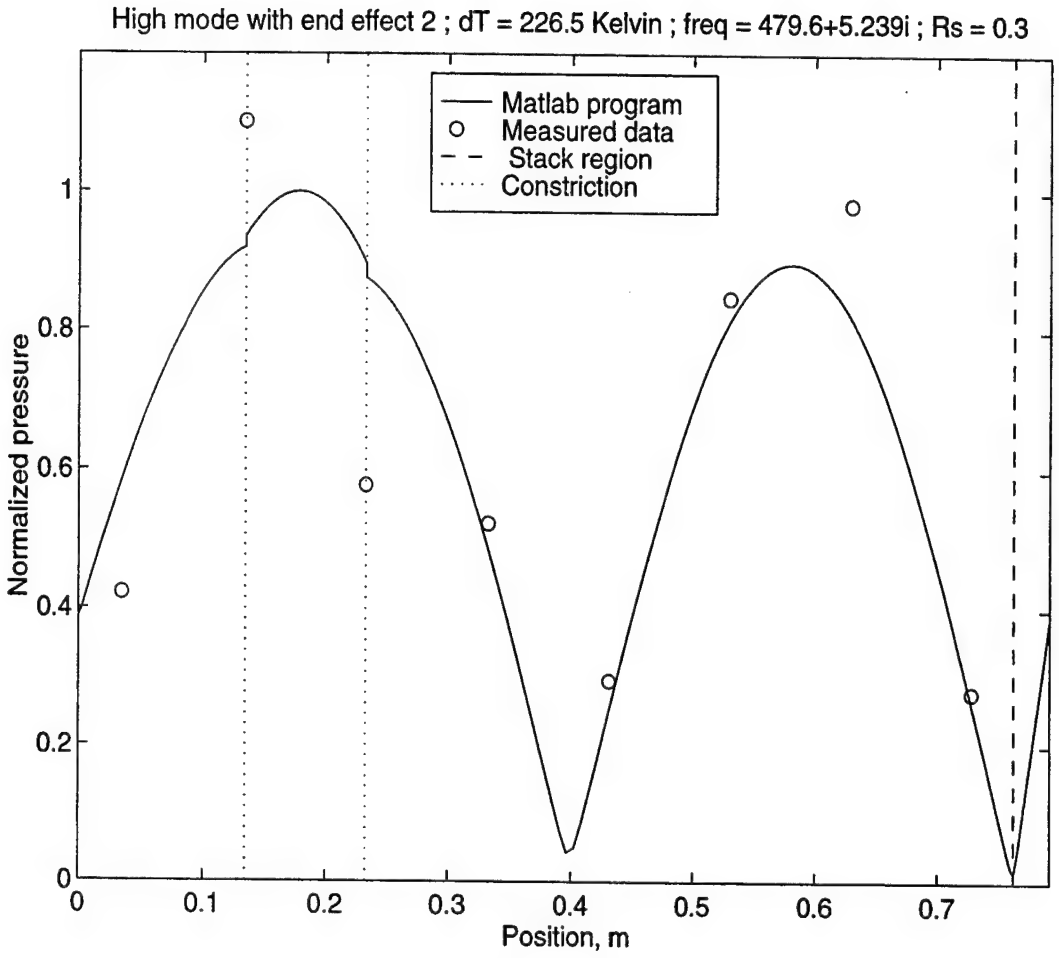

Figure F.1-17 Mode shape of the high mode of the constricted prime mover (Rs=0.3) when the driver is located 45° from the stack and ΔT=227 K. The calculated results are based on the higher order mode method. The frequency is the calculated value.

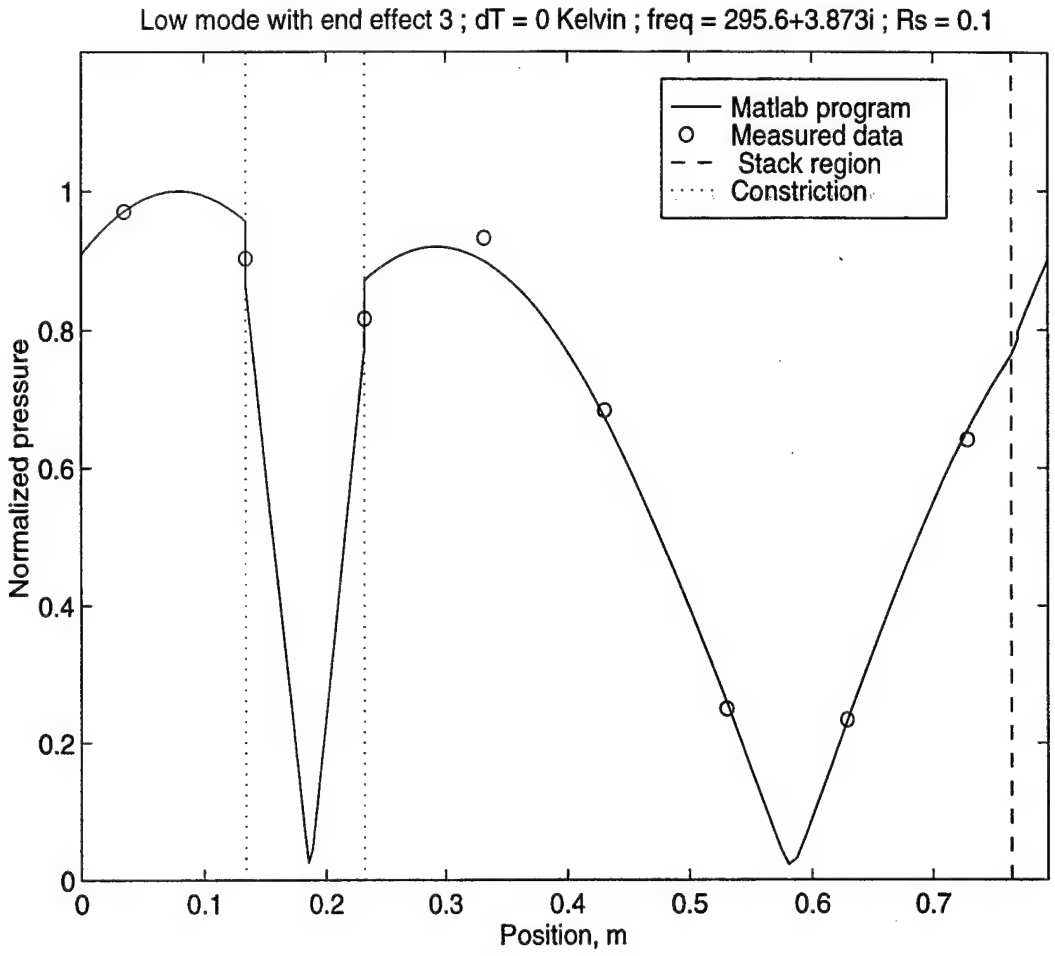

Figure F.1-18 Mode shape of the low mode of the constricted prime mover (Rs=0.1) when the driver is located 45° from the stack and ΔT=0 K. The calculated results are based on the higher order mode method and the end corrections of the stack are included. The frequency is the calculated value.

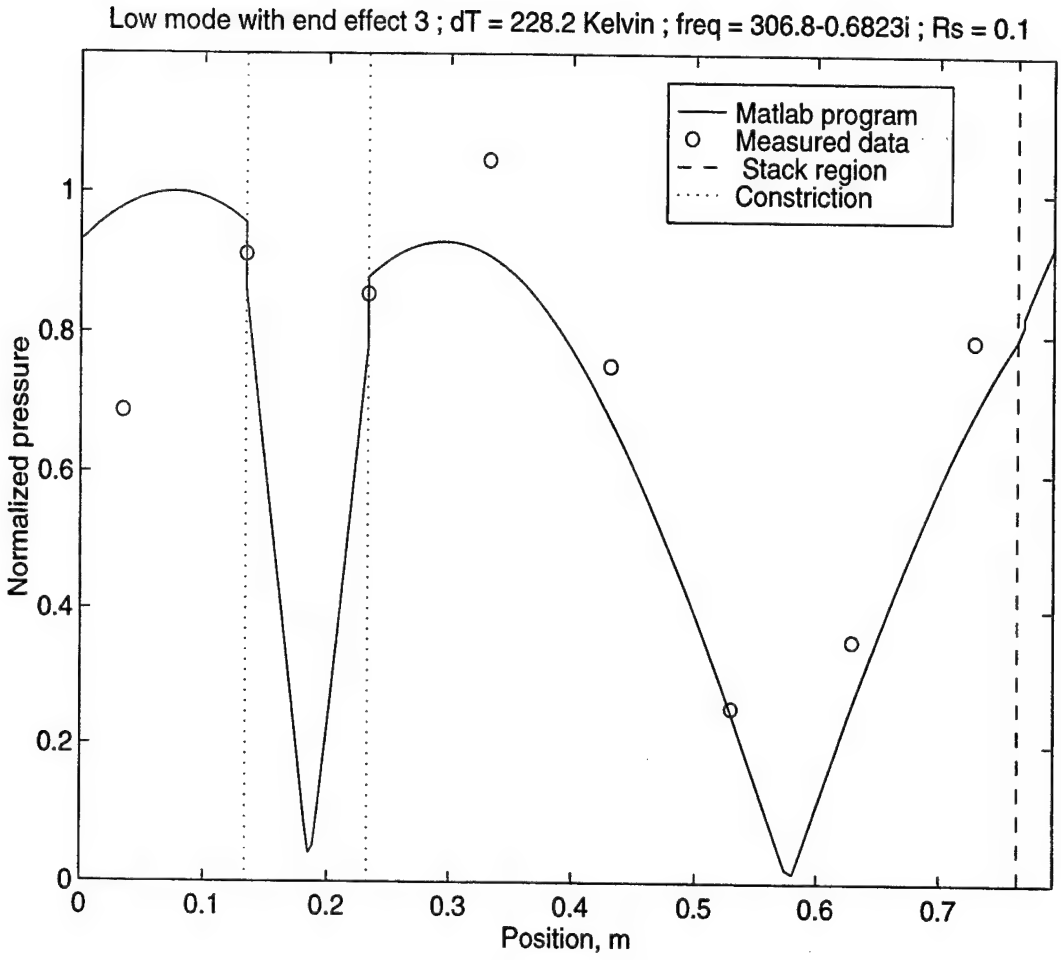

Figure F.1-19 Mode shape of the low mode of the constricted prime mover (Rs=0.1) when the driver is located 45° from the stack and ΔT=228 K. The calculated results are based on the higher order mode method and the end corrections of the stack are included. The frequency is the calculated value.

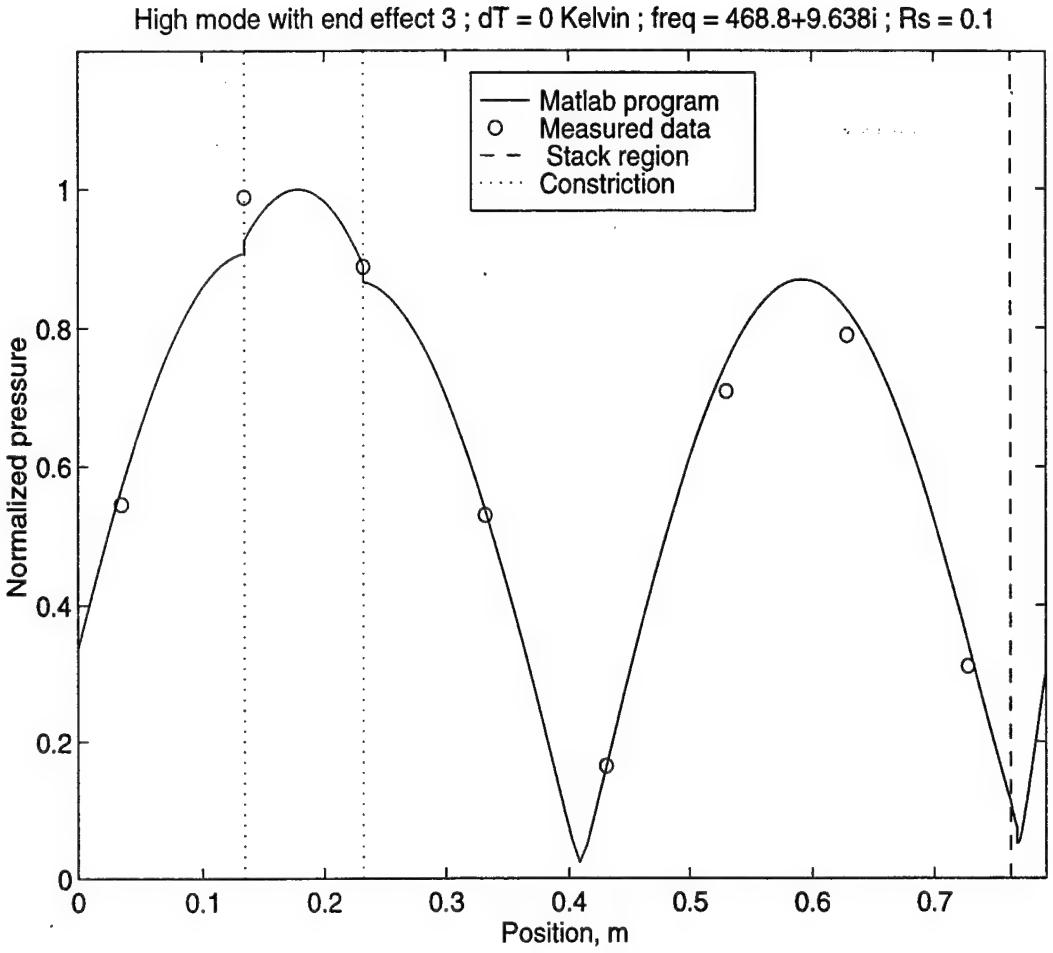

Figure F.1-20 Mode shape of the high mode of the constricted prime mover (Rs=0.1) when the driver is located 45° from the stack and ΔT=0 K. The calculated results are based on the higher order mode method and the end corrections of the stack are included. The frequency is the calculated value.

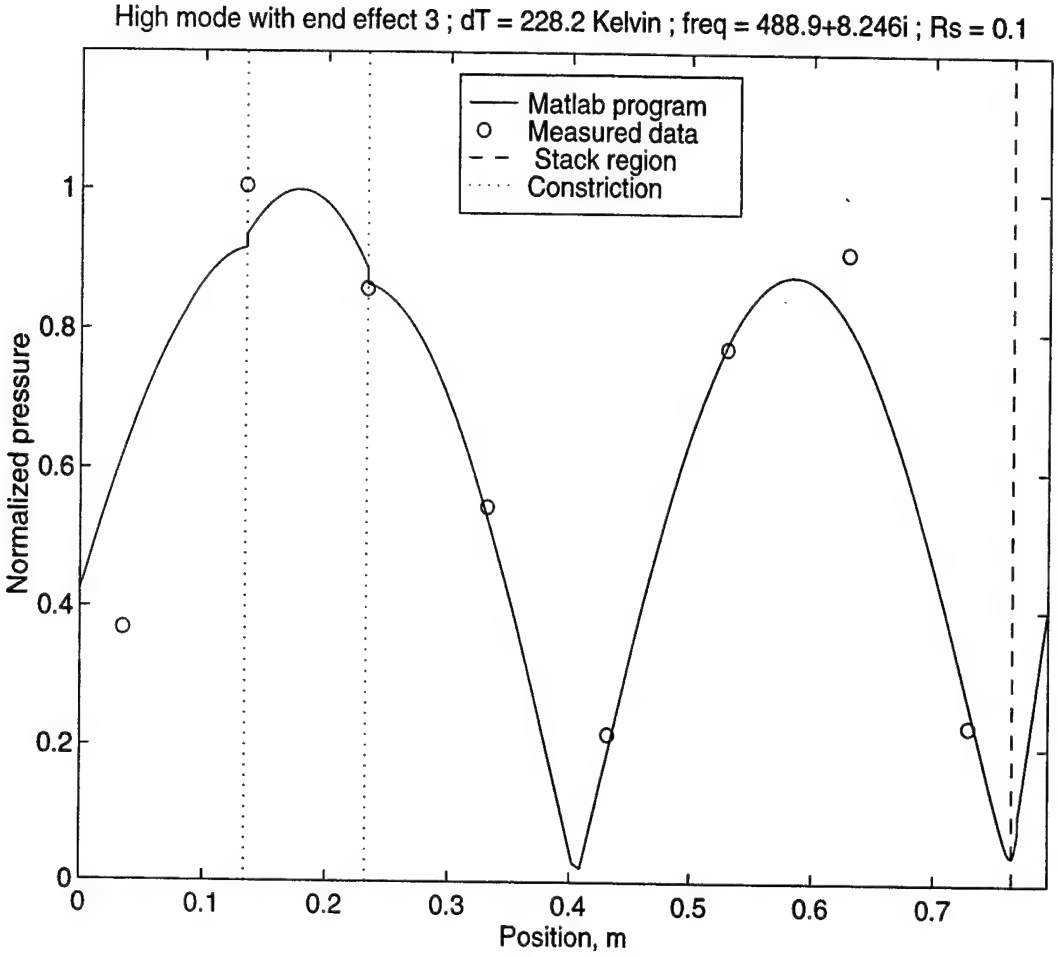

Figure F.1-21 Mode shape of the high mode of the constricted prime mover (Rs=0.1) when the driver is located 45° from the stack and ΔT=228 K. The calculated results are based on the higher order mode method and the end corrections of the stack are included. The frequency is the calculated value.

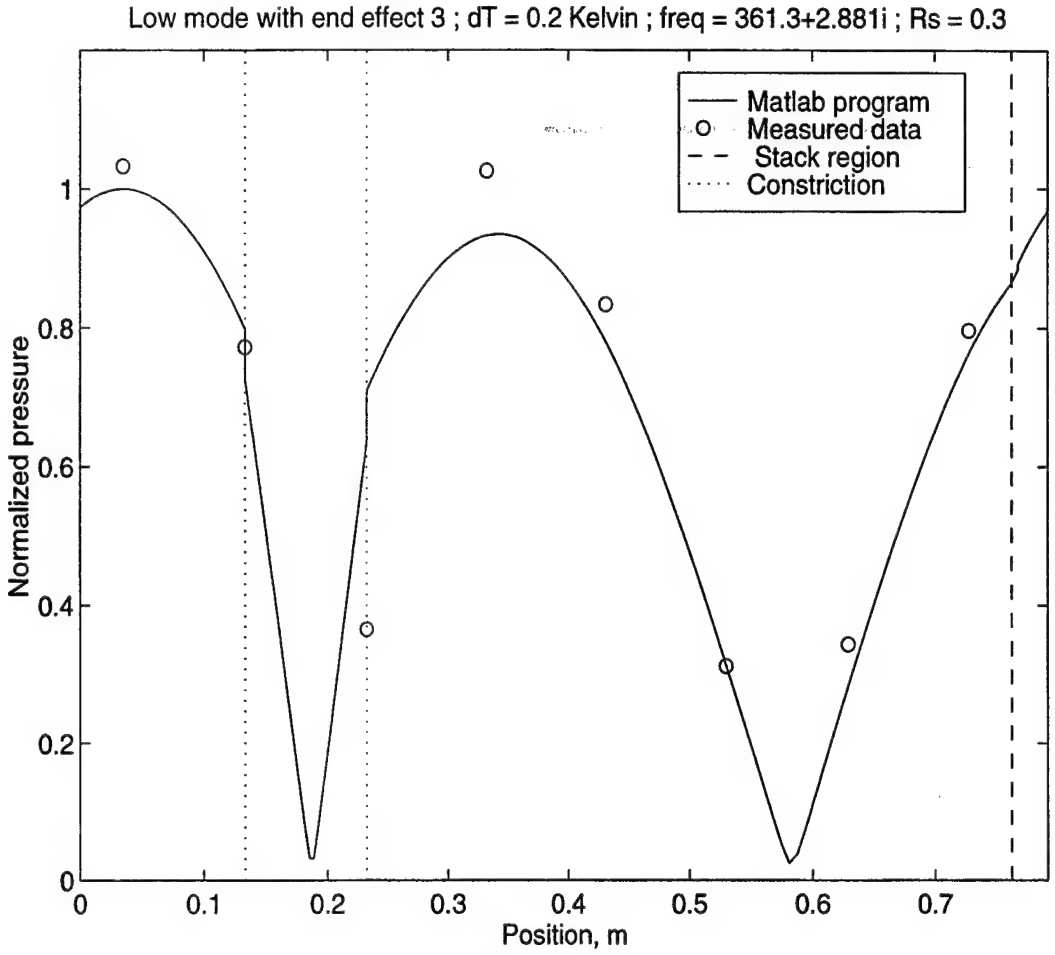

Figure F.1-22 Mode shape of the low mode of the constricted prime mover (Rs=0.3) when the driver is located 45° from the stack and ΔT=0 K. The calculated results are based on the higher order mode method and the end corrections of the stack are included. The frequency is the calculated value.

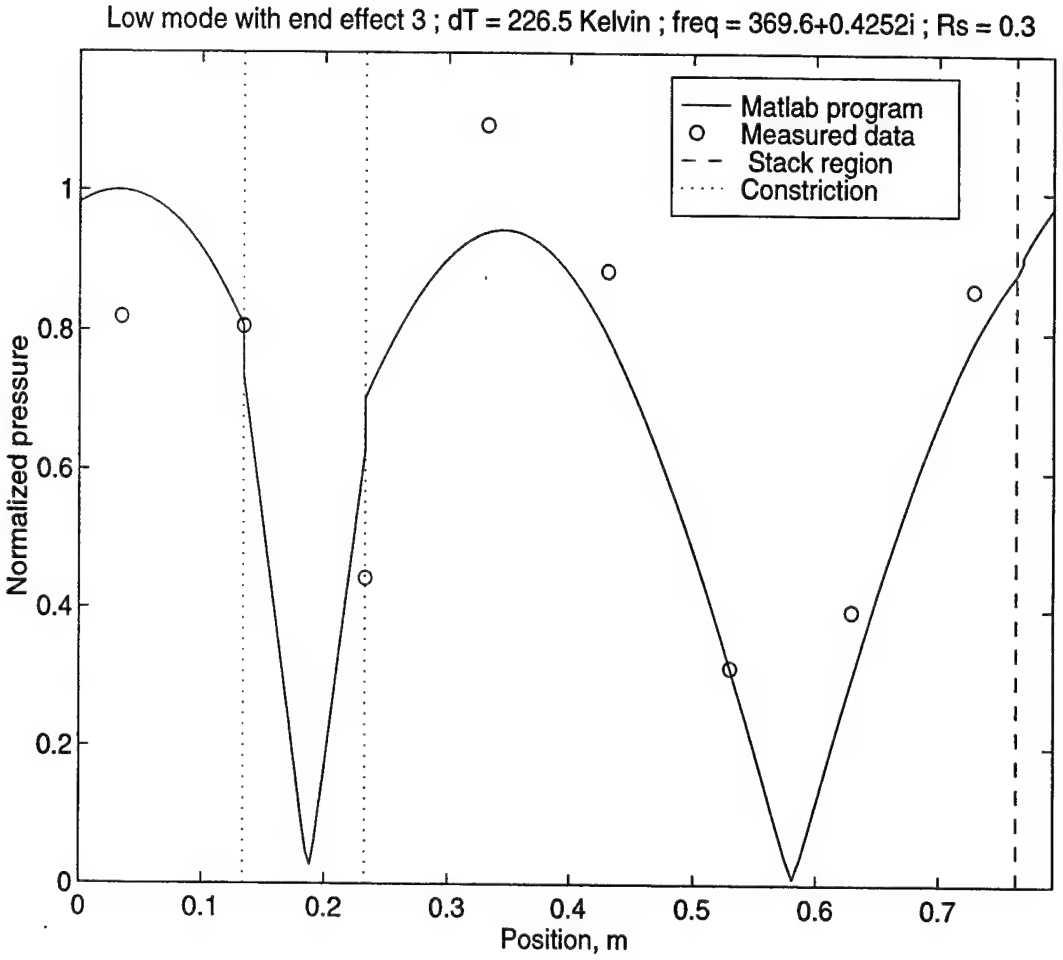

Figure F.1-23 Mode shape of the low mode of the constricted prime mover (Rs=0.3) when the driver is located 45° from the stack and ΔT=227 K. The calculated results are based on the higher order mode method and the end corrections of the stack are included. The frequency is the calculated value.

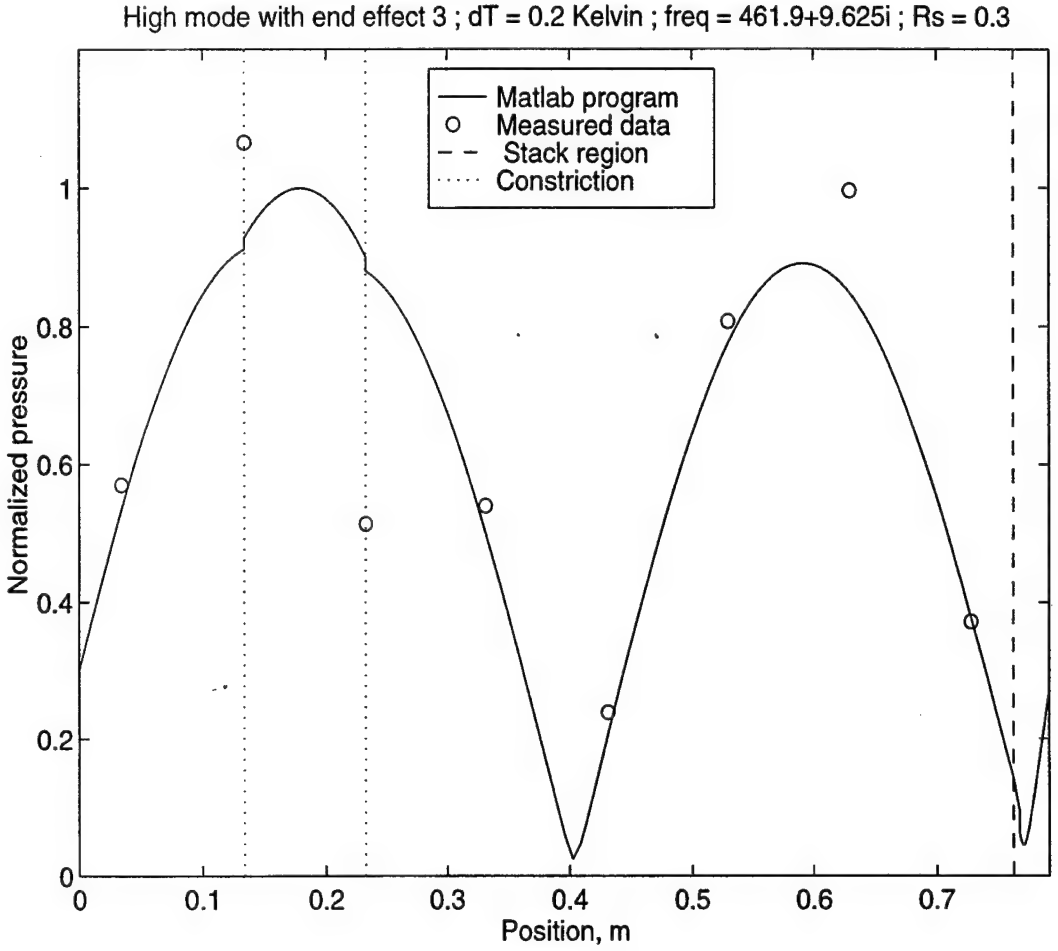

Figure F.1-24 Mode shape of the high mode of the constricted prime mover (Rs=0.3) when the driver is located 45° from the stack and ΔT=0 K. The calculated results are based on the higher order mode method and the end corrections of the stack are included. The frequency is the calculated value.

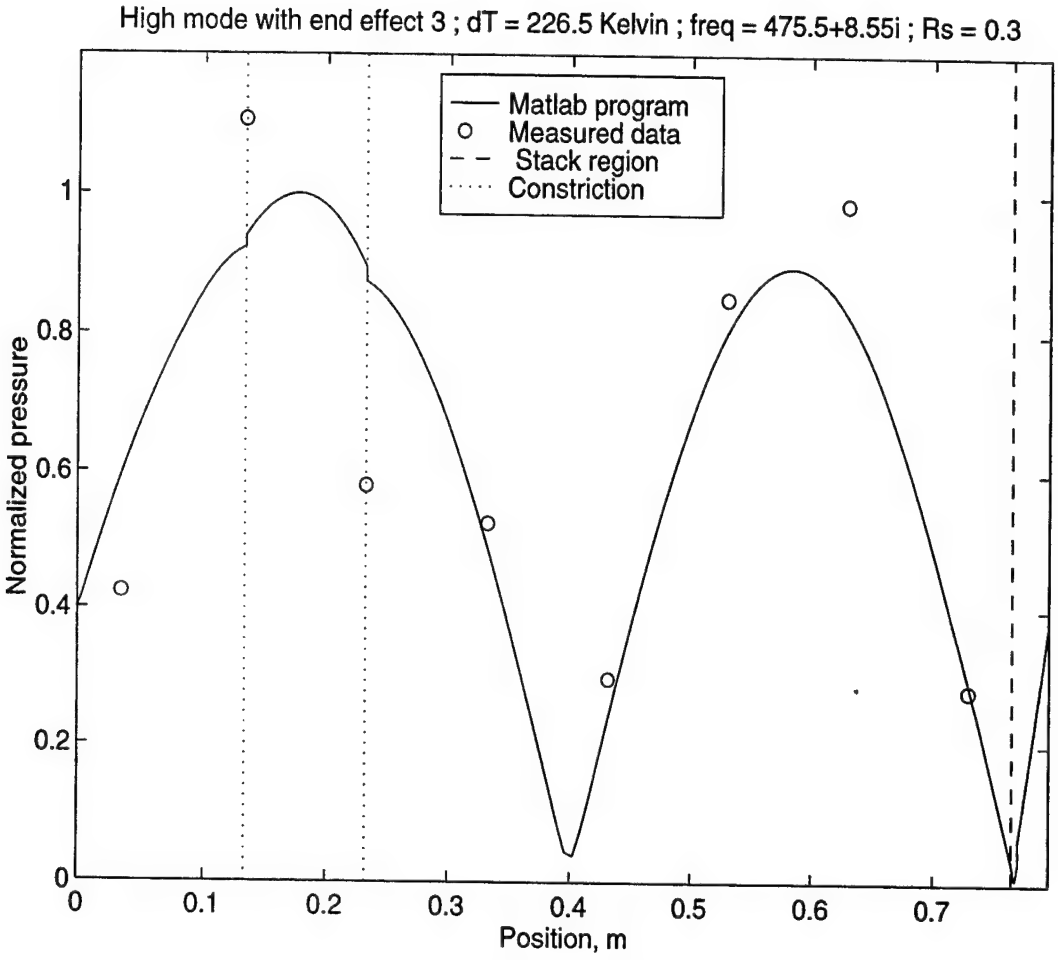

Figure F.1-25 Mode shape of the high mode of the constricted prime mover (Rs=0.3) when the driver is located 45° from the stack and ΔT=227 K. The calculated results are based on the higher order mode method and the end corrections of the stack are included. The frequency is the calculated value.

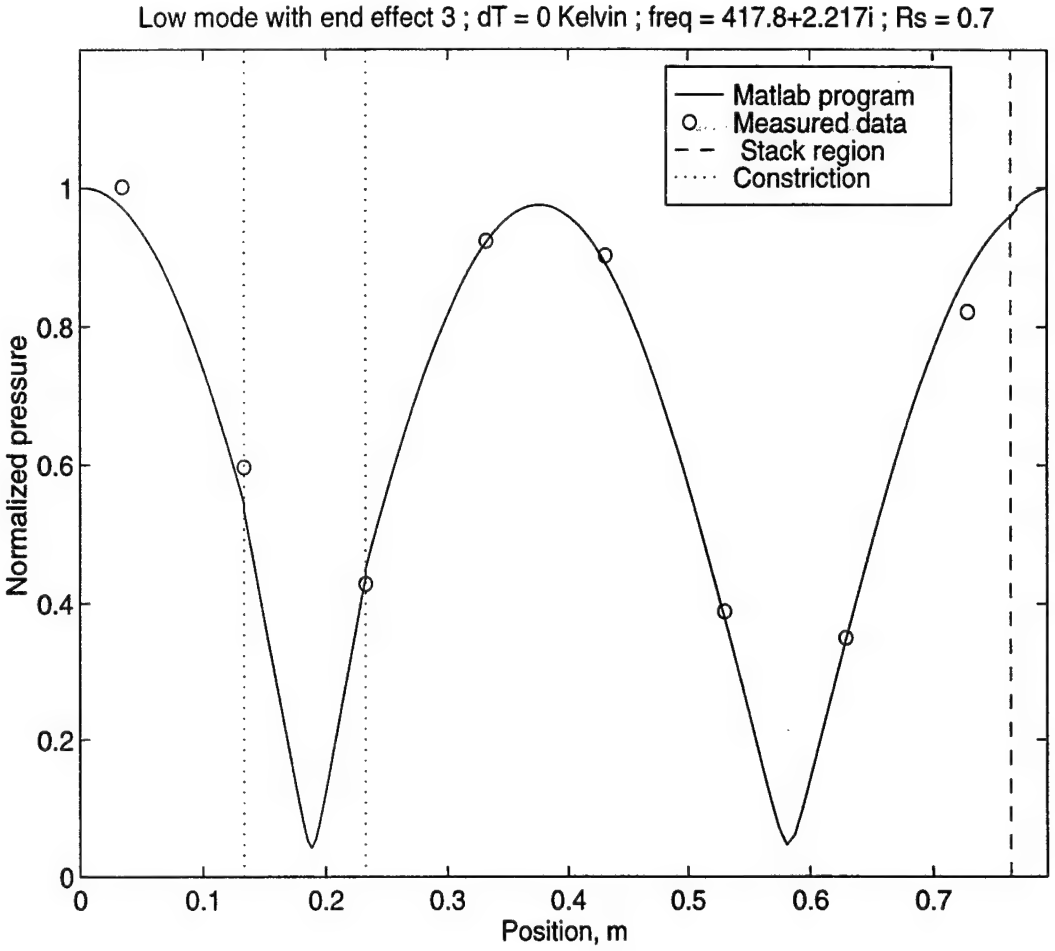

Figure F.1-26 Mode shape of the low mode of the constricted prime mover (Rs=0.7) when the driver is located 45° from the stack and ΔT=0 K. The calculated results are based on the higher order mode method and the end corrections of the stack are included. The frequency is the calculated value.

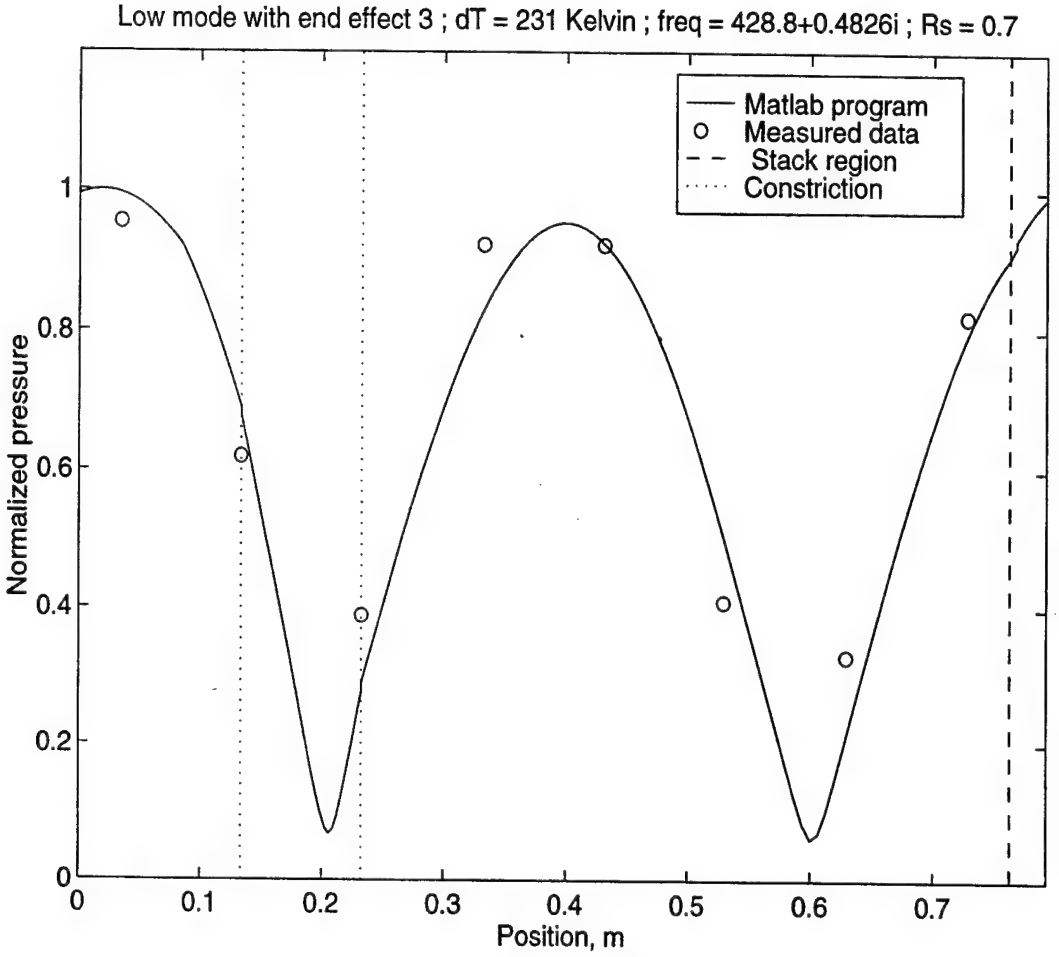

Figure F.1-27 Mode shape of the low mode of the constricted prime mover (Rs=0.7) when the driver is located 45° from the stack and ΔT=231 K. The calculated results are based on the higher order mode method and the end corrections of the stack are included. The frequency is the calculated value.

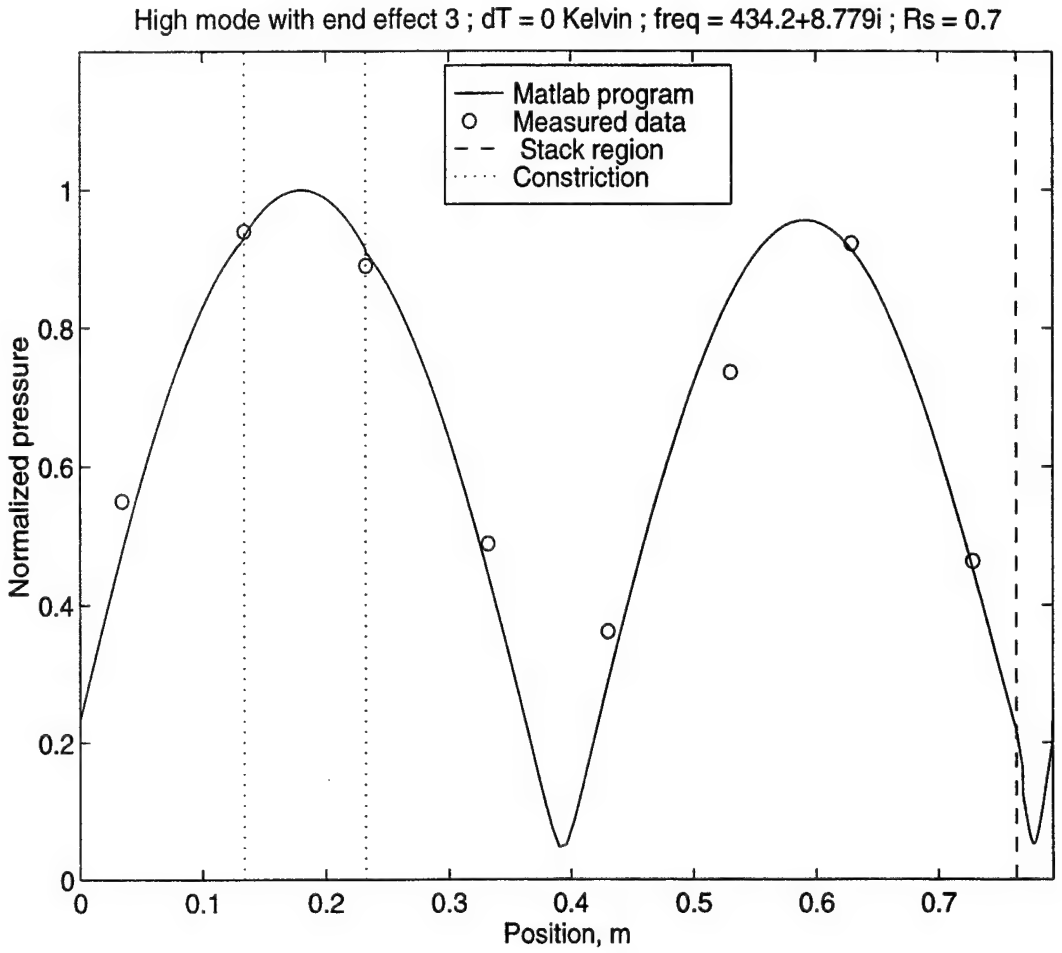

Figure F.1-28 Mode shape of the high mode of the constricted prime mover (Rs=0.7) when the driver is located 45° from the stack and ΔT=0 K. The calculated results are based on the higher order mode method and the end corrections of the stack are included. The frequency is the calculated value.

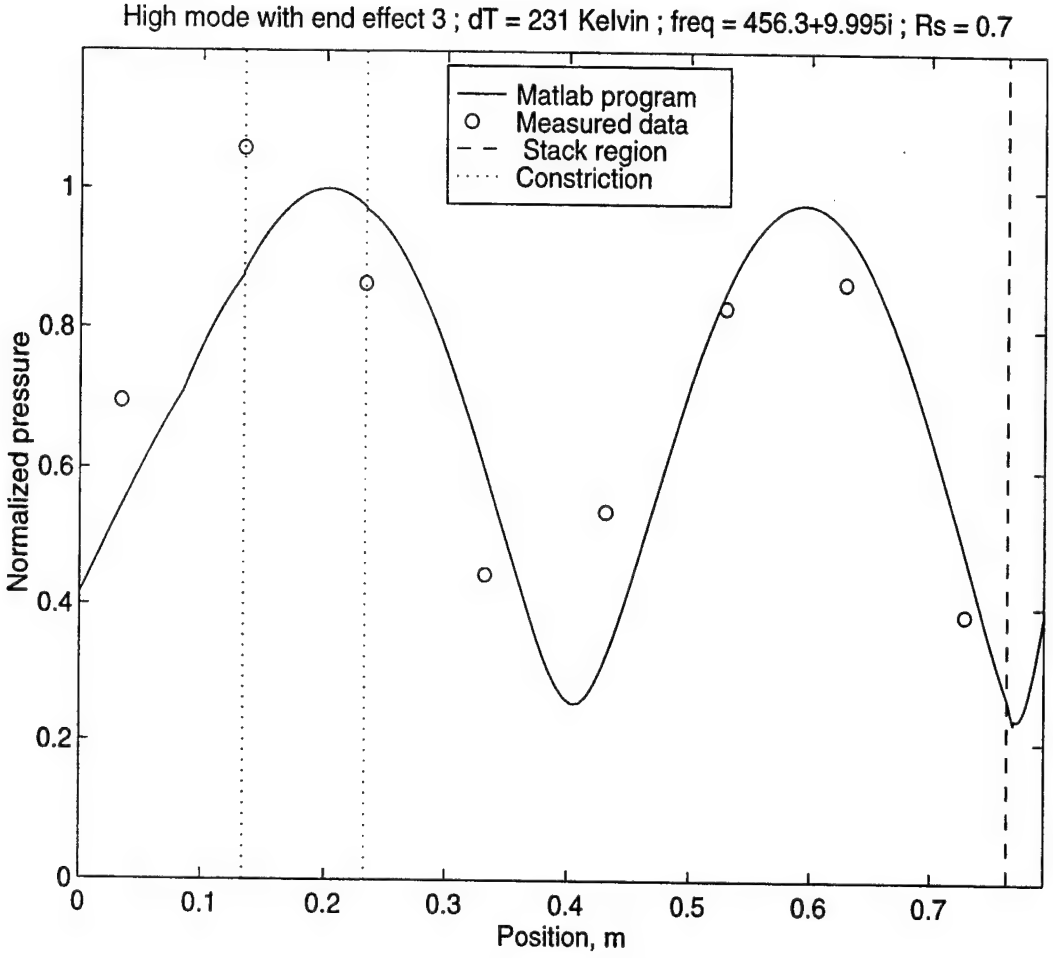

Figure F.1-29 Mode shape of the high mode of the constricted prime mover (Rs=0.7) when the driver is located 45° from the stack and ΔT=231 K. The calculated results are based on the higher order mode method and the end corrections of the stack are included. The frequency is the calculated value.

APPENDIX F.2 RESULTS OF THE TWO STACK ANNULAR PRIME MOVER

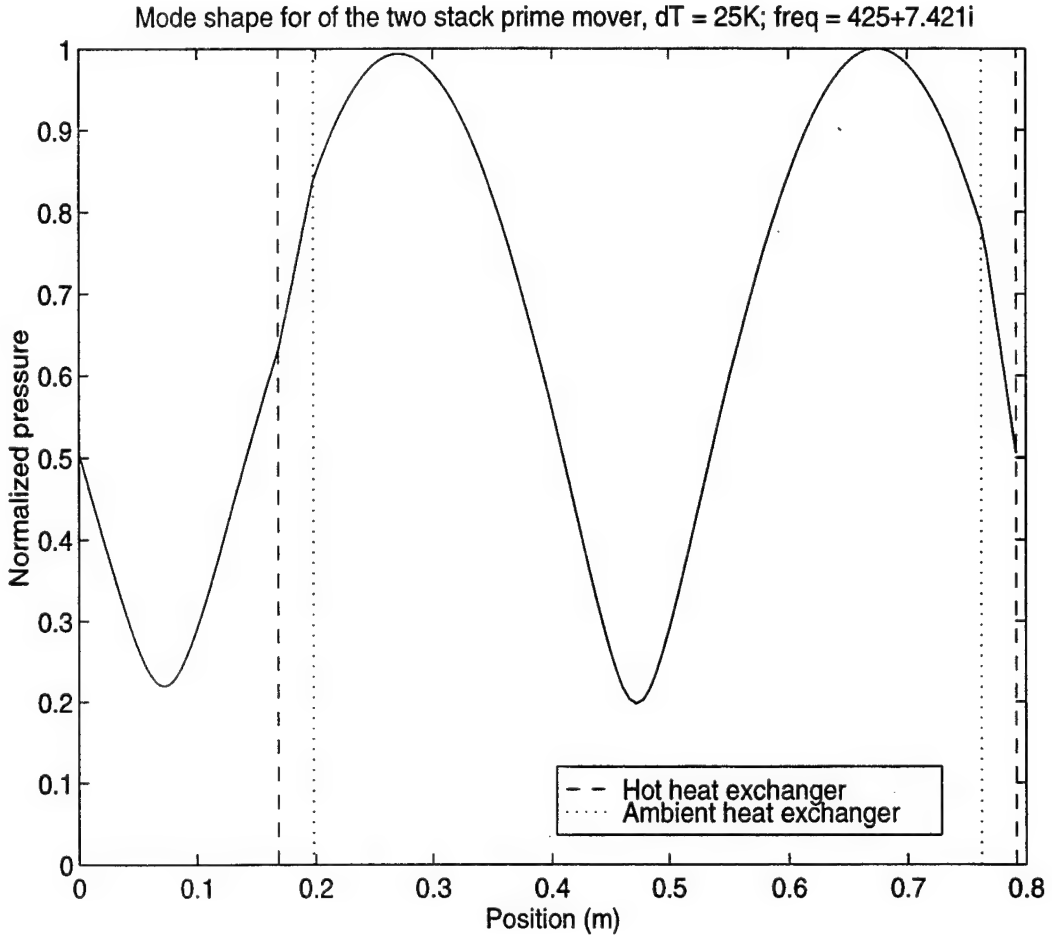

Figure F.2-1 The calculated mode shape of the high mode of the two stack annular prime mover at $\Delta T = 25$ K. Case 1: The duct between the two hot heat exchangers is held at T_a.

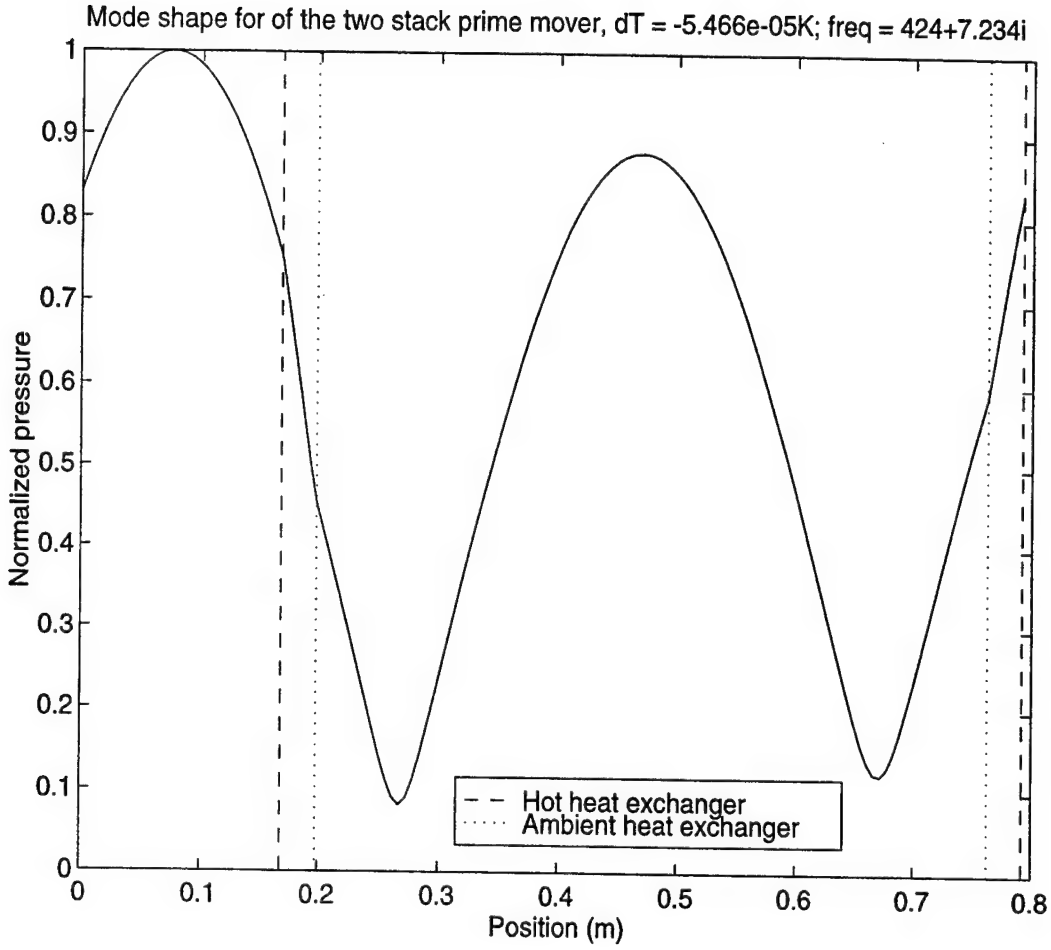

Figure F.2-2 The calculated mode shape of the low mode of the two stack annular prime mover at $\Delta T = 0$ K. Case 1: The duct between the two hot heat exchangers is held at T_a.

LIST OF REFERENCES

Al-Charchafchi, S. H. and Dawson, C. P ., "Analysis of Asymmetrically Coupled Microstrip Ring Resonators," Int. J. Electronics, vol. **68**, no. 2, pp. 275-282, 1990.

Al-Charchafchi, S. H. and Boulkos, J., "Frequency Splitting in Microstrip Rhombic Resonators," IEEE Proceeding, vol. **137**, Pt. H, no. 3, pp. 179-183, 1990.

Al-Charchafchi, S. H. and Schreck, H. G., "Model Predicts Resonator Frequency-Splitting Effects," Microwaves & RF, pp. 117-120, September 1994.

Arnott, W. P., Bass, H. E., and Raspet, R., "General Formation of Thermoacoustics for Stacks Having Arbitrarily Shaped Pore Cross Section," J. Acoust. Soc. Am. **90**(6), pp. 3228-3237, 1991.

Arnott, W. P., Belcher, J. R., Raspet, R., and Bass, H. E., "Stability Analysis of a Helium-Filled Thermoacoustic Engine," J. Acoust. Soc. Am. **96**(1), pp. 370-375, 1994.

Arnott, W. P., Lightfoot, J. A., Raspet, R., and Moosmuller, H., "Radial Wave Thermoacoustic Engines: Theory and Examples for Refrigerators and High-Gain Narrow-Bandwidth Photoacoustic Spectrometers," J. Acoust. Soc. Am. **99**(2), pp. 734-745, 1996.

Atchley, A. A., Bass, H. E. and Hofler, T. J., "Development of Nonlinear Waves in a Thermoacoustic Prime Mover," *Frontiers of Nonlinear Acoustics 12th ISNA*, edited by M. F. Hamilton and D. T. Blackstock, pp. 603-608, Elsevier Applied Science, New York, 1990.

Atchley, A. A., Bass, H. E., Hofler, T. J., and Lin, H. T., "Study of a Thermoacoustic Prime Mover Below Onset of Self-oscillation," J. Acoust. Soc. Am. **91**(2), pp. 734-743, 1992.

Atchley, A. A., "Standing Wave Analysis of a Thermoacoustic Prime mover Below Onset of Self-oscillation," J. Acoust. Soc. Am. **92**(5), pp. 2907-2914, 1992.

Atchley, A. A. and Kuo, F. M., "Stability Curves for a Thermoacoustic Prime Mover," J. Acoust. Soc. Am. **95**(3), pp. 1401-1404, 1994.

Atchley, A. A., "Analysis of the Initial Buildup of Oscillations in a Thermoacoustic Prime Mover," J. Acoust. Soc. Am. **95**(3), pp. 1661-2495, 1994.

Borg, G. G. and Wit D. D., "The Properties of the Frequency Splitting of the Axisymmetric Magnetoacoustic Wave and an Application to Current Profile Diagnosis," Phys. Fluids **B3** (5), pp. 1191-1197, 1991.

Cap, F. and Deutsch, R., "Toroidal Resonators for Electromagnetic Waves," IEEE Tran. on Microwave Theory and Techniques, vol. **MTT-26**, no. 7, pp. 478-486, 1978.

Cap, F. and Deutsch, R., "Toroidal Resonators for Electromagnetic Waves-II," IEEE Tran. on Microwave Theory and Techniques, vol. **MTT-28**, no. 7, pp. 700-703, 1980.

Castro, N. C., "Experimental Heat Exchanger Performance in a Thermoacoustic Prime mover," Master's Thesis, Naval Postgraduate School, California, December 1993.

Celia, M. A and Gray, W. G., *Numerical Methods for Differential Equations : Fundamental Concepts for Scientific and Engineering Applications*, pp. 10 and pp. 67-70, Prentice-Hall, Inc., 1992.

Ceperley, P. H., "A Pistonless Stiring Engine-The Traveling Wave Heat Engine," J. Acoust. Soc. Am. **66**(5), pp. 1508-1513, 1979.

Ceperley, P. H., "Gain and Efficiency of a Traveling Wave Heat Engine," J. Acoust. Soc. Am. **72**(6), pp. 1688-1694, 1982.

Ceperley, P. H., "Gain and Efficiency of a Short Traveling Wave Heat Engine," J. Acoust. Soc. Am. **77**(5), pp. 1239-1244, 1985.

Choe, S. Y., "An Investigation of a Constricted Annular Resonator," Master's Thesis, Naval Postgraduate School, California, June 1997.

Clement, J. R. and Gaffney, J., "Thermal Oscillations in Low-Temperature Apparatus," Adv. Cryog. Eng., **1**, pp. 302, 1954.

Coppens, A. B., "Theoretical Study of Finite-amplitude Traveling Waves in Rigid-walled Ducts: Behavior for Strengths Precluding Shock Formation," J. Acoust. Soc. Am. **49**, pp. 306-318, 1971.

Gabrielson, T. B., "Radiation from a Submerged Thermoacoustic Source," J. Acoust. Soc. Am. **90**(5), pp. 2628-2636, 1991.

Gamaletsos, A. L., "Computer Implementation of Arnott's Formulation of Thermoacoustic Using Matlab," Master's Thesis, Naval Postgraduate School, California, December 1993.

Garrett, S. L. and Swift, G. W., "Thermoacoustic Refrigeration and Its Relationship to the Stirling Cycle," *Proc. of the 7th International Conference on Stirling Cycle Machines*, Tokyo, November 1995.

Gaitan, D. F. and Atchley, A. A., "Finite Amplitude Standing Waves in Harmonic and Anharmonic Tubes," J. Acoust. Soc. Am. **93**(5), pp. 2489-2495, 1993.

Gerald, C. F. and Wheatley, P. O., *Applied Numerical Analysis*, fifth edition, pp. 403-409 and pp. 647-479, Addison-Wesley Publishing Company, 1994.

Gibson, R. J., Nessler F. S., and Keolian R. M., "A Thermoacoustic Pin Stack for Improved Efficiency," *Proc. of the National Heat Transfer Conference*, Baltimore, MD., August 1997.

Heiserman, J. D., "A Study of the Trapping of Superfluid Persistent Currents in Superleaks," Ph.D. dissertation, University of California Los Angeles, December 1975.

Hofler, T. J., "Concepts for Thermoacoustic Refrigeration and a Practical Device," *Proc. Int. Cryocooler Conf.* V, pp. 93-101, August 1988.

Janaki, M. S. and Dasgupta, B., "Eigenmodes for Electromagnetic Waves Propagating in a Toroidal Cavity," IEEE Tran. on Plasma Science, vol. **18**, no. 1, pp. 78-85, 1990.

Johanson Companies, *Thermal Conductivity of Selected Common Materials*, Johanson Companies, New Smyrna Beach, Florida, April 1996.

Karal, F. C., "The Analogous Acoustical Impedance for Discontinuities and Constrictions of Circular Cross Section," J. Acoust. Soc. Am. **25**(2), pp. 327-334, 1953.

Keller, H. B., *Numerical Methods for Two-Point Boundary-Value Problems*, pp. 7-30 and pp. 199-203, Dover Publications, Inc., 1992.

Landau, L. D. and Lifshitz, E. M., *Fluid Mechanics*, pp. 49 and pp. 185, Pergamon Press, 1975.

Larraza, A. and Denardo B., "The Wilberforce Pendulum Lattice: A Model System for Mode Level Repulsion," to be submitted to Am. J. Phys., 1997.

Leon, S. J., *Linear Algebra with Applications*, 4th edition, pp. 378-381, Macmillan College Publishing Company, Inc., 1994.

Lindfield, G. and Penny, J., *Numerical Methods Using MATLAB*, pp. 47-51, Ellis Horwood Limited, 1995.

Lin, H. T., "Investigation of a Heat Driven Thermoacoustic Prime Mover," Master's Thesis, Naval Postgraduate School, California, December 1989.

Meng, C. K., "Transient Phenomena in Thermoacoustic Prime Movers," Master's Thesis, Naval Postgraduate School, California, June 1996.

Migliori, A. and Swift, G. W., "Liquid-Sodium Thermoacoustic Engine," App. Phy. Lett. **53**, pp. 355-357, 1988.

Miles, J. W., "The Analysis of Plane Discontinuities in Cylindrical Tubes. Part I," J. Acoust. Soc. Am. **17**(3), pp. 259-271, 1945.

Miles, J. W., "The Analysis of Plane Discontinuities in Cylindrical Tubes. Part II," J. Acoust. Soc. Am. **17**(3), pp. 272-284, 1945.

Morse, P. M. and Ingard, K. U., *Theoretical Acoustics*, pp. 467-492, Princeton University Press, 1968.

Muehleisen, R. T., "Reflection, Radiation, and Coupling of Higher Order Modes at Discontinuities in Finite Length Rigid Walled Rectangular Ducts," Ph.D. dissertation, Graduate Program in Acoustics, Pennsylvania State University, Pennsylvania, May 1996.

Muehleisen, R. T. and Swanson D. C., "Matrix Methods for Obtaining the Lumped Acoustic Impedance of a Waveguide Step Discontinuity," to be submitted to J. Acoust. Soc. Am, 1997.

Nesslere, F. S., "Comparison of Pin Stack to a Conventional Stack in a Thermoacoustic Prime Mover," Master's Thesis, Naval Postgraduate School, California, December 1994.

Olson, J. R. and Swift, G. W., "Similitude in Thermoacoustics," J. Acoust. Soc. Am. **95**(3), pp. 1405-1412, 1994.

Organ, A. J., "*Thermodynamics and Gas Dynamics of the Stirling Cycle Machine*," pp. 3, pp. 95-99, and pp. 306-321, Cambridge University Press, 1992.

Pierce, A. D., *Acoustics: An Introduction to its Physical Principles and Applications*, pp. 319-330, Acoustical Society of America, 1991.

Pippard, A. B., *Response and Stability: An Introduction to Physical Theory*, pp. 77-86, Cambridge University Press, 1985.

Pippard, A. B., *The Physics of Vibration*, pp. 366-384, Cambridge University Press, 1989.

Press, H. W., Teukolsky, S. A., Vetterling, W. T., and Flannery, B. P., *Numerical Recipes in FORTRAN: The Art of Scientific Computing*, second edition, pp. 372-381 and pp. 745-751, Cambridge University Press, 1992.

Putnam, A. A. and Dennis, W. R., "Survey of Organ-Pipe Oscillations in Combustion Systems," J. Acoust. Soc. Am. **28**, pp. 246, 1956.

Ring, R., "On Frequency Shift and Splitting Induced by a Deformation of the Cross-section of a Pinch," Plasma Physics and Controlled Fusion, vol. **31**, no. 7, pp. 1161-1177, 1989.

Rott, N., "Damped and Thermally Driven Acoustic Oscillations in Wide and Narrow Tubes," Z. Angew. Math. Phys. **20**, pp. 230-243, 1969.

Rott, N., "Thermoacoustic engines," Adv. Appl. Mech., vol. **20**, pp. 135-175, 1980.

Rudnick, I., Kojima, H., Veith, W., and Kagiwada, R. S., "Observation of Superfluid-helium Persistent Current by Doppler-shifted Splitting of Fourth-sound Resonance," Phys. Rev. Lett., vol. **23**, pp. 1220-1223, 1969.

Sondhauss, C., "Ueber die Schallschwingungen der Luft erhitzten Glasrohren und in gedeckten Pfeifen vön ungleicher Weite," Ann. Phys. (leipzig) **79**, pp. 1, 1850.

Swift, G. W., "Thermoacoustic engines," J. Acoust. Soc. Am. **84**, pp. 1145-1180, 1988.

Swift, G. W., "Liquid-Sodium Thermoacoustic Engine," J. Acoust. Soc. Am. **92**(3), pp. 1551-1563, 1992.

Swift, G. W. and Keolian, R. M., "Thermoacoustics in Pin-array Stacks," J. Acoust. Soc. Am. **94**, pp. 941-943, 1993.

Swift, G. W., *Encyclopedia of Acoustics*, Edited by Crocker, M. J., vol **2** part V 61, pp. 695-701, John Wiley & Sons, Inc., 1997.

The Math Works, *MATLAB Reference Guide*, pp. 286-288 and pp. 318-320, The MathWorks, Inc., 1992.

Ward, W. and Swift, G., "Design Environment for Low-amplitude Thermo-acoustic Engines," J. Acoust. Soc. Am. **95**(6), pp. 3671-3672, 1994.

Ward, W. and Swift, G., *Design Environment for Low-amplitude Thermo-acoustic Engines DeltaE Tutorial and User's Guide*, Los Alamos National Laboratory, January 1996.

Ward, W., private communication, February and March 1997.

Wested, J. and Andersen, E., "Resonance Splitting in Nonuniform Ring Resonators," Electronics Letters, vol. **8**, no. 12, pp. 301-302, 1972.

Wheatley, J., Hofler, T., Swift, G. W., and Migliori, A., "An Intrinsically Irreversible Thermoacoustic Heat Engines," J. Acoust. Soc. Am. **74**(1), pp. 153-170, 1983.

Wheatley, J., Hofler, T., Swift, G. W., and Migliori, A., "Understanding Some Simple Phenomena in Thermoacoustics with Applications to Acoustical Heat Engines," Am. J. Phys. , **53**(2), pp. 147-161, 1985.

Wu, H. N., Carrera R., Dong, J., and Oakes, M. E., "Resonant Mode Analysis in Toroidal Cavities with Elliptical Sections," IEEE Tran. on Plasma Science, vol. **20**, no. 1, pp. 19-23, 1992.

Yang, S. W., "Design of a Toroidal Thermoacoustic Prime Mover," Master's Thesis, Naval Postgraduate School, California, June 1995.

BIBLIOGRAPHY

Acton, F. S., *Numerical Methods That Work*, pp. 157-198, The Mathematical Association of America, 1990.

Ahmadian, H., Galdwell, G. M. L., and Ismail, F., "Extracting Real Modes from Complex Measured Modes," *Proc. of the 13th International Modal Analysis Conference*, Society for Experimental Mechanics, Bethel, CT., 1995.

Beranek, L. L., *Acoustics*, pp. 132-143, 1986 edition, the Acoustic Society of America, 1986.

Bradley, C. E., "Linear and Nonlinear Acoustic Bloch Wave Propagation in Periodic Waveguides," Ph.D. dissertation, University of Texas at Austin, May 1993.

Ceperley, P. H., "Rotating Wave," Am. J. Phys. **60**(1), pp. 938-942, 1992.

Ceperley, P. H., "Tuning a Rotating Wave Resonator," Rev. Sci. Instrum., **66**(1), pp. 256-260, 1995.

Chen, C. L., "Experimental Investigation of Energy Dissipation in Finite-amplitude Standing Waves," Master's Thesis, Naval Postgraduate School, California, June, 1991.

Coppens, A. B. and Sanders, J. V., "Finite-amplitude standing Waves within Real Cavities," J. Acoust. Soc. Am. **58**, pp. 1133-1140, 1975.

Imregun, M. and Ewins, D. J., "Complex Modes- Origins and Limits," *Proc. of the 13th International Modal Analysis Conference*, Society for Experimental Mechanics, Bethel, CT., 1995.

Kinsler L. E., Frey, A. R., Coppens, A. B., and Sanders, J. V., *Fundamentals of Acoustics*, third edition, pp. 206-208, John Wiley & Sons, Inc., 1982.

Richardson, M. H., "Is It a Mode Shape, or an Operating Deflection Shape?," Sound and Vibration, vol. **31**, no 1, pp. 54-61, 1997.

Lallement, G., Gray, R. D., and Inman, D. J., "A Tutorial on Complex Eigenvalues," *Proc. of the 13th International Modal Analysis Conference*, Society for Experimental Mechanics, Bethel, CT., 1995.

Skudrzyk, E., *Simple and Complex Vibratory Systems*, pp. 75-81, Pennsylvania State University Press, 1981.

Taconis, K. W., "Vapor-Liquid Equilibrium of Solutions of ^{3}He in ^{4}He," Physica **15**, pp. 738, 1949.

Wheatley, J., Cox, A., "Natural Engines," Physics Today., pp. 50-57, August 1985.

Yazaki, T., Tominaga, A., and Narahara, Y., "Experiments on Thermally Driven Acoustic Oscillations of Gaseous Helium," J. Acoust. Soc. Am. **84**, pp. 1145-1180, 1988.

Yazaki, T., Okada, A., Mizutani, F., Tominaga, A., and Narahara, Y.," Quasiperiodic and Chaotic states Observed in Taconis Oscillations," Jpn. J. Appl. Phys. **26**, Suppl, **26**-3, pp. 1747, 1987.

INITIAL DISTRIBUTION LIST

1. Defense Technical Information Center 2
   8725 John J. Kingman Rd, STE 0944
   Ft. Belvoir, Virginia 22060-6218

2. Dudley Knox Library.....2
   Naval Postgraduate School
   411 Dyer Rd.
   Monterey, California 93943-5101

3. Professor. Anthony A Atchley , Code PH/Ay 4
   Graduate Program in Acoustics
   Pennsylvania State University
   P. O. Box 30
   State College, Pennsylvania16804

4. Professor Robert M. Keolian, Code PH/Kn 1
   Department of Physics
   Naval Postgraduate School
   Monterey, California 93943-5117

5. Professor Andres Larraza, Code PH/La 1
   Department of Physics
   Naval Postgraduate School
   Monterey, California 93943-5117

6. Professor Thomas J. Hofler, Code PH/Hf 1
   Department of Physics
   Naval Postgraduate School
   Monterey, California 93943-5117

7. Dr. Ralph T. Muehleisen.....1
   Department of Physics, Code PH/Mu
   Naval Postgraduate School
   Monterey, California 93943-5117

8. Professor Steven Baker, Code PH/Ba 1
   Department of Physics
   Naval Postgraduate School
   Monterey, California 93943-5117

9. Professor Ashok Gopinath, Code ME/Gk.....1
   Department of Mechanical Engineering
   Naval Postgraduate School
   Monterey, California 93943-5146

10. Professor Christopher Frenezn, Code MA/Fr.....1
Department of Mathematics
Naval Postgraduate School
Monterey, California 93943-5216

11. Dr. Logan E. Hargrove 1
ONR 331 Room 503-13
Office of Naval Research
800 North Quincy Street
Arlington, Virginia 22217-5660

12. Dr. William Ward.....1
Los Alamos National Laboratory
Grope ESA-EPE
MS J576
Los Alamos, New Mexico 87545

13. Professor James H. Miller.....1
Department of Ocean Engineering, 114 Middleton Building
University of Rhode Island
Narragansett, Rhode Island 02882

14. Maj. Lin, Hsiao-Tseng.....5
Department of Vehicle Engineering
Chung Cheng Institute of Technology
Ta-Shi, Tao-Yuan 33509
Taiwan, R.O.C.

15. Library of Chung Cheng Institute of Technology.....1
Ta-Shi, Tao-Yuan 33509
Taiwan, R.O.C.

16. Library of Chung San Institute of Science and Technology 1
P.O. Box 1
Lung-Tan, Ta-Shi, Tao-Yuan 33500
Taiwan, R.O.C.

17. Dr. Wang, K. L. 1
Chairman of Department of Vehicle Engineering
Chung Cheng Institute of Technology
Ta-Shi, Tao-Yuan 33509
Taiwan, R.O.C.